VNIVERSITAT DE VALÈNCIA

Universitat de València – IFIC/CSIC
Departament de Física Teòrica
Programa de Doctorado en Física

NONCANONICAL APPROACHES TO INFLATION

Ph.D. Dissertation

Héctor Ariel Ramírez Rodríguez

Under the supervision of
Dr. Olga Mena Requejo

Valencia, March 2019

Front cover (adapted) figure by *The Voorhes*
for Scientific American, February 2017

Dr. Olga Mena Requejo, científico titular del Consejo Superior de Investigaciones Científicas (CSIC),

Certifica:

Que la presente memoria, "**Noncanonical Approaches to Inflation**", ha sido realizada bajo su dirección en el Instituto de Física Corpuscular, centro mixto de la Universidad de Valencia y del CSIC, por **Héctor Ariel Ramírez Rodríguez**, y constituye su Tesis para optar al grado de Doctor en Ciencias Físicas.

Y para que así conste, en cumplimiento de la legislación vigente, presenta en el Departamento de Física Teórica de la Universidad de Valencia la referida Tesis Doctoral, y firma el presente certificado.

Valencia, a 4 de marzo de 2018,

Olga Mena Requejo

V.° B.° de la tutora, Dr. Nuria Rius Dionis

Comité Evaluador

Tribunal titular

Prof. Gabriela Barenboim	Universitat de València
Prof. Nick E. Mavromatos	King's College London
Prof. David Wands	University of Portsmouth

Tribunal suplente

Prof. Mar Bastero Gil	Universidad de Granada
Dr. Daniel G. Figueroa	École Polytechnique Fédérale de Lausanne
Dr. Gonzalo Olmo	Universitat de València

Agradecimientos / Acknowledgments

First and foremost, a Olga, porque solo gracias a ella esta tesis fue posible. Por haberme dado la oportunidad de trabajar con ella y haber confiado en mí desde el primer día. Han pasado más de cinco años desde entonces y nunca ha dejado de alentarme, aconsejarme y motivarme a hacer las cosas lo mejor posible. Nunca dejaré de agradecer la fortuna que fue haberla conocido y haber trabajado a su lado.

Many thanks to Lotfi Boubekeur for introducing me to Inflation, for teaching me the basics of it and helping me grow as a researcher. Also for all the help, patience and friendship throughout these years. Many thanks to Hayato Motohashi as well, for his teaching and his enormous patience during the hours I spent in his office. Thanks both for the advice in work, physics and life, and for the reading and comments on the manuscript of this thesis.

I owe a great debt of gratitude to Prof. Wayne Hu for his time and teaching during my two visits to U. Chicago, and also for his help and patience regarding our project. I would also like to greatly thank Prof. David Wands for hosting me at ICG and making me feel at home every second since the beginning, but also for his time and endless help and support. Finally, to Prof. Shinji Tsujikawa for his interest, great support and help during the realization of our project and towards my academic life.

I'm obviously in debt to the rest of my collaborators for their help and contribution: Elena Giusarma, Stefano Gariazzo and Lavinia Heisenberg. But in particular, to Sam Passaglia for his friendship, help, motivation, advice and the good times in Japan. Además, muchísimas gracias también

a todos los miembros de mi grupo en el IFIC por su ayuda y amistad a lo largo de estos años.

Agradecimientos especiales a los amigos más cercanos que me acompañaron a lo largo de estos años. A Miguel Escudero por absolutamente todo: amistad, compañía, ayuda, consejos, colaboración; desde el primer momento en el que empezó el máster y hasta el último minuto de doctorado, pasando por todos los group meetings, congresos, viajes y estancias. A José Ángel, por ser mi primer gran amigo desde mi primera etapa en Valencia, y por continuar siéndolo desde entonces, por los infinitos coffee breaks, charlas de la vida y su sana (e innecesaria) competitividad en todo. A Quique y a Gomis por su compañía todos estos años, ayuda, consejos y su (aún más innecesaria) competitividad dentro y fuera del despacho. También, al resto de mis amigos de Valencia que de una u otra forma se han distanciado pero de los que siempre tendré grandes recuerdos y agradecimientos por haberme incluido en el grupo cuando llegué. Last but not least, special thanks to Sam Witte for all his advice, help, grammar corrections and friendship inside and outside work.

I would also like to thank every single friend I made during these years not only in IFIC but also in Trieste, in Chicago, in Tokyo and in Portsmouth, who somehow contributed to this thesis, either through their help, advice, company or friendship. Many special thanks to every single friend I made in Portsmouth, I wish all the research institutes were like the ICG. Also, thanks a lot to every person I met in my visits to other institutes, people who hosted me or spent some time discussing my work. Finally, thanks to all the people I played football with in all these cities, I hope you enjoyed the games as much as I did.

Finalmente, a mi mamá, mi papá y mis hermanos. Porque, aunque hemos estado alejados, esta tesis no hubiera sido posible sin ellos, sin su apoyo incondicional.

HR

"And the end of all our exploring
Will be to arrive where we started
And know the place for the first time."

— Frank Wilczek & Betsy Devine,
Longing for the Harmonies

List of Publications

This PhD thesis is based on the following publications:

- *Phenomenological approaches of inflation and their equivalence* [1]
  L. Boubekeur, E. Giusarma, O. Mena and H. Ramírez.
  Phys. Rev. D **91** (2015) no.8, 083006, [1411.7237].

- *Do current data prefer a nonminimally coupled inflaton?* [2]
  L. Boubekeur, E. Giusarma, O. Mena and H. Ramírez.
  Phys. Rev. D **91** (2015) 103004, [1502.05193].

- *The present and future of the most favoured inflationary models after Planck 2015* [3]
  M. Escudero, H. Ramírez, L. Boubekeur, E. Giusarma and O. Mena.
  JCAP **1602** (2016) 020, [1509.05419].

- *Reconciling tensor and scalar observables in G-inflation* [4]
  H. Ramírez, S. Passaglia, H. Motohashi, W. Hu and O. Mena.
  JCAP **1804** (2018) no.04, 039, [1802.04290].

- *Inflation with mixed helicities and its observational imprint on CMB* [5]
  L. Heisenberg, H. Ramírez and S. Tsujikawa.
  Phys. Rev. D **99** (2019) no.2, 023505, [1812.03340].

Other works not included in this thesis are:

- *Primordial power spectrum features in phenomenological descriptions of inflation* [6]
  S. Gariazzo, O. Mena, H. Ramírez and L. Boubekeur.
  Phys. Dark Univ. **17** (2017) 38, [1606.00842].

- *Running of featureful primordial power spectra* [7]
  S. Gariazzo, O. Mena, V. Miralles, H. Ramírez and L. Boubekeur.
  Phys. Rev. D **95** (2017) no.12, 123534, [1701.08977].

Preface

The Universe is *some* 13,800,000,000 years old. From its first moments to its current stage, the Universe has undergone several different thermodynamical processes that transformed and deformed it, going between hot and cold, and from dark to bright. Despite the immense complexity of these transformations, when we look at the sky, we can gain access to its *story*. It is a story written in the stars and in the galaxies that we observe, and in the light coming from distant corners of the Universe. Thus, when we look at the sky, we are able to look into the past, and even into the *far* past, back in time to what cosmologists call the *early universe*. There, the *tale* of Inflation is drafted—as an incomplete account of events that theoretical physicists are eager to fulfill. These events took place at *some instant* during the first[1] 0.00000000000000000000000000000000001 seconds after the *big bang*. At that moment, the Universe is believed to have undergone an accelerated expansion and *how was that so?* is the question we, theoretical physicists, wish to answer.

In this thesis we attempt to address a part of this fundamental question. We cover both phenomenological and theoretical approaches to the study of inflation: from model-independent parametrizations to modifications of the laws of gravity. It is divided in four parts. The first one, containing five chapters, consists of an introduction to the research carried out during the PhD: Chapter §1 provides a short introduction to the standard cosmological model, in particular focusing on the epochs and the observables which motivate the need for the inflationary paradigm. In Chapter §2, we review the dynamics of the canonical single-field inflationary scenario, showing that

[1] There are 35 zeros there to the right of the decimal mark.

a scalar quantum field can produce an accelerated expansion of the Universe which effectively solves the problems identified in §1. Furthermore, we review the dynamics and the evolution of the primordial quantum fluctuations and their signatures on current observations. In Chapter §3, we discuss the Mukhanov parametrization, a model-independent approach to study the allowed parameter space of the canonical inflationary scenario. An alternative approach, using modified gravity, is proposed in Chapter §4. There, we review the construction of the most general scalar-tensor and scalar-vector-tensor theories of gravity yielding second-order equations of motion. Additionally, we discuss the main models of inflation developed within these frameworks. Finally, in Chapter §5, we demonstrate new techniques that move beyond the slow-roll approximation to compute the inflationary observables more accurately, in both canonical and noncanonical scenarios. These chapters are complemented with detailed appendices on the cosmological perturbation theory and useful expressions for the main chapters.

Part II is based on the most relevant peer-reviewed publications for this thesis. There, the reader can find the main results obtained during the Ph.D. In Part III we summarize these results and draw our conclusions.

Finalmente, en la Parte IV se ofrece un resumen detallado en español de la Tesis donde se discuten los objetivos, motivación, metodología, resultados y conclusiones.

Contents

Part I

The Inflationary Universe

"The reader may well be surprised that scientists dare to study processes that took place so early in the history of the universe. On the basis of present observations, in a universe that is some 10 to 20 billion years old, cosmologists are claiming that they can extrapolate backward in time to learn the conditions in the universe just one second after the beginning! If cosmologists are so smart, you might ask, why can't they predict the weather? The answer, I would argue, is not that cosmologists are so smart, but that the early universe is much simpler than the weather!"

— Alan H. Guth, The Inflationary Universe

CHAPTER 1

An introduction to ΛCDM

At the beginning of the past century, the common belief was that the Universe we live in was static in nature, a space-time with infinite volume which would neither expand nor contract. When Albert Einstein was formulating the General Theory of Relativity (GR), during the second decade of the century, the equations he obtained would predict a scenario in which the Universe would collapse due to the gravitational force pulling on galaxies and clusters of galaxies. In order to counteract this effect, in 1917, Einstein introduced a *cosmological constant*, Λ, into his equations, a term that induces a repulsive force, counterbalancing the attractive force of gravity, leading to a static universe.

Soon after, and during the course of the last and current centuries, astronomers obtained an enormous amount of information about the origin and evolution of the Universe. First, in 1929, Edwin Hubble observed that galaxies were receding from us at a rate proportional to their distances [8] (see Fig. 1.1). The *Hubble law*—as it is now called—was then a clear evidence that the Universe was not only evolving but that it was dynamical! Einstein was forced to remove the cosmological constant from his equations in what he called his "biggest blunder".[1]

After the groundbreaking observations made by E. Hubble on the expanding state of the Universe, the equations of GR still suggested that the Universe could come to a halt and eventually start to contract due to the effects of gravity; the question was *when?* or, relatedly, how fast the most

[1] I strongly suggest the reader Ref. [9] for an amazing exposition of the history of the General Theory of Relativity, from its developments to its latests cosmological consequences through the contributions of some of the greatest minds from the last century.

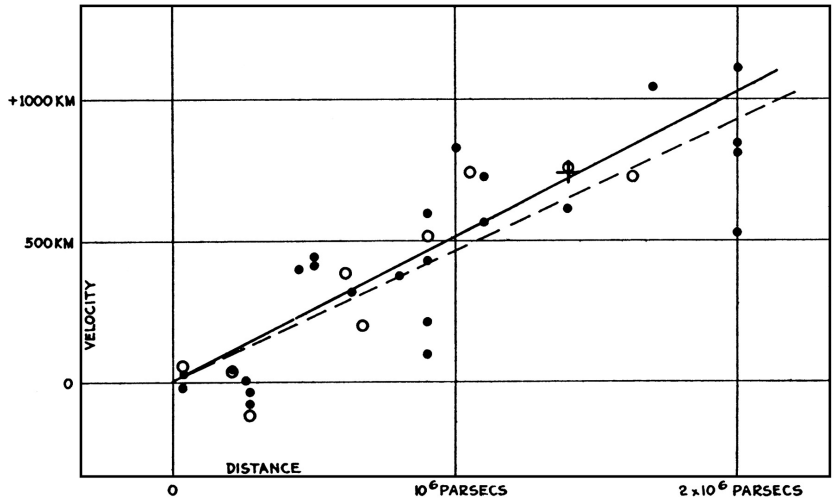

Figure 1.1: Hubble diagram: Velocity-distance relation among galaxies as observed by Edwin Hubble in 1929. The black circles and the solid line give the estimation for individual galaxies whereas white circles and the broken line give the estimation for combined galaxies into groups. The vertical axis is given in units of km/s whereas the horizontal axis is shown in parsecs (1 pc=3.08×10^{16} m). This plot is the original from Ref. [8].

distant galaxies are receding from us. Unexpectedly however, further observations during the last decade of the past century made by the High-Z Supernova Search Team [10] and, independently, by the Supernova Cosmology Project [11], revealed that the Universe was not decelerating, but all the contrary, galaxies are actually receeding from one another at an accelerated rate. Both teams looked at distant Supernovae whose (apparent) luminosity is well-known (this type of supernovae are called Type Ia). These supernovae are *standard candles*: by measuring their flux and knowing their luminosity, we can determine the luminosity distance to these objects and compare to what we expect from the theory. Indeed, the luminosity distance is directly related to the expansion rate of the Universe and its energy content [12, 13]. The two aforementioned independent groups observed that the Type Ia Supernovae were much fainter than what one would expect in a universe with only matter. Consequently, an additional ingredient was mandatory to make our Universe to expand in an accelerated way.

The accelerated nature of the expansion of the Universe has been confirmed by several experiments during the following years, however, its nature remains a mystery. The simplest explanation relies on an intrinsic source of energy of space itself which would act in the same way as the cosmological constant Einstein introduced 100 years ago. Even though the observed value for this vacuum energy density and the value computed from quantum field theory (QFT) calculations differ in many orders of magnitude, the

cosmological constant Λ is now a fundamental part of the standard model of Cosmology and it is referred to as the *dark energy*.

This Chapter provides a brief introduction to the standard model of Cosmology—the so-called ΛCDM—by accounting for the evolution of the Universe from the big bang to the current observations of the late-time accelerated expansion. We shall then review the basic equations for the dynamics of an expanding universe and the main problems of the ΛCDM model, which indicate the strong need for an explanation of the initial conditions of the early universe.

1.1 The expanding universe

In an expanding universe, where each galaxy is receding from one another, one could perform the thought experiment of reversing the time flow. An expanding universe would become a collapsing one where all galaxies get closer and closer to each other. When we then look further back in time, we can see that all the matter and energy content fuse together in a very small and, hence, highly dense and energetic patch of space and time. At this point—dubbed as the hot *big bang*—the equations of GR break down and a new formulation of gravity which includes the laws of quantum mechanics needs to be found. As we currently do not know the principles of such a theory, a given cosmological model must assume some initial conditions which otherwise should come up from a good quantum gravity candidate. As we shall see, these initial conditions need to account for the right amount of initial density perturbations as well as for the observed homogeneity and isotropy of the largest structures of the Universe.

The Universe started to expand soon after the Big Bang, cooling down and following several proceses for a period of approximately 14 billion years[2]—the current age of the Universe. During each of these proceses, the matter and energy content of the Universe went through different phases, each of which left imprints in different direct and indirect cosmological observations we measure nowadays. These indeed have helped us to uncover the history of the Universe we are about to briefly summarize [12, 14–17]. Figure 1.2 shows a schematic summary of the different stages the Universe has gone through.

1.1.1 Cosmological phase transitions

As already pointed out, our starting point is the *hot* big bang—we will see that the event previously described as the big bang is not the expected

[2]As in English: 1 billion = 1 thousand million.

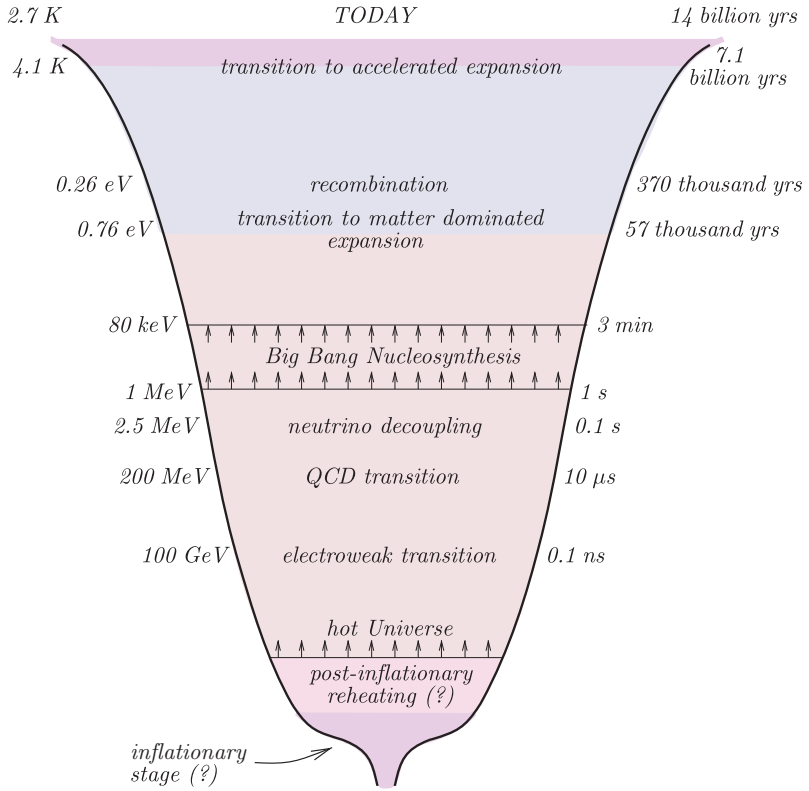

Figure 1.2: Stages of the evolution of the Universe. Adapted from *Introduction to the Theory of the Early Universe* [17] (page 20).

beginning of the Universe, but the residual of the *inflationary* epoch. We call the hot 'Big Bang' to the epoch where all the elementary particles, described in the Standard Model of Particle Physics [18–20], were in thermal equilibrium—they were moving freely in the *primordial plasma*—at energies of a few hundreds of GeV, approximately 10^{15} degrees Kelvin.[3]

As the Universe started to cool down, it experimented phase transitions characterized by the change in the nature of the cosmic fluid. The first one resulted in the spontaneous breaking of the *electroweak* (EW) symmetry [21–23]:[4] at energies above approximately 100 GeV—the energy-scale

[3] 1 GeV=1.16×10^{13} K. Given this equivalence, we shall sometimes refer to a given temperature in eV units.

[4] Let us emphasize that there is a reasonable expectation for a *Grand Unification* epoch, where the QCD and the EW interactions are unified into a single force. Therefore the first phase transition would be at the energy-scale of the Grand Unified Theories (GUT) corresponding to temperatures of around $T \sim 10^{16}$ K. However, even though the idea was proposed in 1974 [24], there are no experimental hints yet that confirm the theory and, furthermore, we will see that inflation is expected to take place at slightly lower energies. Therefore we will ignore the hypothesis of the GUT epoch in this thesis.

of the EW interaction—the EW $SU(2) \otimes U(1)$ gauge symmetry remained unbroken and, consequently, particles in the primordial fluid were massless. Once the temperature dropped, the Higgs field acquired a nonzero vacuum expectation value (vev) which, in turn, breaks the EW symmetry down to the $U(1)$ gauge electromagnetic group. The interaction of particles with the Higgs field provides them with mass (except for the photon which belongs to the unbroken $U(1)$ group) [25,26]. As a result, the new massive particles, as the $W^{\pm}$ and Z gauge bosons, mediate only short-distance interactions.

Another phase transition, the QCD—*Quantum Chromodynamics*—transition, occurred at energies around $\Lambda_{\rm QCD} \sim 200$ MeV. The QCD theory describes the strong force between quarks and gluons, which are subject to an internal charge called *colour* [27–29]. The strong force has the peculiar characteristic of being weaker at shorter (rather than at larger) distances as opposed to the well-known electromagnetic force. This distinctive feature, called *asymptotic freedom* [30, 31], allows the fluid of quarks and gluons to interact only weakly above this energy scale. Once the energy drops below $\Lambda_{\rm QCD}$, quarks and gluons get confined into colourless states, called 'hadrons', of regions with size of $\Lambda_{\rm QCD}^{-1} \simeq 10^{-15}$ m. Consequently, isolated quarks cannot exist below the confinement energy scale.

1.1.2 Neutrino decoupling

Neutrinos are weakly interacting particles. As such, they stopped interacting soon in the early universe, exactly when their interaction rate falls below the rate of the expansion of the Universe, at an approximate temperature of 2-3 MeV [14, 17, 32]. Below this temperature, these relic neutrinos can travel freely through the Universe as they do today. Their temperature and number density are indeed of the same order as the measured relic photons that we shall describe later. However, although direct detection of the relic neutrinos is an extremely difficult task given their feeble interaction with matter [33], their energy density plays an important role on the Universe's evolution [34–36] and thus we are confident of their existence.

1.1.3 Big Bang Nucleosynthesis

Light elements form when freely streaming neutrons bind together with protons into nuclei. These processes happened at energies of a few MeV, corresponding to the binding energy of nuclei and, as a consequence, there was

a production of hydrogen and helium-4, in large amounts, and deuterium, helium-3 and lithium-7 in smaller abundances.[5]

The calculation of the amount of light elements produced during this epoch requires the physics of the previous phase transitions—namely nuclear physics and weak interactions—as well as the use of the equations of GR [37, 38]. Consequently, the measurement of the primordial abundances of such elements and its agreement with the Big Bang Nucleosynthesis (BBN) theory is one of the greatest achievements of the ΛCDM model. This, furthermore, makes the BBN epoch the earliest epoch probed with observations [20] (see however [39, 40] for a discussion on the controversial observed amount of Lithium and the theoretical expectations).

1.1.4 Recombination

We have reached an epoch where the constituents of the primordial fluid were nuclei, electrons and photons. During BBN, the photons were still energetic enough to excite electrons out of atoms. However, once the temperature of the Universe drops at energies around 0.26 eV (∼3000 K), electrons are finally trapped by the nuclei, forming the first stable atoms. This made the remnant of the primordial fluid to become a neutral gas made mostly of hydrogen [41, 42].

It is at this point where a crucial event takes place: photons stopped being actively scattered by the electrons and were able to propagate freely through the Universe, forming a relic radiation which has been freely propagating since then. This radiation is in fact the first light of the Universe and, furthermore, it can be measured today with antennas and satellites as some type of noise coming from all parts of the sky. This photon radiation is the so-called *Cosmic Microwave Background* (CMB) and, as we will see, it plays a crucial role in the understanding of the inflationary epoch because it contains information about the primordial density perturbations and also about the degree of homogeneity and isotropy present during the recombination epoch.

1.1.5 The Cosmic Microwave Background

The energy spectrum of the CMB, as measured today, is precisely that of a black body [43] with a mean temperature of $T_0 = 2.726 \pm 0.001$ K [44]. It was first detected in 1965 by Arno Penzias and Robert Wilson using their antenna from Bell Laboratories [45]. Once they ruled out any known source

[5] Heavier elements need higher densities to form. Carbon and other elements synthesized from it, are the result of thermonuclear reactions in stars once after they have burned out their concentrations of hydrogen and helium.

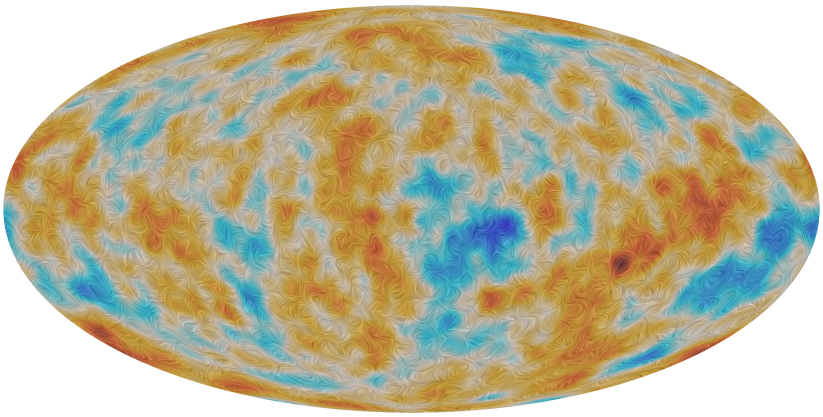

Figure 1.3: Temperature anisotropies and polarization in the Cosmic Microwave Background. Variations in color indicate variations in temperature: the bluer (redder) regions correspond to colder (hotter) temperatures. On the other hand, the texture pattern represents the direction of polarized light. The illustration shows the anisotropies at an angular resolution of 5°, however, the *Planck* satellite has reached a resolution as accurate as $\sim 0.16°$ [47]. *Image Credit:* European Space Agency (ESA) and *Planck* Collaboration.

of noise, Dicke, Peebles, Roll and Wilkinson reported, in the same year, that the source of this radiation could be attributed to the relic photons that decoupled at the recombiation era [46].

The CMB spectrum with mean T_0 temperature is not, however, perfectly isotropic. There are small variations in temperature across the celestial sphere. A map of the CMB is shown in Fig. 1.3 where the changes around the mean temperature—quantified by the differences in color—manifest as anisotropies across the angular scales observed in the sky. These anisotropies are of order of 10^{-5} and are consequence of the slight difference in density across the particle fluid at the time of recombination. Therefore, the CMB is indeed a map of the Universe when it was about 380000 years old.

The differences in temperature across the sphere can be conveniently expanded in spherical harmonics as

$$\frac{\delta T(\hat{n})}{T_0} = \sum_{\ell=1}^{\infty} \sum_{m=-\ell}^{m=\ell} a_{\ell m} Y_{\ell m}(\hat{n}) \ , \tag{1.1}$$

where $\delta T(\hat{n}) \equiv T(\hat{n}) - T_0$ quantifies the deviation between the temperature $T(\hat{n})$ coming from the direction $\hat{n}$ and the mean temperature T_0. The coefficients a_{lm} are themselves related to the amplitud of temperature fluctuations, whereas their ensemble average $\langle a_{\ell m} \rangle$ contains all the statistical information about an average of universes like ours.

One important measurement of the CMB is that the primordial density perturbations must have been close to Gaussian. Given that the a_{lm} coef-

ficients are linear functions of the primordial perturbations, then they are also Gaussian random variables. Hence, the spectrum C_l of the two-point correlation function $\langle a_{\ell m} a^*_{\ell' m'} \rangle$ completely determines the CMB anisotropies.

Furthermore, as we have only one universe to experiment with, the ensemble average can be translated to an average over the single sky we can observe. For higher multipoles ℓ, with a large number of different values for $m = -\ell, ..., \ell$, this is a good approximation and indeed observations are consistent with the Gaussian hypothesis. For lower multipoles, however, the statistical analyses are limited by the cosmic variance. Specifically, the spectrum is defined as

$$C_\ell^{TT} \equiv \frac{1}{2\ell + 1} \sum_{m=-\ell}^{m=\ell} \langle a_{\ell m} a^*_{\ell m} \rangle \ , \tag{1.2}$$

where the statistical error is $1/\sqrt{\ell + 1/2}$, which is clearly larger for a smaller value of ℓ.

Another important type of information contained in the CMB spectrum is its polarization. Figure 1.3 also shows the pattern of polarized light measured in the CMB. The photons decoupled during the recombination era come with polarization states due to the Thompson scattering they experimented before decoupling [48–50]; however, their polarization can be further affected during their subsequent travel by scattering with free electrons during the reionization era[6] or by lensing effects due to massive structures.[7]

As for the temperature anisotropies, we can define two different scalar quantities of polarization in terms of the polarization factors a^E_{lm} and a^B_{lm} as

$$E(\hat{n}) = \sum_{\ell=1}^{\infty} \sum_{m=-\ell}^{m=\ell} a^E_{\ell m} Y_{\ell m}(\hat{n}) \ , \qquad B(\hat{n}) = \sum_{\ell=1}^{\infty} \sum_{m=-\ell}^{m=\ell} a^B_{\ell m} Y_{\ell m}(\hat{n}) \ . \tag{1.3}$$

With these two different types of polarization, we can now define three different types of correlations—TT, EE and BB—plus three cross-correlations—TE, TB and EB,— however, the last two vanish due to symmetry under parity [12, 17].

Measurements of the CMB can then determine the spectra C_ℓ^{TT}, C_ℓ^{TE}, C_ℓ^{EE} and C_ℓ^{BB}. The shape shown in Fig. 1.3 is characteristic of the E-mode polarization, the predominant type of polarization observed, whereas

[6] At late times, star formation processes lead to a *re*ionization period in the Universe. CMB photons can therefore interact with the new free electrons, changing their polarization.

[7] Massive structures bend the light that travels close to them. On one hand, stars, galaxies and galaxy clusters can act as enormous lenses for distant light passing through them, deforming it into *Einstein rings* [51]. On the other hand, light rays traveling long distances during the early universe are also affected by mass sources surrounding their path but in a smaller amount. The statistical account for this effect is commonly known as *weak lensing* and it can also modify the polarization state of the CMB photons.

measurements of the B-mode polarization have only placed upper bounds on the BB spectrum. The B-mode polarization on degree scales is produced by tensor modes present during inflation, thereby a measurement of this type of polarization would extremely help to understand the physics of inflation (see, *e.g.*, Refs. [52–55]).

1.1.6 Structure formation

The starting point of structure formation is the assumption of initial regions of overdensities. During the epoch of radiation domination (before recombination), the amplitude of the density perturbations was small. However, at some point, the Universe becomes matter dominated and then matter starts to get trapped into overdensed regions due to the gravitational potentials.

The way galaxies and clusters of galaxies are currently distributed in space depends crucially on the primordial overdensity. The existence of these initial overdensities is indeed assumed, in the same way as the initial homogeneity and isotropy, as no mechanism within the ΛCDM model is able to produce it. We will see later that inflation, in fact, is exactly a mechanism that provides us with these initial perturbations, with predictions that are amazingly consistent with the data.

Furthermore, the theory of structure formation gives strong hints for the existence of an unknown type of matter which does not have electromagnetic interaction, *i.e.* does not emit light. This *dark matter* is indeed needed to understand the rotation curves of galaxies and to account for the rate of formation of the structures: without dark matter, structures would not have been formed yet! Consequently, the dark matter must be non-relativistic—it must cluster—and therefore it is said that dark matter is *cold*. Current observations show that the dark matter accounts for the 85% of the matter content in the Universe and therefore it is a key element in the development of the ΛCDM (*lambda-cold dark matter*) model, together with the dark energy component.[8]

As the evolution of the structure formation links the current state of the large structures with the initial conditions of the early universe, the observations of the *Large Scale Structure* (LSS) and their statistical signatures have the power of constraining inflation apart from those from the CMB. The first important observation we note is that the Universe, as already stated, is highly homogeneous, *i.e.*, at relatively large scales, it looks the same wherever we look. Figure 1.4 is an example of this fact: it shows the

[8] We shall not further discuss the nature of dark matter as it is not the main topic of this work, see however Refs. [56–58] for reviews on the subject.

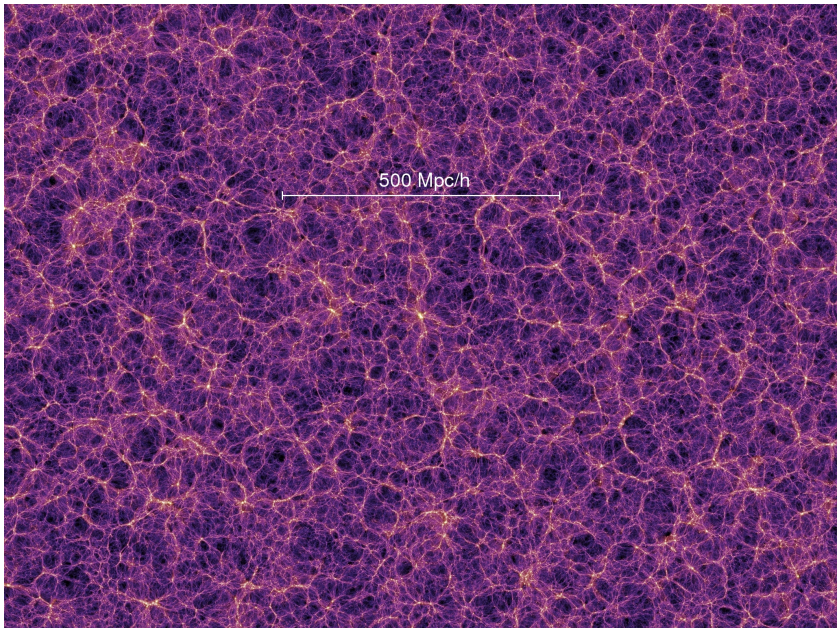

Figure 1.4: N-body simulation of the dark matter density distribution at $t = 13.6$ Gyr (today) using the ΛCDM model [59]. It is shown the scale distance of 500 Mpc/h (see §1.2 for details) above which the distribution of matter is clearly homogeneous and isotropic as assumed by the ΛCDM model.

N-body simulation of 10^{10} particles of a dark matter field evolved following the ΛCDM model [59].

1.2 Dynamics of an expanding universe

So far we have briefly reviewed the evolution of the Universe which is consistent with observations. It can be summarized as a primordial fluid made by elementary particles filling the spacetime. Across this fluid, there must have existed density perturbations in order to lead to structure formation processes due to the gravitational potential wells. As the Universe expanded, this fluid cooled down experiencing several processes which left their imprint both indirectly and directly in the CMB photons and in the structures we measure today. From observations of these two, we can infer the required level of homogeneity and anisotropy the primordial fluid should have had. Let us now set the mathematical grounds upon which the theory is built (see Refs. [12, 15–17, 60, 61] for comprehensive studies in the literature).

1.2.1 Geometry

The geometry of an expanding homogenous and isotropic universe is simply described by the Friedmann-Lemaître-Robertson-Walker metric (FLRW)

$$\begin{aligned} \mathrm{d}s^2 =& g_{\mu\nu}\mathrm{d}x^\mu \mathrm{d}x^\nu \\ =& -\mathrm{d}t^2 + a^2(t) g_{ij}\mathrm{d}x^i \mathrm{d}x^j \ , \end{aligned} \tag{1.4}$$

where g_{ij} is the metric of a unit 3-sphere given by

$$\mathrm{d}l^2 = \mathrm{d}\chi^2 + \Phi(\chi^2)\left(\mathrm{d}\theta^2 + \sin^2\theta \mathrm{d}\phi^2\right) \ . \tag{1.5}$$

Depending on the spatial curvature of the universe, the value of $\Phi(\chi^2)$ is given by

$$\Phi(\chi^2) \equiv \begin{cases} \sinh^2\chi & k=-1 \\ \chi^2 & k=0 \\ \sin^2\chi & k=+1 \end{cases} \ , \tag{1.6}$$

where the curvature parameter k is +1, 0 and -1 for a positive-curvature, flat and negative-curvature universe respectively.

The function $a(t)$, called *scale factor*, grows with time and thus characterizes the distance between two distant objects in space at a given time. We can therefore define the rate of cosmological expansion characterized by the change of the scale factor in time as[9]

$$H(t) = \frac{\dot{a}(t)}{a(t)} \ , \tag{1.7}$$

which is another function of time, and is called the *Hubble rate*. The present value of the Hubble parameter, denoted by H_0, is currently being constrained by the *Planck* satellite. Its measured value is $H_0 = (67.27 \pm 0.6)$ km s^{-1}Mpc^{-1} $= h \cdot 100$ km s^{-1} Mpc^{-1}.[10] However, local estimates from distance ladders find a value of $H_0 = (73.8 \pm 2.4)$ km s^{-1}Mpc^{-1}, showing a discrepancy of around 3.5σ level (see [47] for details).

To understand the value of the intrinsic curvature, *i.e.* the value of k in Eq. (1.6), we again assume a homogeneous and isotropic universe filled with a perfect fluid (*i.e.* with vanishing viscous shear and vanishing heat flux) characterized only by an energy density ρ and an isotropic pressure p. With these ingredients we can define the ratio of energy density relative to

[9] Here and throughout this thesis, dots imply derivatives with respect to cosmic time t.

[10] A megaparsec (Mpc) is a standard cosmological unit of length given by 1 Mpc $= 3.1 \times 10^{24}$ cm. Also, $h \simeq 0.66$ is a dimensionless parameter sometimes used to parametrize the value of H_0 (as in Fig. 1.4).

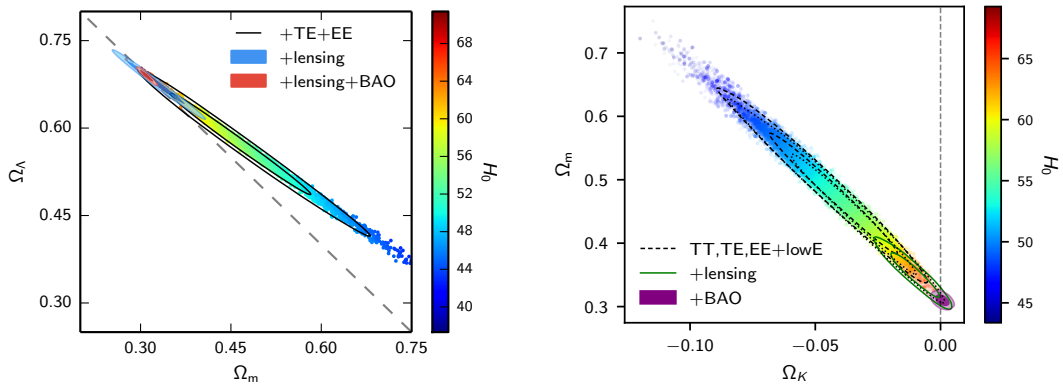

Figure 1.5: *Left: Planck* 2015 constraints in the $\Omega_m - \Omega_\Lambda$ plane [64]. *Right: Planck* 2018 constraints in the $\Omega_k - \Omega_m$ plane [47]. Both constraints are color-coded by the measurement of H_0 and are obtained by using CMB (TT, TE and EE), LSS (weak lensing) and BAO observations.

the *critical* one, ρ_c,[11] as $\Omega = \rho/\rho_c$, and the equation of state as $\omega \equiv p/\rho$. The curvature parameter is related to Ω as

$$1 - \Omega = -\frac{k}{(aH)^2} \ . \tag{1.8}$$

Therefore the intrinsic curvature of the Universe today depends on its total energy density. Current CMB, LSS and BAO[12] combined observations [47] estimate a present value of $\Omega_k \equiv 1 - \Omega_0 = 0.0007 \pm 0.0019$ at 68% confidence level, implying that, to a very good approximation, we are living in a flat universe ($k = 0$).

In the same way, we can define a ratio for both the total matter content, Ω_m, and the contribution due to the dark energy, Ω_Λ, the sum of which equals the total energy content of the Universe. Figure 1.5 shows the current constraints on the three ratios ($\Omega_k = 1 - \Omega_m - \Omega_\Lambda$) using CMB, LSS and BAO observations. We see that around the 70% of the Universe is filled with the mysterious dark energy.

[11] Where ρ_c, the energy density of an exactly flat spacetime, is to be carefully defined in §1.2.2.

[12] Baryon acoustic oscillations (BAO) are pressure waves in the coupled baryon-photon fluid, similar to sound waves, which had visible effects on the CMB and LSS spectra [62, 63].

1.2.2 Evolution

The evolution of the Universe is governed by the Einstein's field equations of General Relativity written as

$$R_{\mu\nu} - \frac{1}{2} g_{\mu\nu} R = 8\pi G T_{\mu\nu} \ , \tag{1.9}$$

where G is Newton's gravitational constant, $R = g^{\mu\nu} R_{\mu\nu}$ is the scalar curvature, and the Ricci tensor $R_{\mu\nu}$ is defined in terms of the Christoffel symbols as

$$R_{\mu\nu} = \Gamma^{\lambda}_{\mu\nu,\lambda} - \Gamma^{\lambda}_{\nu\lambda,\mu} + \Gamma^{\lambda}_{\mu\nu}\Gamma^{\sigma}_{\lambda\sigma} - \Gamma^{\lambda}_{\mu\sigma}\Gamma^{\sigma}_{\lambda\nu} \ . \tag{1.10}$$

Here and throughout this thesis, commas denote partial derivatives $_{,\alpha} \equiv \partial/\partial x^{\alpha}$. The symbols themselves are affine connections defined in GR as

$$\Gamma^{\lambda}_{\mu\nu} = \frac{1}{2} g^{\lambda\sigma} \left(g_{\nu\sigma,\mu} + g_{\mu\sigma,\nu} - g_{\mu\nu,\sigma} \right) \ . \tag{1.11}$$

The energy-momentum tensor $T_{\mu\nu}$, in Eq. (1.9), reads as

$$T^{\mu}_{\nu} = (\rho + p) u^{\mu} u_{\nu} - p \delta^{\mu}_{\nu} \ , \tag{1.12}$$

for a perfect, homogeneous and isotropic, and in a local reference frame fluid, where u^{μ} is its 4-velocity satisfying the condition $g_{\mu\nu} u^{\mu} u^{\nu} = -1$. In cosmology one usually chooses a reference frame which is comoving with the fluid. In this case, $u^{\mu} = (1, 0, 0, 0)$ and then the energy-momentum tensor can be written as a diagonal matrix $T^{\mu}_{\nu} = diag(\rho, -p, -p, -p)$. Furthermore, the energy-momentum tensor is conserved, *i.e.*

$$T^{\mu}_{\nu;\mu} = 0 \ , \tag{1.13}$$

where semicolons denote covariant derivatives $_{;\mu} \equiv \nabla_{\mu} T^{\mu}_{\nu} = T^{\mu}_{\nu,\mu} + \Gamma^{\mu}_{\mu\sigma} T^{\sigma}_{\nu} - \Gamma^{\sigma}_{\mu\nu} T^{\mu}_{\sigma}$. Equation (1.13) leads to the continuity equation

$$\frac{\mathrm{d}\rho}{\mathrm{d}t} + 3\frac{\dot{a}}{a}(\rho + p) = 0 \ , \qquad \leftrightarrow \qquad \frac{\mathrm{d}\ln\rho}{\mathrm{d}\ln a} = -3(1 + \omega) \ , \tag{1.14}$$

where we used the definition of the equation of state $\omega \equiv p/\rho$.

One needs to compute all the components of Eq. (1.9) considering the FLRW spacetime by means of the metric given by Eq. (1.4). The 00-component of the Einstein equations relates the rate of cosmological expansion given by H to the total energy density as[13]

$$\left(\frac{\dot{a}}{a}\right)^2 = \frac{1}{3}\rho - \frac{k}{a^2} \ . \tag{1.15}$$

[13]Here and from now on, we will work in units given by $M_{\rm Pl} = (8\pi G)^{-1/2} = 1$, where $M_{\rm Pl}$ is the Planck mass scale.

This is called the first Friedmann equation. Notice that for a flat ($k = 0$) universe, the energy density reads as $\rho_c = 3H^2$ which we had defined before as the critical density, and therefore Eq. (1.15) can be written as Eq. (1.8).

Taking the derivative of Eq. (1.15) and using the continuity equation (1.14), one obtains the second Friedmann equation:

$$\frac{\ddot{a}}{a} = -\frac{1}{6}(\rho + 3p) \ , \tag{1.16}$$

which gives the acceleration of the scale factor in terms of ρ and p.

The continuity equations (1.14) can also be integrated for $\omega = const.$ to find the behavior of the total energy density as

$$\rho \propto a^{-3(1+\omega)} \ , \tag{1.17}$$

and thus, by plugging it into Eq. (1.16), we could find the behavior of the scale factor for a universe dominated for different components (depending on the value of the equation of state ω):

$$a(t) \propto \begin{cases} t^{2/3(1+\omega)} & \omega \neq -1 \\ e^{Ht} & \omega = -1 \end{cases} \ . \tag{1.18}$$

Notice that an equation of state given by $\omega = p/\rho = -1$ implies that the universe is filled with a fluid with negative pressure. This is exactly the case of a universe dominated by a cosmological constant or by a scalar field driving an accelerated expansion.

1.2.3 Horizons

Information across space can only travel with finite speed, as stated by the Special Theory of Relativity. This defines the causal structure of the Universe: an event originated at some point in spacetime will propagate with a speed which cannot surpass the speed of light. Photons, for instance, —traveling at the speed of light—follow null (light-like) geodesics obeying $\mathrm{d}s^2 = 0$. To better understand the consequences of this simple fact, we define a standard function of time, called *conformal time* τ, given by

$$\mathrm{d}\tau = \frac{\mathrm{d}t}{a(t)} \ . \tag{1.19}$$

In terms of τ, the FLRW line element, Eq. (1.4), with the spatially flat metric $g_{ij} = \delta_{ij}$, can be written as

$$\mathrm{d}s^2 = a^2(\tau)\left(-\mathrm{d}\tau^2 + \delta_{ij}\mathrm{d}x^i\mathrm{d}x^j\right) \ , \tag{1.20}$$

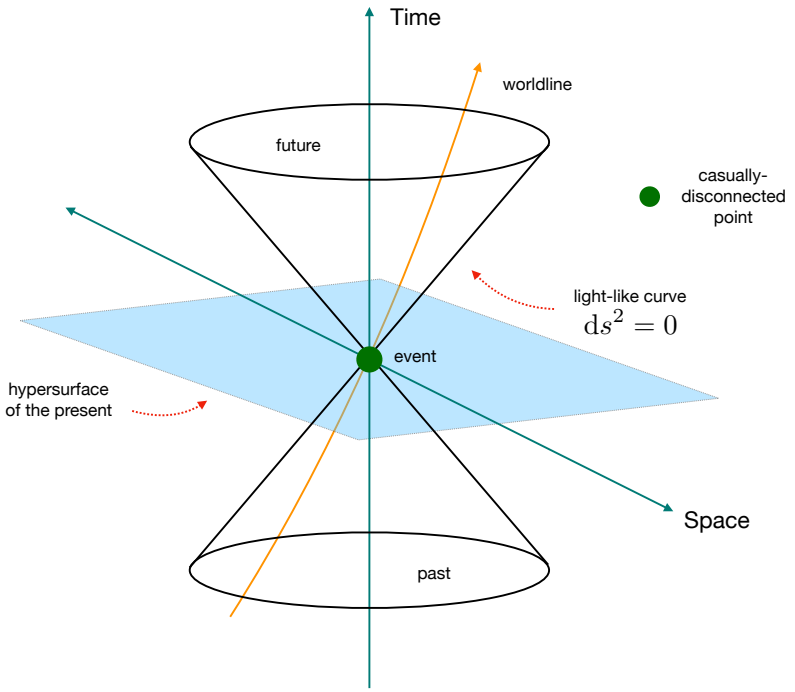

Figure 1.6: Light cone. The information coming from an event produced at a given point in spacetime can only travel with finite speed in time-like worldlines. Light-like curves then enclose all the regions that are and will be causally-connected to that event.

i.e. a static Minkowski metric ($g_{\mu\nu}^{\text{Mink}} = diag\,(-1,1,1,1)$) rescaled by $a(\tau)$. It is simple to see then that null geodesics are described by straight lines of 45°:

$$|\mathrm{d}\vec{x}| = \mathrm{d}\tau \ . \tag{1.21}$$

Figure 1.6 sketches causally connected and disconnected regions of spacetime: null geodesics given by $\mathrm{d}s^2 = 0$ enclose regions causally connected to a given event in a *light cone*; regions outside the light cone do not have access to the event. The light cone grows with time, *i.e.* causally disconnected regions will be reached by the cone at some future time.

Imagine then a photon emitted during the Big Bang; there is a finite physical distance this photon has traveled since then given by

$$d_H(t) = a(t)\tau(t) \ . \tag{1.22}$$

This distance, in fact, defines the radius of a sphere called *cosmological horizon* or *comoving particle horizon* which, for an observer at present time, represents the size of the observable universe.

Now imagine an observer lying at some position $\vec{x} = 0$. For this observer, there will be a future event which will never reach her. For an arbitrary

future time, Eq. (1.21) reads

$$\tau(t \to \infty) - \tau(t) = \int_t^\infty \frac{\mathrm{d}t'}{a(t')} \ , \tag{1.23}$$

which allows us to define the physical size

$$d_e = a(t) \int_t^\infty \frac{\mathrm{d}t'}{a(t')} \ = \frac{1}{H_e}. \tag{1.24}$$

This result implies that such an observer will never know about an event that happens at a distance larger than d_e. This distance is called the *event horizon*.

As we shall see, the event horizon allows us to understand how, without an accelerated expansion during the early universe, most of the observable cosmological scales would have never been in causal contact, which is the core of the ΛCDM problems we are about to discuss.

1.3 Problems of the standard cosmological model

The ΛCDM model just described, consisting on different phases, each driven by very different physical processes, is able to explain with incredible accuracy a large amount of direct and indirect observations. However, as we have already stated several times, it does not provide neither the initial conditions for the primordial fluid in the very early universe—its assumed homogeneity and isotropy—nor the required density perturbations which are the seeds for the structures we observe today in our Universe; these ingredients are just assumed to be there.

On the one hand, it is indeed a puzzle the homogeneity observed in the Universe. Take for instance the CMB anisotropies. The differences in temperature are of order of 10^{-5}, however, the CMB at the time of decoupling consisted of 10^4 causally disconnected patches which should have never been in thermal equilibrium. How is it that they have the same temperature then? (This is the so-called Horizon problem). On the other hand, for our universe to be flat now, it must have been flat to an incredibly degree in the far past, a value uncomfortably small to take as an initial condition. (This is the so-called flatness problem). These two issues are among the main problems of the standard model of Cosmology.

1.3.1 Horizon problem

The particle horizon presented in Eq. (1.19) can be rewritten as

$$\tau = \int_0^{a'} \frac{\mathrm{d}\ln a}{aH} \ . \tag{1.25}$$

Furthermore, from Eq. (1.18) one can use the definition $\mathrm{d}t = a\mathrm{d}\tau$ and find that the combination $(aH)^{-1}$ grows, for a matter (with $\omega = 0$)- or radiation (with $\omega = -1/3$)-dominated universe, as

$$(aH)^{-1} \propto a^{\frac{1}{2}(1+3\omega)} \ , \tag{1.26}$$

and therefore the particle horizon (1.25) grows in a similar way.

The quantity defined as $(aH)^{-1}$ is called the *comoving Hubble radius*, and its implications are quite important: as the comoving Hubble radius has been growing monotonically with time during the evolution of the Universe, observable scales are now entering the particle horizon and, therefore, they were outside causal contact in the far past, at the CMB decoupling for instance. Consequently, the homogeneity problem is manifest: two points with an angular separation exceeding 2 degrees over the observable sky should have never been in thermal equilibrium and yet they have almost exactly the same temperature!

1.3.2 Flatness problem

We have now defined the comoving Hubble radius, which clearly is a function of time that monotonically grows during the evolution of the Universe. Evidently, Eq. (1.8) is therefore a function of time too. It can be then explicitly written as

$$|\Omega(a) - 1| = \left| \frac{k}{(aH)^2} \right| \ , \tag{1.27}$$

where we recall that $\Omega(a) \equiv \rho(a)/\rho_c(a)$. Because $(aH)^{-1}$ grows with time, $|\Omega(a) - 1|$ must diverge and therefore the value $\Omega(a) = 1$ is an unstable fixed point, as seen from the differential equation [60]

$$\frac{\mathrm{d}\ln\Omega}{\mathrm{d}\ln a} = (1 + 3\omega)\,(\Omega - 1) \ . \tag{1.28}$$

For the observed value $\Omega(a) \sim 1$, the initial conditions for Ω then require an extreme fine tuning. For instance, to account for the flatness level observed today, $|\Omega(a_{\rm BBN}) - 1| \leq \mathcal{O}\,(10^{-16})$ or $|\Omega(a_{\rm GUT}) - 1| \leq \mathcal{O}\,(10^{-61})$. Setting these orders of magnitude as initial conditions imply a huge fine-tuning problem.

1.3.3 Initial perturbations problem

Finally, as we have already stated, even though the homogeneity and isotropy are evident, they are not perfect. There exist structures like galaxies, cluster of galaxies and cosmic voids which back in time were seeded by small density perturbations which differed in amplitude by $\delta\rho/\rho \sim 10^{-5}$, according to the level of anisotropy observed in the CMB. These perturbations are, again, assumed and put *by hand*, as the ΛCDM model has no mechanism which can produce them. To that end, a theory providing a mechanism for the generation of these primordial seeds is very appealing.

In the following, we shall see that both the horizon and flatness problems are trivially solved if we account for an epoch in which the comoving Hubble radius decreases before starting to increase again, and that this epoch must consist in an accelerated expansion of the Universe. Furthermore, in the quantum regime, vacuum fluctuations subject to this accelerated expansion could be stretched to classical scales, becoming into the primordial seeds we are looking for. Such a mechanism is now conceived as *inflation* (for reasons we are about to discuss) and it is not only an artifact to solve the horizon and flatness problems, but a theory where the laws of GR and those of quantum mechanics are put to work together, converting inflation in the theory of the primordial quantum fluctuations.

CHAPTER 2

The Physics of Inflation

The *inflationary paradigm* provides the Standard Model of Cosmology with a mechanism which easily solves the horizon and flatness problems and, at the same time, produces the primordial seeds that became the structures we see today in the sky. Independently of the precise nature of the mechanism, it consists on an accelerating stage during the early universe (similar to the current one driven by the dark energy component) which happened only for a *brief* period, soon after the big bang. During this time, the Universe should have exponentially increased—*inflated*—by a factor of 10^{24} in order to fit the current observational constraints. As we shall see, the comoving Hubble radius decreases during this stage and, therefore, observable scales were inside the horizon at the beginning, *i.e.* in causally-connected regions. Hence, this solves the horizon problem. A similar analysis shows that the flatness problem is solved too.

Different mechanisms to inflate the universe have been proposed—the standard picture being that of a new field driving the accelerated expansion. The original one,[1] due to Alan Guth [65], consisted in a new scalar field trapped in a false vacuum state which energy density drives the accelerated expansion. The false vacuum is unstable and decays into a true vacuum by means of a process called *quantum bubble nucleation*. The hot big bang was then generated by bubble collisions whose kinetic energy is obtained from the energy of the false vacuum. A deep analysis of this mechanism, however, showed that this method does not work for our Universe: for

[1] Alan Guth was the first one who proposed a scalar field for the inflationary mechanism and who coined the term 'inflation.' However, historically, the first successful model of inflation is due to Alexei Starobinsky (1979). See §2.3 for a discussion on this model.

sufficiently long inflation to solve the horizon problem, the bubble collision rate is not even small but it does not happen at all as the bubbles get pushed to causally disconnected regions due to the expansion [66–68]. Even though Guth's mechanism did not work, he showed that an accelerated expanding universe could be able to solve the horizon and flatness problems.

Soon after, Andrei Linde [69] and, independently, Andreas Albrecht and Paul Steinhardt [70] introduced a new mechanism in which the new scalar field, instead of being trapped in a false vacuum, is rolling down a smooth potential. Inflation then takes place while the field rolls slowly compared to the expansion rate of the Universe. Once the potential becomes steeper, the field rolls towards the vacuum state, oscillates around the minimum and reheats the Universe. This new mechanism has prevailed up to now and it is the so-called *Slow-Roll inflation*.

In 1981, Viatcheslav Mukhanov and Gennady Chibisov showed an amazing consequence of an accelerated stage of the primordial universe [71]: quantum fluctuations present during this epoch are able to generate the primordial density perturbations and their spectra amplitude are consistent with observations. Later, during the 1982 *Nuffield Workshop on the Very Early Universe*, four different working groups, led by Stephen Hawking [72], Alexei Starobinsky [73], Alan Guth and So-Young Pi [74], and James Bardeen, Paul Steinhardt and Michael Turner [75], computed the primordial density perturbations generated due to quantum fluctuations by the slow-roll mechanism. These calculations made inflation not only an artifact to solve the horizon and flatness problems, but a fully testable theory able to generate the initial conditions of the ΛCDM model.[2]

The simplified picture of inflation consists then in an accelerated epoch driven by the energy density of a new scalar field, dubbed the *inflaton*, which slowly rolls down its potential. Once the inflaton acquires a large velocity, inflation ends and the inflaton oscillates around the minimum of the potential, reheating the Universe *i.e.* giving birth to the hot big bang universe we described in the previous chapter. During the inflaton's evolution, vacuum fluctuations of the inflaton field are continuously created everywhere in space. These fluctuations, which were in causal contact, get stretched to classical levels, exiting the horizon and originating overdensity fluctuations that seeded the structure formation of the Universe.

Along this Chapter, we firstly focus on the classical dynamics of slow-roll inflation: the solution to the ΛCDM problems and the dynamics of a scalar field coupled to Einstein's gravity (GR). Secondly, we shall introduce the

[2] Alan Guth himself is the author of a book on the history of inflation—*The Inflationary Universe: The quest for a new theory of cosmic origins* [76]. I suggest the interested reader to take a look at the book for an extraordinary account of the development of the Inflationary Theory.

theory of cosmological perturbations and follow the quantization prescription for a scalar field in order to compute the predictions for the primordial perturbations. Finally, we shall describe the cosmological observations able to test and discern between different realizations of inflation.

2.1 The horizon and flatness problems revisited

As already pointed out, the core of the ΛCDM problems is the growing nature of the comoving Hubble radius $(aH)^{-1}$—a region enclosing events that are causally-connected at a given time—during the evolution of the Universe. As a consequence, most of the observable scales must have been disconnected in the past. The intuitive solution is then a mechanism which makes the comoving Hubble radius decrease during the early times. This would imply that observable scales were causally-connected at some initial time and then exited the horizon when it decreased. The horizon problem would then be solved as currently disconnected regions across space would have been allowed to be causally-connected in the past.

As we shall see in §2.1.1, during inflation, the Hubble parameter H is approximately constant. Therefore, the particle horizon τ, given by Eq. (1.25), can be integrated explicitly as

$$\tau \simeq -\frac{1}{aH} \,. \tag{2.1}$$

So one can see that a large past Hubble horizon $(aH)^{-1}$ would make τ fairly large today, larger than the present Hubble horizon $(a_0 H_0)^{-1}$, *i.e.* two largely-separated points in the CMB would not communicate today but would have done so in the past if they were inside the particle horizon τ. Figure 2.1 sketches this reasoning.

Furthermore, it is evident from Eq. (1.8) that a decreasing Hubble radius drives the Universe towards flatness, and just deviating from it at present times. Thereby $\Omega = 1$, which previously was an unstable fix point (see Eq. (1.28)), became an attractor solution thanks to inflation, thus also solving the flatness problem.

2.1.1 Conditions for inflation

The shrinking Hubble radius entails important consequences for the evolution of the scale factor a, *i.e.* for the evolution of the Universe. First, lets

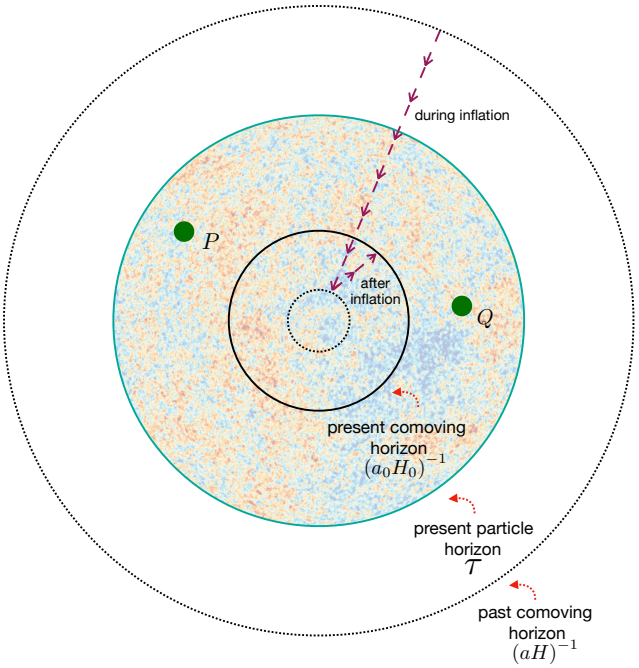

Figure 2.1: Evolution of the comoving Hubble radius $(aH)^{-1}$. At early times, the horizon was large enough so that observable scales were in causal contact. As inflation took place, the horizon shrank and scales came out to disconnected regions. Inflation then finished and the horizon started to grow to the present size. Two casually-disconnected regions, P and Q, were then in causal contact at some point in the past, thus resolving the horizon problem.

note that the change of the decreasing $(aH)^{-1}$ over time is

$$\frac{\mathrm{d}}{\mathrm{d}t}\left(\frac{1}{aH}\right) = -\frac{\ddot{a}}{(aH)^2} < 0 \ , \tag{2.2}$$

and therefore, from the inequality,

$$\ddot{a} > 0 \ , \tag{2.3}$$

is a necessary condition for the shrinking of the Hubble radius. It is evident then that we require an accelerated expansion to solve the horizon and flatness problems.

Furthermore, Eq. (2.3) has implications on the evolution of the Hubble parameter due to the relation $\dot{H} = (\ddot{a}/a) - H^2$, and hence

$$\frac{\ddot{a}}{a} = H^2\left(1 - \epsilon_H\right) \ , \tag{2.4}$$

where we have implicitly defined the first *slow-roll parameter* as

$$\epsilon_H \equiv -\frac{\dot{H}}{H^2} < 1 \ . \tag{2.5}$$

As we shall see, ϵ_H is one of the most important parameters in inflation, as it quantifies its duration and, equivalently, determines when it ends.

Furthermore, from the second Friedmann equation (1.16),

$$\begin{aligned} \frac{\ddot{a}}{a} = H^2 \left(1 - \epsilon_H\right) &= -\frac{1}{6}\left(\rho + 3p\right) \\ &= -\frac{\rho}{6}\left(1 + 3\omega\right) \ , \end{aligned} \tag{2.6}$$

where, for $\epsilon_H \to 0$ and a flat Universe with $\rho = \rho_c = 3H^2$, we find that Eq. (2.6) leads to

$$\omega \to -1 \ , \qquad \leftrightarrow \qquad a \propto e^{Ht} \ , \tag{2.7}$$

as already obtained from Eq. (1.18). This means that the expansion increases exponentially or, in other words, the universe inflates! In a general case, Eq. (2.6) suggests a more general condition for an accelerated expansion:

$$p < -\frac{1}{3}\rho \ , \tag{2.8}$$

which, as discussed in §1.2.2, implies that the accelerated expansion is driven by a fluid with negative pressure.

Finally, notice that Eq. (2.5) shows that during this accelerated expansion, the rate of change of the Hubble parameter is required to be small, meaning that H is approximately constant during inflation. This has important consequences on the conformal time, namely (see Eq. (2.1))

$$\tau = -\frac{1}{aH} \ , \qquad \leftrightarrow \qquad a = -\frac{1}{H\tau} \ , \tag{2.9}$$

and therefore a singularity $a = 0$ corresponds to $\tau \to -\infty$. Consequently, at $\tau = 0$ the scale factor is not well defined and inflation must end before reaching this epoch (that is, $H \simeq const.$ stops being a good approximation). The spacetime defined with these characteristics is called *de Sitter space* and it is exactly the spacetime of inflation. To see the consequences of this in the evolution of two CMB points, let us take Fig. 2.1 and put it in perspective as a function of the conformal time τ, shown in Fig. 2.2. If we take only the period containing the hot big bang (from $\tau = 0$ to τ_0), two CMB points could have never been in contact, whereas once we assume inflation took place, the light cones of these two points intersect in the far past, during inflation, allowing them to be causally connected.

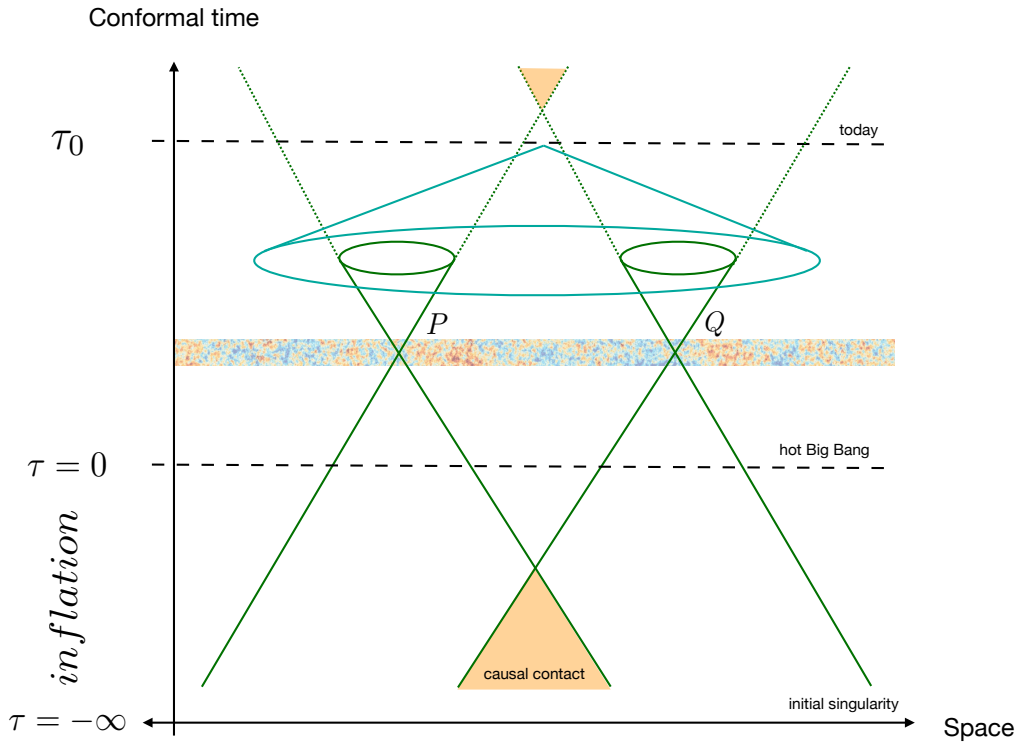

Figure 2.2: Conformal diagram including the inflationary epoch. Inflation shifts the initial singularity to $\tau = -\infty$ (see Eqs. (2.9)) allowing the light cones of two CMB points, P and Q, which are causally disconnected now, to be causally connected at some point in the past, thus solving the horizon problem.

Before continuing, and to summarize, let us emphasize that whatever the mechanism for inflation is, the simple fact that the comoving Hubble radius shrinks implies that the following conditions must be (mutually) satisfied:

$$\ddot{a} > 0 \ , \qquad \epsilon_H \equiv -\frac{\dot{H}}{H^2} < 1 \ , \qquad p < -\frac{1}{3}\rho \ . \tag{2.10}$$

Now, let us discuss how the energy density of a scalar field driving inflation, subject to the *slow-roll approximation*, effectively satisfies these conditions.

2.2 Canonical single-field inflation

At the background level, we consider a single scalar and homogeneous field $\phi(t, x^i) = \phi(t)$, which we shall name the 'inflaton', minimally coupled to Einstein's gravity. The action is then given by the sum of the Einstein-

Hilbert action and the action for the scalar field. It reads as

$$\mathcal{S} = \mathcal{S}_{\rm EH} + \mathcal{S}_\phi = \int \mathrm{d}^4x\sqrt{-g}\left[\frac{1}{2}R + \frac{1}{2}g^{\mu\nu}\phi_{,\mu}\phi_{,\nu} - V(\phi)\right] \ , \tag{2.11}$$

where g =det$(g_{\mu\nu})$, and $V(\phi)$ is the potential energy of the inflaton ϕ. As we shall see, the predictions for a given inflationary model are, in general, highly dependent on the form of $V(\phi)$.

The variation of the Einstein-Hilbert action leads to the Einstein equations in the vacuum $R_{\mu\nu} - \frac{1}{2}g_{\mu\nu}R = 0$. On the other hand, the variation of $\mathcal{S}_\phi$ defines the energy-momentum tensor for the scalar field:

$$\delta\mathcal{S}_\phi = \frac{1}{2}\int \mathrm{d}^4x\sqrt{-g}T_{\mu\nu}\delta g^{\mu\nu} \ , \tag{2.12}$$

which can be solved for $T_{\mu\nu}$ as

$$T_{\mu\nu} = \phi_{,\mu}\phi_{,\nu} - g_{\mu\nu}\left[\frac{1}{2}g^{\rho\sigma}\phi_{,\rho}\phi_{,\sigma} - V(\phi)\right] \ . \tag{2.13}$$

Using the FLRW metric (1.4), the 00- and ii-components of Eq. (2.13) can be related to those in Eq. (1.12) for a perfect fluid. Consequently, the energy density and pressure for a homogeneous minimally coupled scalar field are given by:

$$\rho = \frac{1}{2}\dot{\phi}^2 + V(\phi) \ , \tag{2.14}$$

$$p = \frac{1}{2}\dot{\phi}^2 - V(\phi) \ . \tag{2.15}$$

If we now take the continuity equation (1.14) and substitute Eqs. (2.14)-(2.15) into it, we obtain the Klein-Gordon equation for a scalar field in the gravitational background:

$$\ddot{\phi} + 3H\dot{\phi} + V'(\phi) = 0 \ . \tag{2.16}$$

Here primes denote derivatives with respect to the field, as $' \equiv \mathrm{d}/\mathrm{d}\phi$. Furthermore, it is possible to do the same for the Friedmann equations (1.15) and (1.16) to obtain the evolution equation for the Hubble parameter and the constraint equation respectively as

$$H^2 = \frac{1}{3}\left[\frac{1}{2}\dot{\phi}^2 + V(\phi)\right] \ , \tag{2.17}$$

$$0 = \dot{\phi}^2 - V(\phi) + 3\left(H^2 + \dot{H}\right) \ . \tag{2.18}$$

Together with the Klein-Gordon equation (2.16), Eqs. (2.17)-(2.18) completely determine the dynamics of the scalar field in the gravitational background—and hence are the so-called *background equations of motion*. Now, we shall discuss how this set of equations behaves under the conditions for inflation obtained in §2.1.1.

2.2.1 Conditions for inflation revisited

Recall the conditions for inflation in Eqs. (2.10). The third equation, for the energy density and pressure of ϕ, can be written as

$$\omega_\phi = \frac{p_\phi}{\rho_\phi} = \frac{\frac{1}{2}\dot{\phi}^2 - V(\phi)}{\frac{1}{2}\dot{\phi}^2 + V(\phi)} < -\frac{1}{3} \ , \tag{2.19}$$

which the last inequality can be recast as $\dot{\phi}^2 < V(\phi)$. The same can be noticed from the second equation in (2.10), where the slow-roll parameter can be written, using Eqs. (2.17)-(2.18), as

$$\epsilon_H = \frac{1}{2}\frac{\dot{\phi}^2}{H^2} < 1 \ . \tag{2.20}$$

In this case, the inflationary limit $\epsilon_H \to 0$ places the even stronger condition

$$\dot{\phi} \ll V(\phi) \ . \tag{2.21}$$

In addition, the second derivative, *i.e.* the acceleration of ϕ, must be negligible compared to the rate of expansion. This places the second condition

$$|\ddot{\phi}| \ll |3H\dot{\phi}|, |V'(\phi)| \ . \tag{2.22}$$

This inequality allows us to introduce the second slow-roll parameter η_H, defined as

$$\begin{aligned} \eta_H =& \epsilon_H - \frac{\mathrm{d}\ln\epsilon_H}{2H\mathrm{d}t} \\ =& -\frac{\ddot{\phi}}{\dot{\phi}H} \ . \end{aligned} \tag{2.23}$$

Then, the condition

$$|\eta_H| < 1 \ , \tag{2.24}$$

ensures that the fractional change of ϵ_H is small. We shall sometimes use the slow-roll parameter $\delta_1 = -\eta_H$ which will help us to better define a hierarchy of slow-roll parameters δ_i (see §5).

Therefore, the conditions for inflation Eqs. (2.10) were recast as the slow-roll conditions $\{\epsilon_H, |\eta_H|\} < 1$ which place constraints for the velocity of the field ϕ. Namely, the potential energy $V(\phi)$ should dominate over the kinetic energy $\dot{\phi}^2/2$ or, in other words, the field should *roll slowly* down its potential. This is sketched in Fig. 2.3, where a sufficiently flat potential would make the field roll slowly towards the minimum: once the potential gets steeper, the field acquires a large velocity, breaking the condition (2.20); finally, the field oscillates around the minimum and reheats the Universe. In addition, we illustrate, in Fig. 2.4, the solution for the field ϕ and the first

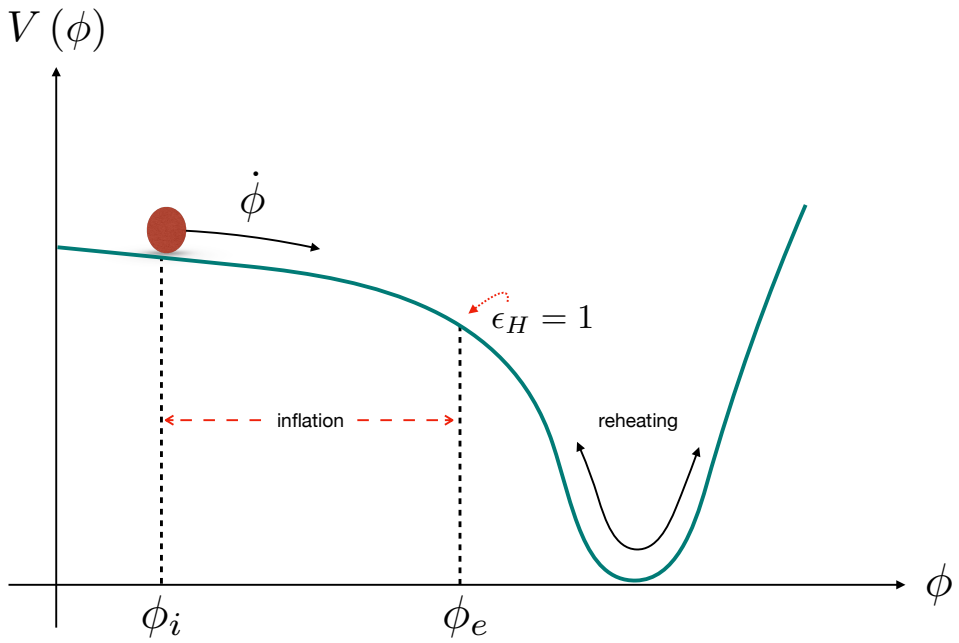

Figure 2.3: Evolution of the inflaton. The inflaton rolls down the potential, inflating the Universe. Once it acquires a large velocity, the slow-roll conditions break and inflation finishes. Afterwards, the inflaton oscillates around the potential's minimum and reheats the Universe. Note that, in general, $\phi_i > \phi_e$, so the field decreases towards the right in this sketch.

slow-roll parameter ϵ_H computed by solving numerically the background equations (2.16)-(2.18) for the α-attractor potential given in Eq. (2.38) with $\alpha_c = 1$. Notice that ϕ and ϵ_H evolve slowly during most of the evolution, parametrized by the number of $e$folds $N = \int H dt$ (quantity that we shall carefully describe in §2.2.4) and that the field enters the oscillatory stage when inflation finishes at $\epsilon_H = 1$, as expected.

2.2.2 Slow-roll approximation

The conditions obtained in §2.2.1 allow us to simplify the Einstein equations for the inflaton, Eqs. (2.16)-(2.18). In particular,

$$\dot{\phi} \simeq -\frac{V'(\phi)}{3H} \ , \tag{2.25}$$

$$H^2 \simeq \frac{1}{3} V(\phi) \ , \tag{2.26}$$

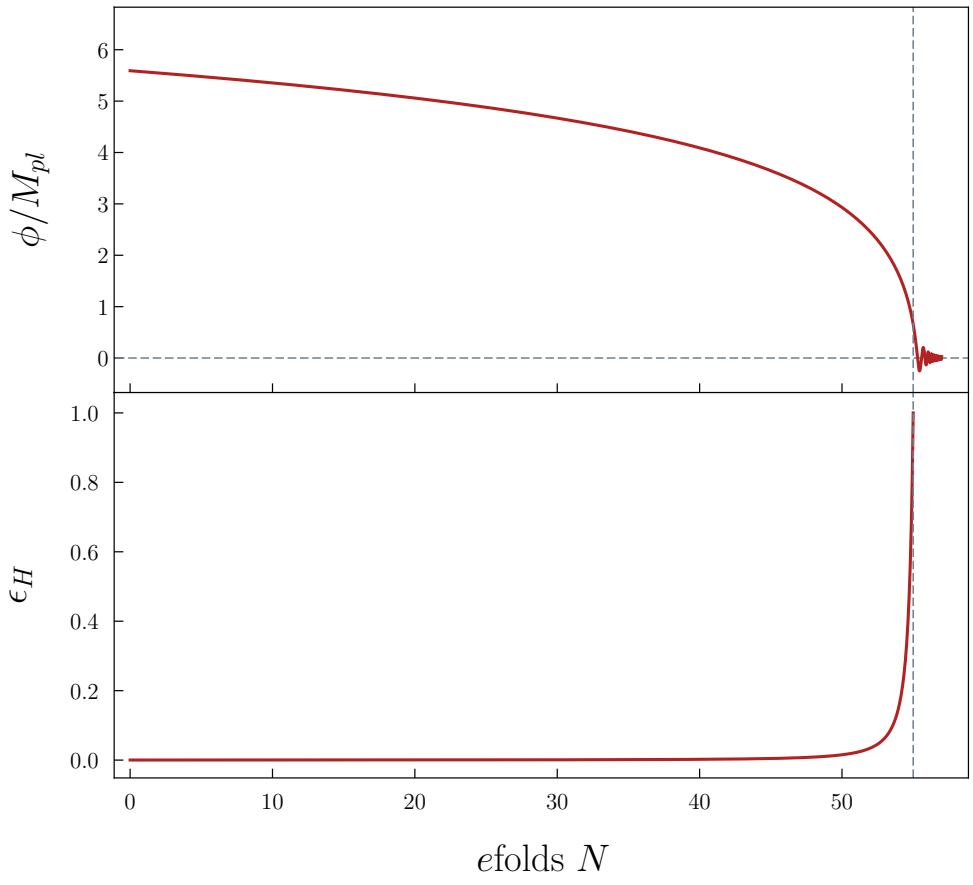

Figure 2.4: Evolution for the field ϕ and the first slow-roll parameters ϵ_H for the model given in Eq. (2.38) with $\alpha_c = 1$, by solving the background equations (2.16)-(2.18) numerically. The plot is normalized such as the end of inflation $\epsilon_H = 1$ coincides with $N = 55$ (gray vertical dashed line).

which is the so-called *slow-roll approximation* (SR).[3] Notice that the second equation also implies that H^2 is approximately constant as expected. Also, from Eqs. (2.25)-(2.26), one can see that the conditions for inflation in terms of the field velocity can be once more recast as conditions for the shape of the potential $V(\phi)$. This allows us to define the potential slow-roll parameters as

$$\epsilon_V \equiv \frac{1}{2}\left(\frac{V'(\phi)}{V(\phi)}\right)^2 , \qquad \eta_V \equiv \frac{V''(\phi)}{V(\phi)} , \tag{2.27}$$

which are related to the *Hubble* slow-roll parameters as $\epsilon_H \simeq \epsilon_V$ and $\eta_H \simeq \eta_V - \epsilon_V$, respectively, as long as the SR approximation (Eqs. (2.25)-(2.26))

[3] Along this thesis, 'SR' shall refer to the (slow-roll) approximation only, which helps to differentiate it from other approximations discussed in §5.

holds. They are also subject to the slow-roll conditions, *i.e.* inflation finishes when ϵ_V, $\eta_V \sim 1$.

2.2.3 Reheating

After inflation has finished, the inflaton rolls to the global minimum of the potential where it oscillates. There will be energy losses due to oscillations, corresponding to the decay of individual ϕ-particles. The equation of motion of ϕ then becomes

$$\ddot{\phi} + 3H\dot{\phi} + \Gamma\dot{\phi} + V'(\phi) = 0 \ , \tag{2.28}$$

after having expanded the potential around the minimum value and where Γ is the decay rate of ϕ, which acts as an additional friction term and depends on how the inflaton couples to the Standard Model particles. One important feature is that reheating occurs at $t \sim H^{-1} \sim \Gamma^{-1}$, *i.e.* the reheating temperature is given by $T_{\rm reh} \sim \sqrt{M_{\rm Pl}\Gamma}$.

As we shall discuss, an important and surprising feature of inflation is that the primordial perturbations freeze after inflation has finished, *i.e.* their subsequent evolution is not affected by the physics of reheating (see Refs. [15, 17, 77–79] for more details on the reheating processes in the early universe).

2.2.4 Duration of inflation

As the expansion is exponentially accelerated, the duration of inflation is parametrized by means of the number of *e*folds $\Delta N \equiv \ln\left(a_{\rm end}/a_{\rm initial}\right)$. Therefore, the number of *e*folds elapsed from a particular epoch to the end of inflation is given by

$$\begin{aligned} N &= \int_t^{t_{\rm end}} H {\rm d}t' \ , \\ &\simeq \int_{\phi_{\rm end}}^{\phi} \frac{V(\phi')}{V'(\phi')} {\rm d}\phi' = \int_{\phi_{\rm end}}^{\phi} \frac{{\rm d}\phi'}{\sqrt{2\epsilon_V}} \ , \end{aligned} \tag{2.29}$$

where in the second line we assumed the SR approximation, and thus we can approximate the duration of inflation by means of the field excursion $\Delta\phi$.

The precise value of N, needed to solve the horizon and flatness problems, depends then on the energy scale of inflation and also on the physics of reheating. The latter in fact provides the following relation [14, 79]:

$$N = 56 - \frac{2}{3}\ln\frac{10^{16}\ {\rm GeV}}{\rho_*^{1/4}} - \frac{1}{3}\ln\frac{10^{9}\ {\rm GeV}}{T_{\rm reh}} \ , \tag{2.30}$$

where ρ_* is the energy density at the end of inflation. Thus, we can estimate N for some well-motivated values of $T_{\rm reh}$. In particular, to solve the aforementioned problems, it is found that $\Delta N \geq 60$ [14, 79]. Furthermore, CMB scales should have exited the horizon around 55 *e*folds before inflation ended (see references in §2.2.3):

$$N_{\rm CMB} = \int_{\phi_{\rm end}}^{\phi_{\rm CMB}} \frac{{\rm d}\phi}{\sqrt{2\epsilon_H}} \simeq 55 \ . \tag{2.31}$$

Before moving on, a comment is in order. Introducing units back, the first slow-roll condition tells us that $|V'(\phi)/V(\phi)| \ll \sqrt{2}/M_{\rm Pl}$, for which $N \gg (\phi - \phi_{\rm end})/\sqrt{2}M_{\rm Pl}$ in Eq. (2.29). This means that we will get a sufficient amount of inflation as long as the excursion $\Delta\phi$ changes at least as large as $\sqrt{2}M_{\rm Pl}$. These *super-Planckian* values (encountered in many inflationary models as the one used in Fig. 2.4) do not represent a breakdown of the classical theory. In fact, the condition for neglecting quantum gravitational effects is that the field energy density is much smaller than the Planck energy density: $|V(\phi)| \ll 2M_{\rm Pl}^2$ [16, 55]. This condition can be simply satisfied by supposing that $V(\phi)$ is proportional to a small coupling constant which, in turn, does not affect the slow-roll conditions nor the value of N.

2.3 Models of inflation

So far we have not made any prediction but just found that, under the assumption that there exists a single field minimally coupled to Einstein's gravity, the conditions for inflation require that the potential energy dominates over the kinetic one. Then, in order to exploit the theory, we need to choose a particular function for $V(\phi)$ and solve the background equations. Their computation is often performed analytically given the simplifications one can do using the SR approximation. However, there exist numerous potentials proposed in the literature which break per se the slow-roll conditions and hence the background equations must be solved numerically. In the following we discuss the usual approximations to choose a model in which we include noncanonical models, which are a central part of this thesis. We do not attempt to give a full list of models but only a taste of the most popular and phenomenologically well-behaved ones. For a well-known and exhaustive classification see Ref. [80].

Single-field canonical models

A general and historical classification of single-field models relies on whether the field in a particular model takes super- or sub-Planckian values.

The former class is dubbed *large-field inflation* whereas *small-field inflation* the latter. The requirement of the flatness of the potential $V(\phi)$ is the same for both and therefore we do not discuss their further conceptual differences but the interested reader is referred to Refs. [55, 79].

Chaotic inflation

Unarguably, the simplest model is given by the potential energy $V(\phi) = m^2\phi^2/2$ which belongs to the class of models called *chaotic inflation* [81], generally written as

$$V(\phi) = \lambda_p \phi^p \ . \tag{2.32}$$

In the next section we shall see that this class of models, in the canonical framework, are in tension with CMB observations [82], however we will often use it as a working example given its simplicity. For instance, the potential slow-roll parameters for this model are simply given by $\epsilon_V = \eta_V = 2/\phi^2$. Furthermore, the end of inflation— $\epsilon_V = 1$ —sets the final value for the field as $\phi_e = \sqrt{2}M_{\rm Pl}$, where we recovered the units for illustration. Then the field value at which CMB fluctuations must have been created can be computed by solving Eq. (2.31). This gives us $\phi_{\rm CMB} = 2\sqrt{N_{\rm CMB} - 1/2} \simeq 15 M_{\rm Pl}$ for $N_{\rm CMB} \simeq 55$. Notice that this model takes super-Planckian values, *i.e.* $\Delta\phi > M_{\rm Pl}$; models with this characteristic produce in general a large amplitud of primordial tensor modes and thus they are in tension with observations [82].

Small-field inflation

A model of inflation with super-Planckian values might be subject to quantum effects which affect the evolution of ϕ in a way we currently do not know. Therefore, models with short excursions $\Delta\phi$ are attractive. Among the most popular ones, *Hiltop inflation*—similar to that sketched in Fig. 2.3—given by the potential [83]

$$V(\phi) = V_0 \left[1 - \left(\frac{\phi}{\mu}\right)^p\right] \ , \tag{2.33}$$

is able to fit observations for $p = 4$ [82].

High-energy physics models

Other class of models are inspired from high-energy theories. Historically, from GUT, the Coleman-Weinberg potential [69, 70]

$$V(\phi) = V_0 \left\{ \left(\frac{\phi}{\mu}\right)^4 \left[\ln\left(\frac{\phi}{\mu}\right) - \frac{1}{4}\right] + \frac{1}{4} \right\} \ , \tag{2.34}$$

was used when inflation was first being studied. However, calculations of the primordial perturbations were incompatible with the phenomenological values of V_0 and μ coming from particle physics. The same problem arises from the widely studied Higgs potential [81, 84].

Along of the lines of GUT theories, supersymmetric realizations provide the potential

$$V(\phi) = \Lambda^4 \left[1 + \alpha_h \log\left(\phi/M_{\rm Pl}\right)\right] \ , \tag{2.35}$$

where $\alpha_h > 0$. In this scenario, inflation is driven by loop corrections in spontaneously broken supersymmetric (SB SUSY) GUT theories [85].

Another widely studied model comes from axion physics, called *natural inflation* [86–89], and is given by a periodic potential of the form

$$V(\phi) = V_0 \left[\cos\left(\frac{\phi}{f}\right) + 1\right] \ . \tag{2.36}$$

However, this model is becoming disfavored by the latest measurements [82].

From string theory, *brane inflation*—driven by a D-brane—is characterized by the effective potential

$$V(\phi) = M^2 M_{\rm pl}^2 \left[1 - \left(\frac{\mu}{\phi}\right)^p + \cdots\right] \ , \tag{2.37}$$

where p and μ are positive constants. In general, one assumes that inflation ends around $\phi \sim \mu$, before the additional terms denoted by the ellipsis contribute to the potential. The models arising from the setup of D-brane and anti D-brane configuration have the power $p = 2$ [90] or $p = 4$ [91, 92].

More recently, from supergravity theories, the α-attractors with the potential energy [82, 93, 94]

$$V(\phi) = \frac{3}{4}\alpha_c M^2 M_{\rm Pl}^2 \left[1 - \exp\left(-\sqrt{\frac{2}{3\alpha_c}}\frac{\phi}{M_{\rm Pl}}\right)\right]^2 \ , \tag{2.38}$$

have been used mainly due to their flexibility to fit observational predictions, depending on the value of α_c (which, interestingly, coincides with Starobinsky inflation, Eq. (2.41), in the limit $\alpha_c = 1$ and with the ϕ^2 model of chaotic inflation in the limit $\alpha_c \to \infty$).

Multifield models

It would be very natural that different species of particles were present during inflation. They may have not played any role in the evolution of the Universe, but any interaction between the inflaton field and other particles will inevitably lead to new phenomenology and to different mechanisms for

the production of perturbations. The study of *multifield inflation* deserves a thesis of its own, but the interested reader is encouraged to look at the comprehensive review by D. Wands [95] or in [17, 79].

Noncanonical models

Here we consider cases in which we do not only choose a potential energy $V(\phi)$ but also modify either the kinetic energy of the field, the gravitational interaction, or both.

k-inflation

Instead of taking $\mathcal{L}_\phi = \frac{1}{2} g^{\mu\nu}\phi_{,\mu}\phi_{,\nu} - V(\phi)$, one can consider more general kinetic terms proportional to ϕ and its velocity $\dot{\phi}$ as

$$\mathcal{L}_\phi = K(\phi, X) - V(\phi) \ , \tag{2.39}$$

where $X \equiv \frac{1}{2} g^{\mu\nu}\phi_{,\mu}\phi_{,\nu}$. These kind of models are called k-inflation and it can be shown that inflation can indeed be driven by the kinetic term and take place even for a steep potential [96, 97].

Nonminimal couplings

Equation (2.11) assumes a minimal coupling between ϕ and R, however, a term like $\xi\phi R$, where ξ is a coupling constant, is also allowed and introduces new phenomenology for different values of the coupling. In this configuration, simple potentials can be reconciled with observations for a range of values of ξ. Furthermore, it can be shown that the theory can be recast as one with a minimal coupling with an effective potential if one performs a conformal transformation of the metric as [2, 84, 98–108]

$$g_{\mu\nu} \to \Omega^2(\phi) g_{\mu\nu} \ . \tag{2.40}$$

Scalar-tensor theories

The two approaches described above can be extended to general theories of modified gravity. In general, any modification of GR will introduce new degrees of freedom, from which a scalar field can be identified as the inflaton. Currently, the most general scalar-tensor theories are the so-called *Horndeski* [109–112] and *beyond Horndeski* [113–120] theories of gravity. These are fully characterized by a few functions, $G_i(\phi, X)$, coupled to the Ricci and Einstein tensors and to derivatives of the field. Therefore, any choice of these functions will inevitably introduce new phenomenology to the inflationary evolution.

Historically, the first successful model of inflation was due to Starobinsky [121]. He realized that an early exponential acceleration comes as a solution of the Einstein equations with quantum corrections, due to the conformal anomaly of free scalar fields interacting with the classical gravitational background.[4] This conformal anomaly contributes with higher-order terms, in the scalar curvature R, to the Einstein-Hilbert action. The action then reads

$$S = \int \mathrm{d}^4x\sqrt{-g}\frac{M_{\rm Pl}}{2}\left(R + \frac{R^2}{6M^2}\right) , \tag{2.41}$$

where, in the absence of a quantum-gravity description of the theory, M is a phenomenological parameter with dimensions of mass. This model belongs to the class of theories called $f(R)$, where suitable functions of R can be written. Furthermore, these classes allow the same conformal transformation, Eq. (2.40), as the nonminimal-coupling models and, in particular, Eq. (2.41) can be recast as a canonical action of a scalar field with the potential given in Eq. (2.38) (with $\alpha_c = 1$), *i.e.* the Starobinsky model is a limit case of the α-attractors [123–126].

The first models of inflation in the framework of general *Horndeski-like* theories were called G-inflation and have been studied for very different potentials. In particular, one can show that simple potentials as those of chaotic inflation can be reconciled with observations for simple choices of $G_i(\phi, X)$ [4, 127–130].

The study of this class of theories for inflation is one of the main goals of this thesis. Consequently, they are fully discussed in §4.

2.4 The theory of primordial quantum fluctuations

We have thus far discussed the classical physics of the inflationary theory: a mechanism able to drive the expansion of the early universe in an accelerated way, solving the horizon and flatness problems. Furthermore, we showed that a scalar field, evolving slowly compared to the expansion rate, satisfies the requirements for the inflationary mechanism.

Yet we are halfway into the story inflation has to tell. As already stated, inflation is also able to provide with the initial conditions for the hot big bang model, *i.e.* with the primordial density perturbations that led to the

[4] In the classical theory, a conformally-invariant free scalar field ($m = 0$), *i.e.* respecting the symmetry given in Eq. (2.40), satisfies $T^{\mu}_{\ \mu} = 0$. However, the quantum expectation value $\langle 0|T^{\mu}_{\ \mu}|0\rangle$ differs from 0, contributing with linear combinations of the scalar curvature R. This is called in the literature a conformal (or *trace*) anomaly (see, *e.g.*, Ref. [122] for details).

CMB anisotropies and the large scale structure. The origin of these lies on the vacuum fluctuations of the inflaton field itself, which is subject to quantum effects.

The inflaton fluctuations backreact on the spacetime geometry, leading to metric perturbations. The full set of quantum perturbations then get stretched to cosmological scales due to the accelerated expansion. As we shall see, these fluctuations in the inflaton field lead to time differences in the evolution of different patches of the Universe, *i.e.* inflation finishes at different times in different places across space. Each of these patches will then evolve as independent causally-disconnected *universes*, each one with different energy density, and it is once these patches come back inside the horizon, during recent times, when they become causally-connected again.

In Appendix A we review the Cosmological Perturbation Theory, useful for this chapter. There we compute the primordial curvature perturbation which power spectrum is related to current CMB measurements. One important feature of this perturbation is that it freezes when it comes out the horizon during inflation. Consequently, its evolution is not modified by reheating processes and, in this way, we can connect the physics at the end of inflation with the density perturbations during the latter epochs, including the CMB anisotropies. We shall study the statistical properties of the primordial curvature and tensor perturbations that inflation creates and, in the next section, compare them to current observations.

We will start by finding the second-order action for scalar and tensor perturbations. Then we will quantize the field perturbations and find their equations of motion. Their solutions are not trivial in general so we will explain different approaches to solve them. Finally we shall give the exact formula for the power spectra of these primordial perturbations.

2.4.1 Scalar and tensor perturbations

To compute the second-order action for perturbations, we first adopt the Arnowitt-Deser-Misner (ADM) formalism which allows us to split the metric in such a useful way that the constraint equations clearly manifest [131]. The line element, following this splitting, then reads

$$\mathrm{d}s^2 = -N^2\mathrm{d}t^2 + g_{ij}\left(\mathrm{d}x^i + N^i\mathrm{d}t\right)\left(\mathrm{d}x^j + N^j\mathrm{d}t\right) \ , \tag{2.42}$$

where g_{ij} is the three-dimensional metric on slices of constant t, $N(x^i)$ is called the *lapse function* and $N_i(x_i)$ is called the *shift function*. As we shall see, both N and N_i are Lagrange multipliers and, furthermore, they contain the same information as the metric perturbations Φ and B introduced in Appendix A.

By inserting Eq. (2.42) into Eq. (2.11), the action becomes

$$\mathcal{S} = \frac{1}{2}\int \mathrm{d}^4x\sqrt{-g}\left[N^{(3)}R - 2NV + N^{-1}\left(E_{ij}E^{ij} - E^2\right) + N^{-1}\left(\dot{\phi} - N^i\phi_{,i}\right)^2 - Ng^{ij}\phi_{,i}\phi_{,j} - 2V\right] , \tag{2.43}$$

where ${}^{(3)}R$ is the three-dimensional curvature and

$$E_{ij} \equiv \frac{1}{2}\left(\dot{g}_{ij} - N_{i;j} - N_{j;i}\right) , \qquad E = E^i_i = g^{ij}E_{ij} . \tag{2.44}$$

One can see that neither N nor N_i have temporal derivatives and therefore they are subject to dynamical constraints (the only dynamical variables are then ϕ and g_{ij}). Consequently, by varying the action (2.43) with respect to N and N^i, we get the following constraint equations

$${}^{(3)}R - 2V - g^{ij}\phi_{,i}\phi_{,j} - N^{-2}\left[E_{ij}E^{ij} - E^2 + \left(\dot{\phi} - N^i\phi_{,i}\right)^2\right] = 0 , \tag{2.45}$$

$$\left[N^{-1}\left(E^i_j - E\delta^i_j\right)\right]_{;i} = 0 . \tag{2.46}$$

Now that the splitting, *i.e.* the foliation of the spacetime is evident, we introduce the metric and inflaton perturbations defined in Appendix A. For this, it is customary to choose the *comoving* gauge to fix time and spatial reparametrizations.[5] In this gauge, the inflaton perturbation $\delta\phi$ and E vanish, and thus we adopt a coordinate system which *moves* with the cosmic fluid; furthermore, most of the energy density is driven by the inflaton field during inflation, *i.e.* $\delta\rho \sim \delta\phi$. A consequence of this is that the curvature perturbation on density hypersurfaces, ζ_ϕ, and the spatial curvature Ψ relate as $\zeta_\phi \simeq -\Psi$ (see Eq. (A.50)) and, therefore, the perturbed spatial metric g_{ij} in the comoving gauge reads as (see Eq. (A.10))[6]

$$g_{ij} = a^2\left[(1 + 2\zeta)\,\delta_{ij} + h_{ij}\right] , \tag{2.47}$$

where we assumed that the vector perturbation F_i is subdominant. Also, h_{ij} is the only tensor perturbation and obeys the equation of a gravitational wave (see Eq. (A.55)), *i.e.* the generation of a background of primordial tensor modes h_{ij} is equivalent to the generation of a background of primordial gravitational waves (primordial GW). This waves could polarize the CMB, as discussed in §1.1.5.

We then expand the lapse and shift into background and perturbed quantities. Furthermore, the shift admits a helicity decomposition (see Appendix A for details) in such a way that we can write N and N^i as

$$N = \overline{N} + N_{(1)} , \qquad N_i = \overline{N_i} + \chi_{(1),i} + \omega_{i(1)} , \tag{2.48}$$

[5] See, *e.g.*, Refs. [15, 60, 132] for relations in this and other gauges.

[6] We drop the subscript 'ϕ' as the distinction between ζ and ζ_ϕ is not further neccesary.

to first order in perturbations.

Plugging Eqs. (2.48) into the constraint equations (2.45)-(2.46) we find to zero order the Friedmann equation (2.17), which means that it is a constraint equation and not an equation of motion. On the other hand, to first order in perturbations, we find that [133]

$$N_{(1)} = \frac{\dot{\zeta}}{H} \ , \qquad \text{and} \qquad \chi_{(1)} = -\frac{\zeta}{H} + a^2 \frac{\dot{\phi}^2}{2H^2} \partial^{-2} \dot{\zeta} \ , \tag{2.49}$$

where ∂^{-2} is defined through the relation $\partial^{-2} \left(\partial^2 \phi \right) = \phi$.

Finally, by expanding the action Eq. (2.43) to first order in scalar perturbations and substituting Eqs. (2.49) into it, we arrive to the quadratic action for scalar perturbations[7]

$$\mathcal{S}_\zeta^{(2)} = \frac{1}{2} \int \mathrm{d}^4 x a^3 \frac{\dot{\phi}}{H^2} \left[\dot{\zeta}^2 - a^{-2} \left(\partial \zeta \right)^2 \right] \ . \tag{2.50}$$

For tensor perturbations, the computation of the quadratic action is much simpler, given that we only have h_{ij}. The tensor perturbation can be decomposed into its polarization states as

$$h_{ij} = \gamma_+ e_{ij}^+ + \gamma_\times e_{ij}^\times \ , \tag{2.51}$$

and thus we only study the evolution of the scalar components γ_+ and $\gamma_\times$. The quadratic action for tensor perturbations then reads as

$$\mathcal{S}_\gamma^{(2)} = \sum_{\lambda=+,\times} \frac{1}{8} \int \mathrm{d}^4 x a^3 \left[\dot{\gamma}_\lambda^2 - a^{-2} (\partial \gamma_\lambda)^2 \right] \ , \tag{2.52}$$

where the sum is over the two polarization states.

2.4.2 Quantization

We define the scalar and tensor *Mukhanov variables*, $u_s \equiv z_s \zeta$ and $u_t \equiv z_t \gamma$ with

$$z_s^2 \equiv a^2 \frac{\dot{\phi}^2}{H^2} = 2a^2 \epsilon_H \ , \qquad z_t^2 \equiv \frac{a^2}{2} \ . \tag{2.53}$$

In terms of these variables, the quadratic actions become

$$\mathcal{S}_p^{(2)} = \frac{1}{2} \int \mathrm{d}\tau \mathrm{d}^3 x \left[\left(u_p' \right)^2 - \left(\partial u_p \right)^2 + \frac{z_p''}{z_p} u_p^2 \right] \ , \tag{2.54}$$

[7] This equation is popularly identified with the '(2)' superscript and called 'quadratic', although it is composed with *first*-order perturbations identified in this thesis with the '(1)' subscript.

where $p = s, t$ stands for either scalars or tensors. Also, we changed to conformal time and, therefore, from now on primes refer to derivatives with respect to τ, unless otherwise stated.

In order to quantize the field u_p, we define its Fourier expansion as

$$u(\tau, x^i) = \int \frac{\mathrm{d}^3 k}{(2\pi)^3} u_{k_i}(\tau) e^{i k_i x^i} \ , \tag{2.55}$$

where we omit here the subscript 'p' in both $u(\tau, x^i)$ and $u_{k_i}(\tau)$ to simplify the notation. By varying the quadratic action Eq. (2.54) with respect to u_p one obtains the *Mukhanov-Sasaki* equation in Fourier space as

$$u_p'' + \left(k^2 - \frac{z_p''}{z_p}\right) u_p = 0 \ , \tag{2.56}$$

where here $u_p = u_k(\tau)$, from Eq. (2.55), after removing the vector subscript i for the wavenumbers k, given that equation (2.56) depends only on their magnitude.

To specify the solutions of the evolution equation (2.56) we first need to promote u_p to a quantum operator in the standard way as

$$\hat{u} = \int \frac{\mathrm{d}k_i^3}{(2\pi)^3} \left[u_k(\tau) \hat{a}_{k_i} e^{i k_i x^i} + u_k^*(\tau) \hat{a}_{k_i}^\dagger e^{-i k_i x^i} \right] \ , \tag{2.57}$$

where the creation and annihilation operators satisfy the usual commutation relation

$$\left[\hat{a}_{k_i}, \hat{a}_{k_i'}^\dagger\right] = (2\pi)^3 \delta\left(k_i - k_i'\right) \ , \tag{2.58}$$

only if the following normalization condition of u_k and its conjugate momenta $\pi = u_k'$ is satisfied:

$$u_k' u_k^* - u_k u_k'^* = i \ . \tag{2.59}$$

Secondly, we need to choose a vacuum state. In the far past, *i.e.* for $\tau \to -\infty$ (or, equivalently $k \gg aH$), Eq. (2.56) becomes

$$u_p'' + k^2 u_p = 0 \ , \tag{2.60}$$

which is the equation of a (quantum) simple harmonic oscillator with time-independent frequency. It can thus be shown that the requirement of the vacuum state to be the state with minimum energy implies that [15]

$$u_p\left(\tau \to -\infty\right) = \frac{1}{\sqrt{2k}} e^{-ik\tau} \ , \tag{2.61}$$

which defines a unique physical vacuum—the *Bunch-Davies vacuum*—and, along with Eq. (2.59), completely fixes the mode functions.

2.4.3 Solutions to the Mukhanov-Sasaki equation

The Mukhanov-Sasaki equation (2.56) is not simple to solve in general, as it depends on the specific inflationary background, encoded in z_p. For canonical inflation, *i.e.* a background with a smooth inflaton evolution, one can simplify the z_p''/z_p factor by assuming that the evolution is close to a *de Sitter* phase and find analytic solutions by means of the SR approximation. Conversely, the background could not be smooth—features in the inflaton potential can be present—or can be given by a scalar-tensor theory different than GR. In these cases, different techniques must be used or numerical integration must be performed.

Quasi-de Sitter solution

In de Sitter space where de Hubble parameter H is constant, Eq. (2.56) reduces to

$$u_p'' + \left(k^2 - \frac{2}{\tau^2}\right) u_p = 0 \ , \tag{2.62}$$

which, using the initial condition Eq. (2.61), has as solution

$$u_k(\tau) = \frac{e^{-ik\tau}}{\sqrt{2k}} \left(1 - \frac{i}{k\tau}\right) \ , \tag{2.63}$$

which is the same solution for either scalars or tensors, so we dropped the subscript p.

Observations are to be compared with the spectrum of the primordial quantum fluctuations. In this case, the spectrum of u_p is defined as

$$\langle \hat{u}_{k_i}(\tau), \hat{u}_{k_i'} \rangle = (2\pi)^3 \, \delta \left(k_i + k_i'\right) \mathcal{P}_{u_p}(k) \ , \tag{2.64}$$

where $\mathcal{P}_{u_p}(k) \equiv |u_k(\tau)|^2$ is the *power spectrum* of the variable u_p, while the dimensionless power spectrum, $\Delta^2(k)$, reads as

$$\Delta^2_{u_p}(k) \equiv \frac{k^3}{2\pi^2} \mathcal{P}_{u_p}(k) \ . \tag{2.65}$$

Notice that on superhorizon scales, $|k\tau| \ll 1$,

$$|u_k(\tau)|^2 = \frac{1}{2k^3\tau^2} \left(1 + k^2\tau^2\right) \simeq \frac{a^2 H^2}{2k^3} \ , \tag{2.66}$$

where, in the approximation, we took the de Sitter condition on the conformal time Eq. (2.9). Furthermore, using the relations $\zeta = u_s/z_s$ and

$\gamma = u_t/z_t$, we can compute the dimensionless power spectrum for the primordial scalar and tensor perturbations in quasi-de Sitter space, using therefore the solution given in Eq. (2.63), as

$$\Delta^2_\zeta(k) = \frac{k^3}{2\pi^2}\left|\frac{u_p(\tau)}{z_s}\right|^2 = \left.\frac{H^2}{8\pi^2\epsilon_H}\right|_{k=aH} , \tag{2.67}$$

$$\Delta^2_\gamma(k) = \frac{k^3}{2\pi^2}\left|\frac{u_p(\tau)}{z_t}\right|^2 = \left.\frac{H^2}{2\pi^2}\right|_{k=aH} , \tag{2.68}$$

where it has been explicitly stated that they must be evaluated at horizon crossing $k = aH$.

First-order in slow-roll solution

We can take weaker restrictions for the z_p''/z_p factor in Eq. (2.56) if we expand it in slow-roll parameters. On the one hand, the tensor sector is not modified as $z_t^2 = a/2$ does not contain any slow-roll parameter. On the other hand, the scalar factor z_s''/z_s can be expanded as

$$\frac{z''}{z} = a^2H^2\left(2 + 2\epsilon_H + \epsilon_H^2 + 3\delta_1 + 4\delta_1\epsilon_H + \delta_2\right) , \tag{2.69}$$

where we dropped the subscript s to make the notation simpler, and we employed the Hubble slow-roll parameter convention:

$$\delta_1 \equiv \frac{1}{2}\frac{\mathrm{d}\ln\epsilon_H}{\mathrm{d}N} - \epsilon_H , \qquad \delta_2 \equiv \frac{\mathrm{d}\delta_1}{\mathrm{d}N} + \delta_1\left(\delta_1 - \epsilon_H\right) . \tag{2.70}$$

Equation (2.69) is exact, *i.e.* no slow-roll hierarchy approximation has been used at that point (namely, we kept $\mathcal{O}(\epsilon_H^2)$ terms).[8]

To first order in SR approximation, where the quasi-de Sitter condition reads as

$$aH = -\frac{1}{\tau}(1+\epsilon_H) , \qquad \text{(first order in SR)} \tag{2.71}$$

Eq. (2.69) is reduced to

$$\frac{z''}{z} \simeq \frac{1}{\tau^2}\left(2 + 6\epsilon_H + 3\delta_1\right) \equiv \frac{\nu^2 - \frac{1}{4}}{\tau^2} , \qquad \text{(first order in SR)} \tag{2.72}$$

where

$$\nu^2 \equiv \frac{9}{4} + 6\epsilon_H + 3\delta_1 , \quad \leftrightarrow \quad \nu \simeq \frac{3}{2} + 2\epsilon_H + \delta_1 . \tag{2.73}$$

[8] See §5 for details on the hierarchy of slow-roll parameters.

Hence, to first order in slow-roll parameters, the scalar Mukhanov-Sasaki equation (2.56),

$$u_k'' + \left(k^2 - \frac{\nu^2 - \frac{1}{4}}{\tau^2}\right) u_k = 0 \ , \tag{2.74}$$

can be recast as a Bessel equation and thus it has an exact solution given by

$$u_k(\tau) = \sqrt{-\tau}\left[\alpha H_\nu^{(1)}\left(-k\tau\right) + \beta H_\nu^{(2)}\left(-k\tau\right)\right] \ , \tag{2.75}$$

where $H_\nu^{(1)}$ and $H_\nu^{(2)}$ are the Hankel functions of the first and second kind, respectively. These functions are equal, $H_\nu^{(1)}(x) = H_\nu^{(2)}(x)$, for a real argument x and have the following asymptotic limits:

$$H_\nu^{(1)}(x \to \infty) \simeq \sqrt{\frac{2}{\pi x}} e^{i\left[x - \left(\nu + \frac{1}{2}\right)\frac{\pi}{2}\right]} \ , \tag{2.76}$$

$$H_\nu^{(1)}(x \to 0) \simeq -i\frac{(\nu-1)!}{\pi}\left(\frac{2}{x}\right)^\nu = \sqrt{\frac{2}{\pi}}\left(2^{\nu-\frac{3}{2}}\right)\frac{\Gamma(\nu)}{\Gamma\left(\frac{3}{2}\right)} x^{-\nu} e^{-i\frac{\pi}{2}} \ . \tag{2.77}$$

Therefore, in the far past $|k\tau| \to -\infty$, Eq. (2.75) is written as

$$\begin{aligned} u_k(\tau \to -\infty) &= \sqrt{\frac{2}{\pi}}\left[\alpha\frac{e^{-ik\tau}}{\sqrt{k}} + \beta\frac{e^{ik\tau}}{\sqrt{k}}\right] \ , \\ &= \sqrt{\frac{\pi}{2}}\sqrt{-\tau}H_v^{(1)}(-k\tau) \ , \end{aligned} \tag{2.78}$$

where we dropped the factors $e^{\pm i\frac{\pi}{2}\left(\nu+\frac{1}{2}\right)}$ and, in the second line, we took $\alpha = \sqrt{\pi/2}$ and $\beta = 0$ by comparison with Eq. (2.61), *i.e.* Eq. (2.78) fixes the Bunch-Davies mode functions to first order in the slow-roll parameters.

Finally, the dimensionless power spectrum, computed in the limit $k\tau \ll 1$, reads as

$$\begin{aligned} \Delta_\zeta^2(k) &= \frac{k^3}{2\pi^2}\left|\frac{u_k(\tau \to 0)}{z}\right|^2 \\ &= \frac{2^{2\nu-3}}{(2\pi)^2}\left[\frac{\Gamma(\nu)}{\Gamma\left(\frac{3}{2}\right)}\right]^2\left(\frac{H}{-a\tau\dot{\phi}}\right)^2(-k\tau)^{3-2\nu}\Big|_{k=aH} \ , \end{aligned} \tag{2.79}$$

where one can notice that in the limit $\epsilon_H = \delta_1 \to 0$ (or, equivalently, $\nu \to 3/2$), Eq. (2.79) reduces to Eq. (2.67) as expected.

Integral solutions

In the previous approximate solutions, the validity of the slow-roll conditions, Eqs. (2.20) and (2.24), was assumed. The first condition, $\epsilon_H \ll 1$, is

required to not terminate inflation prematurely, whereas $|\delta_1| \ll 1$ [9] enforces that ϵ_H evolves slowly and thus the only deviation from quasi-de Sitter is due to the end of inflation, which ensures that the SR approximation remains valid. However, in canonical inflation, the evolution of these parameters depends on the shape of the potential, meaning that an irregular potential—with features of some sort—would make one of the parameters increase before the end of inflation, violating the slow-roll conditions. This does not necessarily mean that inflation is terminated, but that the SR approximation cannot be trusted. This has become an issue as more models with features in the potential have become popular due to their particular signatures in the power spectrum. For such cases, numerical integration of Eq. (2.56) has been usually performed.

Alternatively, new techniques to solve the Mukhanov-Sasaki equation in a semi-analytical way have been developed to overcome the deficiencies of the SR approximation. In §5 we will carefully review two powerful methods: the *Generilized slow-roll* (GSR) [134–143], and the *Optimized slow-roll* (OSR) [144,145] approximations. The former relies on an integral, iterative solution of Eq. (2.56), whereas the latter relies on analytical formulas in terms of the slow-roll parameters as in the standard SR approximation, but with a different and more accurate order counting of slow-roll parameters. In both cases, ϵ_H is still required to be small in amplitude, so inflation is not terminated, but its evolution can be as fast as the $e$folding scale. As we shall see in §5, both techniques were recently extended to include the full Horndeski background described in §2.3 and to be detailed in §4.1.1.1, making these methods even more powerful.

In the case in which neither the conditions for the SR approximation nor those for the GSR/OSR techniques are satisfied, direct numerical integration of Eq. (2.56) is required, for each wavenumber k and with the initial condition given by Eq. (2.63).

2.4.4 Scale dependence, the amplitude of gravitational waves and current observational bounds

The scale dependence of the primordial spectra of scalar and tensor perturbations is quantified through the spectral indices

$$n_s - 1 \equiv \frac{\mathrm{d}\ln\Delta^2_\zeta}{\mathrm{d}\ln k}\,, \qquad\qquad n_t \equiv \frac{\mathrm{d}\ln\Delta^2_\gamma}{\mathrm{d}\ln k}\,. \tag{2.80}$$

Equations (2.67) and (2.68) allow to relate the spectral indices (sometimes called 'primordial tilts') with the slow-roll parameters and thus, working to

[9] Recall that $\eta_H = -\delta_1$.

linear order, we can write them as

$$n_s - 1 = -4\epsilon_H - 2\delta_1 \ , \qquad \text{(first order in SR)} \tag{2.81}$$

$$n_t = -2\epsilon_H \ , \qquad \text{(first order in SR)} \tag{2.82}$$

where the slow-roll parameters should be evaluated at some fixed scale k_*—usually being when CMB scales left the horizon, in order to compare the spectral indices with CMB observations.

Moreover, another parameters obtained from a further quantification of the scale-dependence of the scalar spectral index have been proved to be useful while testing models of inflation against observations [3, 146, 147]. In particular, the running of the scalar spectral index and its own running can be written, respectively, as

$$\alpha_s \equiv \frac{\mathrm{d}n_s}{\mathrm{d}\ln k} \ , \qquad \beta_s \equiv \frac{\mathrm{d}\alpha_s}{\mathrm{d}\ln k} \ , \tag{2.83}$$

and analogously for tensors. Notice that, by taking Eq. (2.81), α_s and β_s can also be written in terms of the slow-roll parameters, and that the hierarchy of these parameters implies that $\alpha_s = \mathcal{O}(\epsilon_H^2)$ and $\beta_s = \mathcal{O}(\epsilon_H^3)$. Therefore, it is customary to parametrize the scalar spectrum in a power-law form, in terms of the scalar parameters, as

$$\Delta_\zeta^2(k) = A_s \left(\frac{k}{k_*}\right)^{n_s - 1 + \frac{1}{2}\alpha_s \ln(k/k_*) + \frac{1}{3!}\beta_s \ln^2(k/k_*)} \ , \tag{2.84}$$

where $A_s = \Delta_\zeta^2(k_*)$. *Planck* 2018 measurements take a pivot scale of $k_* = 0.05\ \mathrm{Mpc}^{-1}$, for which the scalar power spectrum amplitude A_s is measured as

$$A_s = (2.0989 \pm 0.014) \times 10^{-9} \ , \tag{2.85}$$

at 68% confidence level (CL), using the *Planck* TT,TE,EE+lowE+lensing[10] constraints [82] (we shall take the same constraints throughout this thesis unless otherwise stated). At this k_*, the measurements on the scalar parameters then read

$$n_s = 0.9625 \pm 0.0048 \ , \tag{2.86}$$

$$\alpha_s = 0.002 \pm 0.010 \ , \tag{2.87}$$

$$\beta_s = 0.010 \pm 0.013 \ , \tag{2.88}$$

[10] Here, 'TT', 'TE' and 'EE' stand for the combined likelihood using TT, TE, and EE spectra, introduced in §1.1.5, at $\ell \geq 30$; 'lowE' stands for the low-ℓ temperature-only likelihood plus the low-ℓ EE-only likelihood in the range $2 \leq \ell \leq 29$; and 'lensing' stands for the *Planck* 2018 lensing likelihood which uses the lensing trispectrum to estimate the power spectrum of the lensing potential [82].

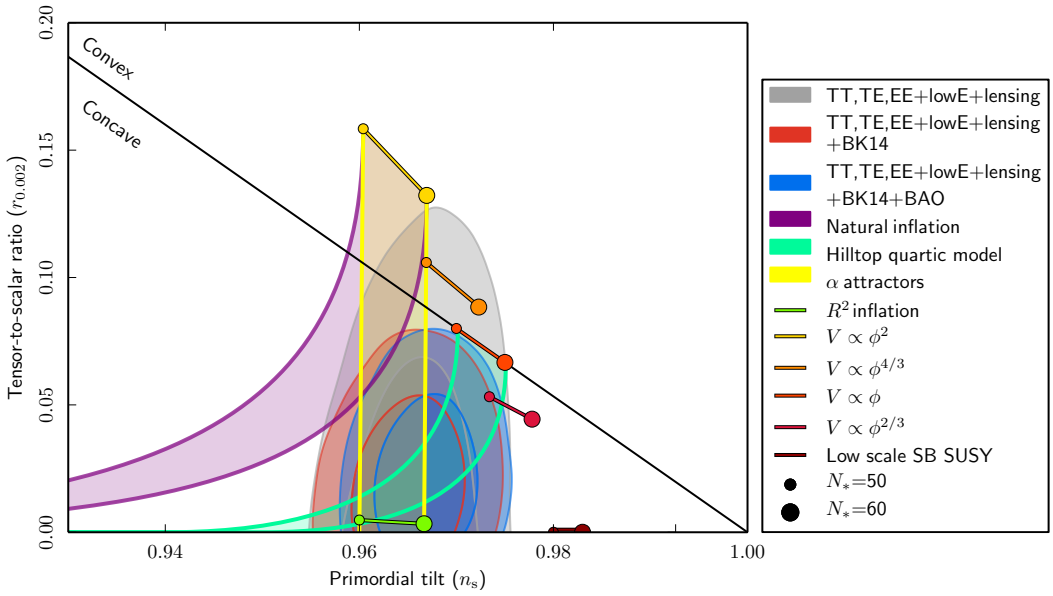

Figure 2.5: *Planck* 2018 constraints on the scalar spectral index n_s and the tensor-to-scalar ratio r at $k_* = 0.002$ Mpc^{-1} from *Planck* measurements alone and in combination with BK14 or BK14+BAO data. The 68% and 95% CL regions are shown and compared to the theoretical predictions of selected inflationary models. Adapted from [82].

at 68% CL, which is consistent with the expectations of the slow-roll hierarchy.

Additionally, the amplitude of tensor perturbations is parametrized through the *tensor-to-scalar ratio* as

$$r \equiv \frac{4\Delta_\gamma^2}{\Delta_\zeta^2} \ , \tag{2.89}$$

where the factor 4 comes after taking into account the two different polarizations of tensor modes. Using Eqs. (2.67) and (2.68), one can see that the tensor-to-scalar ratio can be related to the slow-roll parameters, in which case, using the quasi-de Sitter approximation, it reads as $r = 16\epsilon_H$. By using Eq. (2.82), it is straightforward to see that the tensor-to-scalar ratio is related to the tensor tilt as

$$r = -8n_t \ , \tag{2.90}$$

which is called the *consistency relation*. Any deviation from Eq. (2.90) would be a signature of noncanonical inflationary physics.

Figure 2.5, adapted from [82], shows the 68% and 95% CL constraints coming from *Planck* TT,TE,EE+lowE+lensing measurements alone and also from the combined BICEP2/Keck Array 2014 polarization data [148].

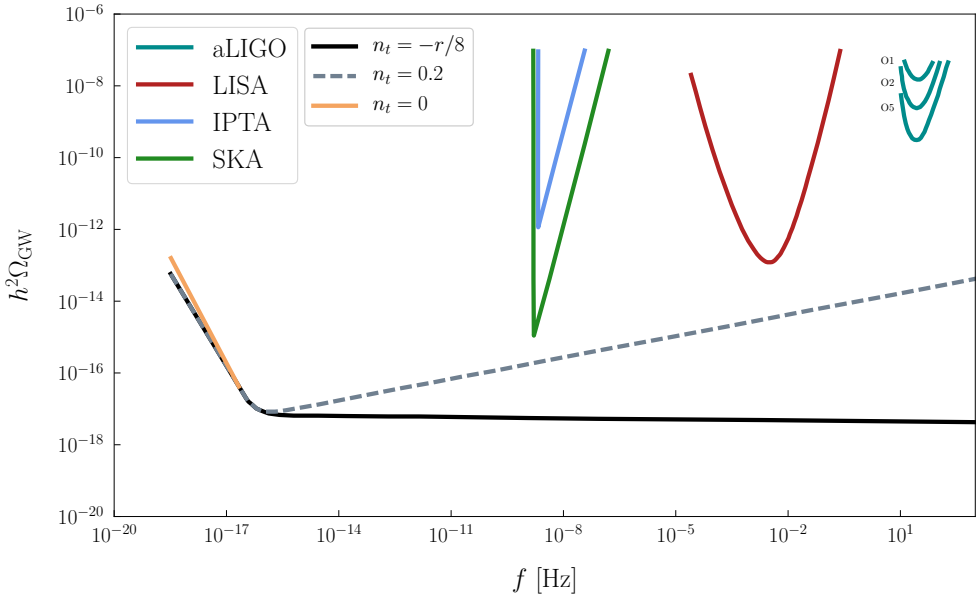

Figure 2.6: Gravitational-wave sensitivity curves for different detectors: Advanced LIGO [152,153]—showing the first (O1) and second (O2) runs and at designed sensitivity (O5)—, LISA [154], IPTA [155], and SKA [156]; along with the GW energy density, given by Eq. (2.92), of three different inflationary scenarios: canonical inflation given by the consistency relation (solid black), a blue-tilted model (dashed gray) and a flat spectrum (orange), all of them by taking the saturated bound $r = 0.064$.

Superimposed are several inflationary models, all of them reviewed in §2.3,[11] and the theoretical line separating concave- and convex-shaped potentials where one can see that the latter are in tension with observations. Notice that all the predictions for the theoretical models are shown for a window of values of the number of $e$folds $N_{\rm CMB} = 50 - 60$, this given the uncertainty in Eq. (2.30). Furthermore, notice that the tensor-to-scalar ratio is consistent with a negligible amplitude of primordial GW, being the current upper bound

$$r < 0.064 \ , \tag{2.91}$$

at $k_* = 0.002$ Mpc^{-1}, using *Planck* TT,TE,EE+lowE+lensing+BK14 constraints. This comes from the fact that no signal of B-mode polarization generated by the primordial GW has yet been detected. Future experiments as, *e.g.*, CORE (a CMB space satellite [149–151]), could be able to improve the current sensitivity to r.

Additionally, current GW experiments, as the ground-based interferometer aLIGO [152,153], have proved their efficacy in measuring GW coming

[11] Notice that the monomial potentials ϕ^p fall into the class of chaotic inflation given by Eq. (2.32).

from astrophysical processes [157–166]. Even though the main goal of these interferometers is to measure astrophysically-sourced GW, a detection of primordial GW is potentially viable. Figure 2.6 shows the gravitational wave-sensitivity curves of several experiments able to detect GW [167,168]. Theoretically, for primordial GW, the GW spectrum is given in terms of the primordial scalar spectrum and the tensor-to-scalar ratio as [168]

$$\Omega_{\rm GW}(f) = \left(\frac{3}{128}\right)\Omega_{\rm rad}\Delta_\zeta^2\left(\frac{f}{f_*}\right)^{n_t}\left[\frac{1}{2}\left(\frac{f_{\rm eq}}{f}\right)^2 + \frac{4}{9}\left(\sqrt{2}-1\right)\right] r \ , \qquad (2.92)$$

where $f_* = k_*/(2\pi\, a_0)$ is the pivot frequency related to the pivot scale k_* and $f_{\rm eq} = H_0\Omega_m/\left(\pi\sqrt{2\Omega_{\rm rad}}\right)$ is the frequency entering the horizon at matter-radiation equality. Using Eq. (2.92), one can compute the predictions of a given inflationary model in terms of the tensor tilt n_t as shown in Fig. 2.6. By taking the bound in Eq. (2.91) as a true value for r, it is shown the theoretical predictions for three different scenarios: the consistency relation in canonical inflation, Eq. (2.90), a blue-tilted scenario with $n_t = 0.2$ and a flat spectrum ($n_t = 0$). In particular, some inflationary scenarios, belonging to the classes discussed in §2.3, predict a large-enough blue tilt of tensor perturbations which could reach future interferometer sensitivities [169–171].

To finish this section, let us notice that although we do not yet know the true nature of inflation, we can still estimate the energy scale at which it took place given the bound (2.91). Recall that $\Delta_t^2 \propto H^2$ and, because of the SR approximation, $H^2 \propto V(\phi)$. Hence, from Eq. (2.89), the energy at CMB scales was approximately

$$E \equiv V^{1/4} \simeq \left(\frac{3\pi^2}{2} r\Delta_\zeta^2\right)^{1/4} M_{\rm Pl} < 7\times 10^{-3} M_{\rm Pl} \ , \qquad (2.93)$$

i.e. the final stages of inflation occurred at sub-Planckian energy densities (if Nature chose canonical slow-roll inflation).

CHAPTER 3

Model-independent approaches

Whenever a new well-motivated model of inflation is found, its dynamics must be tested against observations, as discussed in §2.4.4. While this is the standard approach in *testing* inflation, not much information (if any) about the inflationary period is gained. For instance, on the one side, it may be argued that canonical chaotic inflation is in tension with the data and that this particular class of models could be ruled-out in the near future (see Fig. 2.5). On the other side, it would be a strong claim to say that inflation is noncanonical.

Furthermore, from the observational side, the consistency relation of canonical inflation, Eq. (2.90), may be more challenging to test than expected. With the final results of the *Planck* satellite already released [82], a new generation of experiments is required for an improvement on the measurement (or, in the absence of a signal, on the upper limit) on the amplitude of primordial gravitational waves through the tensor-to-scalar ratio r. Moreover, the subsequent measurement of its scale dependence, n_t, entails an additional experimental challenge.

With all these considerations, it is desirable to look for more robust ways to formulate inflation by capturing its generic features without committing to a specific model. Such features may be simply given by the conditions for inflation, Eqs. (2.10), and the required amount of inflation to solve the inflationary problems, Eq. (2.31), consistent with CMB and LSS data. Indeed, a model independent approach, developed by V. Mukhanov [172], relies on these conditions by parametrizing the equation of state w during inflation.

3.1 Mukhanov parametrization

As discussed in §2.1.1, the equation of state during inflation is given by (see Eq. (2.6))

$$\omega \equiv \frac{p}{\rho} = -1 + \frac{2}{3}\epsilon_H \ , \tag{3.1}$$

i.e. well before the end of inflation, $\epsilon_H \to 0$, the Universe is driven by a fluid with negative pressure, $p = -\rho$. On the other hand, ω approaches to $-1/3$ when $\epsilon_H \to 1$.

This behavior can be instead parametrized in terms of the number of (remaining) *e*folds of inflation $\mathcal{N}$.[1] One can thus propose the ansatz [1,172, 173]

$$\omega = -1 + \frac{\beta}{(\mathcal{N}+1)^\alpha} \ , \tag{3.2}$$

which reproduces the same aforementioned behavior for the positive and order-unity parameters α and β. However, more interesting is the fact that we can further parametrize the scalar tilt n_s and the tensor-to-scalar ratio r with the same parameters. Indeed, recall that $n_s - 1 = -4\epsilon_H - 2\delta_1 = -2\epsilon_H - \mathrm{d}\ln\epsilon_H/\mathrm{d}N$ to first order in slow-roll parameters, and in single-field canonical inflation (see §2.4.4). Then, substituting Eq. (3.1), the scalar tilt can be written as

$$\begin{aligned} n_s - 1 &= -3(\omega+1) - \frac{\mathrm{d}}{\mathrm{d}N}\left[\ln(\omega+1)\right] \\ &= -\frac{3\beta}{(\mathcal{N}+1)^\alpha} - \frac{\alpha}{\mathcal{N}+1} \ , \end{aligned} \tag{3.3}$$

where the ansatz (3.2) was applied in the second line. In the same manner, the canonical-inflation consistency relation, Eq. (2.90), written as $r = 16\epsilon_H$ to first order in slow-roll parameters, can be parametrized as

$$r = \frac{24\beta}{(\mathcal{N}+1)^\alpha} \ . \tag{3.4}$$

Notice then that Eqs. (3.3) and (3.4) provide generic, model-independent predictions for canonical single-field inflation. For instance, notice that for $\alpha > 1$, the second term in Eq. (3.3) dominates and n_s approximates to $n_s - 1 \approx -\alpha/\mathcal{N}_*$ at CMB scales. Then, taking the central value of n_s in Eq. (2.86) and $\mathcal{N}_* \sim 55$, it follows that $\alpha \lesssim 2$. This in turn places a lower bound on r:

$$r \gtrsim \left(6 \times 10^{-3}\right)\beta \ , \tag{3.5}$$

[1] *i.e.* $\mathcal{N}$ approaches to 0 as $\epsilon_H \to 1$.

where, again, $\beta = \mathcal{O}(1)$. Consequently, we were allowed to predict a lower bound on the tensor-to-scalar ratio—assuming that inflation is driven by a canonical single field and for a given measured value of n_s—just by following the conditions for inflation provided the ansatz (3.2). Notice that the bound in Eq. (3.5) is one order of magnitude smaller than the current observational upper bound (2.91) and thus it could be reached with future CMB experiments [174].

In addition, the behavior of the majority of single-field scenarios can be recovered for specific values of α and β as discussed in Ref. [172]. To mention a few examples, chaotic inflation corresponds to $\alpha = 1$ for which the observables read $n_s - 1 = -(3\beta + 1)/(\mathcal{N} + 1)$ and $r = 24\beta/(\mathcal{N} + 1)$; for $\alpha = 2$ and $\beta = 1/2$, $n_s - 1 \approx -2/\mathcal{N}$ and $r \approx 12/\mathcal{N}^2$, which corresponds to the Starobisnky model, Eq. (2.41). For further examples and details, see Ref. [172].

Finally, let us mention that this hydrodynamical approach can be easily extended to k-inflation (see §2.3) where another two phenomenological parameters are required in order to parametrize the nontrivial sound speed of primordial perturbations as

$$c_s = \frac{\gamma}{(\mathcal{N}+1)^{\delta}} \ . \tag{3.6}$$

Here, $\delta \geq 0$ but γ is an arbitrary positive number *i.e.* the sound speed grows towards the end of inflation. With this addition, the scalar tilt and the tensor-to-scalar ratio change to

$$n_s - 1 = -\frac{3\beta}{(\mathcal{N}+1)^{\alpha}} - \frac{\alpha+\delta}{\mathcal{N}+1} \ , \qquad r = \frac{24\beta\gamma}{(\mathcal{N}+1)^{\alpha+\delta}} \ . \tag{3.7}$$

Notice then that the lower bound (3.5) can be further suppressed. On the other hand, it is well known that a too small sound speed induces large non-Gaussianities, for which c_s cannot be much lower than 0.1 [6, 172]. In this case, the lower bound on r would be further pushed one order of magnitude at maximum.

CHAPTER 4

Inflation beyond General Relativity

We have seen that the simplest scenarios of inflation, *i.e.* monomial potentials, are in tension with current CMB observations (see §2.4.4). In this regard, the straightforward model-building approach is to consider more complicated potential functions $V(\phi)$ for the inflaton field ϕ which fit observations. Currently, our corresponding approach relies on finding inflationary models that come from well-motivated high-energy theories of particle physics. However, one drawback of considering these models is the lack of simpler (and perhaps more natural) predictions of such a high-energy theory or, even worst, their failure on experimental confirmation.[1]

Canonical inflation, being driven by a (new) quantum field, is also a theory of gravity based on General Relativity. Einstein's theory of GR is perhaps one of the most successful theories in physics. It has passed the most stringent solar-system tests and predicted several observations over the course of the last century, being one of its most amazing confirmations just achieved in 2015 with the measurement of the gravitational waves produced by a two black-hole merger [157–166].

Yet, there are huge hints on the incompleteness of GR, the most intriguing one being posed by the dark energy (DE) issue. As discussed in §1, there is no natural explanation for the DE, although several proposals have been studied. In a similar way that for inflation, a new scalar field

[1] Take for instance supersymmetry (SUSY), a very elegant solution to many problems in the Standard Model. It was developed in the 1970's and it is actively searched for mainly in accelerators. Hints of a minimal supersymmetric theory were already expected at the current working energies of the Large Hadron Collider (LHC) (see, *e.g.*, Ref. [175]); yet, many inflationary models based on SUSY are still being considered.

could be able to drive the current expansion, however, due to the low energy scale of the current acceleration, new difficulties arise when one tries to construct consistent particle physics models for this new field [13]. A second approach relies on modifying GR at large scales such that these modifications are able to explain the accelerated expansion without modifying the local dynamics, where GR has been tested to be highly accurate. In fact, this approach is one of the most active research lines in Cosmology and has provided numerous kinds of modifications of GR to explain the nature of the DE.[2]

The same modifications of GR proposed to explain the DE, if realized during the early universe, are able to produce different predictions for the same inflationary potentials $V(\phi)$ previously studied. Indeed, there exist simple modifications of GR which lead to a better agreement of the monomial potentials, previously ruled-out, with the current CMB observations. This is in fact one common approach: instead of proposing complicated potential functions $V(\phi)$, we could keep the simplest realizations and just find well-motivated modifications of GR which predict observables satisfying current constraints. While this well-motivated modifications were originally kept simple too—as in the noncanonical models of inflation reviewed in §2.3—in the recent years several classes and, as we shall see, frameworks of generalizations of GR have been worked out. Their study started with a simple question: *what is the most general modification of GR, respecting its symmetries and principles, and which propagates only physical degrees of freedom?*

Indeed, the construction of such frameworks became itself a research line in the fields of gravitation and also of cosmology, where new terms and interactions between the inflaton and the gravity sector have been considered. In this chapter, we shall review the most popular frameworks of general modifications of GR involving new fields (scalars and vectors) coupled to the gravity sector. Indeed, by keeping its symmetries and constraints—namely Lorentz invariance, unitarity, locality and a (pseudo-)Riemannian spacetime—any modification of GR will inevitably introduce new degrees of freedom which could either be in the form of new scalar, vector or tensor fields [176].[3]

We shall follow a bottom-up approach: we start by reviewing the motivations for the construction of the aforementioned frameworks and the considerations one should take. Then, first, we shall review the scalar-tensor interactions which lead to the so-called *Horndeski theory*; second, we

[2]The interested reader is referred to Ref. [13] for a pedagogical review of the different approaches to DE.

[3]In other words, GR is the only Lorentz-invariant theory of gravity for a massless spin-2 particle.

move into the discussion of vector-tensor interactions which, in turn, lead to the *generalized Proca theories*; third, we shall discuss the more general framework which aims to join the first two into the most general class of scalar-vector-tensor (SVT) interactions. In a second part, we shall review some of the most popular models of cosmological inflation that are developed within these general frameworks.[4]

4.1 Towards the most general SVT framework

General Relativity describes a theory of a massless spin-2 particle which propagates only two degrees of freedom as a result of constraints coming from the invariance under differentiable coordinate transformations—*diffeomorphism invariance*. As already stated, any modification of GR will introduce new degrees of freedom in the form of scalar, vector or tensor fields. Take for instance the addition of a mass term for a gravitational field $h_{\mu\nu}$: Lorentz invariance restricts the metric combinations allowed for the mass term to be proportional to[5]

$$m^2 \left(h_{\mu\nu}^2 - h^2 \right) \ , \tag{4.1}$$

where $h_{\mu\nu}$ is a symmetric tensor field. The presence of this mass term makes the theory no longer diffeomorphism invariant and thus more degrees of freedom, apart of the two tensor polarizations, must propagate. This symmetry, however, can be restored by means of the *Stueckelberg trick*, a field redefinition $h_{\mu\nu} \to h_{\mu\nu} + 2\chi_{(\mu,\nu)}$ which introduces additional Stueckelberg fields χ^α, and which transforms the mass term into[6]

$$m^2 \left[\left(h_{\mu\nu} + 2\chi_{(\mu,\nu)} \right)^2 - \left(h + 2\chi^\alpha{}_{,\alpha} \right)^2 \right] \ . \tag{4.2}$$

Furthermore, the Stueckelberg field can be split into its transverse and longitudinal parts $\chi^\alpha \to A^\alpha + \partial^\alpha \pi$ in order to make the degrees of freedom explicitly shown. In this way, the mass term becomes

$$m^2 \left(h_{\mu\nu}^2 - h^2 \right) - m^2 F_{\mu\nu}^2 - 2m^2 \left(h_{\mu\nu} A^{\mu,\nu} - h \partial_\mu A^\mu \right) - 2m^2 \left(h_{\mu\nu} \pi^{,\mu\nu} - h \partial_\mu \partial^\mu \pi \right) \ , \tag{4.3}$$

[4] We would like to emphasize that these are mathematical frameworks rather than physical theories (as the name may suggests), *i.e.* they only provide us with a full set of modifications of GR allowed by physical symmetries and other constraints, and not with a fixed set of fundamental laws of gravity.

[5] Only scalar combinations of the metric are allowed. In this regard, $h_{\mu\nu}^2 = h_{\mu\nu} h^{\mu\nu}$ and $h^2 = h^\mu_\mu h^\nu_\nu$.

[6] $\chi_{(\mu,\nu)} \equiv \left(\partial_\mu \chi_\nu + \partial_\nu \chi_\mu \right) / 2$.

i.e. the Stueckelberg trick produced the kinetic terms proportional to $h_{\mu\nu}\pi^{,\mu\nu}$ and $F^2_{\mu\nu} = (A_{\mu,\nu} - A_{\nu,\mu})^2$ for the scalar field π and the vector field A_μ, respectively.[7] Therefore, a fully consistent theory of *massive gravity*—where diffeomorphism invariance is broken—propagates five degrees of freedom (compared to the two of GR): two tensor (helicity-2) modes from $h_{\mu\nu}$, two vector (helicity-1) modes from A_μ [8] and the scalar (helicity-0) mode π, the last two coming from the Stueckelberg field χ^α.

Also interesting, apart from the kinetic terms for the Stueckelberg fields, the mass term further produces interaction terms of the form

$$m^2 \left(h_{\mu\nu}\pi^{,\mu\nu} - h\partial_\mu\partial^\mu\pi\right) \ , \qquad m^2 \left(h_{\mu\nu}A^{\nu,\mu} - h\partial_\mu A^\mu\right) \ , \tag{4.4}$$

i.e. mixing terms between different helicity modes. Phenomenologically, it has been shown that the helicity-0 mode present in a consistent theory of massive gravity provides a self-accelerating solution and thus it could potentially explain DE [178]; therefore, one would expect interesting cosmological implications from several different mixing combinations coming from more general modifications of GR.

These mixings can be classified as scalar-tensor, vector-tensor or scalar-vector interactions. In this sense, one could follow the theory-independent approach of constructing all the different possible combinations allowed by Lorentz invariance and further restrictions as locality and unitarity, and write down all the possible combinations between scalar and tensor modes, vector and tensor modes, and scalar and vector modes coupled to gravity. In doing so, one would notice that combinations of arbitrarily high-order derivatives are allowed; however, it is well known that a nondegenerate Lagrangian, with temporal derivatives higher than order one, yields equations of motion (EoM) higher than order two. This fact incorporates new pathologies: in the Hamiltonian picture, a Lagrangian of this kind yields a Hamiltonian which is unbounded from below and thus the energy of the system in consideration can take either positive or negative values, *i.e.* it can excite either positive or negative degrees of freedom. A negative degree of freedom of this type is known as *Ostrogradsky instability* or, colloquially, *Ostrogradsky's ghost*.[9] We can therefore state *Ostrogradsky's theorem* as: *'Higher-derivative theories contain extra degrees of freedom, and are usually plagued by negative energies and related instabilities'*. Consequently, and in order to maintain a pathologically-free theory of gravity, any modification of GR, involving higher derivatives, must still yield second-order

[7] This happens after performing a canonical normalization $A_\mu \to A_\mu/m$ and $\pi \to \pi/m^2$. See [176, 177] for details.

[8] The other two degrees of freedom from A_μ are removed by means of the gauge invariance.

[9] See Footnote 2 in Ref. [179] for a discussion on the terminology of the instability and the associated theorem.

EoM.[10] We shall see that this is achieved by imposing constraints which allow us to remove the *ghostly* terms from the EoM.

4.1.1 Scalar-tensor interactions

The simplest terms allowed in a scalar-tensor theory are given in the Lagrangian for a scalar field minimally coupled to GR (shown in Eq. (2.11)), namely those of a canonical kinetic energy, $X \equiv -\frac{1}{2}g^{\mu\nu}\phi_{,\mu}\phi_{,\nu}$, and a potential energy, $V(\phi)$—this term being already a generalization of the even simpler $m^2\phi^2$ mass term. This theory is of first order in derivatives and thus it propagates only real (positive-energy) fields.

In order to construct more general terms, the first natural step relies in combining the canonical kinetic and potential terms into a general function of the field, $f(X,\phi)$. Theories of this type, known as *k-essence*, have been widely considered in the context of both DE and inflation (named as *k-inflation* in the latter context). In particular, terms such as $f(\phi)X+G(\phi)X^2$ or $G(\phi)\sqrt{1-f(\phi)X}$ show up naturally in models inspired from string theory and supersymmetry realizations (see Ref. [13] and references therein for details). Indeed, several new interactions have been discovered in the context of higher-dimensional theories. Another example comes from the Dvali-Gabadadze-Porrati (DGP) model of brane cosmology where in a 3+1 spacetime, embedded in a 4+1 dimensional Minkowski space, the graviton helicity-0 mode appears with a self-interaction term, $\Box\phi\,(\partial\phi)^2$ [11], able to drive an accelerated expansion [180]. Notice that this term contains two derivatives acting on the scalar field ϕ, however, its EoM, $\Box\phi^2-(\phi_{,\mu\nu})^2=0$, are still second-order and thus the model avoids the Ostrogradsky instability. Following this spirit, one could carefully construct higher-order derivative terms which, by means of some particular constraints which remove the higher-order terms, yield second-order equations of motion. This task led to the development of the Galileon theories—a general scalar-tensor theory in flat spacetime, with second-order EoM, which is invariant under the Galilean transformations $\phi \to \phi + x_\mu b^\mu + c$ [110]. The generalization to

[10] This condition is in fact respected in Nature, as no higher order EoM describe physical phenomena—for instance, Newton's, Maxwell's and, again, Einstein's equations are all of them of second-order.

[11] We define the d'Alambertian operator in the standard way: $\Box\phi \equiv \nabla^\mu\nabla_\mu\phi := \phi^{;\mu}_{;\mu}$. Notice however that the interaction present in the DGP model comes from a theory in flat spacetime and, moreover, a covariant derivative acting on a scalar quantity is just a partial differentiation, *i.e.* we are still writing partial derivatives.

a nonflat spacetime was named *covariant Galileons* [112], now known as *Horndeski theory* [109].[12]

4.1.1.1 Horndeski theory

It is possible to construct a theory order by order in derivatives following the generalization procedure mentioned above. We can write the Lagrangians $\mathcal{L}_2 = G_2(\phi, X)$ and $\mathcal{L}_3 = G_3(\phi, X)\Box\phi$ where the subscript makes reference to the number of times the field ϕ appears. The fourth Lagrangian allows two types of interactions: $\alpha_1 G_4(\phi, X)\left(\Box\phi\right)^2$ and $\alpha_2 G_4(\phi, X)\left(\phi_{,\mu\nu}\right)^2$; however, by inspection of the EoM, one notices that in order to maintain only second-order terms, the constraint $\alpha_1 = -\alpha_2$ must be satisfied—this then fixes the form of $\mathcal{L}_4$. Following this procedure, one finds that as long as we restrict ourselves to second-order EoM in four dimensions, only four Lagrangians can be written down, *i.e.* up to $\mathcal{L}_5$. Next, we shall promote the partial derivatives to covariant derivatives and thus *covariantize* the theory. In doing so, the number of derivatives increases and therefore the order of the EoM changes accordingly. The correct order is recovered by introducing nonminimal couplings to gravity into the Lagrangians at the desired order (see [176] for details).

The application of the previous algorithm leads to the full Lagrangian of the Horndeski theory which is then given by four Lagrangians, $\mathcal{L}_{\mathcal{H}} = \sum_{i=2}^{5}\mathcal{L}_i$, each of them proportional to an arbitrary function $G_i(\phi, X)$:

$$\begin{aligned}\mathcal{L}_{\mathcal{H}} = {} & G_2 \\ & + G_3\Box\phi \\ & + G_4 R + G_{4,X}[(\Box\phi)^2 - \phi^{;\mu\nu}\phi_{;\mu\nu}] \\ & + G_5 G^{\mu\nu}\phi_{;\mu\nu} - \frac{G_{5,X}}{6}[(\Box\phi)^3 - 3(\Box\phi)\phi_{;\mu\nu}\phi^{;\mu\nu} + 2\phi_{;\mu\nu}\phi^{;\mu\sigma}\phi^{;\nu}{}_{;\sigma}]\ ,\end{aligned} \tag{4.5}$$

where $G_{i,X} \equiv \partial G_i/\partial X$, R is the scalar curvature and $G_{\mu\nu} = R_{\mu\nu} - \frac{1}{2}g_{\mu\nu}R$ the Einstein tensor. Notice that the canonical Lagrangian, Eq. (2.11), is recovered for the choice $G_2 = X - V(\phi)$, $G_4 = 1/2$, and $G_3 = G_5 = 0$. Equation (4.5) represents therefore the most general theory of gravity involving scalar and tensor fields which yields second-order EoM and is free of Ostrogradsky ghosts.

Horndeski gravity is not however the most general theory of gravity free from instabilities. It is now known that having second-order EoM as a condition for the avoidance of Ostrogradsky instabilities is actually not necessary as long as there exists an additional constraint equation which

[12] In 1974, Gregory Horndeski precisely studied the most general four-dimensional scalar-tensor theory of gravity which yield second-order EoM. His work was rather unnoticed until its rediscovery as the covariant Galileons.

helps to remove the higher-order terms. This inspired the construction of the *Degenerate Higher-Order Scalar-Tensor* (DHOST) theories of gravity which are now the most general theories of gravity, at cubic order in second-order derivatives, with additional primary constraints ensuring the propagation of only three physical degrees of freedom [114, 118, 119, 181]. In the rest of this thesis, we shall however restrict ourselves to the phenomenology of the Horndeski theory for simplicity.

4.1.2 Vector-tensor interactions

We are now in the pursuit of the most general theory of a spin-1 field A_μ, coupled to gravity, yielding second-order EoM, *i.e.* propagating only real vector and tensor modes. As we shall see, the total number or physical degrees of freedom will depend on whether we restrict ourselves to maintain the *gauge* symmetry or not—equivalently, whether we allow the field to be massive. Both theories provide new interesting phenomenology and thus one has the freedom to choose either one. Nevertheless, each case is constructed in the same spirit as the covariant Galileons were obtained: we need to write down all possible combinations order by order by respecting the second-order EoM condition, then covariantize the theory by promoting the partial derivatives to covariant ones and reduce to the correct order by introducing nonminimal couplings to the gravity sector.

4.1.2.1 Maxwell theory

For a massless U(1) field A_μ, the allowed interactions linear in derivatives have the form $\alpha_1 \partial_\mu A_\nu \partial^\mu A^v + \alpha_2 \partial_\mu A_\nu \partial^\nu A^\mu$. The number of propagating degrees of freedom is fixed by the existence of a primary constraint that imposes $\alpha_1 = -\alpha_2$ which makes the temporal mode A_0 nondynamical. Furthermore, $\alpha_1 < 0$ must be satisfied in order to ensure that the Hamiltonian is bounded from below (see [176] for details). These conditions generate a gauge symmetry which further removes the longitudinal mode. Consequently, we obtain a Lorentz invariant theory of a massless spin-1 field invariant under gauge transformations, $A_\mu \to A_\mu + \partial_\mu \theta$ (where θ is a real arbitrary constant) which guarantees that only two vector degrees of freedom propagate. This theory is nothing but the Maxwell's theory of electromagnetism (in absence of external currents)

$$\mathcal{L}^{\text{Maxwell}}_{A_\mu} = -\frac{1}{4} F^2_{\mu\nu} \,, \qquad F_{\mu\nu} \equiv \partial_\mu A_\nu - \partial_\nu A_\mu \,, \tag{4.6}$$

after canonically normalizing the vector field by setting $\alpha_1 = -1/2$. Similar to the Galileons case, one might look for higher-order self-interactions; however, a no-go theorem states that it is the Maxwell kinetic term the only

possible combination yielding second-order EoM for an Abelian vector field as long as we restrict ourselves to keep the gauge symmetry [182–185].

By promoting the partial derivatives to covariant ones, nonminimal couplings are required as in the scalar-tensor case. Additionally, in order to preserve gauge invariance, only couplings of the field strength $F_{\mu\nu}$, and not direct couplings of the vector field, must be considered. In this case, it can be shown that $F_{\mu\nu}$ can only couple to the double dual Riemann tensor $L^{\mu\nu\alpha\beta} = \frac{1}{4}\mathcal{E}^{\mu\nu\rho\sigma}\mathcal{E}^{\alpha\beta\gamma\delta}R_{\rho\sigma\gamma\delta}$, where $\mathcal{E}^{\mu\nu\alpha\beta}$ is the antisymmetric Levi-Civita tensor satisfying the normalization $\mathcal{E}^{\mu\nu\alpha\beta}\mathcal{E}_{\mu\nu\alpha\beta} = -4!$. Consequently, the most general Lagrangian for a massless vector field on curved spacetime yielding second-order EoM is given by [186–188]

$$\mathcal{L}_{\text{Maxwell}} = \frac{1}{2}R - \frac{1}{4}F_{\mu\nu}^2 + \frac{1}{4M}L^{\alpha\beta\gamma\delta}F_{\alpha\beta}F_{\gamma\delta} \ , \tag{4.7}$$

where M is the relevant mass scale.

4.1.2.2 Proca theory

The Proca theory describes a massive U(1) vector field. The mass term proportional to $A^\mu A_\mu$ breaks the gauge symmetry and therefore one degree of freedom more is allowed to propagate—three in total. Nevertheless, as in the massive gravity case, the gauge symmetry can be restored using the Stueckelberg trick by means of the change of variables $A_\mu \to A_\mu + \partial\phi$, where ϕ is a scalar Stueckelberg field. Under this change, the Proca theory becomes

$$\mathcal{L}_{A_\mu}^{\text{Proca}} = -\frac{1}{4}F_{\mu\nu}^2 - \frac{1}{2}m_A A_\mu^2 - \frac{1}{2}\left(\partial\phi\right)^2 - m_A A_\mu \partial^\mu\phi \ , \tag{4.8}$$

where we have canonically normalized the scalar field as $\phi \to \phi/m_A$. Now, Eq. (4.8) in invariant under simultaneous gauge, $A_\mu \to A_\mu + \partial_\mu\phi$, and shift, $\phi \to \phi - \theta$, symmetries and, more interestingly, the Stueckelberg trick produced an interaction term between the vector field and the scalar Stueckelberg field, where the latter comes with a kinetic term. Therefore, associating ϕ to the longitudinal vector mode, the third degree of freedom is explicitly shown—indeed, the change of variables $A_\mu \to A_\mu + \partial\phi$ can be seen as a helicity decomposition of the vector field.

Unlike the massless case, the Proca theory allows for more general interactions made by higher-order derivatives and thus avoiding the aforementioned no-go theorem. Then, to construct Galileon vector theories, called *generalized Proca* in the Literature, we keep the second-order EoM restriction and add a second restriction: the temporal mode A_0 most remain nondynamical, otherwise it would unavoidably be a ghost mode. The algorithm is similar to the one previously discussed for scalar Galileons and

therefore we shall focus on the covariantized version (see [176, 189–191] for details). By replacing partial derivatives with covariant ones and introducing the corresponding nonminimal couplings, the generalized Proca theories in curved space become:

$$\begin{aligned}\mathcal{L}_{\rm Proca} &= G_2(X,F,Y)\\ &\quad + G_3(X)A^{\mu}{}_{;\mu}\\ &\quad + G_4(X)R + G_{4,X}(X)\left[(A^{\mu}{}_{;\mu})^2 - A_{\rho;\sigma}A^{\sigma;\rho}\right]\\ &\quad + G_5(X)G_{\mu\nu}A^{\mu;\nu} - \frac{1}{6}G_{5,X}(X)\Big[(A^{\mu}{}_{;\mu})^3 - 3A^{\mu}{}_{;\mu}A_{\rho;\sigma}A^{\sigma;\rho}\\ &\qquad + 2A_{\rho;\sigma}A^{\sigma;\gamma}A_{\gamma}{}^{;\rho}\Big] - \tilde{G}_5(X)\tilde{F}^{\alpha\mu}\tilde{F}^{\beta}{}_{\mu}A_{\beta;\alpha}\\ &\quad + G_6(X)L^{\mu\nu\alpha\beta}A_{\nu;\mu}A_{\beta;\alpha} + \frac{1}{2}G_{6,X}(X)\tilde{F}^{\alpha\beta}\tilde{F}^{\mu\nu}A_{\mu;\alpha}A_{\nu;\beta}\ ,\end{aligned} \tag{4.9}$$

where $\tilde{F}^{\mu\nu} = \mathcal{E}^{\mu\nu\alpha\beta}F_{\alpha\beta}/2$ is the dual of the strength tensor, and we explicitly showed the dependence of the G_i functions in terms of the quantities

$$X = -\frac{1}{2}A_\mu A^\mu\ , \qquad F = -\frac{1}{4}F_{\mu\nu}F^{\mu\nu}\ , \qquad Y = A^\mu A^\nu F_\mu{}^\alpha F_{\nu\alpha}\ . \tag{4.10}$$

Consequently, Eq. (4.9) is the most general theory of gravity with a vector field A_μ yielding second-order EoM, *i.e.* propagating only real fields—two tensor modes, two transverse vector modes and the longitudinal mode. These theories have brought important new phenomenology in the study of DE [192–196] and compact objects as black holes and neutron stars [197–204].

Beyond Generalized Proca theories have been constructed in the same spirit as beyond Horndeski theories. We shall not discuss them in this thesis but the interested reader is referred to Refs. [176, 205].

4.1.3 Scalar-vector-tensor interactions

Recall that the Stueckelberg trick performed to the Proca theory, Eq. (4.8), produced a kinetic term for the scalar field ϕ and a genuine new interaction between ϕ and A_μ. Nothing has been said about this scalar field, however it can lead to interesting dynamics while being coupled to the Proca vector field in a gravitational background. Bearing this in mind, it is interesting to consider different kind of combinations between these two helicity modes and to construct a general theory of gravity with both scalar and tensor fields. As in the case of the Proca theories, one can construct interactions depending on whether the gauge symmetry is kept or not. As we shall see, both theories contain new interesting phenomenology that can be applied to different physical scenarios.

4.1.3.1 Gauge-invariant theory

On the one hand, it is possible to allow independent self-interactions of the scalar field via derivative terms—such as the third term in Eq. (4.8)—which, restricting to second-order EoM, lead to shift-symmetric Horndeski interactions $\mathcal{L}_{\mathcal{H}}^{\text{shift}}$. On the other hand, it is also possible to construct order by order interactions between the vectorial combinations in Eqs. (4.10) and the $\nabla\phi$ term and its derivatives. By restricting to gauge-invariant combinations and explicitly breaking the shift symmetry to allow more general ones, one obtains the most general gauge-invariant scalar-vector-tensor theory yielding second-order EoM [206]:

$$\begin{aligned}\mathcal{L} = \mathcal{L}_{\mathcal{H}} \\ + f_2(F, \tilde{F}, Y) \\ + \mathcal{M}_3^{\mu\nu}\phi_{;\mu\nu} \\ + \mathcal{M}_4^{\mu\nu\alpha\beta}\phi_{;\mu\alpha}\phi_{;\nu\beta} + f_4(\phi, X)L^{\mu\nu\alpha\beta}F_{\mu\nu}F_{\alpha\beta}\ ,\end{aligned} \tag{4.11}$$

where $\mathcal{L}_{\mathcal{H}}$ is given in Eq. (4.5) and here $Y = \nabla_\mu\phi\nabla_\nu\phi F^{\mu\alpha}F^{\nu}{}_{\alpha}$. We also defined the rank-2 and rank-4 tensors, $\mathcal{M}_3^{\mu\nu}$ and $\mathcal{M}_4^{\mu\nu\alpha\beta}$, respectively, as

$$\mathcal{M}_3^{\mu\nu} = \left[f_3(\phi, X)g_{\rho\sigma} + \tilde{f}_3(\phi, X)\phi_\rho\phi_\sigma\right]\tilde{F}^{\mu\rho}\tilde{F}^{\nu\sigma}\ , \tag{4.12}$$

$$\mathcal{M}_4^{\mu\nu\alpha\beta} = \left[\frac{1}{2}f_{4,X}(\phi, X) + \tilde{f}_4(\phi)\right]\tilde{F}^{\mu\nu}\tilde{F}^{\alpha\beta}\ , \tag{4.13}$$

where we note that the function $\tilde{f}_4$ depends on ϕ alone. Notice that in the limit of constant ϕ and f_4 one recovers the Maxwell theory in Eq. (4.7).

4.1.3.2 Broken gauge-invariant theory

Abandoning the gauge invariance, the vector field cannot only enter via the terms in Eqs. (4.10) but also via $S_{\mu\nu} = \nabla_\mu A_\nu + \nabla_\nu A_\mu$. In this regard, we can introduce an effective metric tensor constructed from possible combinations of $g_{\mu\nu}$, A_μ, and $\nabla_\mu\phi$, given as [206]

$$\mathcal{G}_{\mu\nu}^{h_n} = h_{n1}(\phi, X_i)g_{\mu\nu} + h_{n2}(\phi, X_i)\phi_{;\mu}\phi_{;\nu} + h_{n3}(\phi, X_i)A_\mu A_\nu + h_{n4}(\phi, X_i)A_\mu\phi_{;\nu}$$

where the X_i are defined below. Then, following the same procedure as before, the most general broken gauge-invariant scalar-vector-tensor theories yielding second-order EoM are written as

$$\begin{aligned}\mathcal{L}_{\text{SVT}} = f_2(\phi, X_1, X_2, X_3, F, \tilde{F}, Y_1, Y_2, Y_3) \\ + f_3(\phi, X_3)g^{\mu\nu}S_{\mu\nu} + \tilde{f}_3(\phi, X_3)A^\mu A^\nu S_{\mu\nu} \\ + f_4(\phi, X_3)R + f_{4,X_3}(\phi, X_3)\left[(A^\mu{}_{;\mu})^2 - A_{\mu;\nu}A^{\mu;\mu}\right]\end{aligned} \tag{4.14}$$

$$
\begin{aligned}
&+ f_5(\phi, X_3) G^{\mu\nu} A_{\mu;\nu} - \frac{1}{6} f_{5,X_3}(\phi, X_3) \Big[(A^{\mu}{}_{;\mu})^3 - 3 A^{\mu}{}_{;\mu} A_{\rho;\sigma} A^{\sigma;\rho} \\
&\quad + 2 A_{\rho;\sigma} A^{\sigma;\gamma} A_{\gamma}{}^{;\rho} \Big] + \mathcal{M}_5^{\mu\nu} \phi_{;\mu\nu} + \mathcal{N}_5^{\mu\nu} S_{\mu\nu} \\
&+ f_6(\phi, X_1) L^{\mu\nu\alpha\beta} F_{\mu\nu} F_{\alpha\beta} + \mathcal{M}_6^{\mu\nu\alpha\beta} \phi_{\mu\alpha} \phi_{\nu\beta} + \tilde{f}_6(\phi, X_3) L^{\mu\nu\alpha\beta} F_{\mu\nu} F_{\alpha\beta} \\
&\quad + \mathcal{N}_6^{\mu\nu\alpha\beta} S_{\mu\alpha} S_{\nu\beta} \ ,
\end{aligned}
$$

where we now use the notation

$$
X_1 = -\frac{1}{2} \phi_{;\mu} \phi^{;\mu} \ , \qquad X_2 = -\frac{1}{2} A^{\mu} \phi_{;\mu} \ , \qquad X_3 = -\frac{1}{2} A_{\mu} A^{\mu} \ , \tag{4.15}
$$

and

$$
Y_1 = \phi_{;\mu} \phi_{;\nu} F^{\mu\alpha} F^{\nu}{}_{\alpha} \ , \qquad Y_2 = \phi_{;\mu} A_{\nu} F^{\mu\alpha} F^{\nu}{}_{\alpha} \ , \qquad Y_3 = A_{\mu} A_{\nu} F^{\mu\alpha} F^{\nu}{}_{\alpha} \ , \tag{4.16}
$$

the latter of which corresponds to the interactions arising from pure vector modes. Furthermore, the rank-2 tensors $\mathcal{M}_5^{\mu\nu}$ and $\mathcal{N}_5^{\mu\nu}$, which encode intrinsic vector interactions, are given by

$$
\mathcal{M}_5^{\mu\nu} = \mathcal{G}^{h_5}_{\rho\sigma} \tilde{F}^{\mu\rho} \tilde{F}^{\nu\sigma} \ , \qquad \mathcal{N}_5^{\mu\nu} = \mathcal{G}^{\tilde{h}_5}_{\rho\sigma} \tilde{F}^{\mu\rho} \tilde{F}^{\nu\sigma} \ , \tag{4.17}
$$

where the functions h_{5j} and $\tilde{h}_{5j}$ ($j = 1, 2, 3, 4$) appearing in $\mathcal{G}^{h_5}_{\rho\sigma}$ and $\mathcal{G}^{\tilde{h}_5}_{\rho\sigma}$ are functions of ϕ and X_1, X_2, X_3. On the other hand, the rank-4 tensors $\mathcal{M}_6^{\mu\nu\alpha\beta}$ and $\mathcal{N}_6^{\mu\nu\alpha\beta}$ are defined as

$$
\mathcal{M}_6^{\mu\nu\alpha\beta} = 2 f_{6,X_1}(\phi, X_1) \tilde{F}^{\mu\nu} \tilde{F}^{\alpha\beta} \ , \qquad \mathcal{N}_6^{\mu\nu\alpha\beta} = \frac{1}{2} \tilde{f}_{6,X_3}(\phi, X_3) \tilde{F}^{\mu\nu} \tilde{F}^{\alpha\beta} \ . \tag{4.18}
$$

Notice that the functions $f_3, \tilde{f}_3, f_4, f_5, \tilde{f}_6$ depend on ϕ and X_3, whereas f_6 has dependence on ϕ and X_1. Furthermore, the Generalized Proca theories, Eq. (4.9), are recovered by using the correspondence

$$
\begin{aligned}
&\phi \to 0 \ , \qquad X_{1,2} \to 0 \ , \qquad X_3 \to X \ , \qquad Y_{1,2} \to 0 \ , \qquad Y_3 \to Y \ , \\
&f_2 \to G_2(X, F, Y) \ , \qquad 2 f_3 \to G_3(X) \ , \qquad \tilde{f}_3 \to 0 \ , \qquad f_4 \to G_4(X) \ , \\
&f_5 \to G_5(X) \ , \qquad h_{5j} \to 0 \ , \qquad \tilde{h}_{51} \to -\frac{1}{2} \tilde{G}_5(X), \qquad \tilde{h}_{52}, \tilde{h}_{53}, \tilde{h}_{54} \to 0 \ , \\
&f_6 \to 0 \ , \qquad 4 \tilde{f}_6 \to G_6(X) \ .
\end{aligned}
$$

Finally, we note that the full scalar-vector-tensor theory with second-order EoM is completed by adding the Horndeski interactions $\mathcal{L}_{\mathcal{H}}$, in Eq. (4.5), to $\mathcal{L}_{\rm SVT}$, Eq. (4.14). Therefore, we end up with a theory with six propagating degrees of freedom: two tensor modes, two vector modes and two scalar modes. This general theory has been developed just recently, but applications for DE [207], black holes [208] and inflation [5] (to be discussed in §4.3.1) have already been performed.

4.2 Inflation in scalar-tensor theories

Our goal here is to apply the Horndeski theory and the SVT theories to the physics of inflation. To that end, one needs to consider a background FLRW spacetime and compute the EoM for the background and for the primordial perturbations, the latter of which will lead us to compute the power spectra of these perturbations and to make predictions from the theory (see §2.4.4).

The background EoM and the quadratic actions of primordial scalar and tensor perturbations for the Horndeski theory, Eq. (4.5), were computed in Ref. [209] and are shown in Appendix §B. Here, we shall focus on the novel phenomenology coming from specific models of inflation already tested, some of which constitute a part of the original results presented in this thesis. We shall firstly discuss the addition of nonminimal couplings between the scalar field and the scalar curvature R to the canonical action, mediated by some coupling ξ which alleviates the tension between the canonical model and the data. Secondly, we shall discuss the class of models named as *G-inflation*, derived from taking into account a nonvanishing function G_3 in Eq. (4.5)—this class of models has been studied due to its ability to reconciling simple inflationary potentials $V(\phi)$ with the data.

4.2.1 Nonminimal coupling to gravity

The Horndeski theory has become a rich framework to construct phenomenological models of both early- and late-time cosmology. The most common modification of the canonical action, Eq. (2.11), comes from accounting for a nonminimal coupling between the scalar field and the gravity sector via the term $f(\phi)R$. From Eq. (4.5), notice that this term can be obtained by setting $G_4(\phi, X) = f(\phi)$. However, nonminimal couplings of this form have been considered long before the Galileon theories were formulated [98–102, 106], and reconsidered when such coupling was found in the framework of supergravity theories [210–215]. In particular, the simple function $f(\phi) = (1 + \xi\phi^2)/2$ has been extensively studied, where ξ is a dimensionless coupling expected to be small in this model in order for ϕ to successfully reheat the Universe. Indeed, *Planck* places the lower bound on this parameter to be $\log_{10}\xi > -1.6$ at 95% CL for the quartic potential ϕ^4 which is highly disfavored in the canonical picture [82].

By introducing the nonminimal coupling, the action of such a theory is given by

$$\mathcal{S}_{\rm NM} = \int \mathrm{d}^4x\sqrt{-g}\left[\frac{1}{2}\left(1+\xi\phi^2\right)R - \frac{1}{2}g^{\mu\nu}\phi_{,\mu}\phi_{,\nu} - U(\phi)\right] , \tag{4.19}$$

where $U(\phi)$ is the potential function in the *Jordan frame*. Indeed, it can be shown that the theory in Eq. (4.19) can be recast as a canonical action (the *Einstein frame*) by means of a *conformal transformation* of the form

$$g^{\rm E}_{\mu\nu} = \Omega(\phi) g_{\mu\nu} \ , \tag{4.20}$$

where, in this case,

$$\Omega(\phi) \equiv 1 + \xi\phi^2 \ . \tag{4.21}$$

Under this transformation, the action (4.19) becomes

$$\mathcal{S}^{\rm E}_{\rm NM} = \int {\rm d}^4x\sqrt{-g_{\rm E}}\left(\frac{1}{2}R_{\rm E} - \frac{1}{2}g^{\mu\nu}_{\rm E}\varphi_{,\mu}\varphi_{,\nu} - V\left[\varphi\left(\phi\right)\right]\right) \ , \tag{4.22}$$

where the index 'E' emphasizes that the action is written in the Einstein frame, *i.e.* in canonical form, with an effective potential function

$$V\left[\varphi(\phi)\right] = \frac{U(\phi)}{\Omega^2(\phi)} \ , \tag{4.23}$$

of the rescaled field

$$\left(\frac{{\rm d}\varphi}{{\rm d}\phi}\right)^2 = \frac{1}{\Omega} + \frac{3}{2}\left(\frac{\Omega_{,\phi}}{\Omega}\right)^2 \ . \tag{4.24}$$

As already stated, for a range of values of ξ, several canonical models of inflation can be reconciled with CMB observations, among which the chaotic model $m^2\phi^2$ and the quartic potential $\lambda\phi^4$ have been exhaustively studied [2, 107, 108, 216–219]. The explanation for this is quite simple, as seen in the Einstein frame: any different value of ξ changes the shape of the effective potential and consequently its inflationary predictions; namely, the ability of ξ to make the potential $V(\varphi)$ flatter will induce a suppression in the tensor-to-scalar ratio r and thus make the potentials $U(\phi)$ more favored with respect to CMB observations (see Fig. 4.1).

4.2.2 G-inflation

Notice from Eq. (4.5) that the simplest nontrivial modification of the canonical action, Eq. (2.11), beyond linear order, comes from the third-order Lagrangian proportional to G_3. With this term, the action becomes

$$\mathcal{S}_G = \int {\rm d}^4x\sqrt{-g}\left[\frac{1}{2}R + G_2(\phi, X) + G_3(\phi, X)\Box\phi\right] \ , \tag{4.25}$$

where we have set $G_4(\phi, X) = 1/2$ in order to account for the Einstein-Hilbert term. This class of models is called 'G-inflation' in the literature, and its cosmological implications have been extensively explored—it

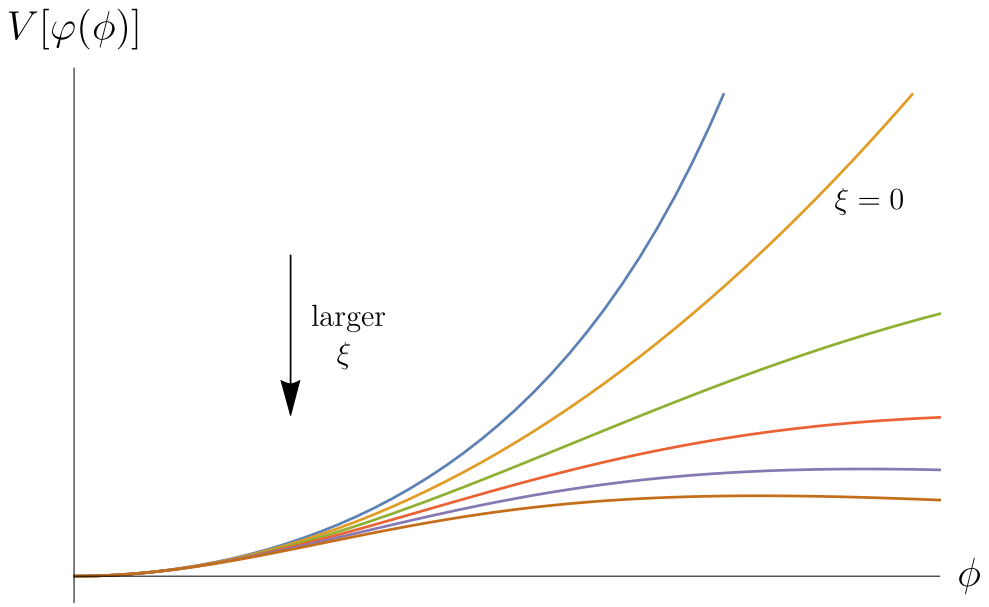

Figure 4.1: Schematic representation of the effective potential (4.23) for $U(\phi) \propto \phi^2$. The different lines represent different values of the coupling constant ξ in the function $\Omega = 1 + \xi\phi^2$, where a larger ξ corresponds to a flatter potential (a less concave one). From the observationally point of view, a flatter potential gives rise to a suppression of the tensor-to-scalar ratio r and, consequently, a larger value of ξ drives the canonical model to be in a better agreement with observations (see §2.4.4).

was first studied in Ref. [220] as a kinetically-driven model of inflation, *i.e.* $G_2(\phi, X) = G_2(X)$ and thus no potential term was introduced. However, potential-driven versions, considered in subsequent works, realized that simple potentials as the ones of chaotic inflation, Eq. (2.32), could be reconciled with CMB observations in the same spirit as in the presence of a nonminimal coupling (see Ref. [129]). Further extensions as, for instance, a Higgs boson driving inflation in this framework [128, 130], and studies on potential signatures on higher correlation functions [221] or reheating [222], have also been carried out.

The equations of motion, for the full theory in Eq. (4.5) were computed in Ref. [209] (also shown in Appendix §B) assuming a homogeneous field $\phi = \phi(t)$ and the flat FLRW spacetime metric $\mathrm{d}s^2 = -N^2(t)\mathrm{d}t^2 + a^2(t)g_{ij}\mathrm{d}x^i\mathrm{d}x^j$ (where the lapse function $N(t)$ is introduced for convenience and later set to one). Particularly, for the G-inflation model in Eq. (4.25), the variation of the action with respect to $N(t)$ yields the Friedmann equation

$$3H^2 + G_2 - 2XG_{2,X} - 2XG_{3,\phi} + 6X\dot{\phi}HG_{3,X} = 0 \ . \tag{4.26}$$

On the other hand, variation with respect to the scale factor $a(t)$ gives the evolution equation

$$3H^2 + 2\dot{H} + G_2 + 2X\left(G_{3,\phi} + \ddot{\phi}G_{3,X}\right) = 0 \ . \tag{4.27}$$

Finally, the variation with respect to $\phi(t)$ gives the scalar-field equation of motion

$$3H\dot{\phi} - G_2 - 6\left(3H^2 + \dot{H}\right)G_3 + (1 - 2G_{3,\phi\phi})\,X + \left(1 + 4G_{3\phi} - 6H\dot{\phi}G_{3X}\right)\ddot{\phi} = 0 \ . \tag{4.28}$$

Furthermore, the quadratic actions for scalar and tensor perturbations, from the full Horndeski background, were also computed in Ref. [209] and are given by

$$\mathcal{S}_\zeta^{(2)} = \int \mathrm{d}^4x \frac{a^3 b_s \epsilon_H}{c_s^2}\left(\dot{\zeta}^2 - \frac{c_s^2 k^2}{a^2}\zeta^2\right) \ , \tag{4.29}$$

$$\mathcal{S}_\gamma^{(2)} = \sum_{\lambda=+,\times}\int \mathrm{d}^4x \frac{a^3 b_t}{4c_t^2}\left(\dot{\gamma}_\lambda^2 - \frac{c_t^2 k^2}{a^2}\gamma_\lambda^2\right) \ , \tag{4.30}$$

where $c_{s,t}^2$ and $b_{s,t}$ are normalization factors which depend on the background, *i.e.* on the $G_i(\phi, X)$ functions, as it is shown in §B.1.1. Particularly, for the model in Eq. (4.25), they read as

$$\begin{aligned} b_s &= \frac{2\mu_1 H - 2\dot{\mu}_1 - \mu_1^2}{\epsilon_H} \ , & b_t &= 1 \ , \\ c_s^2 &= \frac{3\left(2\mu_1 H - 2\dot{\mu}_1 - \mu_1^2\right)}{4\mu_2 + 9\mu_1^2} \ , & c_t^2 &= 1 \ , \end{aligned} \tag{4.31}$$

where

$$\begin{aligned} \mu_1 &= 2H + 2\dot{\phi}G_3 \ , \\ \mu_2 &= -9H^2 + 6\dot{\phi}^2 G_{3,\phi} + \frac{3}{2}\left(\dot{\phi} - 24HG_3\right)\dot{\phi} \ . \end{aligned} \tag{4.32}$$

Notice that the tensor normalization factors correspond to those of the canonical tensor quadratic action, meaning that the choice $G_4 = 1/2$ and $G_5 = 0$ does not modify the tensor sector.[13]

In order to compute the Mukhanov-Sasaki equations for the quadratic actions (4.29)-(4.30), in terms of the Mukhanov variables $u_s = z_s\zeta$ and $u_t = z_t\gamma$, we need to redefine the z_p variables, Eqs. (2.53), as

$$z_s = \frac{a\sqrt{2b_s\epsilon_H}}{c_s} \ , \qquad z_t = \frac{a}{c_s}\sqrt{\frac{b_t}{2}} \ , \tag{4.33}$$

[13] This statement holds for any choice of G_2 and G_3, see Refs. [129, 209].

for which the evolution equations read

$$u_p'' + \left(c_p^2 k^2 - \frac{z_p''}{z_p} \right) u_p = 0 \ . \tag{4.34}$$

As already stated, for the model in Eq. (4.25), the tensor sector is not modified and thus the evolution equations and their solutions remain as in canonical inflation. On the other hand, for scalar perturbations, the solution of Eq. (4.34) is not trivial—one should study carefully the background evolution for a given choice of the $G_i(\phi, X)$ functions and, from there, determine whether the SR approximation is suitable or numerical integration must be performed. Furthermore, closer attention needs to be devoted to the evolution of the normalization factors b_p and c_p^2 as they may develop instabilities; namely, c_p^2 represent the sound speeds of primordial perturbations that need to be positive defined in order to avoid for *Laplacian* instabilities, whereas the factors b_p are required with the same condition so they do not contribute with a wrong sign to the kinetic term, otherwise they would represent a ghost instability.

Until recently, the avoidance of instabilities at the perturbations level represented a severe problem on the construction of G-inflation models. Reference [129], for instance, studied a potential driven-version based on the function $G_3(\phi, X) = -X/(2M^3)$ and found that they could reconcile the quadratic potential $m^2\phi^2$ (among others) with CMB observations for small values of the mass scale M compared to $M_{\rm Pl}$, however with a lower bound of $M = 4.2 \times 10^{-4} M_{\rm Pl}$. Although the tension between the model and the data is recovered when we consider the most recent *Planck* data (see Ref. [4]), the issue with smaller values of M remained interesting as it was due to the appearance of Laplacian instabilities during reheating. Indeed, the G_3 term still affects the dynamics of the inflaton field after the end of inflation, which translates into the lack of coherent oscillations during the reheating epoch. Nevertheless, it has been shown that these instabilities can be avoided by terminating the influence of G_3 before the end of inflation; this mechanism can be simply achieved by a transition from a G-inflation domain to a canonical inflationary era able to properly reheat the Universe. Furthermore, this transition should be carefully introduced after CMB scales in order to contrast with the canonical predictions of a given potential $V(\phi)$. This can be seen from Fig. 4.2, where the slow-roll parameter ϵ_H, Eq. (2.5), is shown for a transient model which was carefully constructed in order to be placed after CMB scales ($N = 0$) and before the end of inflation ($N = 55$). In addition, recall that under the SR approximation, the tensor-to-scalar-ratio at CMB scales reads as $r = 16\epsilon_H$, *i.e.* a suppression of r is expected for the *Transient* model in comparison with the canonical quadratic scenario for the same value of n_s. Consequently, such a

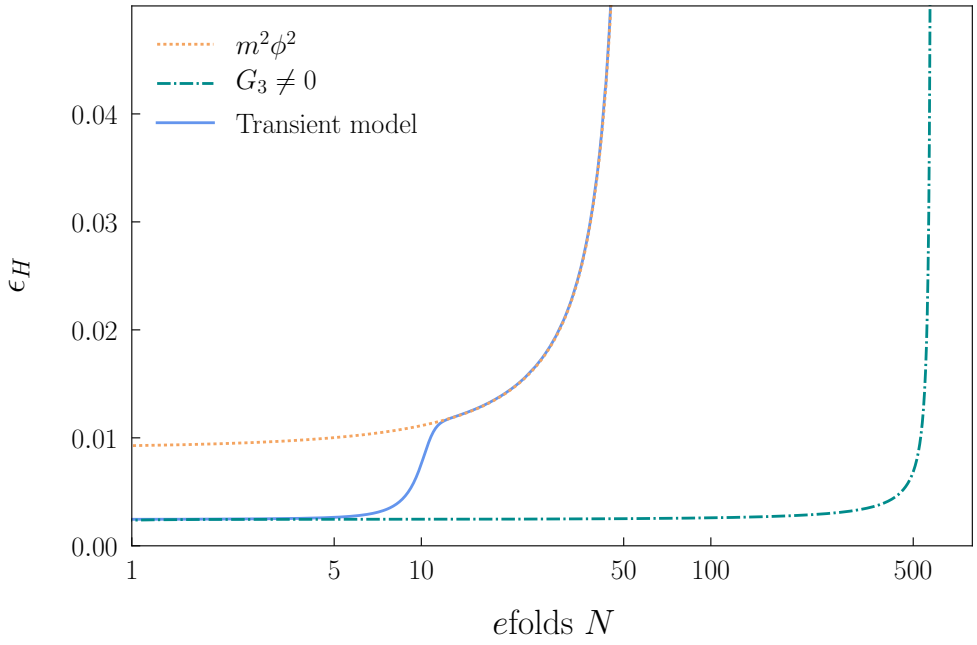

Figure 4.2: Slow-roll parameter $\epsilon_H = -\dot{H}/H^2$ for three different models: the canonical quadratic potential $V(\phi) = m^2\phi^2/2$ (dotted, orange), the quadratic potential plus $G_3(\phi, X) = -X/(2M^3)$ (dash-dotted, green), and a transient model given by $G_3(\phi, X) = -X\left[1 + \tanh\left((\phi - \phi_r)/d\right)\right]/(2M^3)$ with $\{M, m, \phi_r, d\} = \left\{1.303 \times 10^{-4}, 2.58 \times 10^{-6}, 13.87, 0.086\right\}$. The hyperbolic tangent provides a mechanism to switch off the contribution of the G_3 term and thus to transition to the canonical regime. As a consequence, the transient model safely reheats the Universe and suppresses the tensor to scalar ratio, $r = 16\epsilon_H$, at CMB scales ($N = 0$)—the plot is normalized such as in both canonical and transient models inflation ends at $N = 55$. However, CMB scales for the model in green lie at $N \sim 500$, *i.e.* the suppression of r in such a model is small. See Ref. [4] for details.

transient model is able to reconcile chaotic inflation with observations and avoid Laplacian instabilities (see [4] for details).

4.3 Inflation in scalar-vector-tensor theories

The background EoM and the quadratic actions of primordial scalar, vector and tensor perturbations for the SVT theories, Eq. (4.14), were fully computed in Ref. [223] and are shown in Appendix §B. Here, we shall review their consequences on inflation by constructing a simple model, yet with phenomenological implications, with a scalar-vector coupling of the form $A^\mu \nabla_\mu \phi$. As we shall see, the longitudinal vector is able to affect the cosmic expansion during inflation which will be translated into a suppression of the tensor-to-scalar ratio for large-field models [5].

4.3.1 Inflation with mixed helicities

The scalar-vector-tensor theories allow for extra interactions in the form of scalar-vector mixings. In the context of inflation, the vector field is able to modify the dynamics of the expansion driven by the scalar field and, consequently, the predictions for a given potential function $V(\phi)$. As it can be noticed from Eq. (4.14), a scalar-vector mixing can be included in several different forms. Among these possible forms, the simplest one is given by $X_2 = -A^\mu \nabla_\mu \phi/2$, already present in f_2. This term is genuine, coming from the helicity decomposition provided by the Stueckelberg trick and therefore it is interesting to study the dynamics it offers when added to a canonical model of inflation.

We then focus here on a model of inflation driven by a helicity-0 mode, ϕ, mixed with a helicity-1 mode, A_μ, where both fields are allowed to propagate, *i.e.* the vector kinetic and self-interaction terms are included. [14] The action then reads as

$$\mathcal{S}_{\rm mix} = \int \mathrm{d}^4x\sqrt{-g}\left[\frac{1}{2}R + F + X_1 - V(\phi) + \beta_m M X_2 + \beta_A M^2 X_3\right] \ , \quad (4.35)$$

where we recall that

$$X_1 = -\frac{1}{2}\nabla_\mu\phi\nabla^\mu\phi \ , \qquad X_2 = -\frac{1}{2}A^\mu\nabla_\mu\phi \ , \qquad X_3 = -\frac{1}{2}A_\mu A^\mu \ , \quad (4.36)$$

and where M is the positive, constant vector mass, and β_m and β_A are dimensionless constants. The equations of motion, computed on a FLRW spacetime metric (1.4), with a compatible vector profile $A_\mu = (A_0(t), 0, 0, 0)$ and a homogeneous scalar field $\phi(t)$, read as

$$3H^2 - \frac{1}{2}\dot\phi^2 - V(\phi) + \frac{1}{2}\beta_A M^2 A_0^2 = 0 \ , \quad (4.37)$$

$$2\dot H + \dot\phi^2 + \frac{1}{2}\beta_m M\dot\phi A_0 = 0 \ , \quad (4.38)$$

$$\ddot\phi + 3H\dot\phi + V_{,\phi} + \frac{1}{2}M\beta_m\left(\dot A_0 + 3HA_0\right) = 0 \ , \quad (4.39)$$

$$2\beta_A M A_0 + \beta_m\dot\phi = 0 \ . \quad (4.40)$$

Notice that we now have a fourth EoM corresponding to the variation of the action with respect to A_0. Interestingly enough, Eq. (4.40) tells us that the ratio $A_0/\dot\phi$ remains constant during the evolution, as depicted in Fig. 4.3. This fact allows us to substitute $\dot\phi \propto A_0$ into Eqs. (4.37)-(4.39) and to introduce the parameter

$$\beta \equiv 1 - \frac{\beta_m^2}{4\beta_A} \ , \quad (4.41)$$

[14] Recall, however, that $F = -F_{\mu\nu}F^{\mu\nu}/4$ does not contribute to the dynamics on a FLRW spacetime due to the conformal invariance of the Maxwell Lagrangian.

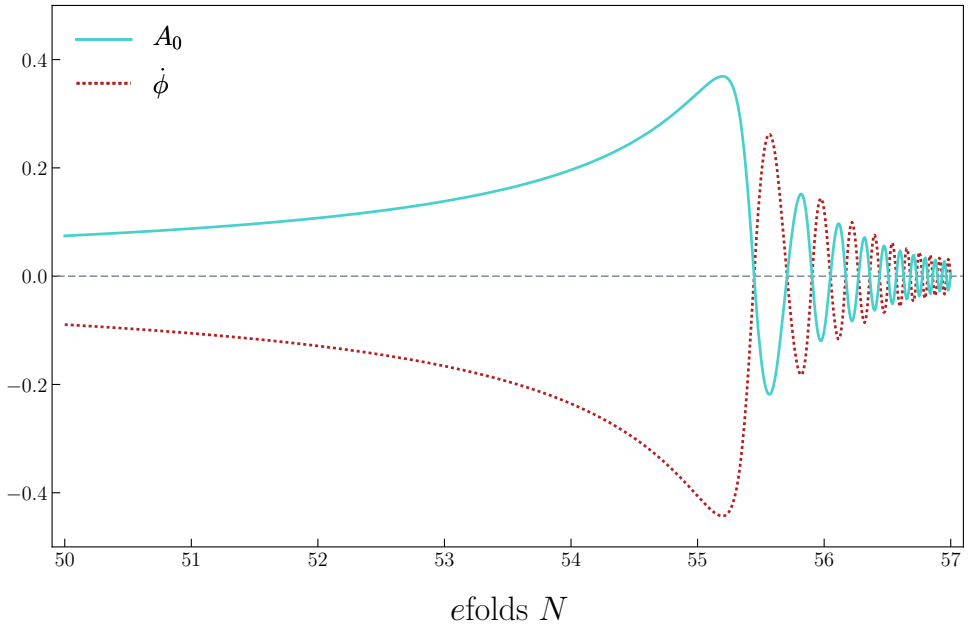

Figure 4.3: Background evolution of the temporal mode A_0 and the scalar-field velocity $\dot{\phi}$, by the end of inflation ($N = 55$) and during reheating, computed for the model given in Eq. (4.35) and for the potential given in Eq. (2.38) with $\alpha_c = \sqrt{6}/3$. Notice that, as expected from Eq. (4.40), the ratio $A_0/\dot{\phi}$ remains constant during the whole evolution.

for convenience, as we shall see. Furthermore, we can define a rescaled field φ in terms of β as

$$\mathrm{d}\varphi = \sqrt{\beta}\mathrm{d}\phi \ , \tag{4.42}$$

and rewrite the EoM as

$$3H^2 - \frac{1}{2}\dot{\varphi}^2 - V(\varphi) = 0 \ , \tag{4.43}$$

$$2\dot{H} + \dot{\varphi}^2 = 0 \ , \tag{4.44}$$

$$\ddot{\varphi} + 3H\dot{\varphi} + V_{,\varphi} = 0 \ , \tag{4.45}$$

i.e. the proportionality between A_0 and $\dot{\phi}$ leads to an effective single-field dynamics driven by the φ field—therefore the computation of the power spectra can be easily performed using the standard SR approximation.

The conditions for the avoidance of scalar ghosts, worked out in Ref. [223] for the full Lagrangian, trivially provide the constraint $4\beta_A > \beta_m^2 \geq 0$ for this model and, consequently, β lies in the range $0 < \beta \leq 1$ (see Eq. (4.41)). The deviation of β from unity, induced by a nonvanishing scalar-vector mixing, makes the rescaled field φ to evolve slower compared to the inflaton field ϕ, which in turns makes the expansion shorter—there are fewer $e$folds N for the same field excursion—as seen from Fig. 4.4. This has important consequences on the inflationary observables. Namely, in order to have

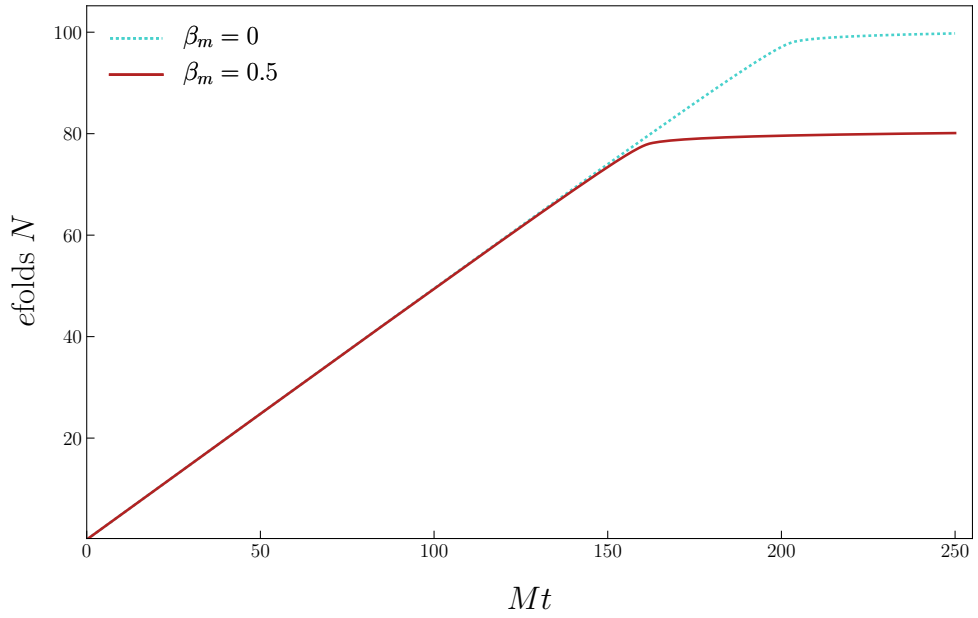

Figure 4.4: Number of $e$folds of inflation $\mathrm{d}N = H\mathrm{d}t$, as a function of time rescaled by the vector mass M, for the same specifications than those in Fig. 4.3. Notice that for a nonvanishing scalar-vector mixing, mediated by β_m, the expansion is shorter; regarding the inflationary observables, a shorter expansion would require to start the inflaton's evolution from a flatter part of the potential in order to have enough inflation which, in turn, translates into a suppression of the tensor-to-scalar ratio r (see [5]).

enough inflation, the field φ needs to evolve from a flatter part of the potential $V(\varphi)$ which will produce a suppression on the tensor-to-scalar ratio r specially noticeable for small-field models—while small-field models currently satisfy the CMB bounds on r, they could be in tension in the near future and thus a scalar-vector-mixing model may reconcile such potential with observations (see Ref. [5] for details).

The complete, general quadratic actions for scalar, vector and tensor perturbations, along with the conditions for the avoidance of ghosts and Laplacian instabilities for the theory in Eq. (4.14), were computed in Ref. [223] (which we omit to show here for brevity), whereas their particularizations for the model in Eq. (4.35) were computed in Ref. [5], as well as the power spectra for the three helicity modes and the predictions for several inflationary potentials; and thus we refer the interested reader to these works for details. Further studies concerning the epoch of reheating, imprints on higher correlation functions and more complicated mixings with potential new phenomenology as, for instance, a non-negligible amplitude of vector perturbations, are expected to be carried out in the near future.

CHAPTER 5

Generalized Slow-Roll Approximation

In §2.1.1 we discussed the conditions required for a successful period of inflation—in doing so, we defined the slow-roll parameters ϵ_H and η_H, Eqs. (2.5) and (2.23). The condition $\epsilon_H \ll 1$ is required so the evolution remains close to de Sitter and inflation does not end earlier than expected; whereas $|\eta_H (= -\delta_1)| \ll 1$ ensures that the evolution of ϵ_H is slow, which is usually understood as a requirement for the inflaton's slow evolution, needed for a sufficient amount of inflation.

Satisfying the slow-roll conditions unwittingly defines a hierarchy of the so-called *Hubble slow-roll* parameters

$$\delta_p \equiv \frac{1}{H^p \dot{\phi}} \left(\frac{\mathrm{d}}{\mathrm{d}t} \right)^{p+1} \phi \ , \tag{5.1}$$

where a given parameter δ_p is of order $\mathcal{O}(\epsilon_H^p)$. This hierarchy is helpful to obtain approximative solutions of the Mukhanov-Sasaki equation (2.56), as discussed in §2.4.3. Furthermore, a consequential hierarchy of inflationary observables, $n_s - 1 = \mathcal{O}(\epsilon_H)$, $\alpha_s = \mathcal{O}(\epsilon_H^2)$, $\beta_s = \mathcal{O}(\epsilon_H^3)$, etc., is implicitly defined (see Eqs. (2.83)). As discussed in §2.4.4, this hierarchy of observational parameters is compatible with the current data (given the large uncertainties on both α_s and β_s), however, it is not really required by the observations. Furthermore, it is not a consequence of the slow-roll (SR) approximation either. Interpretations of the aforementioned CMB constraints in terms of the slow-roll parameters could then provide misleading results, even so at second-order in the SR approximation which is usually assumed to be more accurate.

Features in the inflationary potential $V(\phi)$ translate into oscillations or other type of glitches in the primordial power spectra. These features leave the spectra nearly scale-invariant although no longer scale-free [224–229]. Consequently, treating models of this sort with the standard SR approximation is known to fail, even in canonical inflation, due to large local[1] tilt and running of the tilt (being equivalently to a large $|\delta_1|$), *i.e.* numerical integration of the mode-function equation is usually performed.

In this chapter, we review the *Generalized Slow-Roll* (GSR) approximation, which was developed to overcome the deficiencies of the standard SR approximation. Here, the evolution of the first slow-roll parameter ϵ_H, sourced by features, is only assumed to be small in amplitude, *i.e.* nothing is assumed for its frequency. Conversely, if their frequency is of order $\Delta N \geq 1$, a Taylor expansion of the sources around an optimized horizon exit epoch leads to analytical expressions for the power spectra observables with a correct order counting of the slow-roll parameters. This approach is named *Optimized Slow-Roll* (OSR). In addition, we shall assume a general scalar-tensor background given by the Horndeski framework, Eq. (4.5), for which the mode-function evolution equations are given by Eq. (4.34).[2]

For convenience, we define several new variables: a rescaling of the mode functions

$$y = \sqrt{2c_{s,t}k}u_{s,t} \ , \tag{5.2}$$

a horizon epoch x, in terms of the sound horizons $s_{s,t}$,

$$x \equiv ks_{s,t} \ , \qquad\qquad s_{s,t}(N) \equiv \int_N^{N_f} \frac{c_{s,t}}{aH}\mathrm{d}N \ , \tag{5.3}$$

and the source functions

$$\begin{aligned} f_s &\equiv 2\pi z_s\sqrt{c_s}s_s = \sqrt{8\pi^2\frac{b_s\epsilon_H c_s}{H^2}}\frac{aHs_s}{c_s} \ , \\ f_t &\equiv 2\pi z_t\sqrt{c_t}s_t = \sqrt{2\pi^2\frac{b_t c_t}{H^2}}\frac{aHs_t}{c_t} \ , \end{aligned} \tag{5.4}$$

for scalars and tensors, respectively. In terms of these variables, the Mukhanov-Sasaki equation (4.34), can be written as

$$\frac{\mathrm{d}^2y}{\mathrm{d}x^2} + \left(1 - \frac{2}{x^2}\right)y = \frac{f'' - 3f'}{f}\frac{y}{x^2} \ , \tag{5.5}$$

[1] At a specific scale k.

[2] The original GSR approximation was developed by E. Stewart [230] in the framework of canonical inflation to remove the assumptions yielding to the hierarchy of the inflationary observables. However, this approximation still required $|\eta_H| \ll 1$ and thus only applied for small deviations from scale-invariance. The techniques reviewed in this chapter were developed to improve the original GSR and later extended to noncanonical models.

where primes will represent derivatives with respect to $\ln x$ along this chapter. As it can be noticed, Eq. (5.5) resembles the mode-function equation in de Sitter space, Eq. (2.62), with an extra term sourced by the function

$$g(x) = \frac{f'' - 3f'}{f} \ . \tag{5.6}$$

Therefore, $g(x)$ encodes all the deviations from the de Sitter solution due to excitations of the source functions f. Bear in mind that so far we have not made any assumption for the evolution of ϵ_H or the other slow-roll parameters and therefore, in these variables, the dimensionless power spectra, Eqs. (2.65), are given by

$$\Delta^2_{\zeta,\gamma} = \lim_{x\to 0} \left| \left(\frac{xy}{f}\right)_{s,t} \right|^2 . \tag{5.7}$$

Notice now that in the case where the source function f remains nearly constant, the scalar and tensor power spectra, to the lowest order in excitations, approximate to [145]

$$\Delta^2_\zeta \approx \frac{1}{f_s^2} \approx \frac{H^2}{8\pi^2 \epsilon_H c_s b_s} \ , \qquad \Delta^2_\gamma \approx \frac{1}{f_t^2} \approx \frac{H^2}{2\pi^2 c_t b_t} \ , \tag{5.8}$$

which correspond to the de Sitter results for the spectra in the Horndeski background [231].

5.1 Generalized Slow-Roll

Equation (5.5) can be solved using Green function techniques provided that the amplitude of f remains small, *i.e.* the solution does not deviate considerably from the de Sitter solution, the Bunch-Davies vacuum,

$$y_0(x) = \left(1 + \frac{i}{x}\right) e^{ix} \ . \tag{5.9}$$

Again, this requirement only assumes small deviations of scale invariance over an average of time, but nothing on the local tilt. The formal solution to Eq. (5.5) then reads as

$$y(x) = y_0(x) - \int_x^\infty \frac{\mathrm{d}u}{u^2} \frac{f'' - 3f'}{f} y(u) \mathrm{Im}\left[y_0^*(u) y_0(x)\right] \ , \tag{5.10}$$

from which we can replace $y \to y_0$ on the right-hand side and iteratively improve the solution order by order in deviations from de Sitter. To first

order we obtain,[3]

$$\begin{aligned}\ln \Delta^2_{\zeta,\gamma}(k) &\approx G(\ln x_*) + \int_{x_*}^{\infty} \frac{\mathrm{d}x}{x} W(x) G'(\ln x) \ , \\ &\approx -\int_0^{\infty} \frac{\mathrm{d}x}{x} W'(x) G\left(\ln x\right) \ ,\end{aligned} \tag{5.11}$$

where $x_* \ll 1$ and integration by parts was performed in the second line. Furthermore, $G(\ln x)$ is a source function that now encodes all the deviations from the de Sitter solution, written as

$$G \equiv -2 \ln f + \frac{2}{3} (\ln f)' \ , \tag{5.12}$$

and $W(x)$ is a window function given by

$$W(x) = \frac{3\sin(2x)}{2x^3} - \frac{3\cos(2x)}{x^2} - \frac{3\sin(2x)}{2x} \ , \tag{5.13}$$

which determines the freezout of the mode functions [134].

Equation (5.11) is known as the *Generalized Slow-Roll* formula. It still requires numerical integration, though it is more computationally efficient than solving Eq. (4.34). Moreover, the source function G can be used as a model-independent mean to connect observational constraints with any inflationary model that belongs to the *effective field theory* class [232, 233]. In addition, the tilts $n_{s,t}$ and the higher-order running parameters can also be efficiently computed by taking derivatives of Eq. (5.11) with respect to the scale k, whereas the tensor-to-scalar ratio is computed in the standard way, using Eq. (2.89).

5.2 Optimized Slow-Roll

In the GSR expansion, Eq. (5.11), local scale-dependence of the power spectra is encoded in a nonvanishing $G'(\ln x)$. The condition for small departures from the de Sitter solution then implies that the average of G', over several $e$folds, is of order $\mathcal{O}(1/N)$, which is consistent with CMB and LSS observations where $N \sim 55$. On the other hand, as previously stated, the sources are allowed to vary on a shorter scale ΔN and, consequently, $G'' = \mathcal{O}(1/\Delta N) G'$. In general, there exists a hierarchy of $G^{(p)}$ functions given by

$$G^{(p)} \equiv \frac{\mathrm{d}^p G}{\mathrm{d}\ln x^p} = \mathcal{O}\left(\frac{1}{N \Delta N^{p-1}}\right) \ , \tag{5.14}$$

[3] See, *e.g.*, Refs. [134, 144] for details and the formulas to second order in deviations from the de Sitter background.

which therefore can be distinguished from the standard $\mathcal{O}(1/N^p)$ slow-roll hierarchy.

It can be shown that the source in the GSR formula can be expanded in Taylor series around the horizon exit epoch, provided that $1 \lesssim \Delta N \leq N$ [144]. Compared with the usual SR approximation, this expansion creates a hierarchy of parameters separated by $1/\Delta N$ rather than $1/N$.[4] For the first-order GSR formula, the expansion reads as [144, 145]

$$\ln \Delta^2_{\zeta,\gamma} \approx G(\ln x_f) + \sum_{p=1}^{\infty} q_p(\ln x_f) G^{(p)}(\ln x_f) \ , \tag{5.15}$$

where the $q_p(\ln x_f)$ coefficients are given by

$$q_1(\ln x_f) = \ln x_1 - \ln x_f \ , \qquad \ln x_1 \equiv \frac{7}{3} - \ln 2 - \gamma_{\rm E} \ , \tag{5.16}$$

and

$$q_p(\ln x_f) = \sum_{n=0}^{p} \frac{c_{p-n}}{n!} q_1^n(\ln x_f) \ , \tag{5.17}$$

$$c_p = \frac{1}{p!} \lim_{z\to 0} \frac{\mathrm{d}^p}{\mathrm{d}z^p} \left[e^{-z\left(\frac{7}{3}-\gamma_{\rm E}\right)} \cos\left(\frac{\pi z}{2}\right) \frac{3\Gamma\left(2+z\right)}{(1-z)(3-z)} \right] \ . \tag{5.18}$$

Here, $\gamma_{\rm E}$ is the Euler-Mascheroni constant. The coefficients q_p depend only on the evaluation epoch x_f and thus they do not depend on the inflationary model and are equal for scalars and tensors.

5.2.1 Optimization

The sound horizon exit epoch corresponds to $\ln x_f = 0$, for which the standard slow-roll results are recovered by truncating Eq. (5.15) to leading order, *i.e.* $\ln \Delta^2 \approx G(0)$. In this case, the next-to-leading (NLO) order slow-roll (SR) correction ($p = 1$) is suppressed by $q_1(0)/\Delta N$.

However, we can improve the truncation of Eq. (5.15) by optimizing the evaluation point x_f. For instance, notice that $q_1(\ln x_f)$ vanishes for $x_f = x_1$ and therefore the NLO order correction vanishes as well. The first correction would then come from the next-to-next-to-leading (NNLO) order optimized (OSR) correction $q_2(\ln x_1)/\Delta N^2$.

For large features, $\Delta N \sim N$, both NLO SR and NNLO OSR corrections are small and thus the leading-order solutions are accurate enough, as expected. On the other hand, if the sources vary, for instance, as $\Delta N \sim 3$,

[4] For $\Delta N \sim 1$ numerical integration is needed, either by exactly solving the Mukhanov-Sasaki equation (4.34) or by performing the GSR approximation by means of Eq. (5.11). On the other hand, if $\Delta N \ll 1$, the hierarchy is inverted and different techniques can be performed (see [234]).

the first SR correction (NLO) is expected to be of 35%, as usual, whereas the first OSR correction (NNLO) is just about 4%. Consequently, more accurate approximations for the observables are obtained by optimizing the evaluation point x_f. Since $\ln x_1 \approx 1.06$, notice that the optimization corresponds to evaluate the observables at around ~ 1 *e*fold before the sound horizon exit.

We can therefore establish the p-th order optimization by fixing the evaluation epoch to be $\ln x_f = \ln x_{p+1}$, so that the next-order correction identically vanishes as a consequence of the $q_{p+1}(\ln x_{p+1}) = 0$ solution.

The tilts and the higher order running parameters can be obtained by differentiating Eq. (5.15) and using the fact that [144, 145]

$$\frac{\mathrm{d}G^{(p)}(\ln x_f)}{\mathrm{d}\ln k} = -G^{(p+1)}(\ln x_f) \ . \tag{5.19}$$

Therefore the first observables read, to leading order, as $\mathrm{d}\ln\Delta^2/\mathrm{d}\ln k \approx -G'(\ln x_f)$ and $\alpha \approx G''(\ln x_f)$. As previously stated, this implies a hierarchy of the $G^{(p)}$ functions defined by Eq. (5.14). However, it is more convenient to relate the observables to the standard Hubble slow-roll parameters.

5.2.2 Correspondence to the Hubble slow-roll parameters

In the context of a general scalar tensor theory, parametrized by $\epsilon_H = -\mathrm{d}\ln H/\mathrm{d}N$ and the normalization factors $c_{s,t}^2$ and $b_{s,t}$, the Hubble slow-roll parameter convention is given by the hierarchies[5]

$$\begin{aligned}
\delta_1 &\equiv \frac{1}{2}\frac{\mathrm{d}\ln\epsilon_H}{\mathrm{d}N} - \epsilon_H \ , \qquad \delta_{p+1} \equiv \frac{\mathrm{d}\delta_p}{\mathrm{d}N} + \delta_p\left(\delta_1 - p\epsilon_H\right) \ , \\
\sigma_{i,1} &\equiv \frac{\mathrm{d}\ln c_i}{\mathrm{d}N} \ , \qquad\qquad \sigma_{i,p+1} \equiv \frac{\mathrm{d}\sigma_{i,p}}{\mathrm{d}N} \ , \\
\xi_{i,1} &\equiv \frac{\mathrm{d}\ln b_i}{\mathrm{d}N} \ , \qquad\qquad \xi_{i,p+1} \equiv \frac{\mathrm{d}\xi_{i,p}}{\mathrm{d}N} \ ,
\end{aligned} \tag{5.20}$$

where here $i = s, t$ and $p \geq 1$.

The previously stated assumptions, $G' = \mathcal{O}(1/N)$ and $G^{(p+1)} \sim \mathcal{O}(1/\Delta N)G^{(p)}$, then fix the expectations for the slow-roll parameters as

$$\begin{aligned}
\{G', \epsilon_H, \delta_1, \sigma_{i,1}, \xi_{i,1}\} &= \mathcal{O}\left(\frac{1}{N}\right) \ , \\
\left\{G^{(p+1)}, \delta_{p+1}, \sigma_{i,p+1}, \xi_{i,p+1}\right\} &= \mathcal{O}\left(\frac{1}{N\Delta N^p}\right) \ .
\end{aligned} \tag{5.21}$$

[5] Consistent with the Horndeski theory parametrization (§4.1.1.1), for which the normalization factor are given in Eqs. (B.16). However, the OSR approximation holds for more general theories belonging to the effective field theory class, see Ref. [145] for details.

Therefore, a relation between the $G^{(p)}$ functions and the slow-roll parameters can be established by means of Eq. (5.12), using Eqs. (5.4). In doing so, a convention regarding the expansion in inverse powers of N and ΔN is adopted, namely, expressions are expanded up to $\mathcal{O}(1/N^2)$, *i.e.* terms of order $\mathcal{O}(1/N\Delta N^p)$ are kept but not $\mathcal{O}(1/N^2\Delta N^p)$ terms (see Refs. [144,145] for details).

The first order optimized slow-roll formulas, in terms of the slow-roll parameters, then read as [145]

$$\begin{aligned}
\ln\Delta^2_\zeta &\simeq \ln\left(\frac{H^2}{8\pi^2 b_s c_s \epsilon_H}\right) - \frac{10}{3}\epsilon_H - \frac{2}{3}\delta_1 - \frac{7}{3}\sigma_{s1} - \frac{1}{3}\xi_{s1}\Big|_{x=x_1}\,,\\
n_s - 1 &\simeq -4\epsilon_H - 2\delta_1 - \sigma_{s1} - \xi_{s1} - \frac{2}{3}\delta_2 - \frac{7}{3}\sigma_{s2} - \frac{1}{3}\xi_{s2}\Big|_{x=x_1}\,,\\
\alpha_s &\simeq -2\delta_2 - \sigma_{s2} - \xi_{s2} - \frac{2}{3}\delta_3 - \frac{7}{3}\sigma_{s3} - \frac{1}{3}\xi_{s3} - 8\epsilon_H^2 - 10\epsilon_H\delta_1 + 2\delta_1^2\Big|_{x=x_1}\,,
\end{aligned} \tag{5.22}$$

for scalar, and

$$\begin{aligned}
\ln\Delta^2_\gamma &\simeq \ln\left(\frac{H^2}{2\pi^2 b_t c_t}\right) - \frac{8}{3}\epsilon_H - \frac{7}{3}\sigma_{t1} - \frac{1}{3}\xi_{t1}\Big|_{x=x_1}\,,\\
n_t &\simeq -2\epsilon_H - \sigma_{t1} - \xi_{t1} - \frac{7}{3}\sigma_{t2} - \frac{1}{3}\xi_{t2}\Big|_{x=x_1}\,,\\
\alpha_t &\simeq -\sigma_{t2} - \xi_{t2} - \frac{7}{3}\sigma_{t3} - \frac{1}{3}\xi_{t3} - 4\epsilon_H^2 - 4\epsilon_H\delta_1\Big|_{x=x_1}\,,
\end{aligned} \tag{5.23}$$

for tensor perturbations. Notice then that the OSR approximation introduces corrections to the standard slow-roll results, Eqs. (5.8), even at leading order, aided by the different and optimized evaluation point $x = x_1$. Furthermore, the OSR expressions (5.22) can accurately relate inflationary models to the standard power-law, Eq. (2.84), in cases when $|\alpha_s|$ is of order $|n_s - 1|$, unlike the traditional second-order SR approximation [4,144].

Finally, the tensor-to-scalar ratio can be computed in the standard way through Eq. (2.89). Note however that it is taken at fixed scale k which in general corresponds to an evaluation point $x = x_1$ at two different epochs N due to the different sound speeds c_s^2 and c_t^2 for scalars and tensors, respectively.

The efficiencies of the GSR and OSR approximations have been tested and compared to the standard leading and NLO SR approximation for models with features in the potential as well as for noncanonical models as G-inflation (see, *e.g.*, Refs. [4, 138, 139, 142, 144, 235]) and have been further extended for the computation of the bispectrum [136, 236–238].

In the following, we present two appendices which complement some of the topics discussed in this Part I: the *Cosmological perturbation theory* (Appendix A) sets the basis for the calculations performed in §2.4, whereas Appendix B provides the complete set of equations of motion for the theories discussed in §4.

After these appendices, Part II contains the publications where the main original research developed during the realization of this thesis is presented.

APPENDIX A

Cosmological perturbation theory

In this appendix we review the cosmological perturbation theory for a FLRW spacetime. We start by defining the group of gauge transformations—coordinate changes—that a given perturbation is subject to. Then, starting from the most general perturbed FLRW metric, we explicitly show the scalar, vector and tensor perturbations composing the perturbed line element, as well as the perturbations composing the energy-momentum tensor of an ideal fluid, as the one described in §1. We later describe how these perturbations transform under the gauge transformations and thus we compute the gauge-invariant variables used in §2, relevant for the inflationary theory. Here we mainly follow Refs. [15, 60, 132] and, for the sake of simplicity, we will work only to first-order in perturbations—which suffices for the computation of the power spectrum of primordial perturbations (the computation of the bispectrum requires going to second order, however we do not discuss it in this thesis).

A.1 Gauge transformations

Now that we want to study perturbations living in a spacetime, the choice of a coordinate system is not as straightforward as in an homogeneous universe. In the latter, we were used to define the threading—curves of constant spatial coordinates x^i—as curves corresponding to the motion of free-falling observers with zero momentum density, and the slicing—hypersurfaces of constant time t—corresponding to a homogeneous universe.

When perturbations are present, there is no preferred coordinate system anymore and, furthermore, the threading and slicing choice is not unique. This implies that we would be defining the perturbations by specifying the coordinates. It is then important for Cosmology to find how perturbations transform under a change of coordinates—a *gauge* transformation—and to study the evolution of gauge-invariant variables in order to avoid ambiguities due to a given gauge choice.

In general, any quantity can be split in its background component and its perturbations as

$$\begin{aligned} T(t,x^i) &= \overline{T}(t) + \delta T(t,x^i) \\ &= \overline{T}(t) + \sum_{n=1}^{\infty} \left(\frac{\epsilon^n}{n!}\right) \delta T_{(n)}(t,x^i) \ , \end{aligned} \tag{A.1}$$

where overlines represent unperturbed background quantities and n represents the order of the perturbation. Furthermore, $T(t,x^i)$ transforms under a gauge transformation as

$$\widetilde{T} = e^{\pounds_\xi} T \ , \tag{A.2}$$

where $\pounds$ denotes a Lie derivative with respect to an auxiliary vector field ξ generating the transformation.[1] Under such a transformation, the right-hand side of Eq. (A.1) transforms as

$$\begin{aligned} \widetilde{T} =& \left(1 + \epsilon^1 \pounds_{\xi_1} + \frac{1}{2}\epsilon^2 \pounds_{\xi_1}^2 + \frac{1}{2}\epsilon^2 \pounds_{\xi_2}^2 + \mathcal{O}(\epsilon^3)\right) \left[\overline{T} + \epsilon^1 \delta T_{(1)} + \frac{1}{2}\epsilon^2 \delta T_{(2)} + \mathcal{O}(\epsilon^3)\right] \\ =& \overline{T} + \epsilon^1 \left(\delta T_{(1)} + \pounds_{\xi_1} \overline{T}\right) + \epsilon^2 \left(\frac{1}{2}\delta T_{(2)} + \pounds_{\xi_1} \delta T_{(1)} + \frac{1}{2}\pounds_{\xi_1}^2 \overline{T} + \frac{1}{2}\pounds_{\xi_2} \overline{T}\right) + \mathcal{O}(\epsilon^3) \ . \end{aligned} \tag{A.3}$$

Then, it is evident that background quantities are gauge invariant, whereas first- and second-order perturbations transform as

$$\widetilde{\delta T}_{(1)} = \delta T_{(1)} + \pounds_{\xi_1} \overline{T} \ , \tag{A.4}$$

$$\widetilde{\delta T}_{(2)} = \delta T_{(2)} + \pounds_{\xi_2} \overline{T} + \pounds_{\xi_1}^2 \overline{T} + 2\pounds_{\xi_1} \delta T_{(1)} \ . \tag{A.5}$$

Notice that the specific form of the Lie-derivative terms depends on whether the perturbation is a scalar, a vector or a tensor.

Lie derivatives

The Lie derivatives with respect to the vector field ξ^μ applied to a scalar φ, a covariant vector v_μ and a covariant tensor $t_{\mu\nu}$ are given, respectively, by [132]

$$\pounds_\xi \varphi = \varphi_{,\alpha} \xi^\alpha \ , \tag{A.6}$$

[1] The gauge transformations form a Lie group with an associated Lie algebra of group generators [132].

$$\pounds_\xi v_\mu = v_{\mu,\alpha}\xi^\alpha + v_\alpha \xi^\alpha{}_{,\mu} \ , \tag{A.7}$$

$$\pounds_\xi t_{\mu\nu} = t_{\mu\nu,\alpha}\xi^\alpha + t_{\mu\alpha}\xi^\alpha{}_{,\nu} + t_{\alpha\nu}\xi^\alpha{}_{,\mu} \ , \tag{A.8}$$

where we recall that the notation $_{,\alpha} \equiv \partial/\partial x^\alpha$ is used.

In the following, we shall define the cosmological perturbations and apply the transformation rules obtained here to them, where we will keep the analyses to first-order in perturbations.

A.2 Metric perturbations

We start by reviewing the metric perturbations of a FLRW line element given by

$$\mathrm{d}s^2 = \left(\overline{g}_{\mu\nu} + \delta g_{\mu\nu}\right) \mathrm{d}x^\mu \mathrm{d}x^\nu \ , \tag{A.9}$$

where $\overline{g}_{\mu\nu}(t)$ is the homogeneous FLRW metric given in Eq. (1.4) and $\delta g_{\mu\nu}(t, x_i)$ is composed by the perturbations. Therefore, the most general first-order perturbed FLRW metric can be written as

$$\mathrm{d}s^2 = -\left(1+2\Phi\right)\mathrm{d}t^2 + 2aB_i \mathrm{d}x^i \mathrm{d}t + a^2\left[\left(1-2\Psi\right)\delta_{ij} + E_{ij}\right]\mathrm{d}x^i \mathrm{d}x^j \ . \tag{A.10}$$

Here Φ—the *lapse*, which specifies the relation between t and the proper time along the threading—and Ψ—the spatial *curvature* perturbation—are 3-scalars, whereas the vector and tensor perturbations B_i—the *shift*, which specifies the velocity between the threading and the worldlines orthogonal to the slicing—and E_{ij}—the *shear*—can be further decomposed as[2]

$$B_i \equiv B_{,i} - S_{,i} \ , \qquad \text{where} \quad S_i{}^{,i} = 0 \ , \tag{A.11}$$

and

$$E_{ij} \equiv 2E_{,ij} + F_{i,j} + F_{j,i} + h_{ij} \ , \qquad \text{where} \quad F_i{}^{,i} = 0 \ , \quad h^i_i = 0 \ , \quad h_{ij}{}^{,i} = 0 \ . \tag{A.12}$$

Consequently, we have defined two more scalar perturbations, B and E, two vector perturbations, S_i and F_i, with zero divergence, and a 3-tensor perturbation h_{ij} that is traceless and transverse.

Gauge transformations of metric perturbations

Using the gauge transformation properties obtained in §A.1, we now explicitly show how the scalar metric perturbations Φ, B, Ψ and E transform to first order. Conversely, one can show that vector perturbations S_i

[2]This is called the scalar-vector-tensor decomposition of perturbed quantities into different helicity modes: scalar, vector and tensor perturbations have helicity 0, ±1 and ±2, respectively. Perturbations of different helicity evolve independently and thus they can be studied separately.

and F_i decay very quickly during the expansion and they are actually not produced during inflation [16]. Furthermore, the tensor perturbation h_{ij} is gauge invariant— it does not change under coordinate transformations [15].

For scalar perturbations then, the perturbed metric components are given as

$$\delta g_{00} = -2\Phi \ , \tag{A.13}$$
$$\delta g_{0i} = aB_{,i}\Phi \ , \tag{A.14}$$
$$\delta g_{ij} = -2a^2 \left(\Psi\delta_{ij} - E_{,ij}\right) \ , \tag{A.15}$$

which transform to first order, according to Eq. (A.4), as

$$\widetilde{\delta g}_{00} = \delta g_{00} - 2\dot{\alpha} \ , \tag{A.16}$$
$$\widetilde{\delta g}_{0i} = \delta g_{0i} - \alpha_{,i} + a^2\dot{\beta}_{,i} \ , \tag{A.17}$$
$$\widetilde{\delta g}_{ij} = \delta g_{ij} + a^2 \left[2H\alpha\delta_{ij} + 2\beta_{,ij}\right] \ , \tag{A.18}$$

where we have decomposed the generating vector as $\xi^\mu = (\xi^0, \xi^i) \equiv (\alpha, \beta^{,i} + \gamma^i)$, and set $\gamma^i = 0$. Equations (A.16)-(A.18) give the transformation of each of the scalar perturbations respectively as

$$\widetilde{\Phi} = \Phi + \dot{\alpha} \ , \tag{A.19}$$
$$\widetilde{B} = B - a^{-1}\alpha + a\dot{\beta} \ , \tag{A.20}$$
$$\widetilde{\Psi} = \Psi - H\alpha \ , \tag{A.21}$$
$$\widetilde{E} = E + \beta \ . \tag{A.22}$$

A.3 Matter perturbations

We consider perturbations present in an ideal fluid characterized by its energy density ρ, pressure p, 4-velocity u^μ and anisotropic stress $\Sigma^{\mu\nu}$. Recall that the 4-velocity obeys $g_{\mu\nu}u^\mu u^\nu = -1$ and its only nonvanishing background components are $\overline{u}^0 = -\overline{u}_0 = 1$. Therefore we write the perturbed 4-velocity to first order in perturbations, using Eq. (A.10), as

$$u^0 = \overline{u}^0 + \delta u^0 = 1 - \Phi \ , \qquad u_0 = \overline{u}_0 + \delta u_0 = -1 - \Phi \ , \tag{A.23}$$

and

$$u^i = \delta u^i = \frac{1}{a}\left(v^i - B^i\right) \ , \qquad u_i = \delta u_i = a v_i \ , \tag{A.24}$$

where the linear perturbation v^i is the physical velocity of the fluid (defined with respect to its proper time).

Furthermore, the energy density and pressure can be split in the standard way as

$$\rho(t, x^i) = \overline{\rho}(t) + \delta\rho(t, x^i) \ , \qquad p(t, x^i) = \overline{p}(t) + \delta p(t, x^i) \ . \tag{A.25}$$

With these definitions, we can construct the perturbed energy momentum tensor, $T^\mu_\nu = (\rho + p)\, u^\mu u_\nu + p\delta^\mu_\nu + \Sigma^\mu_\nu$, to first order, as

$$T^0_0 = -\left(\overline{\rho} + \delta\rho\right) \ , \tag{A.26}$$
$$T^0_i = \left(\overline{\rho} + \overline{p}\right) a v_i \ , \tag{A.27}$$
$$T^i_0 = -\frac{1}{a}\left(\overline{\rho} + \overline{p}\right)\left(v^i - B^i\right) \ , \tag{A.28}$$
$$T^i_j = \left(\overline{p} + \delta p\right)\delta^i_j + \Sigma^i_j \ . \tag{A.29}$$

The anisotropic stress tensor Σ^μ_ν vanishes for the homogeneous FLRW Universe and, furthermore, it is constrained by $\Sigma^{\mu\nu}u_\nu = 0$ and $\Sigma^\mu_\mu = 0$, *i.e.* only its spatial components are nonzero and define a perturbation.

Gauge transformations of matter perturbations

In a very similar way as for the metric scalar perturbations, the energy density, pressure and momentum density perturbations transform as

$$\widetilde{\delta}\rho = \delta\rho + \dot{\overline{\rho}}\alpha \ , \tag{A.30}$$
$$\widetilde{\delta}p = \delta p + \dot{\overline{p}}\alpha \ , \tag{A.31}$$
$$\widetilde{\delta}q = \delta q - \left(\overline{\rho} + \overline{p}\right)\alpha \ , \tag{A.32}$$

where the momentum density perturbation was defined as $(\delta q)_{,i} \equiv \left(\overline{\rho} + \overline{p}\right) v_i$. Furthermore, the anisotropic stress Σ^i_j is gauge invariant.

Analogously, a scalar particle field decomposed as $\phi = \overline{\phi} + \delta\phi$ transforms to first order as

$$\widetilde{\phi} = \overline{\phi} + \delta\phi_{(0)} + \dot{\overline{\phi}}\alpha \ . \tag{A.33}$$

Finally, we consider a vector field $A^\mu = (A^0, A^i)$. This field could be present during inflation and play some role in the evolution. We split its temporal and spatial components as

$$A^0 = -\overline{A} + \delta A \ , \qquad A_i = \psi_{,i} \ , \tag{A.34}$$

in which case, the new scalar perturbations transform according to Eq. (A.4) as

$$\widetilde{\delta A} = \delta A - \dot{A}_0\alpha + A_0\dot{\alpha} \ , \qquad \widetilde{\psi} = \psi + A_0\alpha \ . \tag{A.35}$$

A.4 The primordial curvature perturbation

We have defined the transformation rules for metric and matter perturbations. However, it is desirable to study the evolution of gauge-invariant variables instead of keeping track of the full set of perturbations plus the generators α and β, once a particular threading and slicing is defined. By studying only gauge-invariant combinations of these perturbations, we can avoid *fictitious* perturbations or avoid to remove real ones—as James Bardeen stated: *'only quantities that are explicitly invariant under gauge transformations should be considered'.*

A.4.1 Gauge invariant variables

The first two gauge invariant combinations are called *Bardeen potentials* and are written as [239]

$$\Phi_{\rm B} \equiv \Phi - \frac{\mathrm{d}}{\mathrm{d}t}\left[a^2\left(\dot{E} - \frac{B}{a}\right)\right] \ , \tag{A.36}$$

$$\Psi_{\rm B} \equiv \Psi + a^2 H\left(\dot{E} - \frac{B}{a}\right) \ . \tag{A.37}$$

One can see that $\Phi_{\rm B}$ and $\Psi_{\rm B}$ are invariant under gauge transformations, *i.e.* a change of coordinates. Furthermore, if both are equal to zero, then metric perturbations, if present, must be fictitious.

Regarding matter perturbations, we define the following gauge-invariant combinations:

$$-\zeta \equiv \Psi + \frac{H}{\dot{\overline{\rho}}}\delta\rho \ , \tag{A.38}$$

$$\mathcal{R} \equiv \Psi - \frac{H}{\overline{\rho}+\overline{p}}\delta q \ , \tag{A.39}$$

where ζ is the curvature perturbation on uniform density hypersurfaces, whereas $\mathcal{R}$ is the comoving curvature perturbation. In the following, we shall see that ζ is conserved after inflation and, therefore, its power spectrum $\mathcal{P}_\zeta$ directly relates the CMB statistical properties with the physics of inflation. ζ is therefore called *the primordial curvature perturbation.*

A.4.2 Einstein equations

Matter perturbations in a curved spacetime backreact creating geometric perturbations. Consequently, the Einstein equations (1.9), written as

$$\delta R_{\mu\nu} - \frac{1}{2}\delta g_{\mu\nu}\delta R = \delta T_{\mu\nu} \ , \tag{A.40}$$

determine the evolution of the perturbations previously defined.

The evolution of a given perturbation is usually described in Fourier space, where each perturbed quantity can be decomposed as

$$\delta T(t,k_i) = \int \mathrm{d}^3x^i \delta T(t,x^i) e^{-ik^i x^i} \ , \tag{A.41}$$

where, due to translation invariance, different wavenumbers k evolve independently at linear order [60].

Scalars

In Fourier space, the Einstein equations can then be written as [55, 60]

$$3H\left(\dot{\Psi}+H\Phi\right)+\frac{k^2}{a^2}\left[\Psi+H\left(a^2\dot{E}-aB\right)\right]=-\frac{1}{2}\delta\rho \ , \tag{A.42}$$

$$\dot{\Psi}+H\Phi=-\frac{1}{2}\delta q \ , \tag{A.43}$$

$$\ddot{\Psi}+3H\dot{\Psi}+H\dot{\Phi}+\left(3H^2+2\dot{H}\right)\Phi=\frac{1}{2}\left(\delta\rho-\frac{2}{3}k^2\delta\Sigma\right) \ , \tag{A.44}$$

$$(\Psi_{\mathrm{B}}-\Phi_{\mathrm{B}})=a^2\delta\Sigma \ . \tag{A.45}$$

In addition, the energy-momentum conservation gives the continuity equation and the Euler equation as

$$\dot{\delta\rho}+3H\left(\delta\rho+\delta p\right)=\frac{k^2}{a^2}\delta q+\left(\overline{\rho}+\overline{p}\right)\left[3\dot{\Psi}+k^2\left(\dot{E}-\frac{B}{a}\right)\right] \ , \tag{A.46}$$

$$\dot{\delta q}+3H\delta q=-\delta p+\frac{2}{3}k^2\delta\Sigma-\left(\overline{\rho}+\overline{p}\right)\Phi \ . \tag{A.47}$$

Using Eq. (A.38), Eq. (A.46) can be written as

$$\dot{\zeta}=-H\frac{\delta p_{\mathrm{en}}}{\overline{\rho}+\overline{p}}+\frac{k^2}{3H}\left[\dot{E}-\frac{B}{a}+\frac{\delta q}{a^2\left(\overline{\rho}+\overline{p}\right)}\right] \ , \tag{A.48}$$

where we have introduced

$$\delta p_{\mathrm{en}}\equiv\delta p-\frac{\dot{\overline{p}}}{\dot{\overline{\rho}}}\delta\rho \ , \tag{A.49}$$

which measures the non-adiabatic part of the pressure perturbation. In inflation, perturbations are adiabatic in general, *i.e.* δp_{en} vanishes; furthermore, on superhorizon scales where $k/(aH)\ll 1$, the second term vanishes as well, *i.e.* the curvature perturbation ζ remains constant after inflation until scales enter the again the horizon. Consequently, and because the energy density during inflation is $\delta\rho\sim\delta\phi$, we are interested in computing the primordial power spectrum of

$$-\zeta_\phi\simeq\Psi+\frac{H}{\dot{\overline{\phi}}}\delta\phi \ , \tag{A.50}$$

at horizon exit $k \sim aH$, and ignore the subsequent physics.

In the same way, one can define the curvature perturbation ζ_ψ for the scalar component of a vector field A_i as

$$-\zeta_\psi \simeq \Psi + \frac{H}{A_0}\psi \ , \tag{A.51}$$

and, furthermore, define a total curvature perturbation in the case in which both fields, ϕ and A^μ, are playing a role in the inflationary dynamics, as

$$-\zeta = \Psi - \frac{H\left(\dot{\phi}\delta\phi + A_0\psi\right)}{\dot{\phi}^2 + A_0^2} \ , \tag{A.52}$$

which is analogous to a two-field model of inflation [132].

Vectors

The evolution equations for vector perturbations are sourced by an anisotropic stress perturbation $\delta\Sigma_i$ and are given by

$$\dot{\delta q}_i + 3H\delta q_i = k^2\delta\Sigma_i \ , \tag{A.53}$$

$$k^2\left(\dot{F}_i + \frac{S_i}{a}\right) = 2\delta q_i \ . \tag{A.54}$$

However, $\delta\Sigma_i$ is not created by inflation and, in its absence, δq_i decays with the expansion, *i.e.* the perturbation $\dot{F}_i + S_i/a$ vanishes. Therefore, vector perturbations are, in general, subdominant.

Tensors

The evolution equation for the tensor perturbation h_{ij} is given by

$$\ddot{h}_{ij} + 3H\dot{h}_{ij} + \frac{k^2}{a^2}h = 0 \ , \tag{A.55}$$

which is the equation for a gravitational wave. They are produced by inflation and, in the same way as vectors, they decay with the expansion; however some models of inflation predict an observable amount of gravitational waves during the recombination epoch, *i.e.* they can be distinguished in the CMB polarization spectrum.

APPENDIX B

Equations of motion of general theories of gravity

In this appendix we show the equations of motion for the full Horndeski and SVT theories in a FLRW spacetime. The former were first computed in Ref. [209] whereas the latter can be found in Ref. [223].

B.1 Horndeski theory

We take a homogeneous scalar field $\phi = \phi(t)$ and assume a flat FLRW background with the line element given as

$$\mathrm{d}s^2 = -N^2(t)dt^2 + a^2(t)\delta_{ij}\mathrm{d}x^i\mathrm{d}x^j \ , \tag{B.1}$$

to the action

$$\mathcal{S}_{\mathcal{H}} = \int \mathrm{d}^4x\sqrt{-g}\mathcal{L}_{\mathcal{H}} \ , \tag{B.2}$$

where $\mathcal{L}_{\mathcal{H}}$ is given by Eq. (4.5). The variation of Eq. (B.2) with respect to $N(t)$ gives the constraint equation

$$\sum_{i=2}^{5}\mathcal{E}_i = 0 \ , \tag{B.3}$$

where

$$\mathcal{E}_2 = 2XG_{2,X} - G_2 \ , \tag{B.4}$$

$$\mathcal{E}_3 = 2XG_{3,\phi} - 6X\dot{\phi}HG_{3,X} \ , \tag{B.5}$$

$$\mathcal{E}_4 = -6H^2G_4 + 24H^2X\left(G_{4,X} + XG_{4,XX}\right) - 12HX\dot{\phi}G_{4,\phi X}$$

$$- 6H\dot{\phi}G_{4,\phi} \ , \tag{B.6}$$

$$\mathcal{E}_5 = 2H^3X\dot{\phi}\left(5G_{5,X} + 2XG_{5,XX}\right) - 6H^2X\left(3G_{5,\phi} + 2XG_{5,\phi X}\right) \ . \tag{B.7}$$

The variation with respect to $a(t)$ yields the evolution equation

$$\sum_{i=2}^{5} \mathcal{P}_i = 0 \ , \tag{B.8}$$

where

$$\mathcal{P}_2 = G_2 \ , \tag{B.9}$$

$$\mathcal{P}_3 = 2X\left(G_{3,\phi} + \ddot{\phi}G_{3,X}\right) \ , \tag{B.10}$$

$$\begin{aligned}\mathcal{P}_4 =& 2\left(3H^2 + 2\dot{H}\right)G_4 - 4\left(3H^2X + H\dot{X} + 2\dot{H}X\right)G_{4,X} - 8HX\dot{X}G_{4,XX} \\ &+ 2\left(\ddot{\phi} + 2H\dot{\phi}\right)G_{4,\phi} + 4XG_{4,\phi\phi} + 4X\left(\ddot{\phi} - 2H\dot{\phi}\right)G_{4,\phi X} \ ,\end{aligned} \tag{B.11}$$

$$\begin{aligned}\mathcal{P}_5 =& -2X\left(2H^3\dot{\phi} + 2H\dot{H}\dot{\phi} + 3H^2\ddot{\phi}\right)G_{5X} - 4H^2X^2\ddot{\phi}G_{5,XX} + 4HX\dot{\phi}G_{5,\phi\phi} \\ &+ 4HX\left(\dot{X} - HX\right)G_{5,\phi X} + 2\left[2\left(\dot{H}X + H\dot{X}\right) + 3H^2X\right]G_{5,\phi} \ .\end{aligned} \tag{B.12}$$

Finally, the variation with respect to $\phi(t)$ gives the scalar-field equation of motion

$$\frac{1}{a^3}\frac{\mathrm{d}}{\mathrm{d}t}\left(a^3J\right) = P_\phi \ , \tag{B.13}$$

where

$$\begin{aligned}J =& \dot{\phi}G_{2,X} - 6HXG_{3,X} + 2\dot{\phi}G_{3,\phi} + 6H^2\dot{\phi}\left(G_{4,X} + 2XG_{4,XX}\right) - 12HXG_{4,\phi X} \\ &+ 2H^3X\left(3G_{5,X} + 2XG_{5,XX}\right) - 6H^2\dot{\phi}\left(G_{5,\phi} + XG_{5,\phi X}\right) \ ,\end{aligned} \tag{B.14}$$

$$\begin{aligned}P_\phi =& G_{2,\phi} + 2X\left(G_{3,\phi\phi} + \ddot{\phi}G_{3,\phi X}\right) + 6\left(2H^2 + \dot{H}\right)G_{4,\phi} + 6H\left(\dot{X} + 2HX\right)G_{4,\phi X} \\ &- 6H^2XG_{5,\phi\phi} + 2H^3X\dot{\phi}G_{5,\phi X} \ .\end{aligned} \tag{B.15}$$

For the particular choice of $G_4 = 1/2$ and $G_5 = 0$, the above equations reduce to the set of equations (4.26)-(4.28) corresponding to the G-inflation model discussed in §4.2.2.

B.1.1 Normalization factors

Additionally, let us show the dependence on the $G_i(\phi, X)$ functions of the normalization factors $c_{s,t}^2$ and $b_{s,t}$ appearing in the quadratic actions of primordial perturbations, Eqs. (4.29) and (4.30). As given in Ref. [209], they read as

$$c_{s,t}^2 = \frac{\mathcal{F}_{s,t}}{\mathcal{G}_{s,t}} \ , \qquad b_s = \frac{\mathcal{F}_s}{\epsilon_H} \ , \qquad b_t = 4\mathcal{F}_t \ , \tag{B.16}$$

where

$$\mathcal{F}_s = \frac{1}{a}\frac{\mathrm{d}}{\mathrm{d}t}\left(\frac{a}{\Theta}\mathcal{G}_t^2\right) - \mathcal{F}_t \ , \qquad \mathcal{G}_s = \frac{\Sigma}{\Theta^2}\mathcal{G}_t^2 + 3\mathcal{G}_t \ , \tag{B.17}$$

and

$$\begin{aligned}
\mathcal{F}_t =& 2\left[G_4 - X\left(\ddot{\phi}G_{5,X} + G_{5,\phi}\right)\right] \ , \\
\mathcal{G}_t =& 2\left[G_4 - 2XG_{4,X} - X\left(H\dot{\phi}G_{5,X} - G_{5,\phi}\right)\right] \ , \\
\Sigma =& XG_{2,X} + 2X^2G_{2,XX} + 12H\dot{\phi}XG_{3,X} + 6H\dot{\phi}X^2G_{3,XX} - 2XG_{3,\phi} \\
& - 2X^2G_{3,\phi X} - 6H^2G_4 + 6\Big[H^2\left(7XG_{4,X} + 16X^2G_{4,XX} + 4X^3G_{4,XXX}\right) \\
& - H\dot{\phi}\left(G_{4,\phi} + 5XG_{4,\phi X} + 2X^2G_{4,\phi XX}\right)\Big] + 30H^3\dot{\phi}XG_{5,X} + 26H^3\dot{\phi}X^2G_{5,XX} \\
& + 4H^3\dot{\phi}X^3G_{5,XXX} - 6H^2X\left(6G_{5,\phi} + 9XG_{5,\phi X} + 2X^2G_{5,\phi XX}\right) \ , \\
\Theta =& -\dot{\phi}XG_{3,X} + 2HG_4 - 8HXG_{4,X} - 8HX^2G_{4,XX} + \dot{\phi}G_{4,\phi} + 2X\dot{\phi}G_{4,\phi X} \\
& - H^2\dot{\phi}\left(5XG_{5,X} + 2X^2G_{5,XX}\right) + 2HX\left(3G_{5,\phi} + 2XG_{5,\phi X}\right) \ .
\end{aligned} \tag{B.18}$$

B.2 Scalar-vector-tensor theories

We assume the line element in Eq. (B.1) and consider homogeneous scalar and vector field configurations, $\phi(t)$ and $A_\mu(t)$, the latter of which is given by

$$A_\mu(t) = (A_0(t)N(t), 0, 0, 0) \ , \tag{B.19}$$

where $A_0(t)$ is a time-dependent temporal vector component. Furthermore, the quantities $\{F, Y_1, Y_2, Y_3\}$, the last row of Eq. (4.14), corresponding to the sixth-order Lagrangian $\mathcal{L}_6$, and the interactions proportional to $\mathcal{M}_5^{\mu\nu}$ and $\mathcal{N}_5^{\mu\nu}$, do not affect the background cosmology. [1] Finally, the quantities X_1, X_2, X_3 are given, respectively, by

$$X_1 = \frac{\dot{\phi}^2}{2N^2} \ , \qquad X_2 = \frac{\dot{\phi}A_0}{2N} \ , \qquad X_3 = \frac{A_0^2}{2} \ . \tag{B.20}$$

With the above considerations, varying the action

$$\mathcal{S}_{\rm SVT} = \int \mathrm{d}^4x\sqrt{-g}\mathcal{L}_{\rm SVT} \ , \tag{B.21}$$

[1] Furthermore, the parity-violating term $\tilde{F}$ in f_2, Eq. (4.14), is not considered in this chapter as it was originally not considered in Ref. [223] for simplicity.

on the spacetime metric (B.1), with respect to N gives the constraint equation

$$6f_4H^2+f_2-\dot{\phi}^2f_{2,X_1}-\frac{1}{2}\dot{\phi}A_0f_{2,X_2}+6H\left(\dot{\phi}f_{4,\phi}-HA_0^2f_{4,X_3}\right)+2A_0H^2\left(3\dot{\phi}f_{5,\phi}-A_0^2Hf_{5,X_3}\right)=0\ . \quad \text{(B.22)}$$

Varying the action (B.22) with respect to the scale factor $a(t)$ yields the evolution equation

$$\begin{aligned}2f_4\left(2\dot{H}+3H^2\right)+f_2+2\dot{A}_0A_0^2\left(f_{3,X_3}+\tilde{f}_3\right)+2\dot{\phi}A_0f_{3,\phi}+2\left(\ddot{\phi}+2H\dot{\phi}\right)f_{4,\phi}\\ -2A_0\left[A_0\left(2\dot{H}+3H^2\right)+2\dot{A}_0H\right]f_{4,X_3}+2\dot{\phi}\dot{A}_0A_0f_{4,X_3\phi}+2\dot{\phi}^2f_{4,\phi\phi}\\ -4HA_0^2\left(\dot{A}_0A_0f_{4,X_3X_3}+\dot{\phi}f_{4,X_3\phi}\right)+\Big[2A_0\left(H\ddot{\phi}+\dot{H}\dot{\phi}\right)\\ +\dot{\phi}\left(2H\dot{A}_0+3H^2A_0\right)\Big]f_{5,\phi}-HA_0^2\left[2A_0\left(\dot{H}+H^2\right)+3\dot{A}_0H\right]f_{5,X_3}\\ +H\dot{\phi}A_0^2\left(2\dot{A}_0-HA_0\right)f_{5,X_3\phi}+HA_0\left(2\dot{\phi}^2f_{5,\phi\phi}-\dot{A}_0A_0^3Hf_{5,X_3X_3}\right)=0\ .\end{aligned} \quad \text{(B.23)}$$

The variation with respect to $\phi(t)$ gives the scalar-field equation of motion

$$\begin{aligned}\left(f_{2,X_1}+\dot{\phi}^2f_{2,X_1X_1}+\dot{\phi}A_0f_{2,X_1X_2}+\frac{1}{4}A_0^2f_{2,X_2X_2}\right)\ddot{\phi}+3Hf_{2,X_1}\dot{\phi}-f_{2,\phi}\\ +\dot{\phi}^2f_{2,X_1\phi}-6\left(\dot{H}+2H^2\right)f_{4,\phi}+\Bigg[\frac{1}{2}f_{2,X_2}+\frac{1}{2}\dot{\phi}^2f_{2,X_1X_2}+2f_{3,\phi}-3H^2f_{5,\phi}\\ +A_0\left(\dot{\phi}f_{2,X_1X_3}+\frac{1}{4}\dot{\phi}f_{2,X_2X_2}-6Hf_{4,X_3\phi}\right)+\frac{A_0^2}{2}\Big(f_{2,X_2X_3}-4\tilde{f}_{3,\phi}\\ -6H^2f_{5,X_3\phi}\Big)\Bigg]\dot{A}_0+\Bigg[\frac{1}{2}\dot{\phi}f_{2,X_2\phi}+\frac{3}{2}Hf_{2,X_2}+6Hf_{3,\phi}-6A_0H^2f_{4,X_3\phi}\\ -3H\left(2\dot{H}+3H^2\right)f_{5,\phi}-A_0^2H^3f_{5,X_3\phi}\Bigg]A_0=0\ ,\end{aligned} \quad \text{(B.24)}$$

whereas the variation with respect to A_0 gives the temporal-vector equation of motion

$$\begin{aligned}2\left(f_{2,X_3}+6H^2f_{4,X_3}-6H\dot{\phi}f_{4,X_3\phi}\right)A_0+12H^2f_{4,X_3X_3}A_0^3+2H^3f_{5,X_3X_3}A_0^4\\ -2\left(6Hf_{3,X_3}+6H\tilde{f}_3+2\dot{\phi}\tilde{f}_{3,\phi}-3H^3f_{5,X_3}+3H^2\dot{\phi}f_{5,X_3\phi}\right)A_0^2\\ +\left(f_{2,X2}+4f_{3,\phi}-6H^2f_{5,\phi}\right)\dot{\phi}=0\ .\end{aligned} \quad \text{(B.25)}$$

Notice from Eqs. (B.24) and (B.24) that the scalar field ϕ and the temporal vector component A_0 are coupled to each other in a non-trivial way (see Ref. [223] for an exhaustive discussion on the implications of this fact). For the particular model in Eq. (4.35), Eqs. (B.22)-(B.25) simplify to those given by Eqs. (4.37)-(4.40).

Part II

Scientific Research

PHYSICAL REVIEW D **91,** 083006 (2015)

Phenomenological approaches of inflation and their equivalence

Lotfi Boubekeur,[1,2] Elena Giusarma,[3] Olga Mena,[1] and Héctor Ramírez[1]

[1]*Instituto de Física Corpuscular (IFIC), CSIC-Universitat de Valencia, Apartado de Correos 22085, Valencia E-46071, Spain*

[2]*Laboratoire de Physique Mathématique et Subatomique (LPMS), Université de Constantine I, Constantine 25000, Algeria*

[3]*Physics Department and INFN, Università di Roma "La Sapienza," Ple Aldo Moro 2, 00185 Rome, Italy*

(Received 10 December 2014; published 20 April 2015)

In this work, we analyze two possible alternative and model-independent approaches to describe the inflationary period. The first one assumes a general equation of state during inflation due to Mukhanov, while the second one is based on the slow-roll hierarchy suggested by Hoffman and Turner. We find that, remarkably, the two approaches are equivalent from the observational viewpoint, as they single out the same areas in the parameter space, and agree with the inflationary attractors where successful inflation occurs. Rephrased in terms of the familiar picture of a slowly rolling, canonically normalized scalar field, the resulting inflaton excursions in these two approaches are almost identical. Furthermore, once the Galactic dust polarization data from Planck are included in the numerical fits, inflaton excursions can safely take sub-Planckian values.

DOI: 10.1103/PhysRevD.91.083006 PACS numbers: 98.70.Vc, 98.80.Bp, 98.80.Cq

I. INTRODUCTION

Despite its impressive observational success, the inflationary paradigm [1] is still lacking firm confirmation. The crucial missing piece of evidence is the B-mode's polarization pattern imprinted in the cosmic microwave background (CMB) at recombination by the inflationary stochastic gravitational waves (GWs). This observable is usually parametrized through the tensor-to-scalar ratio $r \equiv A_t/A_s$, where A_t and A_s are the amplitudes of the primordial tensor and scalar fluctuations,[1] respectively, at some pivot scale. The measurement of r is extremely useful because its magnitude directly determines the inflationary energy scale, when the modes observed now were stretched out of the horizon [2]. An additional piece of information is given by the scale dependence of the power spectrum of inflationary GWs. The accurate measurement of this last value would allow us to test the so-called standard inflationary *consistency relation* $n_t = -r/8$ [3]. However, such a measurement might turn out to be very challenging, especially when the amplitude of the B-modes is small [4]. In view of that, the measurement of n_t would entail an additional experimental challenge that might or might not be met in the future generation of CMB observations. One could be led to conclude that perhaps testing the inflationary consistency relation is not the best way to test the inflationary paradigm in its simplest realization, i.e. *single-field slow-roll inflation*. An alternative and easier way might be to test the consistency relation in each model of inflation, i.e. the relationship between r and n_s in each of the possible scenarios. For instance, the quadratic model $V \propto \phi^2$ predicts $r = -4(n_s - 1)$ at first order in slow roll. Such a consistency relation would be easier to test than the former one [5], given the present and forecasted accuracy in n_s and r. However, despite this encouraging feature, this approach is not model independent, as it assumes explicitly an underlying scenario with a peculiar inflationary potential to obtain results. On the other hand, more useful and robust ways to formulate the tests of inflation should ideally be model independent, capturing the generic features of inflation, without committing to a specific scenario. Said in other words, it would be more appealing to try to work out the inflationary predictions in a model-independent picture where the inflationary potential does not play a crucial role. This will enable us to avoid treating inflation on a case-by-case basis, but rather in a more general way. In this work, we address this important issue by considering two possible alternative model-independent approaches.

The recent BICEP2 claim of primordial GW detection [6,7] underlined the difficulties faced when trying to extract a primordial polarization signal from the ubiquitous Galactic foregrounds. Despite the general excitement in the community, soon after these results were released, several studies carried out a reassessment of the level of Galactic dust polarization in the BICEP2 field [8,9], questioning the cosmological origin of the BICEP2 signal.

[1]The scalar and tensor amplitudes are given by

$$A_s(k) = A_s\left(\frac{k}{k_0}\right)^{n_s-1+\frac{1}{2}\alpha_s \ln\left(\frac{k}{k_0}\right)},$$

$$A_t(k) = A_t\left(\frac{k}{k_0}\right)^{n_t},$$

where k_0 is the pivot scale, and n_s and n_t are the scalar and tensor spectral indices, respectively, while $\alpha_s \equiv dn_s/d\ln k$ is the running of the scalar tilt.

Recently, the Planck Collaboration [10] has released the results of the polarized Galactic dust emission measurements at 353 GHz in the BICEP2 field. By extrapolating these results to 150 GHz (the frequency where BICEP2 operates), they were able to test the level of dust contamination in the BICEP2 signal. The Planck analysis suggests that the BICEP2 signal could be, in principle, explained fully in terms of a dust component. However, given the large systematic uncertainties on the polarized dust signal, a joint analysis of Planck and BICEP2 data is mandatory, before giving a final interpretation of the BICEP2 signal.

In a previous study [11], we have shown that using a purely phenomenological parametrization of the inflationary period, the tension between the BICEP2 signal and previous upper bounds on r can be reduced significantly. In this work, and along the same lines, we explore two alternative approaches to describe the inflationary paradigm, confronting them with the most recent CMB temperature and polarization data. The first approach, considered in Ref. [11], is the Mukhanov parametrization of inflation [12], while the second one is the so-called inflationary Hubble flow formalism [13,14]. We will see that these two approaches appear to be physically equivalent, because, interestingly, both single out the same regions in the inflationary parameter space. These results suggest that, when analyzing inflationary predictions in a model-independent way, one should restrict attention to these regions in the parameter space, as they are the physical ones, ensuring therefore meaningful and robust constraints.

The rest of the paper is organized as follows: In Sec. II, we review the main features of the Mukhanov parametrization and explain its branches. Next, in Sec. III, we introduce the Hubble flow formalism and analyze its fixed points. Section IV is dedicated to the inflaton excursion. In Sec. V, we carry out the numerical analyses of both approaches. We end up by drawing our conclusions in Sec. VI.

II. MUKHANOV PARAMETRIZATION

In Ref. [12], an alternative and model-independent parametrization of the inflationary period was proposed (see Refs. [15,16] for a similar treatment). Without reference to a specific potential, one can assume the ansatz

$$p/\rho = -1 + \beta/(1+N_e)^{\alpha} \tag{1}$$

for the equation of state during inflation.[2] In the above ansatz, α and β are phenomenological parameters and are both positive and of $\mathcal{O}(1)$, and N_e is the number of remaining e-folds to end inflation. In this hydrodynamical picture, the predictions for the scalar tilt and tensor-to-scalar ratio are

$$n_s - 1 = -3\frac{\beta}{(N_*+1)^{\alpha}} - \frac{\alpha}{N_*+1}, \tag{2a}$$

$$r = \frac{24\beta}{(N_*+1)^{\alpha}}, \tag{2b}$$

where N_* stands for the number of e-folds at horizon crossing and it usually takes values around 60, depending mildly on the reheating details and on r as well. A general prediction of this ansatz is that the tilt is always *negative*, regardless of the inflationary scenario, while the tensor-to-scalar ratio can take any value depending on the parameters α, β, and N_*. Furthermore, the running of the tilt α_s is also always *negative*.

The Mukhanov parametrization captures a wide range of models with completely different predictions [12]. Notice, however, that this phenomenological description of the inflationary phase is not completely equivalent to the slow-roll picture, as there is no more freedom in the signs of both the tilt and the running.

A. Two branches

As noticed and explained in Ref. [11], the Mukhanov parametrization exhibits two distinct branches:

$$\text{Branch I}: \; r \approx 0 \quad \text{and} \quad n_s \leq 1. \tag{3a}$$

$$\text{Branch II}: \; n_s = 1 - \frac{r}{8}. \tag{3b}$$

The first branch contains, for instance, Starobinsky models [18], while the second one contains, among other models, the chaotic scenarios[3] $V(\phi) \propto \phi^n$ [21]. Because of the presence of these two branches, the observationally preferred value of the scalar spectral index $n_s \simeq 0.96$ will correspond to two different possible values of the tensor-to-scalar ratio, see Fig. 1. Coming back to the parametrization in terms of α and β, these two branches are recovered simply as the large- and small-α limits, i.e. $\alpha \gg 1$ and $\alpha \leq 1$, respectively. Indeed, combining Eq. (2a) and Eq. (2b), one gets

$$n_s = 1 - \frac{r}{8} - \frac{\alpha}{N_*+1}. \tag{4}$$

From the above expression, and remembering that both n_s and r still depend on α, we can easily get the two branches according to whether α is bigger or smaller than 1. In principle, the value of the phenomenological parameters α and β is unconstrained; however, as discussed in Ref. [11], it is sufficient to consider the range $0 \leq \beta \lesssim 1$

[2]For an extension of the above ansatz, see e.g. Ref. [17].

[3]The natural inflation scenario [19,20], $V(\phi) \propto [1+\cos(\phi/f)]$, is captured by the Mukhanov parametrization only for large enough decay constants $f \gtrsim 10 M_P$, which is indeed the regime compatible with observations.

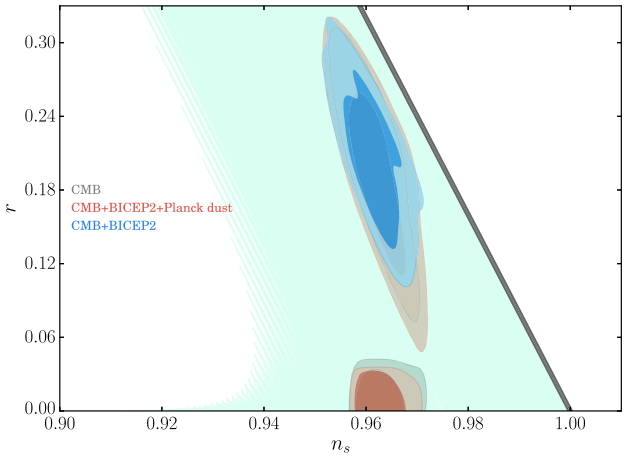

FIG. 1 (color online). Confidence intervals (68% and 95% C.L.) for the derived parameters n_s and r, using the Mukhanov parametrization, from the various data combinations considered in this work. The thick diagonal grey line represents branch II of Eq. (3), while the light green area displays the region covered by the Mukhanov parametrization for $N_* = 40$–70.

and $0 \leq \alpha \lesssim 3$. Let us recall some interesting limits of the parametrization Eq. (1). First, the chaotic scenarios $V \propto \phi^n$ correspond to the limiting case $\alpha = 1$, regardless of β. The power n appearing in the potential is given by $\beta = n/6$. Next, the other interesting limiting case is provided by Starobinski models corresponding to $\alpha = 2$ and $\beta = 1/2$ in Eq. (1). Finally, the special case $\alpha = 0$ corresponds to power-law inflation where the scale factor evolves as $a(t) \propto t^{\frac{2}{3\beta}}$ and $V \propto e^{-\sqrt{3\beta}\phi/M_P}$. In this scenario, inflation has a graceful exit problem; i.e., it never ends, and most probably the end of inflation is triggered by an additional field.

III. THE HUBBLE FLOW FORMALISM

In this picture, the basic parameter is the Hubble rate $H(\phi)$, and the dynamics can be completely specified without reference to a specific inflaton potential. In this *Hamilton-Jacobi* formulation of inflation, starting from $H(\phi)$ and its derivatives, one can construct a hierarchy of slow-roll parameters [13,14]. Such parameters start at first order with the usual slow-roll parameters[4]

$$\epsilon_{\rm H} \equiv 2M_P^2 \left(\frac{H'(\phi)}{H(\phi)}\right)^2, \tag{5}$$

$$\eta_{\rm H} \equiv 2M_P^2 \left(\frac{H''(\phi)}{H(\phi)}\right). \tag{6}$$

At higher orders, the slow-roll hierarchy is given by

$$^{\ell}\lambda_{\rm H} \equiv (2M_P^2)^{\ell} \frac{(H')^{\ell-1}}{H^{\ell}} \frac{d^{(\ell+1)}H}{d\phi^{(\ell+1)}}, \qquad \ell \geq 2. \tag{7}$$

These slow-roll parameters obey the infinite system of first-order differential equations:

$$\frac{d\epsilon_{\rm H}}{dN} = \epsilon_{\rm H}(\sigma_{\rm H} + 2\epsilon_{\rm H}), \tag{8}$$

$$\frac{d\sigma_{\rm H}}{dN} = -5\epsilon_{\rm H}\sigma_{\rm H} - 12\epsilon_{\rm H}^2 + 2(^2\lambda_{\rm H}), \tag{9}$$

$$\frac{d(^{\ell}\lambda_{\rm H})}{dN} = \left[\frac{\ell - 1}{2}\sigma_{\rm H} + (\ell - 2)\epsilon_{\rm H}\right]{}^{\ell}\lambda_{\rm H} + {}^{\ell+1}\lambda_{\rm H}, \tag{10}$$

where the tilt of the scalar spectrum is defined as $\sigma_{\rm H} \equiv 2\eta_{\rm H} - 4\epsilon_{\rm H}$. Notice that these flow equations are invariant under rescaling the Hubble rate. In principle, they can be integrated to arbitrarily high order in slow roll [22]. In practice, however, by truncating them at some order M, imposing $^{M+1}\lambda_{\rm H} = 0$, they become a closed system of differential equations that can be integrated once a set of initial conditions is specified.

A. Two fixed points

By inspection, one can determine the fixed points of the above inflationary flow equations. For instance, truncating at first order, it is straightforward to notice that they exhibit the following fixed points [13]:

$$\text{Fixed point I}: \; r = 0 \quad \text{and} \quad n_s = \text{const.} \tag{11}$$

$$\text{Fixed point II}: \; n_s = 1 - \frac{r}{8}. \tag{12}$$

Fixed point I can be either stable ($n_s - 1 > 1$) or unstable ($n_s - 1 < 0$) according to the sign of the tilt. We call these fixed points I-a and I-b, respectively. The Harrison-Zel'dovich spectrum $n_s = 1$ separates these two regions. Remarkably, the fixed points I-b and II of the Hubble flow equations overlap with the two different branches of the Mukhanov parametrization in Eq. (3). This is the first main result of this paper.

Considering the full set of equations, the fixed points are given by

$$\text{Fixed point I}: \; r = 0 \quad \text{and} \quad n_s = \text{const.} \tag{13}$$

$$\text{Fixed point II}: \; n_s = 1 - \frac{r}{8} \times \left[\frac{1}{1 - r/16}\right]. \tag{14}$$

The first fixed point, Eq. (13), coincides with the first-order one, and the stability analysis is the same. However, the second fixed point Eq. (14) is slightly different and corresponds to power-law scenarios [22], where $a(t) \propto t^{1/\epsilon_{\rm H}}$.

[4]As usual, the reduced Planck mass is given by $M_P = (8\pi G_N)^{-1/2} \simeq 2.43 \times 10^{18}$ GeV.

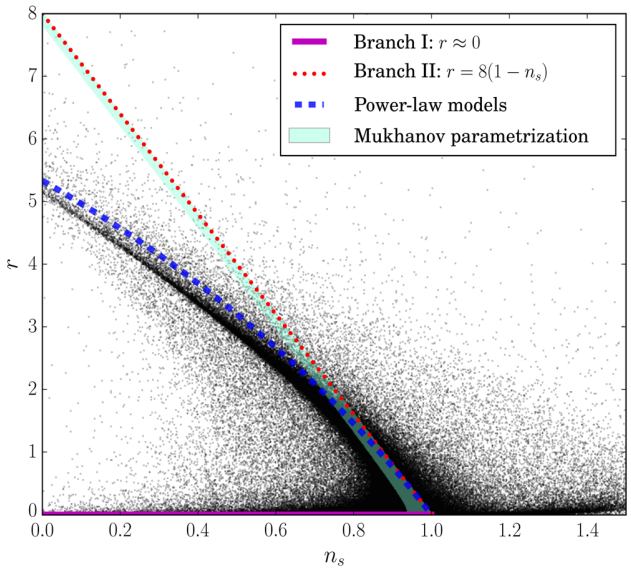

FIG. 2 (color online). The results of the Monte Carlo reconstruction using FLOWCODE1.0 of 2×10^6 models with wider priors than those shown in Eq. (15). The clustering around branch I and branch II is clearly visible. The three different lines refer to the two branches, together with the attractor for power-law models.

Notice that in this case, $\eta_{\rm H} = \epsilon_{\rm H}$, while ${}^{\ell+1}\lambda_{\rm H} = \epsilon_{\rm H}({}^{\ell}\lambda_{\rm H})$ for $\ell \geq 2$. Nevertheless, at small r, these fixed points coincide; the difference shows only at large r; see Fig. 2.

In order to solve the flow equations, we use the publicly available code `Flowcode1.0` [22] that adopts a Monte Carlo approach to reconstruct the inflationary potential. For more details on the methodology, see Refs. [22,23]. For related work using this methodology to obtain cosmological constraints on inflationary models, see also Ref. [24]. We generate a total of 6×10^6 inflationary models by drawing randomly the initial conditions of the slow-roll parameters from the following flat priors[5]:

$$\begin{aligned} N_* &= [50, 70], \\ \epsilon_{\rm H} &= [0., 0.8], \\ \sigma_{\rm H} &= [-0.1, 0.0], \\ {}^2\lambda_{\rm H} &= [-0.05, 0.05], \\ {}^3\lambda_{\rm H} &= [-0.025, 0.025], \\ &\cdots \\ {}^{M+1}\lambda_{\rm H} &= 0. \end{aligned} \tag{15}$$

As in Refs. [23], the slow-roll hierarchy is truncated at order $M = 8$ and the equations are evolved using `Flowcode1.0`. For illustration, we plot the results of reconstructing 2×10^6 inflationary models with wider priors in Fig. 2. As noticed in Ref. [13], models cluster around the attractors given by the fixed points. Figure 2 clearly shows this feature: in the (r, n_s) plane, the models populate the regions I-b and II, while the areas outside these regions are underpopulated.

[5]For orders $\ell \geq 2$, the width of the interval is reduced by a factor of 5 at each order.

IV. THE INFLATON EXCURSION

The Mukhanov parametrization is formulated independently of any scalar field; however, one can always recast the dynamics in the inflaton picture [12], where inflation is driven by a canonically normalized scalar field. In slow roll $\rho \simeq V$, the distance traveled by the inflaton during inflation, i.e. the inflaton excursion, can be written in terms of the Mukhanov phenomenological parameters as

$$\frac{\Delta\phi}{M_P} = \int_0^{N_*} dN \sqrt{\frac{3\beta}{(1+N)^{\alpha}}}. \tag{16}$$

For a related recent appraisal of the inflaton excursion, see e.g. Ref. [15]. The expression in Eq. (16) can be straightforwardly integrated, giving

$$\frac{\Delta\phi}{M_P} = \begin{cases} \sqrt{3\beta}\ln(N_* + 1) & \text{for } \alpha = 2. \\ \frac{\sqrt{3\beta}}{1-\frac{\alpha}{2}}[(N_* + 1)^{\frac{-\alpha+2}{2}} - 1] & \text{for } \alpha \neq 2. \end{cases} \tag{17}$$

For $\alpha \neq 2$, it is useful to consider the small-r limit of Eq. (4). Recall that CMB data prefers $\alpha > 2$ [11]. When $r \ll 8/N_*$, we can expand around $\alpha = 2$, and get

$$\frac{\Delta\phi}{M_P} \simeq \sqrt{\frac{r}{8}}(1 + N_*)\left[\ln(1 + N_*) + \frac{(\alpha - 2)}{4}\ln(1 + N_*)^2\right]. \tag{18}$$

Figure 3 shows the inflation excursion in this limit for the range $40 < N_\star < 70$ and $\alpha = 2.6$. Notice that the field excursion in this limit is small, as expected, due to the smaller r in this case. Meanwhile, for the opposite limit, i.e. for large r such that $r \gtrsim 8/N_*$, $\alpha \simeq 1$ (see Ref. [11]), and one gets

$$\frac{\Delta\phi}{M_P} \simeq 2\sqrt{\frac{r}{8}}N_*, \tag{19}$$

well above the original Lyth bound [25] (see also Refs. [26,27]) and in agreement with the predictions for chaotic inflationary scenarios $V(\phi) \propto \phi^n$. The predictions for the field excursion as a function of r for this regime are also shown in Fig. 3. Note that, in this case, large field excursions are correlated with large tensor-to-scalar ratios, as expected from the Lyth bound.

In Fig. 3, we show the *derived* inflaton excursion $\Delta\phi/M_P$ versus r in the Mukhanov parametrization arising

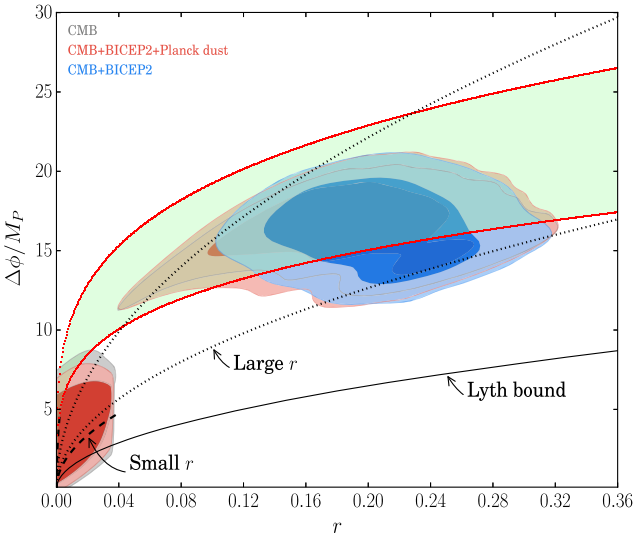

FIG. 3 (color online). Confidence intervals (68% and 95% C.L.) on the inflaton excursion versus the tensor-to-scalar ratio r from the various data combinations in the Mukhanov parametrization. The light green area represents the theoretical prediction of Eq. (21). The area between the dotted lines refers to the large-r limit [Eq. (19)], while the one between the dashed lines refers to the small-r limit [Eq. (18)]. Finally, the black line stands for the original Lyth bound. All the regions are computed for $N_* = 40$–70.

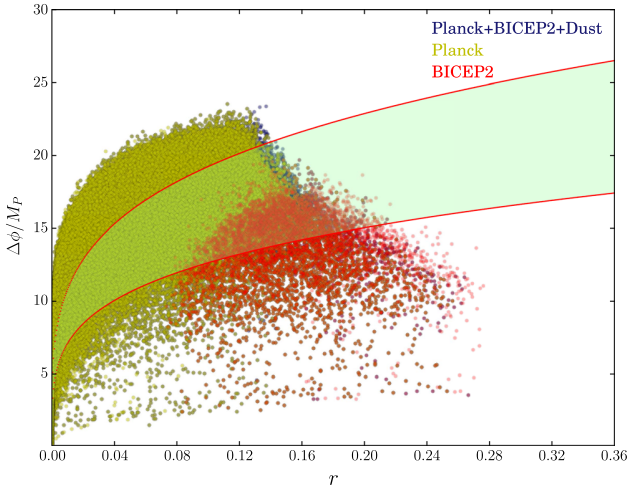

FIG. 4 (color online). The result of the Monte Carlo reconstruction of 6×10^6 inflationary models using FLOWCODE1.0, represented in the (r, n_s) plane. Here, the light green area represents the theoretical prediction in Eq. (21) for $N_* = 40$–70.

from our numerical fits to cosmological data, as we shall explain in the next section. The models cluster around the empirical Efstathiou-Mack relationship[6] [28] (see also Ref. [29])

$$\frac{\Delta\phi}{m_{\rm Pl}} \approx 6r^{1/4}. \tag{20}$$

Such expression has been understood analytically [27] as the prediction of the *quartic hilltop* inflation scenario where $V(\phi) = V_0 - \lambda\phi^4/4$. The general prediction for this scenario reads

$$\frac{\Delta\phi}{m_{\rm Pl}} = \frac{N_*^{3/4}}{2\sqrt{\pi}} r^{1/4}. \tag{21}$$

For $N_* = 60$, Eq. (21) simply reduces to the Efstathiou-Mack relationship, Eq. (20). Furthermore, Eq. (21) is a special case of the more general hilltop potentials parametrized as $V(\phi) = V_0[1 - \lambda_p(\phi/\mu)^p]$, where $p > 2$ and $M_P > \mu > 0$. It is straightforward to check that in the Mukhanov parametrization, this corresponds to setting $\alpha = 4$. The light green areas in Figs. 3 and 4 stand for the prediction given by Eq. (21), for N_* between 40 and 70.

[6]Notice that here we are using the Planck mass $m_{\rm Pl} = \sqrt{8\pi}M_P \simeq 1.22 \times 10^{19}$ GeV, instead of M_P, in order to compare with the original literature.

V. NUMERICAL ANALYSIS

In the following, we will analyze numerically both parametrizations using Markov Chain Monte Carlo (MCMC) methods.

A. Mukhanov parameterization

The Mukhanov scenario is described by

$$\{\omega_b, \omega_c, \Theta_s, \tau, \log[10^{10}A_s], \alpha, \beta, N_\star\}, \tag{22}$$

where $\omega_b \equiv \Omega_b h^2$ and $\omega_c \equiv \Omega_c h^2$ are the physical baryon and cold dark matter energy densities, respectively, Θ_s is the ratio between the sound horizon and the angular diameter distance at decoupling, τ is the reionization optical depth, A_s is the amplitude of the primordial spectrum, and α and β are the parameters governing the Mukhanov parameterization. For the sake of simplicity, we have assumed that the dark energy component is described by a cosmological constant. Table I specifies the priors considered on the cosmological parameters listed above. Notice that this analysis is different from the ones presented in Ref. [11], as we are also varying here the number of e-folds $N_\star$ to compute the inflaton excursion. The commonly used (r, n_s) parameters can be easily recovered using Eqs. (2), and the running for this inflationary scheme is completely fixed, see e.g. Refs. [11,12]. The field excursion is computed using Eq. (17). In our analysis, we also assume the so-called inflation consistency relation ($n_t = -r/8$), which still holds in the Mukhanov phenomenological model.[7] In

[7]For recent cosmological analyses relaxing this condition, see Ref. [30].

TABLE I. Uniform priors on the cosmological parameters used in the CosmoMC analyses of the Mukhanov parametrization.

Parameter	Physical meaning	Prior
$\Omega_b h^2$	Present baryon density	$0.005 \to 0.1$
$\Omega_c h^2$	Present Cold dark matter density	$0.001 \to 0.99$
Θ_s	Ratio between the sound horizon and the angular diameter distance at decoupling	$0.5 \to 10$
τ	Reionization optical depth	$0.01 \to 0.8$
$\log(10^{10} A_s)$	Amplitude of the primordial scalar spectrum	$2.7 \to 4$
α	Phenomenological parameter of the Mukhanov parametrization Eq. (1)	$0 \to 2.5$
β	Phenomenological parameter of the Mukhanov parametrization Eq. (1)	$0 \to 1$
$N_\star$	Number of e-folds at horizon crossing	$50 \to 70$

order to compute the allowed regions in the derived parameter spaces (r, n_s) and $(r, \Delta\phi)$, we make use of the CAMB Boltzmann code [31], deriving posterior distributions for the cosmological parameters by means of a MCMC analysis, performed using `CosmoMC` [32].

The basic data set used for our numerical analyses includes the Planck CMB temperature anisotropies data [33,34] together with the WMAP 9-year polarization data [35]. The total likelihood for the former data is obtained by means of the Planck Collaboration publicly available likelihood code; see Ref. [34] for details. The Planck temperature power spectrum reaches a maximum multipole number $\ell_{\rm max} = 2500$, while the WMAP 9-year polarization data are analyzed up to a maximum multipole $\ell = 23$ [35]. We shall refer to the basic data set in the following as CMB data.

We have also considered the BICEP2 measurements of the tensor-to-scalar ratio $r = 0.2^{+0.07}_{-0.05}$ [6,7]. These measurements are included in our analysis by postprocessing the chains that were previously generated, using the likelihood code released by the BICEP2 experiment, including the nine bandpowers from multipoles $\ell \sim 45$ to $\ell \sim 300$. The recent estimates of the Galactic dust polarized emission carried out by the Planck Collaboration in Ref. [10] have also been included in our numerical fits. For the former purpose, we have added the dust power spectrum measured by Planck in the $40 < \ell < 120$ multipole range, $D^{BB}_\ell \equiv \ell(\ell+1)/2\pi C^{BB}_\ell = 1.32 \times 10^{-2}\ \mu\mathrm{K}^2$, to the theoretical B-mode spectra in the same multipole range, in order to evaluate the likelihood of the total signal resulting from the addition of gravitational lensing, primordial B-modes, and dust B-mode contributions. The statistical and the interpolation-induced uncertainties of the Planck dust analysis are accounted for by including them in the BICEP2 covariance matrix. We then use this Planck-dust-plus-BICEP2 likelihood to postprocess the chains previously obtained by the Planck temperature and WMAP9 polarization likelihoods. We multiply the original weight of each model by the Planck-dust-plus-BICEP2 likelihood, using the new weights to derive the allowed cosmological parameter regions by Planck CMB data, Planck dust polarization measurements and BICEP2.

In Fig. 1, we plot the 68% and 95% confidence regions in the plane of the *derived* parameters n_s and r. We also superimpose the region covered by the Mukhanov parametrization for $40 \leq N_* \leq 70$; see Eqs. (2a) and (2b). We represent the MCMC results for the three possible data combinations. Notice that CMB data alone shows a mild preference for the branch I region (with a negligible tensor-to-scalar ratio r), since there is no 68%-C.L.-allowed contour in the branch II region. The inclusion of BICEP2 measurements to CMB data isolates the branch II region as the allowed one at 95% C.L., favoring inflationary scenarios with a relatively large tensor-to-scalar ratio, like for instance chaotic inflationary models. However, once the Galactic polarized dust emission from the Planck experiment is taken into account in the BICEP2 likelihood, there is no difference between the branch I and branch II regions, as both regions are equally allowed by the data.

Figure 3 shows the 68%- and 95%-C.L.-allowed regions in the plane of the *derived* parameters r and $\Delta\phi$. As previously stated, to derive $\Delta\phi$, we have used Eq. (17). We also plot the theoretical relationship in Eq. (21) for $40 \leq N_\star \leq 70$. Notice that the area covered by this relationship perfectly agrees with the parameter regions preferred by current cosmological data. Notice as well that CMB data alone favours relatively small inflaton excursions, as this is the expected behavior in scenarios in which r is tiny, like for instance in Starobinsky models, belonging to branch I. The inclusion of BICEP2 data favors instead large inflation excursions, i.e. $\Delta\phi/M_P \sim 20$, at 95% C.L. Such large excursions have been argued to render the validity of effective field theory questionable. In this regime, nonrenormalizable operators $\mathcal{O}_{n+4} = c_n \phi^{n+4}/M_P^n$ are expected to dominate the inflationary potential, compromising its flatness, even in the regime of validity of classical general relativity $V \ll M_P^4$. Suppressing such operators is only possible if the shift symmetry $\phi \to \phi + c$ is *only* broken softly at the renormalizable level. However, since in general this symmetry is a mere global symmetry, it is likely to be badly broken by gravity, producing the nonrenormalizable operators $\mathcal{O}_{n+4}$. Furthermore, embedding the theory in a

framework where shift symmetry descends from a local symmetry leads to inconsistencies [36].

However, for sub-Planckian inflaton excursions, the problems discussed above are less severe. Fortunately, once the Planck dust polarization measurements are included in the analyses together with CMB and BICEP2 data, the small excursion region becomes allowed at the 95% C.L., and therefore trans-Planckian field values are no longer absolutely required to explain observations. This is the second main result of this study.

B. The Hubble flow formalism

We have performed as well an analysis of the 6×10^6 models resulting from integrating the Hubble flow equations, using the priors in Eq. (15). For each of these models, we have computed the likelihood by means of the covariance matrices resulting from three different MCMC runs with flat priors in n_s, r and α_s.[8] The former three runs correspond to the three possible data combinations considered in this study, namely, CMB data alone, CMB plus BICEP2 measurements, and finally, CMB plus BICEP2 plus Planck dust polarization measurements. The covariance matrices were previously marginalized over the remaining cosmological parameters that are irrelevant for our purposes.

Figure 4 shows the analogue of Fig. 3 but for the Hubble flow analysis in the $(r, \Delta\phi)$ plane. The models depicted are allowed at the 95% C.L. by the three different data sets. We also include in Fig. 4 the theoretical prediction from Eq. (21) for $40 \leq N_\star \leq 70$. Notice that the allowed regions for the inflationary Hubble flow approach almost coincide with those arising from the Mukhanov parametrization, and consequently these two approaches are equivalent from the point of view of data analyses.

VI. DISCUSSION AND CONCLUSIONS

Unraveling the source of primordial curvature perturbations is one of the key purposes of modern cosmology, both from a theoretical and an observational viewpoint. The inflationary paradigm is the leading mechanism that provides such initial conditions. In this regard, when testing the inflationary predictions against cosmological measurements, the approach used to describe inflation is crucial. The most familiar picture is based on the dynamics of a friction-dominated scalar field. However, this description, although useful, is always model dependent, as the predictions for the cosmological observables will largely depend on the inflationary potential. Furthermore, when embedded in a consistent fundamental theory, the shape of this latter is usually difficult to understand. In this work, we focused on two model-independent approaches that might alleviate the above problems. The first one is a pure theoretical formulation, the Mukhanov parametrization, in which inflation is described via an effective equation of state. The second approach is a pure phenomenological one, which deals with the reconstruction of the inflationary trajectory via the slow-roll hierarchy. We showed that the allowed parameter regions arising from fitting these two approaches to current CMB data (temperature and polarization) agree with the expected fixed-point solutions. Remarkably, the parameter regions recovered from both model-independent methods are almost identical. Our results thus suggest that these two approaches are the most suitable ones to constrain the inflationary parameters, as they are independent of the inflaton potential details while ensuring a successful inflationary period.

Another problem that we touched upon in this work is the issue of super-Planckian inflaton field values. Such large excursions have been argued to cause the breakdown of effective theories (see e.g. Refs. [38,39]). At small inflaton values, the effective theory approach makes sense, and no additional fine-tuning is required to make the potential flat. However, once the inflaton reaches super-Planckian values, it is really difficult to justify the absence, or at most the extreme suppression, of higher-order nonrenormalizable terms in the inflaton potential, without the knowledge of a UV-complete theory. The BICEP2 Collaboration [6] has claimed the detection of B-modes on large scales. If the primordial nature of this signal is confirmed, then it would constitute an unmistakable smoking gun of inflation. Furthermore, the amplitude of the detected signal suggests that, if we insist on describing inflation as a scalar field dynamics, then the regime of super-Planckian excursions should be consistently understood. In this work, we have reconstructed the inflaton excursion using the two approaches described above. Our analyses indicate that the inflaton excursions required to explain the BICEP2 data can take sub-Planckian values once the Galactic dust polarized signal measured by Planck is accounted for. As a consequence, the validity of effective field theories to describe inflation as a scalar field dynamics still holds. The forthcoming polarization data release from the Planck Collaboration will fortunately shed light on this crucial issue.

[8]The authors of Ref. [37] performed a MCMC analysis considering the Hubble flow parameters as free parameters, deriving constraints on n_s, r and α_s. However, the resulting cosmological constraints on these derived parameters are not significantly affected, and their bounds were similar to those found in the case in which the parameters n_s, r and α_s are free parameters in the Monte Carlo. Therefore, we shall use the likelihood in terms of n_s, r and α_s rather than in terms of the Hubble flow parameters.

ACKNOWLEDGMENTS

O. M. is supported by Consolider Ingenio Project No. CSD2007-00060, by PROMETEO/2009/116, by Spanish Ministry Science Project No. FPA2011-29678 and by ITN Invisibles No. PITN-GA-2011-289442. We also thank the Spanish MINECO (Centro de excelencia Severo Ochoa Program) under Grant No. SEV-2012-0249.

[1] A. H. Guth, The inflationary universe: A possible solution to the horizon and flatness problems, Phys. Rev. D **23**, 347 (1981); A. Albrecht and P. J. Steinhardt, Cosmology for Grand Unified Theories with Radiatively Induced Symmetry Breaking, Phys. Rev. Lett. **48**, 1220 (1982).

[2] D. H. Lyth, A bound on inflationary energy density from the isotropy of the microwave background, Phys. Lett. **147B**, 403 (1984);

[3] A. R. Liddle and D. H. Lyth, COBE, gravitational waves, inflation and extended inflation, Phys. Lett. B **291**, 391 (1992).

[4] S. Dodelson, How Much Can We Learn about the Physics of Inflation? Phys. Rev. Lett. **112**, 191301 (2014).

[5] P. Creminelli, D. López Nacir, M. Simonović, G. Trevisan, and M. Zaldarriaga, ϕ^2 or Not ϕ^2: Testing the Simplest Inflationary Potential, Phys. Rev. Lett. **112**, 241303 (2014).

[6] P. A. R. Ade *et al.* (BICEP2 Collaboration), Detection of B-Mode Polarization at Degree Angular Scales by BICEP2, Phys. Rev. Lett. **112**, 241101 (2014).

[7] P. A. R. Ade *et al.* (BICEP2 Collaboration), BICEP2 II: Experiment and three-year data set, Astrophys. J. **792**, 62 (2014).

[8] M. J. Mortonson and U. Seljak, A joint analysis of Planck and BICEP2 B modes including dust polarization uncertainty, J. Cosmol. Astropart. Phys. 10 (2014) 035.

[9] R. Flauger, J. C. Hill, and D. N. Spergel, Toward an understanding of foreground emission in the BICEP2 region, J. Cosmol. Astropart. Phys. 08 (2014) 039.

[10] R. Adam *et al.* (Planck Collaboration), Planck intermediate results. XXX. The angular power spectrum of polarized dust emission at intermediate and high Galactic latitudes, arXiv:1409.5738.

[11] L. Barranco, L. Boubekeur, and O. Mena, A model-independent fit to Planck and BICEP2 data, Phys. Rev. D **90**, 063007 (2014).

[12] V. Mukhanov, Quantum cosmological perturbations: Predictions and observations, Eur. Phys. J. C **73**, 2486 (2013).

[13] M. B. Hoffman and M. S. Turner, Kinematic constraints to the key inflationary observables, Phys. Rev. D **64**, 023506 (2001).

[14] J. E. Lidsey, A. R. Liddle, E. W. Kolb, E. J. Copeland, T. Barreiro, and M. Abney, Reconstructing the inflation potential: An overview, Rev. Mod. Phys. **69**, 373 (1997).

[15] J. Garcia-Bellido, D. Roest, M. Scalisi, and I. Zavala, The Lyth bound of inflation with a tilt, Phys. Rev. D **90**, 123539 (2014).

[16] D. Roest, Universality classes of inflation, J. Cosmol. Astropart. Phys. 01 (2014) 007.

[17] J. Garcia-Bellido and D. Roest, Large-N running of the spectral index of inflation, Phys. Rev. D **89**, 103527 (2014).

[18] A. A. Starobinsky, A new type of isotropic cosmological models without singularity, Phys. Lett. **91B**, 99 (1980).

[19] K. Freese, J. A. Frieman, and A. V. Olinto, Natural Inflation with Pseudo-Nambu-Goldstone Bosons, Phys. Rev. Lett. **65**, 3233 (1990).

[20] F. C. Adams, J. R. Bond, K. Freese, J. A. Frieman, and A. V. Olinto, Natural inflation: Particle physics models, power law spectra for large scale structure, and constraints from COBE, Phys. Rev. D **47**, 426 (1993).

[21] A. D. Linde, Chaotic inflation, Phys. Lett. **129B**, 177 (1983).

[22] W. H. Kinney, Inflation: Flow, fixed points and observables to arbitrary order in slow roll, Phys. Rev. D **66**, 083508 (2002).

[23] R. Easther and W. H. Kinney, Monte Carlo reconstruction of the inflationary potential, Phys. Rev. D **67**, 043511 (2003).

[24] W. H. Kinney, E. W. Kolb, A. Melchiorri, and A. Riotto, Inflation model constraints from the Wilkinson Microwave Anisotropy Probe three-year data, Phys. Rev. D **74**, 023502 (2006); Latest inflation model constraints from cosmic microwave background measurements, Phys. Rev. D **78**, 087302 (2008).

[25] D. H. Lyth, What Would We Learn by Detecting a Gravitational Wave Signal in the Cosmic Microwave Background Anisotropy? Phys. Rev. Lett. **78**, 1861 (1997).

[26] L. Boubekeur and D. H. Lyth, Hilltop inflation, J. Cosmol. Astropart. Phys. 07 (2005) 010.

[27] L. Boubekeur, Theoretical bounds on the tensor-to-scalar ratio in the cosmic microwave background, Phys. Rev. D **87**, 061301 (2013).

[28] G. Efstathiou and K. J. Mack, The Lyth bound revisited, J. Cosmol. Astropart. Phys. 05 (2005) 008.

[29] L. Verde, H. Peiris, and R. Jimenez, Optimizing CMB polarization experiments to constrain inflationary physics, J. Cosmol. Astropart. Phys. 01 (2006) 019.

[30] M. Cortês, A. R. Liddle, and D. Parkinson, Tensors, BICEP2, prior dependence, and dust, arXiv:1409.6530.

[31] A. Lewis, A. Challinor, and A. Lasenby, Efficient computation of CMB anisotropies in closed FRW models, Astrophys. J. **538**, 473 (2000).

[32] A. Lewis and S. Bridle, Cosmological parameters from CMB and other data: A Monte-Carlo approach, Phys. Rev. D **66**, 103511 (2002).

[33] P. A. R. Ade *et al.* (Planck Collaboration), Planck 2013 results. I. Overview of products and scientific results, Astron. Astrophys. **571**, A1 (2014).

[34] P. A. R. Ade *et al.* (Planck Collaboration), Planck 2013 results. XV. CMB power spectra and likelihood, Astron. Astrophys. **571**, A15 (2014).

[35] C. L. Bennett *et al.* (WMAP Collaboration), Nine-year Wilkinson Microwave Anisotropy Probe (WMAP) observations: Final maps and results, Astrophys. J. Suppl. Ser. **208**, 20 (2013).

[36] T. Banks, M. Dine, P. J. Fox, and E. Gorbatov, On the possibility of large axion decay constants, J. Cosmol. Astropart. Phys. 06 (2003) 001.

[37] C. R. Contaldi and J. S. Horner, Planck and WMAP constraints on generalised Hubble flow inflationary trajectories, J. Cosmol. Astropart. Phys. 08 (2014) 050.

[38] J. P. Conlon, Quantum gravity constraints on inflation, J. Cosmol. Astropart. Phys. 09 (2012) 019.

[39] L. Boubekeur, On the scale of New Physics in inflation, arXiv:1312.4768.

PHYSICAL REVIEW D **91,** 103004 (2015)

Do current data prefer a nonminimally coupled inflaton?

Lotfi Boubekeur,[1,2] Elena Giusarma,[3] Olga Mena,[1] and Héctor Ramírez[1]

[1]*Instituto de Física Corpuscular (IFIC), CSIC-Universitat de Valencia, Apartado de Correos 22085, E-46071 Valencia, Spain*

[2]*Laboratoire de Physique Mathématique et Subatomique (LPMS) Université de Constantine I, Constantine 25000, Algeria*

[3]*Physics Department and INFN, Università di Roma "La Sapienza," Ple Aldo Moro 2, 00185 Rome, Italy*

(Received 23 February 2015; revised manuscript received 16 April 2015; published 19 May 2015)

We examine the impact of a nonminimal coupling of the inflaton to the Ricci scalar, $\frac{1}{2}\xi R\phi^2$, on the inflationary predictions. Such a nonminimal coupling is expected to be present in the inflaton Lagrangian on fairly general grounds. As a case study, we focus on the simplest inflationary model governed by the potential $V \propto \phi^2$, using the latest combined 2015 analysis of *Planck* and the BICEP2/*Keck* Array. We find that the presence of a coupling ξ is favored at a significance of 99% C.L., assuming that nature has chosen the potential $V \propto \phi^2$ to generate the primordial perturbations and a number of e-foldings $N = 60$. Within the context of the same scenario, we find that the value of ξ is different from zero at the 2σ level. When considering the cross-correlation polarization spectra from the BICEP2/*Keck* Array and *Planck*, a value of $r = 0.038^{+0.039}_{-0.030}$ is predicted in this particular nonminimally coupled scenario. Future cosmological observations may therefore test these values of r and verify or falsify the nonminimally coupled model explored here.

DOI: 10.1103/PhysRevD.91.103004 PACS numbers: 98.70.Vc, 98.80.Cq

I. INTRODUCTION

Inflation provides the most theoretically attractive and observationally successful cosmological scenario able to generate the initial conditions of our Universe, while solving the standard cosmological problems. Despite this remarkable success, the inflationary paradigm is still lacking firm observational confirmation. The picture that emerges from the latest data from *Planck*, including also the joint analysis of B-mode polarization measurements from the BICEP2 Collaboration [1–4], is compatible with the inflationary paradigm. According to these observations, structure grows from Gaussian and adiabatic primordial perturbations. From the theoretical viewpoint, this picture is usually understood as the dynamics of a single new scalar degree of freedom, *the inflaton*, minimally coupled to Einstein gravity. However, the inflaton ϕ is expected to have a nonminimal coupling to the Ricci scalar through the operator $\frac{1}{2}\xi R\phi^2$, where ξ is a dimensionless coupling. Indeed, successful reheating requires that the inflaton is coupled to the light degrees of freedom. Such couplings, though weak, will induce a nontrivial running for ξ. Thus, even starting from a vanishing value of ξ (away from the conformal fixed point $\xi = -1/6$) at some energy scale, a nontrivial nonminimal coupling will be generated radiatively at some other scale (see e.g. Ref. [5]). Therefore, it is important to study the impact of such a coupling on the inflationary predictions, especially in view of the latest *Planck* 2015 data.

Generically, for successful inflation, the inflaton should be very weakly coupled.[1] It follows that the magnitude of ξ is expected to be small. Yet, even with such a suppressed coupling, the inflationary predictions are significantly altered [6–16]. For instance, and as we will see, a small and positive ξ can enlarge considerably the space of phenomenologically acceptable scenarios (see also [17]). In this paper, we will focus on the simplest inflationary scenario with a potential $V \propto \phi^2$ [18], and a nonzero nonminimal coupling. According to the very recent *Planck* 2015 full mission results, the minimally coupled version of this scenario (i.e. $\xi = 0$) is ruled out at more than 99% confidence level [2,4], for 50 e-folds of inflation. Nevertheless, the $N = 60$ case is only moderately disfavoured at 95% C.L. Thus, before discarding it definitely from the range of theoretical possibilities, it is worthwhile to explore this scenario in all generality (considering as well different possibilities for the number of e-folds), given that, as explained earlier, the presence of nonminimal couplings in the inflaton Lagrangian is quite generic.

[1]This requirement is also dictated by the nondetection of large primordial non-Gaussianities [3] and the soft breaking of the shift symmetry $\phi \to \phi + c$, necessary to protect the flatness of the potential.

II. NONMINIMALLY COUPLED INFLATON

The dynamics of a nonminimally coupled scalar field ϕ with a potential $U(\phi)$ is governed, in the Jordan frame, by the following action[2]:

$$S=\int \mathrm{d}^4x\sqrt{-g}\left[\frac{M_P^2}{2}R+\frac{\xi}{2}R\phi^2-\frac{1}{2}(\partial\phi)^2-U(\phi)\right], \quad (1)$$

where indices are contracted with the metric $g_{\mu\nu}$, defined as $\mathrm{d}s^2=-\mathrm{d}t^2+a^2(t)\mathrm{d}x^2$. Inflation can be conveniently studied in the Einstein frame, after performing a conformal transformation $g^E_{\mu\nu}=\Omega(\phi)g_{\mu\nu}$, with $\Omega\equiv 1+\xi\phi^2/M_P^2$ and canonically normalizing the scalar field. Up to a total derivative, the action takes the familiar form

$$S=\int \mathrm{d}^4x\sqrt{-g_E}\left(\frac{M_P^2}{2}R_E-\frac{1}{2}g_E^{\mu\nu}\partial_\mu\varphi\partial_\nu\varphi-V[\phi(\varphi)]\right), \quad (2)$$

where now φ is the canonically normalized inflaton, related to the original nonminimally coupled scalar field ϕ through

$$\left(\frac{\mathrm{d}\varphi}{\mathrm{d}\phi}\right)^2=\frac{1}{\Omega}+\frac{3}{2}M_P^2\left(\frac{\Omega'}{\Omega}\right)^2. \quad (3)$$

In terms of the original scalar field ϕ, the physical potential takes the simple form

$$V[\varphi(\phi)]=U(\phi)/\Omega^2(\phi). \quad (4)$$

In the following, as previously stated, we shall focus on the simplest inflationary model. A generalization to other interesting inflationary scenarios, as for instance, the Higgs inflation model [19], will be carried out elsewhere [20]. The simplest scenario is given by the quadratic potential $U(\phi)=\frac{1}{2}m^2\phi^2$, with a nonvanishing coupling ξ. In order to derive the primordial scalar and tensor perturbation spectra within the nonminimally coupled ϕ^2 theory, we shall make use of the slow-roll parameters[3]:

$$\epsilon\equiv\frac{M_P^2}{2}\left(\frac{V_\varphi}{V}\right)^2, \qquad \eta\equiv M_P^2\frac{V_{\varphi\varphi}}{V}, \qquad \xi_{\mathrm{SR}}\equiv M_P^4\frac{V_\varphi V_{\varphi\varphi\varphi}}{V^2}. \quad (5)$$

It is straightforward to derive the expressions for the spectral index of the primordial scalar perturbations $n_s\equiv 1+2\eta-6\epsilon$, its running $\alpha\equiv \mathrm{d}n_s/\mathrm{d}\ln k\equiv -24\epsilon^2+16\epsilon\eta-2\xi_{\mathrm{SR}}$, and the tensor-to-scalar ratio $r\equiv 16\epsilon$ from the above slow-roll parameters.[4]

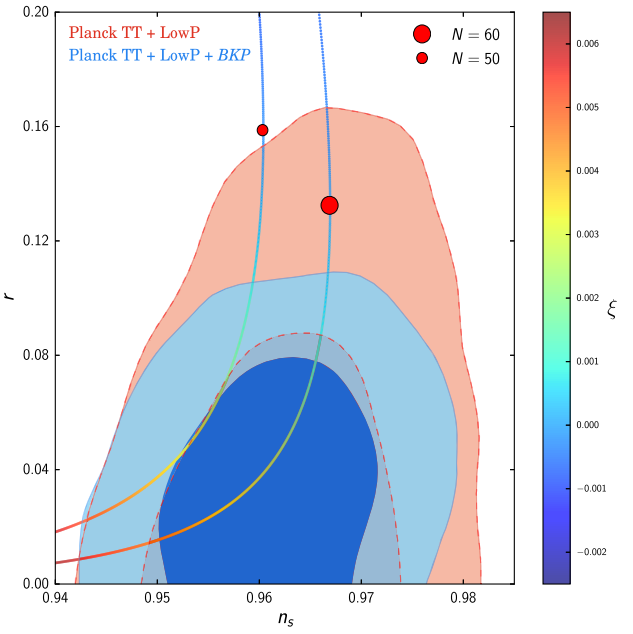

FIG. 1 (color online). Theoretical predictions for the chaotic model $V\propto\phi^2$ with a nonminimal coupling ξ in the (n_s, r) plane for $N=50$ and $N=60$. The red circles represent the $\xi=0$ case, corresponding to the usual predictions of the chaotic inflationary scenario. We show as well the 68% and 95% confidence level regions arising from the usual analyses in the (n_s, r) plane using the various data combinations considered here.

Within the slow-roll approximation, one can easily solve numerically the inflationary dynamics governed by the action Eq. (2). The number of e-folds is given by

$$N=\frac{1}{M_P}\int_{\varphi_{\mathrm{end}}}^{\varphi_*}\frac{\mathrm{d}\varphi}{\sqrt{2\epsilon(\varphi)}}=\frac{1}{M_P}\int_{\phi_{\mathrm{end}}}^{\phi_*}\frac{\mathrm{d}\phi}{\sqrt{2\epsilon(\phi)}}\left(\frac{\mathrm{d}\varphi}{\mathrm{d}\phi}\right), \quad (6)$$

where $\epsilon(\phi)\equiv\frac{M_P^2}{2}[V'(\phi)/V(\phi)]^2$.

The inflationary theoretical predictions for the $N=50$ and $N=60$ cases are depicted in Fig. 1, in the (n_s, r) plane, for both positive and negative values of the coupling ξ. The case of $\xi=0$ corresponds to the usual predictions of the chaotic inflationary scenario, with $n_s=1-2/N\simeq 0.967$ ($n_s\simeq 0.96$) and $r=8/N\simeq 0.13$ ($r\simeq 0.16$) for $N=60$ ($N=50$), and it is represented by red circles. Notice that negative values of ξ lead to a larger tensor-to-scalar

[2]As usual, $M_P=1/\sqrt{8\pi G_N}\simeq 2.43\times 10^{18}$ GeV is the reduced Planck mass.

[3]Here, we use the notation $\xi_{\mathrm{SR}}(\varphi)$ to refer to the usual slow-roll parameter ξ, in order to avoid confusion with the nonminimal coupling to gravity ξ.

[4]Notice that the expressions for both n_s and r are first order in slow roll, while α involves second order slow-roll terms. However, we have checked numerically that such second order corrections in slow roll leave unchanged the constraints on the inflationary observables (n_s, r). Therefore, higher order slow-roll corrections can be safely neglected.

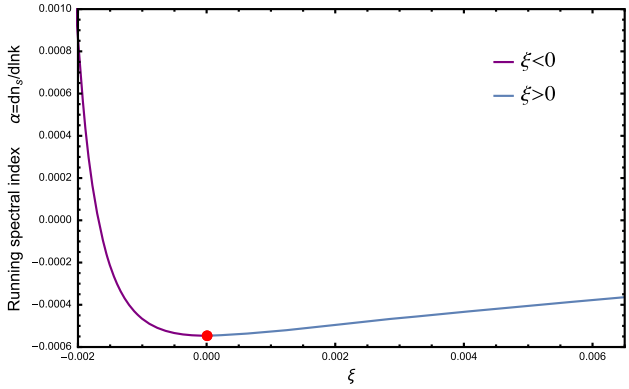

FIG. 2 (color online). The running α as a function of the nonminimal coupling ξ. The red circle represents the minimal coupling case $\xi = 0$.

ratio. Positive values of ξ, on the other hand, will reduce the tensor contribution, while also pushing n_s significantly below scale invariance as ξ increases. For instance, for $\xi > 0.002$ and $N = 60$, the scalar spectral index will always be smaller than the observationally preferred value $n_s \simeq 0.96$.

The predicted running of the spectral index α is shown in Fig. 2 as a function of the nonminimal coupling ξ. In general, negative (positive) values of ξ lead to positive (negative) values of the running. Although the large positive values of the running shown in Fig. 2 are compatible with the recent *Planck* 2015 constraints [2], $\alpha = -0.0065 \pm 0.0076$, they are nevertheless associated with values of the tensor-to-scalar ratio $r > 0.5$, which are excluded observationally. The red circle in Fig. 2 refers to the $\xi = 0$ case, corresponding to $\alpha = -2/N^2 \simeq -0.00056$ for $N = 60$.

III. OBSERVATIONAL CONSTRAINTS ON ξ IN THE QUADRATIC INFLATIONARY MODEL

In this paper, we restrict our numerical fits to cosmic microwave background (CMB) measurements. The inclusion of external data sets, such as baryon acoustic oscillation measurements, or a Hubble constant prior from the HST team will not affect the constraints presented in the following. Our data sets are the *Planck* temperature data (hereafter TT) [21–23], together with the low-ℓ WMAP 9-year polarization likelihood, that includes multipoles up to $\ell = 23$ (hereafter WP; see Ref. [24]), and the recent multicomponent likelihood of the joint analysis of the BICEP2/*Keck* Array and *Planck* polarization maps (hereafter BKP), following the data selection and foreground parameters of the fiducial analysis presented in Ref. [1].[5]

[5]This fiducial analysis assumes a tensor spectral index $n_T = 0$, the *BB* bandpowers of BICEP2/*Keck* Array and the 217 and 353 GHz bands of *Planck*, in the multipole range $20 < \ell < 200$.

TABLE I. Uniform priors for the cosmological parameters considered in the present analysis.

Parameter	Physical meaning	Prior
$\omega_b \equiv \Omega_b h^2$	Present baryon density	$0.005 \to 0.1$
$\omega_c \equiv \Omega_c h^2$	Present cold dark matter density	$0.01 \to 0.99$
Θ_s	$r_s/D_A(z_{\rm dec})$[a]	$0.5 \to 10$
τ	Reionization optical depth	$0.01 \to 0.8$
$\ln(10^{10}A_s)$	Primordial scalar amplitude	$2.7 \to 4$
ξ	Nonminimal coupling	$-0.002 \to 0.0065$

[a]The parameter Θ_s is the ratio between the sound horizon r_s and the angular diameter distance $D_A(z_{\rm dec})$ at decoupling $z_{\rm dec}$.

However, variations of this fiducial model will not change significantly the results presented here.

These data sets are combined to constrain the cosmological model explored here, and described by the parameters[6]

$$\{\omega_b, \omega_c, \Theta_s, \tau, \log[10^{10}A_s], \xi\}. \quad (7)$$

In Table I, we summarize the definition as well as the priors on these parameters. We use the Boltzmann code CAMB [25] and the cosmological parameters are extracted from the data described above by means of a Monte Carlo Markov chain (MCMC) analysis based on the most recent version of cosmomc [26]. The constraints obtained on the nonminimal coupling ξ are then translated into bounds on the usual inflationary parameters n_s, r and α.

Table II shows the 95% C.L. constraints on the parameter ξ as well as on the derived inflationary parameters n_s, r and the running α arising from our numerical analyses using the two CMB data combinations used here and assuming that n_s and r are univocally determined by ξ (for a fixed number of e-folds N, that we consider to be either 60 or 50). For $N = 60$, the preferred value of the nonminimal coupling ξ from *Planck* TT plus WP measurements is positive and slightly larger than the mean value obtained when the cross-correlated polarized maps from BICEP2/*Keck* and *Planck* experiments are included in the numerical analyses. This preference for a slightly larger ξ (and consequently, smaller r) is clear from the one-dimensional posterior probability distribution of ξ shown in the left panel of Fig. 4. The mean value of $\xi = 0.0028$ obtained from *Planck* TT plus WP data is translated into a 95% C.L. constraint of the tensor-to-scalar ratio $r = 0.038^{+0.051}_{-0.031}$, as can be seen from the right panel of Fig. 4. When considering BICEP2/*Keck* and *Planck* cross-spectra polarization data, the former constraint on the tensor-to-scalar ratio is very similar to the one

[6]Notice that the inflationary cosmology under study contains less parameters than the standard ΛCDM picture, as once the nonminimal coupling ξ is fixed, n_s, r and α are fully determined, and are thus *derived* parameters.

TABLE II. Inflationary constraints in the context of nonminimally coupled chaotic potential ϕ^2: The upper block of the table refers to the 95% C.L. limits on the nonminimal coupling ξ (the parameter varied in the MCMC analyses) from the two possible CMB data combinations used in this study, for both $N = 60$ and $N = 50$. The lower block of the table contains the 95% C.L. derived ranges of the inflationary parameters n_s, r and α from the limits of ξ illustrated above, in the context of the nonminimally coupled chaotic potential ϕ^2, for both $N = 60$ and $N = 50$.

	Planck TT + WP		BK + Planck TT + WP	
N	60	50	60	50
ξ	$0.0028^{+0.0023}_{-0.0025}$	$0.0024^{+0.0023}_{-0.0023}$	$0.0027^{+0.0023}_{-0.0022}$	$0.0027^{+0.0020}_{-0.0019}$
n_s	$0.958^{+0.010}_{-0.011}$	$0.954^{+0.007}_{-0.009}$	$0.958^{+0.009}_{-0.011}$	$0.953^{+0.007}_{-0.009}$
r	$0.038^{+0.051}_{-0.031}$	$0.063^{+0.056}_{-0.048}$	$0.038^{+0.039}_{-0.030}$	$0.053^{+0.038}_{-0.037}$
$\alpha \equiv \mathrm{d}n_s/\mathrm{d}\ln k$	$-0.0005^{+0.0001}_{-0.0001}$	$-0.0007^{+0.0001}_{-0.0001}$	$-0.0005^{+0.0001}_{-0.0001}$	$-0.0007^{+0.0001}_{-0.0001}$

quoted above. Concerning the running of the spectral index, the two data combinations seem to have a preference for a small negative running $\alpha = -0.0005$, associated to small values of $|\xi|$, as shown in Fig. 2.

Let us now comment on the sensitivity of our constraints to changes in the number of e-folds N. Setting $N = 50$ leads to different, though almost insignificant, changes in the constraints obtained using the two CMB data sets. The theoretically allowed regions in the (n_s, r) plane as a function of ξ for $N = 50$ are indeed slightly different from those corresponding to the $N = 60$ case; see Fig. 1. The net result is a smaller (larger) values of n_s (r) than in the $N = 60$ case. The BICEP2/*Keck* and *Planck* cross-spectra polarization data yield a value $r = 0.053^{+0.038}_{-0.037}$ for the tensor-to-scalar ratio in the context of the nonminimally coupled ϕ^2 model. On the other hand, the resulting central value for the scalar spectra index is only half a σ away (towards smaller values) from the corresponding one for $N = 60$, as expected from the theoretical predictions illustrated in Fig. 1.

Figure 1 shows the 68% and 95% C.L. allowed regions in the (n_s, r) plane resulting from our MCMC analyses to *Planck* TT plus WP data and to the combined BKP in the usual (n_s, r) plane, together with the theoretical predictions for $N = 50$ and $N = 60$ for the nonminimally coupled ϕ^2 scenario.

To address the question of whether or not a nonminimal coupling ξ is favored by current CMB data, we compare the χ^2 test statistics function for the ϕ^2 model in its minimally and nonminimally coupled versions for $N = 60$, albeit very similar results are obtained for $N = 50$. The χ^2 for the case of *Planck* TT plus WP data, evaluated at the best-fit point of the ϕ^2 model minimally coupled to gravity, is $\chi^2[\xi = 0] = 9812.8$. On the other hand, the nonminimally coupled version has a lower χ^2 value at the best-fit point due to the extra parameter ξ introduced in the model, with $\chi^2[\xi \neq 0] = 9806.8$. The difference between these two χ^2 values is $\Delta\chi^2 = 6$, which, for a distribution of 1 degree of freedom, has a p-value of 0.014, and is considered statistically significant. For the case of the combined BKP likelihood, the difference between the test statistics for the minimally coupled and nonminimally coupled ϕ^2 models is $\Delta\chi^2 = 10$, which, for 1 degree of freedom, has a p-value of 0.0016, and is considered very statistically significant. Therefore, according to the most recent CMB data, the presence of a nonminimal coupling ξ within the ϕ^2 model is favored at a significance equal or larger than ∼99% C.L.

Let us now turn to future constraints on ξ. Future observations, as those expected from *PIXIE* [27], *Euclid* [28], *COrE* [29] and *PRISM* [30], could be able to reach an accuracy of $\sigma_r = \sigma_{n_s-1} = 10^{-3}$. With such precision, one could hope to test deviations from the quadratic potential [31], as the one studied here, by constructing quantities

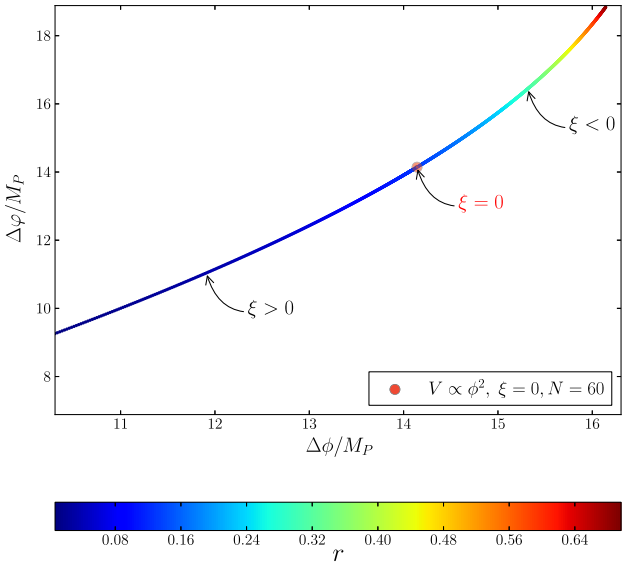

FIG. 3 (color online). Excursion of the canonically normalized inflaton φ versus the one of the original scalar ϕ. The magnitude of the tensor-to-scalar ratio is encoded in the curve through the color bar. Notice that, in both frames, large r correlates with large excursions.

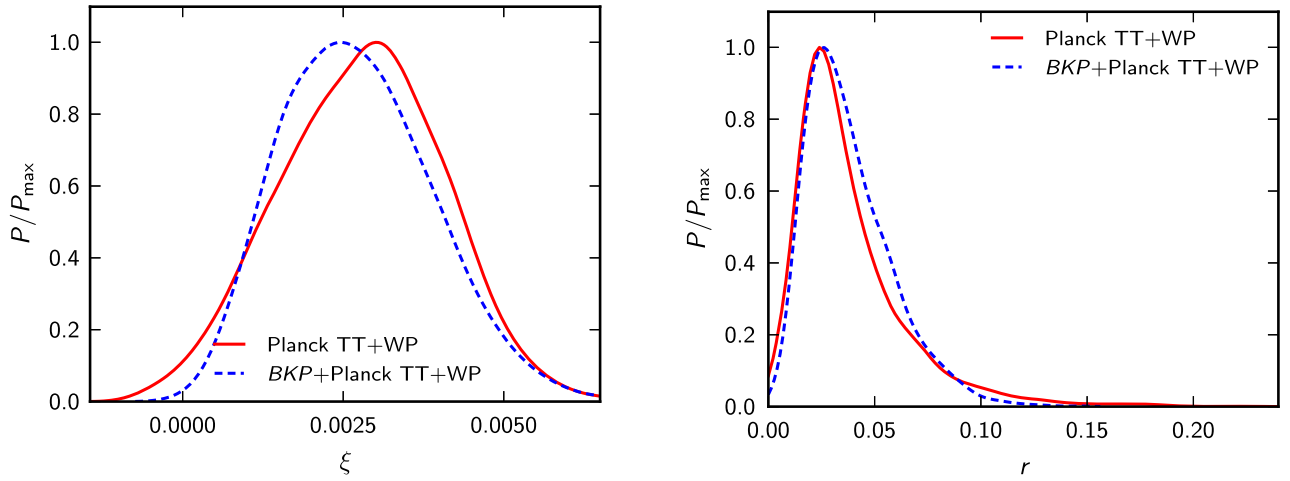

FIG. 4 (color online). The left (right) panel shows the one-dimensional posterior probability distributions of the nonminimal coupling ξ (the tensor-to-scalar ratio r) in the context of a nonminimally coupled chaotic potential ϕ^2, with r a function of ξ, and therefore, a prediction within the model.

independent of N, up to subleading $\mathcal{O}(1/N^3)$ corrections. It is straightforward to get for our case,

$$n_s - 1 + \frac{r}{4} = -20\xi, \tag{8}$$

at leading order both in slow roll and ξ. If it turns out that nature has chosen a very small value of r, future constraints on ξ would be as strong as $\xi \lesssim 10^{-4}$, 1 order of magnitude stronger than the ones obtained in this analysis. Concerning the running α, it is interesting to note that futuristic observations like *SPHEREx* [32], with a forecasted error of $\sigma_\alpha = 10^{-3}$, will be able to falsify the present scenario.

Finally, it is also interesting to explore the impact of the nonminimal coupling on the inflaton excursion. It is well known that large values of the tensor-to-scalar ratio r, as those found by previous BICEP2 measurements[7] [33,34] yield large inflaton excursions $\phi \gg M_P$ [35–38], which are hard to understand in the context of a consistent effective field theory. In particular, successful inflation requires that higher order nonrenormalizable operators, which are expected to be naturally present in the inflationary potential, are sufficiently suppressed. A number of phenomenological studies have recently been devoted to address this problem [39–42]. In Fig. 3, we plot the excursion of both ϕ and φ, together with the corresponding tensor-to-scalar ratio r. It is clear that the excursion of the canonically normalized inflaton φ is lowered for positive values of ξ i.e. $\Delta\varphi < \Delta\phi$. However, this decrease is rather mild and the excursion still takes on super-Planckian values for the phenomenologically acceptable values of ξ. Conversely, negative values of ξ lead to an increase of the excursion of φ. Figure 3 also shows that super-Planckian values of both ϕ and φ are *still* associated with large values of the tensor-to-scalar ratio r, in agreement with the Lyth bound [35]. Thus, once a small nonzero and positive value of the coupling ξ is turned on, both the inflaton excursion and r are slightly lowered, but without alleviating completely the super-Planckian excursion problem.

[7]The joint BKP analysis finds however no evidence for primordial B-modes, but a robust limit of $r < 0.12$ at 95% C.L.; see Ref. [1].

IV. CONCLUSIONS

A small, nonminimal coupling $\frac{1}{2}\xi R\phi^2$ is expected to be present in the inflaton Lagrangian, and modifies the inflationary predictions in an interesting way. Focusing on the simplest quadratic potential scenario, and using the very recent joint analysis of the BICEP2/*Keck* Array and *Planck* polarization maps, we found that a small, positive value of the coupling ξ is favored at the 2σ level, assuming that nature has chosen the ϕ^2 scenario for the generation of primordial perturbations. If only *Planck* TT plus WP data are used in the analyses, the significance is milder. These conclusions have been obtained for a number of e-foldings within the $N = 50$–60 range. It would be interesting to see if upcoming B-mode measurements can reinforce or weaken the statistical significance of these findings. In particular, it would be crucial to discriminate between the presence of a nonminimal coupling in the theory and other departures from the quadratic approximation.

ACKNOWLEDGMENTS

O. M. is supported by PROMETEO II/2014/050, by the Spanish Grant No. FPA2011-29678 of the MINECO and by PITN-GA-2011-289442-INVISIBLES. L. B. and H. R. acknowledge financial support from PROMETEO II/2014/050.

[1] P. A. R. Ade *et al.* (BICEP2 and Planck Collaborations), A Joint Analysis of BICEP2/*Keck* Array and Planck Data, Phys. Rev. Lett. **114**, 101301 (2015).

[2] Planck Collaboration, Planck 2015 results. XIII. Cosmological parameters, arXiv:1502.01589.

[3] P. A. R. Ade *et al.* (Planck Collaboration), Planck 2015 results. XVII. Constraints on primordial non-Gaussianity, arXiv:1502.01592.

[4] P. A. R. Ade *et al.* (Planck Collaboration), Planck 2015. XX. Constraints on inflation, arXiv:1502.02114.

[5] I. L. Buchbinder, S. D. Odintsov, and I. L. Shapiro, *Effective Action in Quantum Gravity* (IOP, Bristol, U.K., 1992), p. 413.

[6] D. S. Salopek, J. R. Bond, and J. M. Bardeen, Designing density fluctuation spectra in inflation, Phys. Rev. D **40**, 1753 (1989).

[7] T. Futamase and K-i. Maeda, Chaotic inflationary scenario in models having nonminimal coupling with curvature, Phys. Rev. D **39**, 399 (1989).

[8] R. Fakir and W. G. Unruh, Improvement on cosmological chaotic inflation through nonminimal coupling, Phys. Rev. D **41**, 1783 (1990).

[9] D. I. Kaiser, Primordial spectral indices from generalized Einstein theories, Phys. Rev. D **52**, 4295 (1995).

[10] E. Komatsu and T. Futamase, Complete constraints on a nonminimally coupled chaotic inflationary scenario from the cosmic microwave background, Phys. Rev. D **59**, 064029 (1999).

[11] M. P. Hertzberg, On inflation with non-minimal coupling, J. High Energy Phys. 11 (2010) 023.

[12] N. Okada, M. U. Rehman, and Q. Shafi, Tensor to scalar ratio in non-minimal ϕ^4 inflation, Phys. Rev. D **82**, 043502 (2010).

[13] A. Linde, M. Noorbala, and A. Westphal, Observational consequences of chaotic inflation with nonminimal coupling to gravity, J. Cosmol. Astropart. Phys. 03 (2011) 013.

[14] D. I. Kaiser and E. I. Sfakianakis, Multifield Inflation after Planck: The Case for Nonminimal Couplings, Phys. Rev. Lett. **112**, 011302 (2014).

[15] T. Chiba and K. Kohri, Consistency relations for large field inflation: Non-minimal coupling, Prog. Theor. Exp. Phys. **2015**, 023E01.

[16] C. Pallis and Q. Shafi, Gravity waves from non-minimal quadratic inflation, J. Cosmol. Astropart. Phys. 03 (2015) 023.

[17] S. Tsujikawa, J. Ohashi, S. Kuroyanagi, and A. De Felice, Planck constraints on single-field inflation, Phys. Rev. D **88**, 023529 (2013).

[18] A. D. Linde, Chaotic inflation, Phys. Lett. **129B**, 177 (1983).

[19] F. L. Bezrukov and M. Shaposhnikov, The Standard Model Higgs boson as the inflaton, Phys. Lett. B **659**, 703 (2008).

[20] L. Boubekeur, E. Giusarma, O. Mena, and H. Ramírez (to be published).

[21] P. A. R. Ade *et al.* (Planck Collaboration), Planck 2013 results. I. Overview of products and scientific results, Astron. Astrophys. **571**, A1 (2014).

[22] P. A. R. Ade *et al.* (Planck Collaboration), Planck 2013 results. XV. CMB power spectra and likelihood, Astron. Astrophys. **571**, A15 (2014).

[23] P. A. R. Ade *et al.* (Planck Collaboration), Planck 2013 results. XVII. Gravitational lensing by large-scale structure, Astron. Astrophys. **571**, A17 (2014).

[24] C. L. Bennett *et al.* (WMAP Collaboration), Nine-Year Wilkinson Microwave Anisotropy Probe (WMAP) observations: Final maps and results, Astrophys. J. Suppl. Ser. **208**, 20 (2013).

[25] A. Lewis, A. Challinor, and A. Lasenby, Efficient computation of CMB anisotropies in closed FRW models, Astrophys. J. **538**, 473 (2000).

[26] A. Lewis and S. Bridle, Cosmological parameters from CMB and other data: A Monte-Carlo approach, Phys. Rev. D **66**, 103511 (2002).

[27] A. Kogut, D. J. Fixsen, D. T. Chuss, J. Dotson, E. Dwek, M. Halpern, G. F. Hinshaw, S. M. Meyer *et al.*, The Primordial Inflation Explorer (PIXIE): A nulling polarimeter for cosmic microwave background observations, J. Cosmol. Astropart. Phys. 07 (2011) 025.

[28] R. Laureijs *et al.* (EUCLID Collaboration), Euclid definition study report, arXiv:1110.3193.

[29] F. R. Bouchet *et al.* (COrE Collaboration), COrE (Cosmic Origins Explorer): A white paper, arXiv:1102.2181.

[30] P. Andre *et al.* (PRISM Collaboration), PRISM (Polarized Radiation Imaging and Spectroscopy Mission): A white paper on the ultimate polarimetric spectro-imaging of the microwave and far-infrared sky, arXiv:1306.2259.

[31] P. Creminelli, D. López Nacir, M. Simonović, G. Trevisan, and M. Zaldarriaga, ϕ^2 or Not ϕ^2: Testing the Simplest Inflationary Potential, Phys. Rev. Lett. **112**, 241303 (2014).

[32] O. Doré, J. Bock, P. Capak, R. de Putter, T. Eifler, C. Hirata, P. Korngut, E. Krause *et al.*, SPHEREx: An all-sky spectral survey, arXiv:1412.4872.

[33] P. A. R. Ade *et al.* (BICEP2 Collaboration), Detection of B-Mode Polarization at Degree Angular Scales by BICEP2, Phys. Rev. Lett. **112**, 241101 (2014).

[34] P. A. R. Ade *et al.* (BICEP2 Collaboration), BICEP2 II: Experiment and Three-Year Data Set, Astrophys. J. **792**, 62 (2014).

[35] D. H. Lyth, What Would We Learn by Detecting a Gravitational Wave Signal in the Cosmic Microwave Background Anisotropy?, Phys. Rev. Lett. **78**, 1861 (1997).

[36] L. Boubekeur, Theoretical bounds on the tensor-to-scalar ratio in the cosmic microwave background, Phys. Rev. D **87**, 061301 (2013).

[37] G. Efstathiou and K. J. Mack, The Lyth bound revisited, J. Cosmol. Astropart. Phys. 05 (2005) 008.

[38] L. Verde, H. Peiris, and R. Jimenez, Considerations in optimizing CMB polarization experiments to constrain inflationary physics, J. Cosmol. Astropart. Phys. 01 (2006) 019.

[39] J. Garcia-Bellido, D. Roest, M. Scalisi, and I. Zavala, Can CMB data constrain the inflationary field range?, J. Cosmol. Astropart. Phys. 09 (2014) 006.

[40] G. Barenboim and O. Vives, Transplanckian inflation as gravity echoes, arXiv:1405.6498.

[41] J. Garcia-Bellido, D. Roest, M. Scalisi, and I. Zavala, Lyth bound of inflation with a tilt, Phys. Rev. D **90**, 123539 (2014).

[42] L. Boubekeur, E. Giusarma, O. Mena, and H. Ramírez, Phenomenological approaches of inflation and their equivalence, Phys. Rev. D **91**, 083006 (2015).

Journal of Cosmology and Astroparticle Physics
An IOP and SISSA journal

The present and future of the most favoured inflationary models after Planck 2015

Miguel Escudero,[a] **Héctor Ramírez,**[a] **Lotfi Boubekeur,**[a,b] **Elena Giusarma**[c] **and Olga Mena**[a]

[a]Instituto de Física Corpuscular (IFIC), CSIC-Universitat de Valencia, Apartado de Correos 22085, E-46071, Spain
[b]Universidad San Francisco de Quito USFQ, Colegio de Ciencias e Ingenierías El Politécnico, campus Cumbayá, calle Diego de Robles y Vía Interocéanica, Quito EC170157, Ecuador
[c]Physics Department and INFN, Università di Roma "La Sapienza", Piazzale Aldo Moro 2, 00185, Rome, Italy

E-mail: miguel.escudero@ific.uv.es, hector.ramirez@ific.uv.es, lboubekeur@usfq.edu.ec, elena.giusarma@roma1.infn.it, olga.mena@ific.uv.es

Received September 24, 2015
Revised January 11, 2016
Accepted January 17, 2016
Published February 8, 2016

Abstract. The value of the tensor-to-scalar ratio r in the region allowed by the latest *Planck 2015* measurements can be associated to a large variety of inflationary models. We discuss here the potential of future Cosmic Microwave Background cosmological observations in disentangling among the possible theoretical scenarios allowed by our analyses of current *Planck* temperature and polarization data. Rather than focusing only on r, we focus as well on the running of the primordial power spectrum, α_s and the running thereof, β_s. If future cosmological measurements, as those from the COrE mission, confirm the current best-fit value for $\beta_s \gtrsim 10^{-2}$ as the preferred one, it will be possible to rule-out the most favoured inflationary models.

Keywords: inflation, cosmological parameters from CMBR, CMBR experiments

ArXiv ePrint: 1509.05419

doi:10.1088/1475-7516/2016/02/020

JCAP02(2016)020

Contents

JCAP02(2016)020

1 Motivations

The smoking-gun of inflation [1–3] is the detection of a stochastic background of gravitational waves. Such primordial signature is characterized by its amplitude, parametrized via the tensor-to-scalar ratio r. Recent analyses from *Planck* 2015 [4] have presented the tightest bounds to date on r using temperature and polarization measurements. Albeit current *Planck* constraints are perfectly compatible with a vanishing tensor-to-scalar ratio, yet there is still enough room for other theoretical possibilities besides the Starobinsky R^2-gravity scenario, which emerges as the best-fit model. Looking forward to the next generation of CMB observations, and depending on the value of r that Nature has chosen, one can envision two distinct possibilities: *(a)* either r turns out to be way too small to be measured by the next generation of CMB observations, or *(b)* the value of r is large enough to be detected. However, in this latter case, the measured tensor-to-scalar ratio will typically correspond to several inflationary models. Given that measuring r (if $r < few \times 10^{-4}$) might be extremely difficult [5–8], and disentangling between the various models that lie in the same regions in

the canonical (n_s, r) plane might not be straightforward either, we explore here the possibility of extending the analysis to other (complementary) inflationary observables.

For the scalar power spectrum of the primordial perturbations, we consider, as additional observables, the running α_s and the running of the running β_s. For the primordial tensor power spectrum, we consider its running n_t. The aim of this paper is to assess the potential of future CMB observations in falsifying inflation (or unraveling the fundamental model among the most favoured candidates after *Planck 2015* data) by looking to these three additional observables. For illustration, we will consider some well-motivated models that are compatible with current data. The structure of the paper is as follows. Section 2 deals with the basic definitions of the different cosmological observables and their current constraints. Section 3 describes the theoretical predictions from the most favoured inflationary scenarios after *Planck* 2015 CMB temperature and polarization measurements. In section 4 we perform Markov Chain Monte Carlo (MCMC) analyses of the *Planck* 2015 data release. Our Fisher matrix forecasts in section 5 show that, if the future preferred value of β_s is close to the current best-fit from *Planck*, future CMB probes may falsify the currently best inflationary scenarios. We shall conclude in section 6.

2 Basic definitions

The power spectrum of the primordial curvature perturbation, ζ, seeding structure formation in the universe is defined as

$$\langle \zeta_{\vec{k}} \zeta_{\vec{p}} \rangle = (2\pi)^3 \delta^{(3)}(\vec{p} + \vec{k}) P_\zeta(k) \,, \tag{2.1}$$

where the dimensionless amplitude of primordial perturbations $\Delta_\zeta(k)$ is defined through

$$P_\zeta(k) = \frac{2\pi^2}{k^3} \Delta^2_\zeta(k). \tag{2.2}$$

The scale dependence of $\Delta^2_\zeta(k)$ is parametrized by the spectral index:

$$n_s = 1 + \frac{\mathrm{d} \ln \Delta^2_\zeta}{\mathrm{d} \ln k} \,. \tag{2.3}$$

Likewise, one can also define the scale dependence of the spectral index, which is called the running, as

$$\alpha_s \equiv \frac{\mathrm{d}n_s}{\mathrm{d} \ln k} \,, \tag{2.4}$$

as well as the running of the running, defined as

$$\beta_s \equiv \frac{\mathrm{d}\alpha_s}{\mathrm{d} \ln k} \,. \tag{2.5}$$

In all these definitions, it is understood that quantities are evaluated at horizon exit $k_* = aH$ ($k_* = 0.05\,\mathrm{Mpc}^{-1}$ throughout this study). In terms of the above parameters, the primordial power spectrum reads

$$\Delta^2_\zeta(k) = \Delta^2_\zeta(k_*) \left(\frac{k}{k_*} \right)^{n_s - 1 + \frac{1}{2}\alpha_s \ln(k/k_*) + \frac{1}{3!}\beta_s \ln^2(k/k_*)} \,. \tag{2.6}$$

JCAP02(2016)020

In the context of slow-roll, one can have a general idea about the magnitude of the above inflationary parameters in terms of the number of e-folds N. If we consider the empirical relation [9–11] $n_s - 1 \propto 1/N$, one expects that

$$\alpha_s \sim \frac{1}{N^2} \lesssim 10^{-4} \quad \text{and} \quad \beta_s \sim \frac{1}{N^3} \lesssim 10^{-5}\,, \tag{2.7}$$

for typical choices of the number of e-foldings $N = 50 - 60$. The latest *Planck* 2015 temperature and polarization TT,TE,EE+lowP [4] data analyses with $r = 0$ provide the following constraints:

$$\begin{aligned} n_s &= 0.9586 \pm 0.0056\,, \\ \alpha_s &= 0.009 \pm 0.010\,, \\ \beta_s &= 0.025 \pm 0.013\,. \end{aligned}$$

What is interesting to notice in these constraints, is a slight preference for a positive $\beta_s \sim 10^{-2}$, while as we will explain shortly, slow-roll inflation predicts typically a smaller and *negative* β_s.

The tensor contribution to the primordial power spectrum is parametrized by the tensor-to-scalar ratio r

$$r = P_t(k_*)/P_\zeta(k_*)\,, \tag{2.8}$$

where $P_t(k) \equiv \frac{2\pi^2}{k^3}\Delta_t^2(k)$ is the tensor power spectrum, and it is parametrized at first order as

$$\Delta_t^2(k) = \Delta_t^2(k_*)\left(\frac{k}{k_*}\right)^{n_t}\,, \tag{2.9}$$

in which n_t is the spectral index of tensor modes. In the slow-roll regime, the magnitude of r can vary within a large range, and this is the main difficulty in testing inflation through the detection of B-modes. This can be understood in the context of phenomenological parametrizations of inflation [9–11]. In such approaches, the (n_s, r) plane appears to be unevenly filled, and one can even argue on the existence of a "forbidden zone",[1] in the r-direction, depending on the precise value of n_s, see figure 1. Future CMB missions aim to reach the important theoretical milestone of $r = 2 \times 10^{-3} \cdot (60/N)^2$ [15], which would signal super-Planckian inflaton excursions [16–18].

3 Most favoured inflationary scenarios

In the following, we shall review the most favoured models (including their predictions for the different inflationary observables: r, n_t, n_s, α_s and β_s) after *Planck 2015* data release.

3.1 Quadratic scenarios

This class of scenarios represents the simplest theoretical possibility. It includes:

[1] This observation has been made previously in different contexts in [12–14].

JCAP02(2016)020

The chaotic scenario, $V \propto \phi^2$, both with minimal and non-minimal coupling to gravity [19–25]. The former is disfavoured with respect to the latter so the non-minimally coupled version is perfectly compatible with current data [26]. The predictions in the (n_s, r), (n_s, α_s), (n_s, β_s) and (n_t, r) planes for these two models (ϕ^2 and $\xi\mathcal{R}\phi^2$) are depicted in figures 1, 2, 3 and 4 for two possible choices for the number of e-folds, $N = 50$ and $N = 60$.[2] Notice, from figure 1, that the trajectories in the (n_s, r) plane for the non-minimally coupled case ($\xi\mathcal{R}\phi^2$) start always at the point corresponding to the ϕ^2 model predictions,[3] and then, as the coupling ξ takes positive values, the tensor contribution is reduced, and the scalar spectral index n_s is pushed below scale invariance, see ref. [26]. Negative values of the coupling ξ (not illustrated here) are highly disfavoured by current CMB observations, since they will lead to large values of the tensor-to-scalar ratio r. Concerning the running of the scalar spectral index α_s, the trajectories for the two quadratic scenarios considered here are depicted in figure 2. Notice that positive values of the coupling ξ will change the predicted value of α_s in the ϕ^2 scenario ($\alpha_s = -2/N^2$, corresponding to $\alpha_s = -0.00056$ for $N = 60$) to slightly larger values, albeit the trajectories always stay in the $\alpha_s < 0$ sub-plane. The running of the running parameter, β_s, barely changes with respect to its predicted value in the non-minimally coupled case (i.e. $\xi = 0$, for which $\beta_s = -4/N^3$, giving $\beta_s \simeq -1.8 \times 10^{-5}$ for $N = 60$) as the coupling ξ gets positive values, see figure 3. Finally, in figure 4 we see that all models follow the theoretical curve $n_t = -r/8$. In particular, the chaotic ϕ^2 model predicts a tensor spectral index of $n_t \simeq -0.019$ ($n_t \simeq -0.016$) for $N = 50$ ($N = 60$); an increasing positive value of ξ, within the non-minimally coupled model, diminishes the predicted value to $n_t \simeq -0.018$ ($n_t \simeq -0.010$) for $\xi \simeq 0.0059$ and $N = 50$ ($N = 60$).

The Natural inflation scenario (minimally coupled to gravity), where the inflaton is a Pseudo-Nambu-Goldstone-Boson (PNGB), which potential is invariant under the shift $\phi \to \phi + 2\pi f$, and it is given by

$$V(\phi) = V_0 \left[1 - \cos(\phi/f)\right] , \tag{3.1}$$

with f the PNGB decay constant [27–29]. It is straightforward to perform the slow-roll analysis and obtain the analytical expressions of the spectral index and the tensor-to-scalar ratio:

$$\begin{aligned} n_s &= 1 - \alpha \left[\frac{e^{\alpha N}\,(1+\alpha/2)+1}{e^{\alpha N}\,(1+\alpha/2)-1}\right] , \\ r &= \frac{8\alpha}{e^{\alpha N}\,(1+\alpha/2)-1} , \end{aligned} \tag{3.2}$$

where the parameter α is defined as[4] $\alpha \equiv M_{\rm pl}^2/f^2$. Notice that for small α (i.e. very large values of f) the predictions of the natural inflation scenario coincide with those of the minimally coupled chaotic inflation model $V \propto \phi^2$. Even if the flatness of the PNGB potential is protected by the shift symmetry, it is not clear whether this structure can be UV completed. For a recent discussion on the issue and some solutions see e.g. [30–34].

Figures 1, 2, 3 and 4 show the predicted trajectories in the (n_s, r), (n_s, α_s), (n_s, β_s) and (n_t, r) planes for $N = 50$ and $N = 60$, and f varying from $3.45 M_{\rm pl}$ to $100 M_{\rm pl}$. For the smallest value of f considered here, $f = 3.45 M_{\rm pl}$, a very small value of $n_s \simeq 0.9152$ is found. Agreement with *Planck* data implies that the decay constant satisfies $f > 5.3 M_{\rm pl}$,

[2] The value of ξ ranges from $\xi = 0$ to $\xi = 0.0065$ in figures 1, 2 and 3.

[3] The case of $\xi = 0$ is equivalent to the standard inflationary chaotic scenario in which the predictions are $n_s = 1 - 2/N$ and $r = 8/N$, corresponding to $n_s = 0.967$ and $r = 0.13$, respectively, for $N = 60$.

[4] $M_{\rm pl} = 1/\sqrt{8\pi G_N} \simeq 2.43 \times 10^{18}$ GeV is the reduced Planck mass.

JCAP02(2016)020

for $N = 50 - 60$. Larger values of f increase the value of the tensor-to-scalar ratio, until the prediction reaches the one of minimal chaotic inflation, as shown in figure 1. In figure 2, we illustrate that large values of f lead to small values for the running of the spectral index, which eventually will reach the predictions for the minimal chaotic scenario. In contrast, the value of β_s, barely changes when f varies, remaining around in $\beta_s \simeq -3 \times 10^{-5}$ and $\beta_s \simeq -1.7 \times 10^{-5}$ for $N = 50$ and $N = 60$, respectively, see figure 3. Concerning the tensor spectral index, for a value of $f = 100 M_{\rm pl}$ the predictions coincide with those of the ϕ^2 model. Whereas lower value of f, corresponds to smaller values n_t. For instance, $n_t \simeq -0.0006$ ($n_t \simeq -0.0002$) for $f = 3.45 M_{\rm pl}$ and $N = 50$ ($N = 60$), following the consistency relation $n_t = -r/8$, as expected (see figure 4).

3.2 Higgs-like scenarios

This class of scenarios is described by a symmetry breaking potential,

$$V(\phi) = \frac{\lambda \left(\phi^2 - v^2\right)^2}{4 \left(1 + \xi \phi^2 / M_{\rm pl}^2\right)^2}\,, \tag{3.3}$$

alike to the one of the standard model Higgs particle, but with a non-minimal-coupling to the Ricci scalar, ξ, see refs. [35–37]. It also includes, as a limiting case (for $\xi \to \infty$), the R^2-gravity Starobinsky scenario [38]. Notice as well that the limiting case $\xi \to 0$ corresponds to the quartic potential scenario, $V \propto \phi^4$. One can find a suitable set of inflaton potentials for different values of the inflaton vacuum expectation value v [25]. In this work we illustrate the predictions of a Higgs-like scenario for $v = 0$ and for different positive values of ξ, as well as for $N = 50$ and $N = 60$ e-folds.[5] Figure 1 clearly shows that the limiting case $\xi \to 0$, corresponding to the quartic potential ϕ^4, is not in good agreement with *Planck* data, as its predictions for the inflationary parameters ($n_s \simeq 0.941$, $r \simeq 0.31$ and $n_s \simeq 0.951$, $r \simeq 0.26$ for $N = 50$ and $N = 60$, respectively) are highly disfavoured. When the non-minimal coupling to gravity, ξ, is increased, the tensor contribution is reduced, while the predictions reach those corresponding to the Starobinsky scenario, as long as $\xi > 10^2$. In this limit, $n_s \simeq 0.961$, $r \simeq 0.0041$ ($n_s \simeq 0.968$, $r \simeq 0.0023$) for $N = 50$ ($N = 60$), values which are in excellent agreement with current CMB data.

Concerning the running of the spectral index, increasing the value of ξ will drive the values of α_s from the one corresponding to the quartic potential to slightly larger ones, corresponding to the Starobinsky scenario, keeping always the trajectory in the $\alpha_s < 0$ sub-plane (see figure 2). The predictions of the running of the spectral index for the quartic (Starobinsky) scenarios are $\alpha_s \simeq -0.0011$ ($\alpha_s \simeq -0.00074$) for $N = 50$, and $\alpha_s \simeq -0.0008$ ($\alpha_s \simeq -0.00052$) for $N = 60$. As in the case of the previous models, the running of running of the spectral index, β_s, remains almost constant as ξ is varied, as shown in figure 3. In particular, in the Higgs-like scenario, $\beta_s \simeq -3.5 \times 10^{-5}$ ($\beta_s \simeq -2.5 \times 10^{-5}$) for $N = 50$ ($N = 60$). This model allows for a wide range of values for the tensor spectral index, starting from the predictions from the ϕ^4 model around $n_t \simeq -0.039$ ($n_t \simeq -0.039$). Then, an increasing value of ξ pushes down the predictions for n_t down to very small values around $n_t \simeq -0.0005$ ($n_t \simeq -0.0003$) for $N = 50$ ($N = 60$), (and thus coinciding with the values predicted from Starobinsky inflation), along the theoretical curve $n_t = -r/8$ depicted in figure 4.

[5] The coupling λ cancels out in the slow-roll calculations.

JCAP02(2016)020

3.3 Hilltop scenarios

For completeness, we should also consider this class of scenarios, described by potentials

$$V(\phi) = V_0 \left[1 - (\phi/\mu)^p\right] , \tag{3.4}$$

since its predictions in the (n_s, r) plane lie very close to the ones associated to the models discussed before [17]. Within these scenarios, we can distinguish two sub-cases:

1. $p = 2$, corresponding to the quadratic hilltop scenario, where inflation takes place close to a local maximum; $V'(\phi) = 0$ and $V''(\phi) < 0$.

2. $p > 2$, corresponding to a generalization of the simplest quadratic case, where here inflation happens close to a local maximum where additionally, higher derivatives of the potential vanish, i.e. $V'(\phi) = V''(\phi) = V'(\phi) = \cdots = V^{(p-1)}(\phi) = 0$ and, again, $V^{(p)}(\phi) < 0$.

We restrict our analysis to the first case, $p = 2$, in which the spectral index and the tensor-to-scalar ratio read as

$$\begin{aligned} n_s &= 1 - 4|\eta_0| \\ r &= 2\,(1 - n_s)^2\, e^{N(n_s-1)}|\eta_0|^{-1} , \end{aligned} \tag{3.5}$$

with $|\eta_0| = \mu^{-2} M_{\rm pl}^2$. In figure 1 we depict the predictions for this model in the plane (n_s, r). The parameter η_0 varies from $\eta_0 = 10^{-4}$ to $\eta_0 \simeq 2 \times 10^{-2}$, pushing n_s to smaller values as η decreases. With $\eta_0 \simeq 8 \times 10^{-3}$ we obtain a tensor-to-scalar ratio of $r = 0.0375$ for the case N=60, and $r \simeq 0.0516$ for $N = 50$, both corresponding to a spectral index $n_s \simeq 0.968$. Notice from figures 2 and 3 that for the same value of $\eta_0 \simeq 8 \times 10^{-3}$ we obtain a running of the spectral index of $\alpha_s \simeq -0.00107$ and a running of the running $\beta_s \simeq -0.000065$ ($\alpha_s \simeq -0.00073$ and $\beta_s \simeq -0.0000386$) for $N = 50$ ($N = 60$). In figure 4 we observe that this scenario predicts almost negligible values of the tensor spectral index for the range of values of η_0 commented above. The predictions reach the smallest values of n_t found in this work: $n_t \simeq -0.0003$ ($n_t \simeq -0.00006$) for $N = 50$ ($N = 60$) and $\eta_0 \simeq 2 \times 10^{-2}$.

4 Current constraints

4.1 Cosmological data and methodology

We consider the new data on CMB temperature and polarization measured by the *Planck* satellite [39–41]. We use the *Planck* TT temperature-only likelihood (hereafter *Planck* TT) and the *Planck* TT,TE, and EE power spectra data (hereafter *Planck* TTTEEE) up to a maximum multipole number of $\ell_{\rm max} = 2500$ combined with the *Planck* low-ℓ multipole likelihood that extends from $\ell = 2$ to $\ell = 29$ (denoted as lowP). We use the Boltzmann code CAMB [42] and generate MCMC chains using the publicly available package cosmomc [43]. We consider a ΛCDM extended model, described by the following set of parameters:

$$\{\omega_b, \omega_c, \Theta_s, \tau, \ln(10^{10} A_s), n_s, r, \alpha_s, \beta_s\} . \tag{4.1}$$

In table 1, the uniform priors considered on the different cosmological parameters are specified. We do not consider the spectral index for tensor perturbations n_t as an additional parameter in our MCMC analyses, since, as recently shown in [44], the current and future error bars on this parameter are considerably larger than the predictions of the different theoretical scenarios explored here. Therefore, the tensor spectral index is fixed in what follows to the slow-roll consistency relation value, $n_t = -r/8$.

JCAP02(2016)020

Parameter	Physical Meaning	Prior
$\omega_b \equiv \Omega_b h^2$	Baryon density	$0.005 \rightarrow 0.1$
$\omega_c \equiv \Omega_c h^2$	Cold dark matter density	$0.01 \rightarrow 0.99$
Θ_s	Angular scale of recombination	$0.5 \rightarrow 10$
τ	Reionization optical depth	$0.01 \rightarrow 0.8$
$\ln(10^{10} A_s)$	Primordial scalar amplitude	$2.7 \rightarrow 4$
n_s	Scalar spectral index	$0.9 \rightarrow 1.1$
α_s	Running of n_s	$-0.04 \rightarrow 0.06$
β_s	Running of α_s	$-0.04 \rightarrow 0.08$
r	Tensor-to-scalar ratio	$0 \rightarrow 2$

Table 1. Uniform priors for the cosmological parameters considered in the present analysis.

4.2 Results

While the latest *Planck* data provide evidence against some of the models explored here [4], these measurements can not single out the responsible mechanism for the inflationary process, nor to falsify this theoretical scenario by themselves.

This can be noticed from the contours shown in figures 1 2 and 3, where it is clear that all the models described above have some trajectories in the (n_s, r), (n_s, α_s) and (n_s, β_s) planes which lie within the current 68% and/or 95% CL allowed regions. Figure 1 depicts the current 68% and 95% CL allowed contours in the (n_s, r) plane from *Planck* TT plus lowP data, as well as from *Planck* TT plus lowP data plus TTEETE measurements, together with the predictions from Natural, Hilltop, Higgs-like, quartic, chaotic[6] and Starobinsky inflationary scenarios, for both $N = 50$ and $N = 60$ e-folds. The addition of EE and TE spectra to *Planck* TT plus lowP data helps in constraining the scalar spectral index n_s, however there is only a mild improvement in the tensor-to-scalar ratio upper bound. Notice, as previously stated, that the predictions for the inflationary parameters n_s and r from these models are all well within the current 68% and/or 95% CL allowed regions and therefore all of them (except for the case of the ϕ^4 potential with $N = 50$) are still feasible. One could ask if current measurements of other inflationary parameters, as the running of the scalar spectral index α_s and/or its running, β_s, may help in disentangling among the plethora of models still allowed by current data. Figure 2, illustrates, together with the trajectories in the (n_s, α_s) plane for the models explored here, the 68% and 95% CL allowed regions from *Planck* TT plus lowP data as well as from TTEETE plus lowP measurements. Notice that current bounds on α_s are unable to discard any of the possible inflationary models. Figure 3 shows the equivalent but in the (n_s, β_s) plane. Interestingly, *Planck* measurements of β_s seem to exclude the value $\beta_s = 0$ at the $\sim 2\sigma$ level. The theoretical scenarios illustrated here could be ruled out with a much higher significance if the value of β_s preferred by *Planck* 2015 measurements (i.e. $\beta \simeq 0.025$) is confirmed by future CMB data. We shall explore this possibility in the next section.

Table 2 shows the 95% CL bounds on the tensor-to-scalar-ratio r as well as the mean values and 68% CL errors of the remaining inflationary parameters n_s, α_s and β_s obtained with the two possible data combinations considered in this study. Notice that the limits

[6]The chaotic model is studied both in its minimally and non-minimally coupled versions.

JCAP02(2016)020

Parameter	*Planck* TT+lowP	*Planck* TT,TE,EE+lowP
r (95% CL)	< 0.27	< 0.23
n_s	0.959 ± 0.008	0.9591 ± 0.0056
α_s	0.0081 ± 0.014	0.0077 ± 0.011
β_s	0.034 ± 0.016	0.0313 ± 0.014

Table 2. 95% CL constraints on the tensor-to-scalar-ratio r and mean values (together with their 68% CL errors) of n_s, α_s and β_s obtained with the two possible data combinations considered in this study.

on r are considerably relaxed when adding the running and the running of the running as additional parameters in the analyses. The mean values and the errors on n_s and β_s are in very good agreement with those found by the *Planck* collaboration and reported in ref. [4].

5 Forecasts

The aim of this section is to forecast the potential of future CMB satellites in constraining the $\{r, n_s, \alpha_s, \beta_s\}$ parameter space via the Fisher matrix formalism.

5.1 CMB likelihood

Assuming that the fraction of sky surveyed $f_{\rm sky}$ is the same for CMB temperature and polarization measurements, the likelihood associated to a single frequency CMB experiment can be written as

$$-2\,\ln\mathcal{L}^{\rm CMB} = \sum_\ell (2\ell+1) f_{sky}\left[\ln\left(\frac{C_\ell^{BB}}{\hat{C}_\ell^{BB}}\right) - \frac{\hat{C}_\ell^{BB}}{C_\ell^{BB}} + \ln\left(\frac{C_\ell^{TT}C_\ell^{EE}-(C_\ell^{TE})^2}{\hat{C}_\ell^{TT}\hat{C}_\ell^{EE}-(\hat{C}_\ell^{TE})^2}\right) - 3 + \frac{\hat{C}_\ell^{TT}C_\ell^{EE}+C_\ell^{TT}\hat{C}_\ell^{EE}-2C_\ell^{TE}\hat{C}_\ell^{TE}}{C_\ell^{TT}C_\ell^{EE}-(C_\ell^{TE})^2}\right], \tag{5.1}$$

where the C_ℓ^{XY} ($\hat{C}_\ell^{XY}$) refer to the theoretical (measured) power spectra for $X, Y = T, E, B$. Due to the finite resolution of the spectra, there will be an induced noise in the map that should be added to the C_ℓ. In addition, following [45] we will also include the foreground contribution to the map as a residual noise, and therefore

$$C_\ell = C_\ell^{th} + N_\ell + R_\ell^F\,, \tag{5.2}$$

where C_ℓ^{th} will be our theoretical power spectra (computed by the Boltzmann solver codes CAMB [42] or CLASS [46]), N_ℓ is the instrumental noise (which is a function of the frequency channel, see below) and R_ℓ^F refers to the residual foreground subtraction (which will also depend on the frequency channel). This latter quantity reads as

$$R_\ell^F(\nu) = \sum_i^{N_{\rm fore}}\left\{\sigma_i(\nu)C_\ell^i(\nu) + N_\ell(\nu)\frac{4}{N_{\rm chan}(N_{\rm chan}-1)}\frac{C_\ell^i(\nu)}{C_\ell^i(\nu_F)}\right\}, \tag{5.3}$$

where the first term corresponds to the uncertainty of a given foreground at a given frequency ν, $C_\ell^i(\nu)$ and $\sigma_i(\nu)$ represent the power spectra and the foreground subtraction level,

JCAP02(2016)020

respectively. The second term in eq. (5.3) takes into account for the instrumental noise of the channel at which the foreground model is constructed, and ν_F is the frequency at which the foreground is modelled. In the case of a multifrequency experiment, as Planck or COrE, the expression for the likelihood eq. (5.1) still holds. However, in such a scenario, the total noise power that should be added to the C_ℓ is written in terms of a weighted combination of the noises from the different channels [45]. Therefore, for a multifrequency experiment, eq. (5.2) reads as

$$C_\ell = C_\ell^{th} + N_\ell^{\rm eff}\,, \tag{5.4}$$

where the effective noise term is given by

$$(N_\ell^{\rm eff})^{-2} = \sum_{i,j\geq i}^{N_{\rm chan}} \left[\left(R_\ell^F(\nu_i) + N_\ell(\nu_i)\right) \left(R_\ell^F(\nu_j) + N_\ell(\nu_j)\right) \frac{1}{2}\left(1+\delta_{ij}\right) \right]^{-1}. \tag{5.5}$$

We focus here on the future satellite experiment COrE [15], covering 70% of the sky. In the next sections we will describe the modelling of the experimental resolution and the main foregrounds for this future CMB mission, and therefore in what follows the numbers quoted will always refer to $f_{\rm sky} = 0.7$.

5.1.1 Instrumental noise

The sensitivity of the detectors of a given CMB experiment is finite; thus, a certain noise will be induced in the map due to the deconvolution of a Gaussian beam, which reads as [47]

$$N_\ell^{XY} = \sigma^X \sigma^Y \delta_{XY} \exp\left[\ell\left(\ell+1\right)\frac{\theta^2}{8\ln 2}\right], \tag{5.6}$$

where σ^X corresponds to the temperature and polarization sensitivity of the channel, respectively ($X = \{T, P\}$), and θ is the Full Width at Half Maximum (FWHM) of the beam. We follow here the specifications for the future COrE mission given in ref. [15], see table 7 of appendix B.

5.1.2 Foregrounds

Foregrounds, consisting of radio emissions from the galaxy and/or other sources at the same frequency to that of the CMB signature, will clearly be the dominant limiting factors in extracting the cosmological information from the maps. In the case of the polarized signal, foregrounds are critical as they are orders of magnitude higher than the primordial signal in some cases. The usual strategy followed to deal with the foregrounds is to exploit their spectral dependence. Several recent works [48–51] have shown that an accurate multifrequency approach to correctly handle foregrounds is mandatory. Here we will briefly discuss the physical origin of the main foregrounds relevant for the COrE mission[7] and their up-to-date modelling, as provided by the *Planck* team.

[7] Other two sources of foregrounds are the Anomalous Microwave Emission and the Free-Free emission (see ref. [54] for details related to their parametrized power spectra) not discussed here, as their impact at the frequency range of interest is negligible.

JCAP02(2016)020

Synchrotron emission. Synchrotron emission results from the interaction of high energy electrons with the magnetic fields of the galaxy, and its signature will be present in both temperature and polarization maps. Giving the dependence of the synchrotron optical depth with frequency, the power of synchrotron emission C_ℓ^S grows with decreasing frequency. It is usually modelled using maps at 408 MHz [52] and with the WMAP K-band at 23 GHz [53]. The synchrotron power spectra is well fitted using a simple power law for both ℓ and ν. The latest *Planck* model [54] is

$$C_\ell^S = A_S \left(\frac{\ell}{\ell_S}\right)^{\alpha_S} \left(\frac{\nu}{\nu_S}\right)^{2\beta_S}, \tag{5.7}$$

where the values of the different parameters are shown in table 3.

Thermal dust. Contrarily to synchrotron emission, the power at which thermal dust radiates grows with frequency. *Planck* has modelled the dust contamination using a Modified Black Body for which $T_D = 19.6\,\mathrm{K}$. The intensity [54] and polarization [51] spectra can be written as

$$C_\ell^D = A_D \left(\frac{\ell}{\ell_D}\right)^{\alpha_D} \left(\frac{\nu}{\nu_D}\right)^{2\beta_D-4} \left(\frac{B_\nu(T_D)}{B_{\nu_D}(T_D)}\right)^2 \tag{5.8}$$

and

$$C_{\ell\,p}^D = \frac{A_D^p}{2\pi} \left(\frac{\ell}{\ell_D^p}\right)^{\alpha_D^p+2} \left(\frac{\nu}{\nu_D^p}\right)^{2\beta_D^p-4} \left(\frac{B_\nu(T_D)}{B_{\nu_D^p}(T_D)}\right)^2 \tag{5.9}$$

respectively, where $B_\nu(T) = 2h\nu^3c^{-2}/(e^{\frac{h\nu}{kT}}-1)$. The values of the different parameters are specified in table 3.

5.1.3 Statistical method

In order to forecast the errors of the different parameters we follow the widely used Fisher matrix formalism [55]. The Fisher matrix is defined as the expectation value of the second derivative around the maximum of the likelihood

$$F_{ij} = -\left\langle \frac{\partial^2 \mathcal{L}}{\partial\theta_i \partial\theta_j} \right\rangle \Big|_{\vec{\theta}=\vec{\theta}_{\rm fid}}, \tag{5.10}$$

where θ_i represent a cosmological parameter, and $\theta_{i,\rm fid}$ represents the fiducial value for the parameter. The Cramér-Rao bound ensures that for unbiased estimators the best achievable 1σ error for a given parameter marginalized over the other parameters is

$$\sigma_{\theta_i} = \sqrt{F_{ii}^{-1}}, \tag{5.11}$$

with F^{-1} the inverse of the Fisher matrix.

5.1.4 Foreground removal

As argued in the previous section, the main limitation for future CMB observations is the foreground contamination. Among the two polarized foregrounds specified above, the most dangerous one when measuring the tensor-to-scalar ratio r is the galactic dust component, as, in general, it gives the largest contribution at the *Planck* and COrE frequencies.

JCAP02(2016)020

Foreground	Parameter	*Planck*
Synchrotron	A_S ($\mu K^2_{\rm CMB}$)	$(4.2 \pm 0.4) \times 10^9$
	ν_S (GHz)	0.408
	ℓ_S	100
	β_{Syn}	-3.00 ± 0.05
	α_{Syn}	-2.5 ± 0.02
Dust	A_D ($\mu K^2_{\rm CMB}$)	40 ± 3 [a]
	ν_D (GHz)	353
	ℓ_D	100
	β_D	1.51 ± 0.01
	α_D	-2.4 ± 0.02
Dust Polarization	A_{EE} ($\mu K^2_{\rm CMB}$)	247 ± 3 [b]
	A_{BB}/A_{EE}	0.53 ± 0.01
	ν^p_D (GHz)	353
	ℓ^p_D	80
	β^p_D	1.59 ± 0.17
	α_{EE}	-0.42 ± 0.02
	α_{BB}	-0.44 ± 0.03

[a] From ref. [54], after applying color corrections and conversion units.

[b] From table 1 of ref. [51], after applying the color corrections.

Table 3. Parameters for the different foregrounds considered in this study, for both the intensity and polarized emissions. For the intensity signal the models are fitted for $\ell < 100$ and, for polarization, for $60 < \ell < 500$. As commonly carried out in the literature, we will extrapolate the models to higher and lower multipoles for both the intensity and polarization spectra.

The issue of foreground removal is a delicate one. Many techniques like template cleaning, bayesian estimation, internal linear combination or independent component analysis are used for this purpose (see [61] for a summary). For example, in ref. [62], a study forecasting errors on r is performed, without any assumption of the properties of the foregrounds. In refs. [60, 63] the errors on the different cosmological parameters are obtained after marginalising over the foregrounds following some simple models for their spectra. Here, following the approach of [45], we will assume a simple model for the foregrounds (see eqs. (5.7), (5.8) and (5.9)). We shall also assume in the following, for simplicity, that the foregrounds will be subtracted by a constant amount. Given that the Planck mission has achieved a less than 10% foreground removal in power, for the COrE mission, due to the high number and the high sensitivity of channels devoted to the study of the dust, one should expect that power could be removed at the 1% level, which is equivalent to set in eq. (5.3) $\sigma_F(\nu) = 0.01$.

5.2 Results

5.2.1 Future satellite CMB missions

In the following, we shall apply the Fisher matrix method to the future CMB mission COrE (see appendix A for a consistency check of our method), although similar results could be

JCAP02(2016)020

Parameter	Fiducial	*Planck* 2015 [a]	*Planck* (Fisher forecast) [b]	COrE $\sigma_F = 0.01$ [c]	COrE $\sigma_F = 0$ [d]
$\Omega_{\rm b}h^2$	0.02223	0.00017	0.00013	0.000065	0.000052
$\Omega_{\rm DM}h^2$	0.1202	0.0015	0.0012	0.00076	0.00036
h	0.6762	0.0069	0.0054	0.0031	0.0014
$\tau_{\rm reio}$	0.079	0.019	0.018	0.0084	0.0024
$\ln(10^{10}A_s)$	3.117	0.037	0.036	0.015	0.0044
n_s	0.9591	0.0056	0.0053	0.0034	0.0023
α_s	0.0077	0.011	0.0077	0.0040	0.0036
β_s	0.0313	0.014	0.019	0.0088	0.0065
r	0	< 0.23	< 0.38	< 0.016	< 0.0001

[a] Using TTTEEE + lowP *Planck* 2015 data.

[b] Using the *Planck* foreground specifications and the 100, 143 and 217 GHz channels.

[c] Using $\sigma_F = 0.01$ and the 105, 135 165 and 195 GHz channels.

[d] Using only resolution noise and the 105, 135 165 and 195 GHz channels.

Table 4. Results for the Fisher Matrix Analysis, 68% CL for all parameters and for r at 95% CL. The fiducial has been assumed to be the same for each run as given in the second column. We have used $\ell^{TT}_{\rm max} = 2000$ and $\ell^{BB}_{\rm max} = 500$.

obtained for other future CMB satellite experiment. We shall use the 105, 135, 165 and 195 GHz channels for all the runs, see table 7 in the appendix B.[8]

We perform two different analyses. The first one considers no foreground contamination. The second one relies on a 1% foreground subtraction in power ($\sigma_F = 0.01$). We assume no *delensing* on the the B-mode signal. The results are shown in table 4. Comparison between the fifth and sixth columns confirm, numerically, the very-well known fact that foregrounds will be the major limitation for future CMB missions when extracting the tensor-to-scalar-ratio r.

5.2.2 Future constraints on inflationary parameters

Figures 1, 2 and 3 show, together with the theoretical predictions and the current constraints from *Planck* measurements, the results of our COrE forecasts for two possible values of the tensor-to-scalar ratio ($r = 0.1$ and 0.01) and two possible fiducial models. The values of the inflationary parameters for the first fiducial model are $n_s = 0.9591$, $\alpha_s = 0.0077$ and $\beta_s = 0.0313$, which correspond to the best-fit to Planck data. For the second fiducial model, which aims to lie within the region covered by the theoretical models explored here, the values are $n_s = 0.9591$, $\alpha_s = -0.0005$ and $\beta_s = 0$. Tables 5 and 6 show the 1σ errors on the inflationary parameters for these two fiducial models. Notice that the uncertainties on the n_s, α_s, and β_s barely depend on the fiducial value of r, as the tensor-to-scalar ratio is not strongly degenerate with these parameters. The quantity σ_r is the expected error from the COrE experiment. Notice that the error is always larger than the COrE sensitivity limit, $\sim 8 \times 10^{-3}$ (higher than the target of ref. [56], which was the theoretical milestone of 2×10^{-3}). However, the parameter space, the treatment of the foreground removal and the *delensing* assumptions of future CMB missions for the present study and those of ref. [56] are different.

[8] For recent CMB forecasts see refs. [56, 57], where however the parameters α_s and β_s where not considered.

JCAP02(2016)020

r	σ_r	σ_{n_s}	σ_{α_s}	σ_{β_s}
0.1	0.0096	0.0034	0.0040	0.0086
0.01	0.0089	0.0034	0.0040	0.0085

Table 5. Results from the Fisher matrix analysis. The fiducial model corresponds to the *Planck* 2015 best-fit values ($n_s = 0.9591$, $\alpha_s = 0.0077$, $\beta_s = 0.0313$) and the forecasted errors are obtained assuming a foreground removal $\sigma_F = 0.01$ for the future COrE mission.

r	σ_r	σ_{n_s}	σ_{α_s}	σ_{β_s}
0.1	0.0096	0.0040	0.0042	0.011
0.01	0.0088	0.0041	0.0043	0.012

Table 6. As table 5 but for a fiducial model based on the values predicted by the theoretical models explored here ($n_s = 0.9591$, $\alpha_s = -0.0005$, $\beta_s = 0$).

From the forecasted errors in tables 5 and 6 and figure 1 we notice that the measurement of r will not be enough to discriminate between the models on the (r, n_s) plane. As figures 2 and 3 show, the forecasted errors on the additional parameters considered here, α_s and β_s, are wider by an order of magnitude or more than the region of values for which the most favoured inflationary models explored in section 3 spread. Thus, there is no hope in disentangling between the different models using these parameters when the data points to their nominal values of $\alpha_s \approx -0.0005$ and $\beta_s \approx -10^{-5}$. However, notice from figure 3, that if the best-fit value of the β_s parameter arising from future CMB data agrees with its current best-fit from *Planck* measurements, then, this parameter could allow to exclude the inflationary models explored here at a high confidence level (with the precise significance level depending on the particular model under consideration). Finally (see also ref. [44]), the error bars on n_t expected from the CorE mission will be $\sim 3-4$ times larger than the spread of the slow-roll predicted values (as shown in figure 4) and therefore this parameter does not help in disentangling among the possible theoretical schemes.

6 Conclusions

The recent 2015 *Planck* measurements still allow many of the possible theoretical scenarios (as quadratic-like, Higgs-like and Hilltop models) as the underlying inflationary mechanism. A firm confirmation of the inflationary paradigm would require a detection of the primordial gravitational wave signal. However, in order to single out a theoretical model, the usual two slow-roll parameters, that is, the scalar spectral index n_s and the tensor-to-scalar ratio r, may not be sufficient. The reason is due to the fact that the (n_s, r) plane appears to be unevenly filled, with a potentially *forbidden zone* and other highly populated regions in which mostly all the theoretical predictions lie. In this regard, we have explored the discriminating power of two other observables, the running α_s and the running thereof β_s. Our analyses of *Planck* temperature and polarization data show that the current errors on the former two quantities are large, and therefore they do not help in discarding some of the possibilities, even if the present mean value of β_s lies 2σ above its predictions in the most favoured inflationary models explored here. However, future CMB measurements, such as the COrE mission, have the potential to rule-out some theoretical possibilities at a much higher significance, provided the best-fit values for these additional parameters do not change significantly from their current estimates. Our forecasts (which rely on both a simple model for foregrounds

JCAP02(2016)020

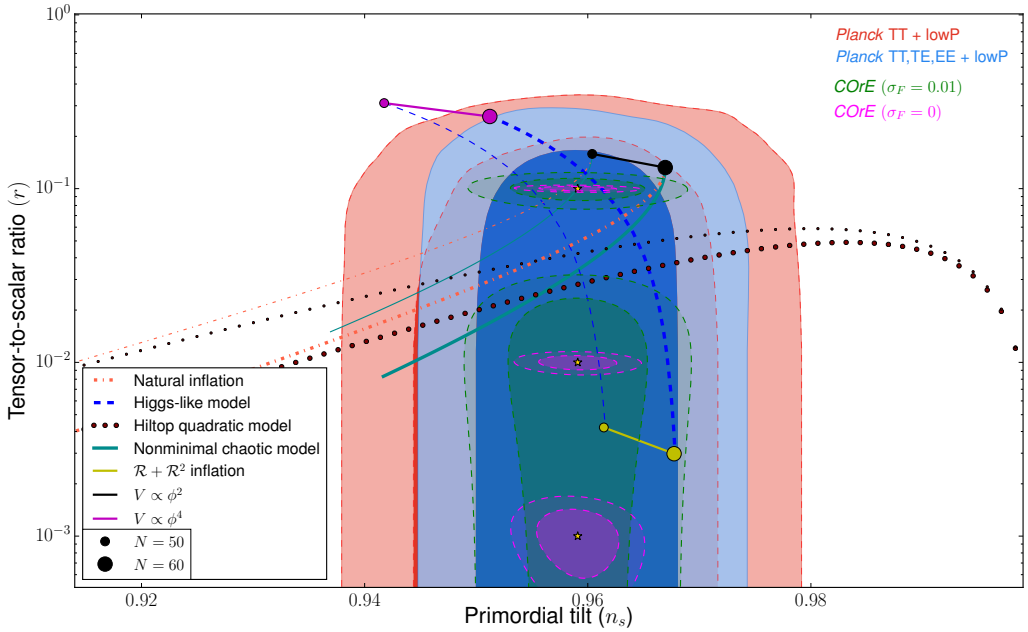

Figure 1. 68% and 95% CL allowed contours from *Planck* TT and lowP and from *Planck* TTTEEE plus lowP in the (n_s, r) plane. We show as well the forecasted 68% and 95% CL contours from the CMB mission COrE considering a 1% foreground removal in power ($\sigma_F = 0.01$) and perfect foreground subtraction ($\sigma_F = 0$). Notice that if the residual foreground emission is only removed to 1% level, the future COrE mission may no disentangle among the different models in the (n_s, r) plane. However, the level at which the foregrounds could be removed may be lower than 1%, but this will only be known once future measurements are performed.

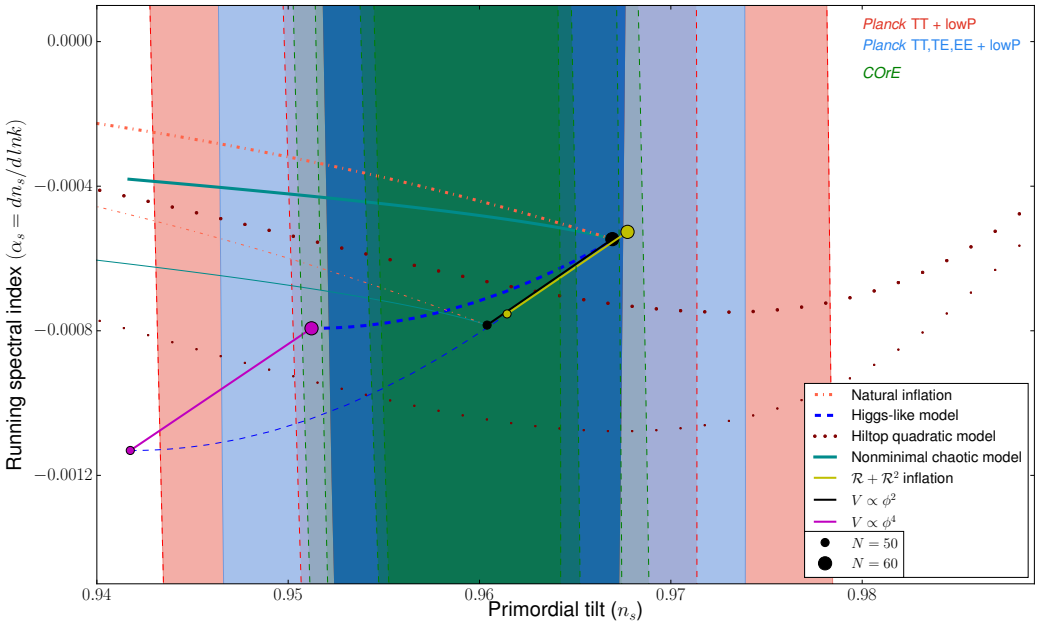

Figure 2. As figure 1 but in the (n_s, α_s) plane, assuming a 1% foreground subtraction in power.

JCAP02(2016)020

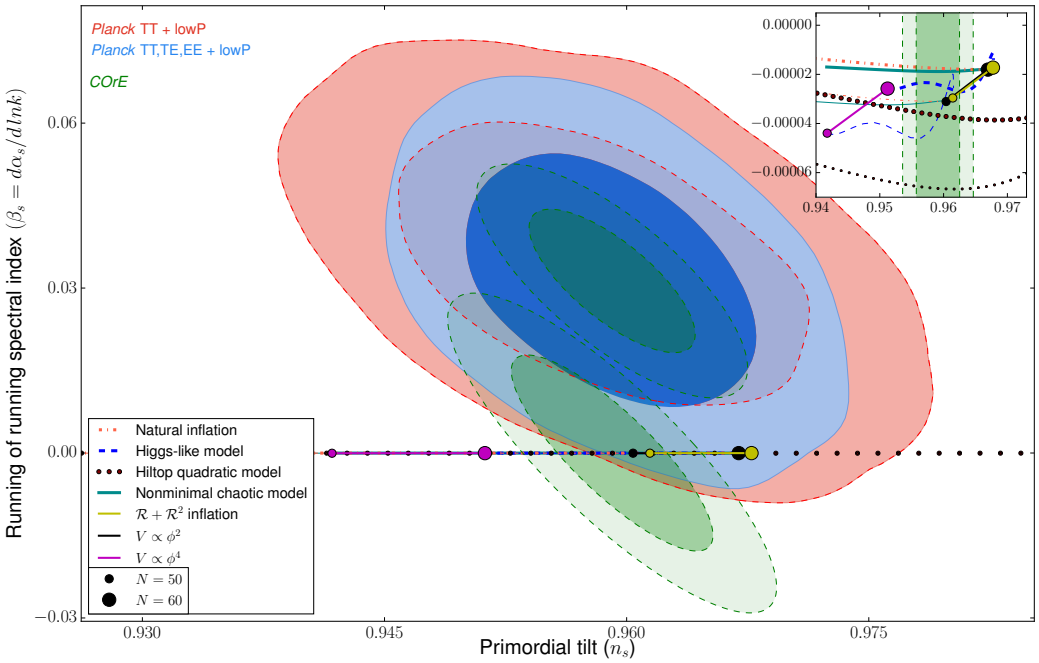

Figure 3. As figure 1 but in the (n_s, β_s) plane, assuming a 1% foreground subtraction in power. If nature has chosen a value of β close to the current best-fit value from *Planck*, then the inflationary models considered here could be excluded by at a high confidence level by future CMB observations.

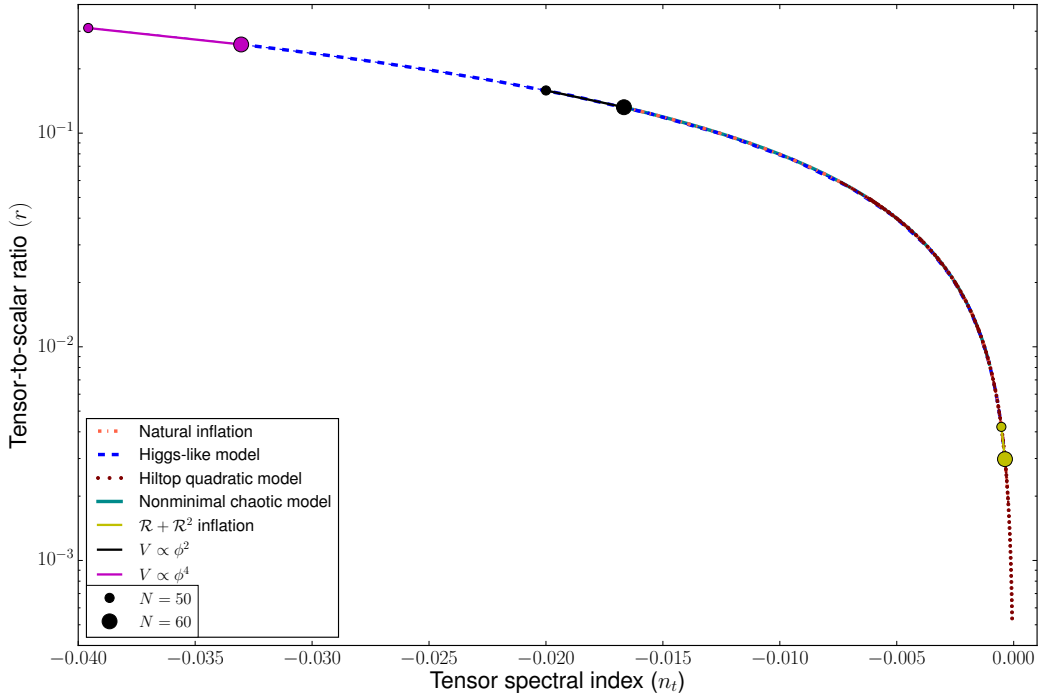

Figure 4. Theoretical predictions in the (n_t, r) plane for the most favoured inflationary models studied here. We do not illustrate the current nor the forecasted contours, as the size of the region depicted here lies well within their 1σ range, showing that n_t can not help much in distinguishing among these theoretical possibilities (see the recent [44]).

JCAP02(2016)020

and assume an *ad-hoc* 1% foreground removal) show that COrE may help enormously in unraveling the inflationary mechanism via its measurement of β_s, especially if Nature has chosen a value of $r \gtrsim 0.005$, which is close to the sensitivity limit found in this study. Other complementary information concerning β_s and/or α_s, as those coming from future planned galaxy surveys [58] (for instance, the SPHEREX project [59]), could significantly improve the sensitivities forecasted here.

Acknowledgments

The authors would like to thank L. Verde for useful comments on the manuscript. OM is supported by PROMETEO II/2014/050, by the Spanish Grant FPA2011–29678 of the MINECO and by PITN-GA-2011-289442-INVISIBLES. LB and HR acknowledge financial support from PROMETEO II/2014/050. ME is supported by Spanish Grant FPU13/03111 of MECD. LB, ME and HR acknowledge the warm hospitality of the HECAP section of the ICTP, where part of this work was done.

A Consistency of the Fisher method

We test the validity of our method by computing our Fisher matrix forecast for the complete *Planck* mission and comparing our results to those obtained by *Planck* measurements. For that purpose, we shall use the 100, 143 and 217 GHz channels of *Planck* with its accounted foreground removal as shown in table 3, and following the specifications detailed in table 7 of the appendix B. From the results depicted in table 4, notice that there is an excellent agreement between the forecasted parameter errors and the errors quoted by the *Planck* collaboration, with the differences always below the 20% level. In addition, we have verified that the correlations between the cosmological parameters are well accounted for.

B CMB mission specifications

Table 7 shows the values used for the sensitivity of *Planck* and COrE missions, as in ref. [15].

JCAP02(2016)020

Mission	Channel (GHz)	FWHM (arcmin)	ΔT ($\mu K_{\rm CMB}$·arcmin)	ΔP ($\mu K_{\rm CMB}$·arcmin)
	30	32.7	203.2	287.4
	44	27.9	239.6	338.9
	70	13.0	221.2	298.7
	100	9.9	31.3	44.2
Planck	143	7.2	20.1	33.3
	217	4.9	28.5	49.4
	353	4.7	107.0	185.3
	535	4.7	1100	-
	857	4.4	8300	-
	45	23.3	5.25	9.07
	75	14.0	2.73	4.72
	105	10.0	2.68	4.63
	135	7.8	2.63	4.55
	165	6.4	2.67	4.61
	195	5.4	2.63	4.54
	225	4.7	2.64	4.57
CORE	255	4.1	6.08	10.5
	285	3.7	10.1	17.4
	315	3.3	26.9	46.6
	375	2.8	68.6	119
	435	2.4	149	258
	555	1.9	227	626
	675	1.6	1320	3640
	795	1.3	8070	22200

Table 7. Specifications of the *Planck* and COrE experiments, from [15].

JCAP02(2016)020

References

[1] A.H. Guth, *The Inflationary Universe: A Possible Solution to the Horizon and Flatness Problems*, *Phys. Rev.* **D 23** (1981) 347 [INSPIRE].

[2] A.D. Linde, *A New Inflationary Universe Scenario: A Possible Solution of the Horizon, Flatness, Homogeneity, Isotropy and Primordial Monopole Problems*, *Phys. Lett.* **B 108** (1982) 389 [INSPIRE].

[3] A. Albrecht and P.J. Steinhardt, *Cosmology for Grand Unified Theories with Radiatively Induced Symmetry Breaking*, *Phys. Rev. Lett.* **48** (1982) 1220 [INSPIRE].

[4] PLANCK collaboration, P.A.R. Ade et al., *Planck 2015 results. XX. Constraints on inflation*, arXiv:1502.02114 [INSPIRE].

[5] L. Knox and Y.-S. Song, *A limit on the detectability of the energy scale of inflation*, *Phys. Rev. Lett.* **89** (2002) 011303 [astro-ph/0202286] [INSPIRE].

[6] M. Kesden, A. Cooray and M. Kamionkowski, *Separation of gravitational wave and cosmic shear contributions to cosmic microwave background polarization*, *Phys. Rev. Lett.* **89** (2002) 011304 [astro-ph/0202434] [INSPIRE].

[7] M. Tucci, E. Martinez-Gonzalez, P. Vielva and J. Delabrouille, *Limits on the detectability of the CMB B-mode polarization imposed by foregrounds*, *Mon. Not. Roy. Astron. Soc.* **360** (2005) 935 [astro-ph/0411567] [INSPIRE].

[8] M. Amarie, C. Hirata and U. Seljak, *Detectability of tensor modes in the presence of foregrounds*, *Phys. Rev.* **D 72** (2005) 123006 [astro-ph/0508293] [INSPIRE].

[9] L. Barranco, L. Boubekeur and O. Mena, *A model-independent fit to Planck and BICEP2 data*, *Phys. Rev.* **D 90** (2014) 063007 [arXiv:1405.7188] [INSPIRE].

[10] L. Boubekeur, E. Giusarma, O. Mena and H. Ramírez, *Phenomenological approaches of inflation and their equivalence*, *Phys. Rev.* **D 91** (2015) 083006 [arXiv:1411.7237] [INSPIRE].

[11] J. García-Bellido and D. Roest, *Large-N running of the spectral index of inflation*, *Phys. Rev.* **D 89** (2014) 103527 [arXiv:1402.2059] [INSPIRE].

[12] G. Efstathiou and S. Chongchitnan, *The search for primordial tensor modes*, *Prog. Theor. Phys. Suppl.* **163** (2006) 204 [astro-ph/0603118] [INSPIRE].

[13] L. Alabidi, *The tensor desert*, *JCAP* **02** (2007) 012 [astro-ph/0608287] [INSPIRE].

[14] S. Bird, H.V. Peiris and R. Easther, *Fine-tuning criteria for inflation and the search for primordial gravitational waves*, *Phys. Rev.* **D 78** (2008) 083518 [arXiv:0807.3745] [INSPIRE].

[15] CORE collaboration, F.R. Bouchet et al., *COrE (Cosmic Origins Explorer) A White Paper*, arXiv:1102.2181 [INSPIRE].

[16] D.H. Lyth, *What would we learn by detecting a gravitational wave signal in the cosmic microwave background anisotropy?*, *Phys. Rev. Lett.* **78** (1997) 1861 [hep-ph/9606387] [INSPIRE].

[17] L. Boubekeur and D. Lyth, *Hilltop inflation*, *JCAP* **07** (2005) 010 [hep-ph/0502047] [INSPIRE].

[18] L. Boubekeur, *Theoretical bounds on the tensor-to-scalar ratio in the cosmic microwave background*, *Phys. Rev.* **D 87** (2013) 061301 [arXiv:1208.0210] [INSPIRE].

[19] A.D. Linde, *Chaotic inflation*, *Phys. Lett.* **B 129** (1983) 177 [INSPIRE].

[20] D.S. Salopek, J.R. Bond and J.M. Bardeen, *Designing Density Fluctuation Spectra in Inflation*, *Phys. Rev.* **D 40** (1989) 1753 [INSPIRE].

[21] T. Futamase and K.-i. Maeda, *Chaotic Inflationary Scenario in Models Having Nonminimal Coupling With Curvature*, *Phys. Rev.* **D 39** (1989) 399 [INSPIRE].

[22] R. Fakir and W.G. Unruh, *Improvement on cosmological chaotic inflation through nonminimal coupling*, *Phys. Rev.* **D 41** (1990) 1783 [INSPIRE].

[23] E. Komatsu and T. Futamase, *Complete constraints on a nonminimally coupled chaotic inflationary scenario from the cosmic microwave background*, *Phys. Rev.* **D 59** (1999) 064029 [astro-ph/9901127] [INSPIRE].

[24] M.P. Hertzberg, *On inflation with non-minimal coupling*, *JHEP* **11** (2010) 023 [arXiv:1002.2995] [INSPIRE].

[25] A. Linde, M. Noorbala and A. Westphal, *Observational consequences of chaotic inflation with nonminimal coupling to gravity*, *JCAP* **03** (2011) 013 [arXiv:1101.2652] [INSPIRE].

[26] L. Boubekeur, E. Giusarma, O. Mena and H. Ramírez, *Does Current Data Prefer a Non-minimally Coupled Inflaton?*, *Phys. Rev.* **D 91** (2015) 103004 [arXiv:1502.05193] [INSPIRE].

[27] K. Freese, J.A. Frieman and A.V. Olinto, *Natural inflation with pseudo-Nambu-Goldstone bosons*, *Phys. Rev. Lett.* **65** (1990) 3233 [INSPIRE].

JCAP02(2016)020

[28] F.C. Adams, J.R. Bond, K. Freese, J.A. Frieman and A.V. Olinto, *Natural inflation: Particle physics models, power law spectra for large scale structure and constraints from COBE*, *Phys. Rev.* **D 47** (1993) 426 [hep-ph/9207245] [INSPIRE].

[29] J.E. Kim, H.P. Nilles and M. Peloso, *Completing natural inflation*, *JCAP* **01** (2005) 005 [hep-ph/0409138] [INSPIRE].

[30] J.P. Conlon, *Quantum gravity constraints on inflation*, *JCAP* **09** (2012) 019 [arXiv:1203.5476] [INSPIRE].

[31] L. Boubekeur, *On the Scale of New Physics in Inflation*, arXiv:1312.4768 [INSPIRE].

[32] A. de la Fuente, P. Saraswat and R. Sundrum, *Natural Inflation and Quantum Gravity*, *Phys. Rev. Lett.* **114** (2015) 151303 [arXiv:1412.3457] [INSPIRE].

[33] B. Heidenreich, M. Reece and T. Rudelius, *Weak gravity strongly constrains large-field axion inflation*, *JHEP* **12** (2015) 108 [arXiv:1506.03447] [INSPIRE].

[34] J. Brown, W. Cottrell, G. Shiu and P. Soler, *On Axionic Field Ranges, Loopholes and the Weak Gravity Conjecture*, arXiv:1504.00659 [INSPIRE].

[35] F.L. Bezrukov and M. Shaposhnikov, *The Standard Model Higgs boson as the inflaton*, *Phys. Lett.* **B 659** (2008) 703 [arXiv:0710.3755] [INSPIRE].

[36] A.O. Barvinsky, A. Yu. Kamenshchik and A.A. Starobinsky, *Inflation scenario via the Standard Model Higgs boson and LHC*, *JCAP* **11** (2008) 021 [arXiv:0809.2104] [INSPIRE].

[37] F. Bezrukov and M. Shaposhnikov, *Standard Model Higgs boson mass from inflation: two loop analysis*, *JHEP* **07** (2009) 089 [arXiv:0904.1537] [INSPIRE].

[38] A.A. Starobinsky, *A New Type of Isotropic Cosmological Models Without Singularity*, *Phys. Lett.* **B 91** (1980) 99 [INSPIRE].

[39] PLANCK collaboration, P.A.R. Ade et al., *Planck 2015 results. XIII. Cosmological parameters*, arXiv:1502.01589 [INSPIRE].

[40] PLANCK collaboration, R. Adam et al., *Planck 2015 results. I. Overview of products and scientific results*, arXiv:1502.01582 [INSPIRE].

[41] PLANCK collaboration, N. Aghanim et al., *Planck 2015 results. XI. CMB power spectra, likelihoods and robustness of parameters*, *Submitted to: Astron. Astrophys.* (2015) [arXiv:1507.02704] [INSPIRE].

[42] A. Lewis, A. Challinor and A. Lasenby, *Efficient computation of CMB anisotropies in closed FRW models*, *Astrophys. J.* **538** (2000) 473 [astro-ph/9911177] [INSPIRE].

[43] A. Lewis and S. Bridle, *Cosmological parameters from CMB and other data: A Monte Carlo approach*, *Phys. Rev.* **D 66** (2002) 103511 [astro-ph/0205436] [INSPIRE].

[44] G. Cabass, L. Pagano, L. Salvati, M. Gerbino, E. Giusarma and A. Melchiorri, *Updated Constraints and Forecasts on Primordial Tensor Modes*, arXiv:1511.05146 [INSPIRE].

[45] L. Verde, H. Peiris and R. Jimenez, *Optimizing CMB polarization experiments to constrain inflationary physics*, *JCAP* **01** (2006) 019 [astro-ph/0506036] [INSPIRE].

[46] J. Lesgourgues, *The Cosmic Linear Anisotropy Solving System (CLASS) I: Overview*, arXiv:1104.2932 [INSPIRE].

[47] L. Knox, *Determination of inflationary observables by cosmic microwave background anisotropy experiments*, *Phys. Rev.* **D 52** (1995) 4307 [astro-ph/9504054] [INSPIRE].

[48] BICEP2, KECK ARRAY collaboration, P.A.R. Ade et al., *BICEP2 /Keck Array V: Measurements of B-mode Polarization at Degree Angular Scales and 150 GHz by the Keck Array*, *Astrophys. J.* **811** (2015) 126 [arXiv:1502.00643] [INSPIRE].

JCAP02(2016)020

[49] BICEP2, Planck collaboration, P. Ade et al., *Joint Analysis of BICEP2/Keck Array and Planck Data*, *Phys. Rev. Lett.* **114** (2015) 101301 [arXiv:1502.00612] [INSPIRE].

[50] Planck collaboration, P.A.R. Ade et al., *Planck 2015 results. XXV. Diffuse low-frequency Galactic foregrounds*, arXiv:1506.06660 [INSPIRE].

[51] Planck collaboration, R. Adam et al., *Planck intermediate results. XXX. The angular power spectrum of polarized dust emission at intermediate and high Galactic latitudes*, arXiv:1409.5738 [INSPIRE].

[52] C.G.T. Haslam, C.J. Salter, H. Stoffel and W.E. Wilson, *A 408 MHz all-sky continuum survey. II. The atlas of contour maps*, *Astron. Astrophys. Suppl. Ser.* **47** (1982) 1.

[53] WMAP collaboration, C. Bennett et al., *First year Wilkinson Microwave Anisotropy Probe (WMAP) observations: Foreground emission*, *Astrophys. J. Suppl.* **148** (2003) 97 [astro-ph/0302208] [INSPIRE].

[54] Planck collaboration, P.A.R. Ade et al., *Planck intermediate results. XXII. Frequency dependence of thermal emission from Galactic dust in intensity and polarization*, *Astron. Astrophys.* **576** (2015) A107 [arXiv:1405.0874] [INSPIRE].

[55] R.A. Fisher, *The Logic of Inductive Inference*, *J. Roy. Statist. Soc.* **1** (1935) 98.

[56] P. Creminelli, D.L. López Nacir, M. Simonović, G. Trevisan and M. Zaldarriaga, *Detecting Primordial B-Modes after Planck*, *JCAP* **11** (2015) 031 [arXiv:1502.01983] [INSPIRE].

[57] Q.-G. Huang, S. Wang and W. Zhao, *Forecasting sensitivity on tilt of power spectrum of primordial gravitational waves after Planck satellite*, *JCAP* **10** (2015) 035 [arXiv:1509.02676] [INSPIRE].

[58] T. Basse, J. Hamann, S. Hannestad and Y.Y.Y. Wong, *Getting leverage on inflation with a large photometric redshift survey*, *JCAP* **06** (2015) 042 [arXiv:1409.3469] [INSPIRE].

[59] O. Doré et al., *Cosmology with the SPHEREX All-Sky Spectral Survey*, arXiv:1412.4872 [INSPIRE].

[60] M. Remazeilles, C. Dickinson, H.K.K. Eriksen and I.K. Wehus, *Sensitivity and foreground modelling for large-scale CMB B-mode polarization satellite missions*, arXiv:1509.04714 [INSPIRE].

[61] J. Dunkley et al., *CMBPol Mission Concept Study: Prospects for polarized foreground removal*, *AIP Conf. Proc.* **1141** (2009) 222 [arXiv:0811.3915] [INSPIRE].

[62] M. Betoule, E. Pierpaoli, J. Delabrouille, M.L. Jeune and J.-F. Cardoso, *Measuring the tensor to scalar ratio from CMB B-modes in presence of foregrounds*, *Astron. Astrophys.* **503** (2009) 691 [arXiv:0901.1056] [INSPIRE].

[63] J. Errard, S.M. Feeney, H.V. Peiris and A.H. Jaffe, *Robust forecasts on fundamental physics from the foreground-obscured, gravitationally-lensed CMB polarization*, arXiv:1509.06770 [INSPIRE].

JCAP02(2016)020

Journal of Cosmology and Astroparticle Physics
An IOP and SISSA journal

Reconciling tensor and scalar observables in G-inflation

Héctor Ramírez,[a,b] **Samuel Passaglia,**[c] **Hayato Motohashi,**[d] **Wayne Hu**[c] **and Olga Mena**[b]

[a]Departamento de Física Teórica, Universidad de Valencia,
Dr. Moliner 50, E-46100 Burjassot, Spain
[b]Instituto de Física Corpuscular (IFIC), Universidad de Valencia-CSIC,
Catedrático José Beltrán 2, E-46980, Paterna, Spain
[c]Kavli Institute for Cosmological Physics & Department of Astronomy and Astrophysics,
The University of Chicago,
5640 South Ellis Avenue, Chicago, IL 60637, U.S.A.
[d]Center for Gravitational Physics, Yukawa Institute for Theoretical Physics,
Kyoto University,
Kitashirakawa-Oiwakecho, Sakyo-Ku, Kyoto 606-8502, Japan

E-mail: hector.ramirez@uv.es, passaglia@uchicago.edu,
hayato.motohashi@yukawa.kyoto-u.ac.jp, whu@background.uchicago.edu,
omena@ific.uv.es

Received February 25, 2018
Accepted April 1, 2018
Published April 11, 2018

Abstract. The simple $m^2\phi^2$ potential as an inflationary model is coming under increasing tension with limits on the tensor-to-scalar ratio r and measurements of the scalar spectral index n_s. Cubic Galileon interactions in the context of the Horndeski action can potentially reconcile the observables. However, we show that this cannot be achieved with only a constant Galileon mass scale because the interactions turn off too slowly, leading also to gradient instabilities after inflation ends. Allowing for a more rapid transition can reconcile the observables but moderately breaks the slow-roll approximation leading to a relatively large and negative running of the tilt α_s that can be of order $n_s - 1$. We show that the observables on CMB and large scale structure scales can be predicted accurately using the optimized slow-roll approach instead of the traditional slow-roll expansion. Upper limits on $|\alpha_s|$ place a lower bound of $r \gtrsim 0.005$ and, conversely, a given r places a lower bound on $|\alpha_s|$, both of which are potentially observable with next generation CMB and large scale structure surveys.

Keywords: inflation, cosmological parameters from CMBR

ArXiv ePrint: 1802.04290

 https://doi.org/10.1088/1475-7516/2018/04/039

JCAP04(2018)039

Contents

1 Introduction

Inflation is a leading paradigm able to solve the main problems of the standard model of cosmology and, at the same time, able to generate the quantum seeds that could have given rise to the structures we see today in the sky. The canonical picture consists of introducing a new scalar field minimally coupled to Einstein gravity, the inflaton, which drives the expansion of the Universe from quantum to cosmological scales at an exponential rate while it slowly rolls towards the minimum of its potential. This potential is required to be sufficiently flat in order to have enough time to form a Universe consistent with the isotropy and homogeneity observed today. Although the paradigm itself is consistent with the latest observational constraints on the scalar and tensor power spectra (see e.g. [1]), simple quadratic and monomial potentials are coming into increasing conflict with these constraints.

Inflationary models with noncanonical terms can arise naturally from particle physics and allow more freedom to satisfy observational constraints [2–8]. Models with nonminimal couplings, for instance, are able to reconcile with current measurements some of the earliest and simplest realizations of inflation, such as those with power-law potentials [9–15].

General scalar-tensor theories of gravity provide a unified framework upon which one can construct new models of inflation or embed known ones in a broader context. The most general four-dimensional scalar-tensor theory in curved space-time which leads to second-order equations of motion — thus free from ghosts and related instabilities — is the Horndeski [16], or generalized Galileon [17–19], theory.[1] Recently there have been efforts to construct models of so-called G-inflation using the Horndeski Lagrangian by explicitly choosing the form of the independent functions of the scalar field and its derivatives. Such models must be carefully constructed to avoid instabilities, given that the Galilean symmetry should be broken in order to have a successful inflation [19, 29–33].

When constructing phenomenologically viable models in the more general parameter space, the usual slow-roll approximation may not always suffice to describe observables. While numerically solving the scalar and tensor equations of motion is always possible, generalized slow-roll (GSR) techniques have been developed to overcome the deficiencies of the traditional

[1] While healthy theories beyond Horndeski have been developed to include higher derivatives in the equations of motion (see [20–28]), we will restrict our analysis to models within the Horndeski framework.

JCAP04(2018)039

slow-roll approach [34–40]. In particular the optimized slow-roll (OSR) expansion of GSR provides an improved way of evaluating scalar and tensor spectra for inflationary models with slow-roll violation on a time scale of a few e-folds or larger [39]. Recently these approaches have been extended to cover the full space of Horndeski models, allowing one to compute the inflationary observables without imposing the slow-roll conditions [41]. Their efficacy have been tested for large slow-roll violations such as those required by primordial black hole (PBH) formation models [42].

In this paper we show that it is possible to reconcile the observational tension between scalar and tensor observables in $m^2\phi^2$ inflation by introducing a transient G-inflation regime, for which the GSR and OSR formulas provide a good description of inflationary observables. In section 2 we review the Horndeski Lagrangian and show why simple models with a constant Galileon interaction mass scale introduced in previous studies [32] can no longer satisfy the latest observational constraints. In section 3 we show how to overcome these difficulties by introducing a transition during inflation that transiently violates the slow-roll approximation. In section 4 we show how the GSR and OSR techniques accurately relate the parameters of these models to the scalar and tensor observables. Finally, we conclude in section 5.

2 Potential-driven G-inflation

Horndeski gravity is the most general scalar-tensor theory in four dimensions which leads to second-order equations of motion. The full Lagrangian is given by

$$\begin{aligned}\mathcal{L}_{\mathcal{H}} = {} & G_2 + G_3\Box\phi + G_4 R \\ & - 2G_{4,X}[(\Box\phi)^2 - \phi^{;\mu\nu}\phi_{;\mu\nu}] + G_5 G^{\mu\nu}\phi_{;\mu\nu} \\ & + \frac{G_{5,X}}{3}[(\Box\phi)^3 - 3(\Box\phi)\phi_{;\mu\nu}\phi^{;\mu\nu} + 2\phi_{;\mu\nu}\phi^{;\mu\sigma}\phi^{;\nu}{}_{;\sigma}]\,,\end{aligned} \tag{2.1}$$

where $G_n = G_n(\phi, X)$ are arbitrary functions of ϕ and $X \equiv g^{\mu\nu}\partial_\mu\phi\partial_\nu\phi$, $G_{n,X} \equiv \partial G_n/\partial X$, $\phi_{;\mu\nu} = \nabla_\mu\nabla_\nu\phi$ and R and $G_{\mu\nu}$ are the Ricci and Einstein tensors respectively. For $G_2 = -X/2 - V(\phi)$, $G_4 = 1/2$, and $G_3 = G_5 = 0$, we recover the Lagrangian for canonical inflation[2].

From eq. (2.1) one can now choose the G_n functions to construct more general phenomenological models of inflation given that the simplest realizations are being ruled out by the latest cosmological measurements. For instance, the chaotic inflation model provides a large value for the tensor-to-scalar ratio r which is disfavored by current observations. Ref. [32] showed that with the introduction of a G_n term the relationship between the tensor and scalar observables can be modified. However, we shall now see that under the slow-roll approximation, this additional freedom is not sufficient to reconcile observations with the predictions of chaotic inflation.

Concretely, ref. [32] considered a model of potential-driven G-inflation of the form

$$\begin{aligned} G_2(\phi, X) &= -\frac{X}{2} - V(\phi)\,, \\ G_3(\phi, X) &= f_3\frac{X}{2}\,, \\ G_4(\phi, X) &= \frac{1}{2}\,, \\ G_5(\phi, X) &= 0\,, \end{aligned} \tag{2.2}$$

[2]Here and throughout we take units where $M_{\rm Pl} = 1/\sqrt{8\pi G} = 1$.

JCAP04(2018)039

with a chaotic inflation potential $V(\phi) = m^2\phi^2/2$ and $f_3 = -M^{-3}$, where m and M are the inflaton and Galileon mass scales respectively.[3]

Taking eqs. (2.2), assuming the general case in which $f_3 = f_3(\phi)$, and working on the flat Friedmann-Lemaître-Robertson-Walker (FLRW) metric,

$$\mathrm{d}s^2 = -\mathrm{d}t^2 + a(t)^2\delta_{ij}\mathrm{d}x^i\mathrm{d}x^j, \tag{2.3}$$

the Einstein and Klein-Gordon equations can be written as

$$\begin{aligned}
V - \left(3 - \frac{1}{2}\phi'^2\right)H^2 + \left(3f_3\phi'^3 - \frac{f_{3,\phi}}{2}\phi'^4\right)H^4 = 0\,,\\
V - 2H'H - \left(3 + \frac{1}{2}\phi'^2\right)H^2 + f_3H^3H'\phi'^3 + \left(f_3\phi'^2\phi'' + \frac{f_{3,\phi}}{2}\phi'^4\right)H^4 = 0\,,\\
V_{,\phi} + HH'\phi' + \left(3\phi' + \phi''\right)H^2 + \left(9f_3H'\phi'^2 - 2f_{3,\phi}H'\phi'^3\right)H^3\\
+ \left(9f_3\phi'^2 + 6f_3\phi'\phi'' - 2f_{3,\phi}\phi'^2\phi'' - \frac{f_{3,\phi\phi}}{2}\phi'^4\right)H^4 = 0\,,
\end{aligned} \tag{2.4}$$

where H is the Hubble parameter and derivatives are defined as $' \equiv \mathrm{d}/\mathrm{d}N$, being $\mathrm{d}N \equiv H\mathrm{d}t = (H/\dot{\phi})\mathrm{d}\phi$ the number of e-foldings of inflation, and ${}_{,\phi} \equiv \mathrm{d}/\mathrm{d}\phi$.

In the slow-roll (SR) approach, eqs. (2.4) may be approximated as [32]

$$\begin{aligned}
3H^2 \approx V,\\
3H^2\phi'(1+\mathcal{A}) + V_{,\phi} \approx 0\,,
\end{aligned} \tag{2.5}$$

and

$$\epsilon_H \equiv -\frac{H'}{H} \approx \frac{1}{2(1+\mathcal{A})}\left(\frac{V_{,\phi}}{V}\right)^2. \tag{2.6}$$

Here

$$\mathcal{A} \equiv 3f_3H^2\phi' \tag{2.7}$$

measures the deviation from canonical inflation: for $|\mathcal{A}| \ll 1$ the Galileon term produces negligible effects. In section 3.1, we use this slow-roll approximation for ϵ_H, eq. (2.6), as a test of the slow-roll approximation itself. For the chaotic inflation potential, $\phi' < 0$ and thus if $f_3 < 0$ the combination of eqs. (2.5) and (2.7) gives

$$\mathcal{A} \approx \frac{\sqrt{1 - 4f_3V_{,\phi}} - 1}{2}. \tag{2.8}$$

The original G-inflation model, hereafter called the "G-model," took a constant $f_3 = -M^{-3}$ so that far up the potential or at early times the Galileon term dominates, whereas the canonical terms come to dominate as the field rolls down. The transition between the two regimes is marked by $\mathcal{A} = 1$ where $V_{,\phi} = -2/f_3 = 2M^3$ [32]. It is therefore interesting to consider the relationship between the tensor and scalar observables as a function of $\mathcal{A}$. The scalar and tensor power spectra, under the slow-roll approximation, can be written as [32]

$$\begin{aligned}
\Delta_\zeta^{2\,(\mathrm{SR})} = \frac{V^3}{12\pi^2V_{,\phi}^2}\frac{(1+\mathcal{A})^2\,(1+2\mathcal{A})^{1/2}}{(1+4\mathcal{A}/3)^{3/2}}\,,\\
\Delta_\gamma^{2\,(\mathrm{SR})} = \frac{V}{6\pi^2}\,,
\end{aligned} \tag{2.9}$$

[3] G-inflation was originally introduced in [19, 29] as a model for inflation driven kinetically by the Galileon field. The models discussed here, on the other hand, are potential-driven versions, first studied in [31].

JCAP04(2018)039

where the tensor power spectrum is defined for each polarization state separately and is not modified from its form in canonical inflation. Therefore for the same position on the potential in field space, the G-model enhances scalar power over tensor power linearly in $\mathcal{A}$ for $\mathcal{A} \gg 1$.

However, given the strong experimental constraints on the tilt, the tensor-to-scalar ratio of the G-model should be compared to chaotic inflation at the same tilt rather than the same field value. The scalar tilt and tensor-to-scalar ratio are defined as usual as

$$n_s - 1 \equiv \frac{\mathrm{d}\ln\Delta^2_\zeta}{\mathrm{d}\ln k}\,, \tag{2.10}$$

$$r \equiv 4\,\frac{\Delta^2_\gamma}{\Delta^2_\zeta}\,. \tag{2.11}$$

For comparison to the CMB observables, these should be evaluated at $k = k_* = 0.05\ \mathrm{Mpc}^{-1}$. These evaluations require converting a given field value ϕ to a wavenumber k. Under slow-roll, scalar fluctuations freeze out[4] when $c_s k = aH$, and therefore this relationship requires a mapping between field values and the number of e-folds to the end of inflation $\Delta N = N_f - N$. From eqs. (2.4) and (2.7),

$$\Delta N \simeq \int_{\phi_f}^{\phi} (1+\mathcal{A})\frac{V}{V_{,\tilde\phi}}\mathrm{d}\tilde\phi\,. \tag{2.12}$$

Putting these relations together ref. [32] found for $\mathcal{A} \gg 1$,

$$n_s - 1 = -\frac{9}{5\Delta N + 2}\,, \qquad r = \frac{64\sqrt{6}}{9}\frac{2}{5\Delta N + 2}\,,$$

where, by eliminating the e-folds to the end of inflation, we obtain the parametric relation

$$r = -\frac{128}{27}\sqrt{\frac{2}{3}}(n_s - 1)\,. \tag{2.13}$$

For the $\mathcal{A} \ll 1$ limit, one recovers the canonical chaotic predictions

$$n_s - 1 = -\frac{4}{2\Delta N + 1}\,, \qquad r = \frac{16}{2\Delta N + 1}\,,$$

which combined give

$$r = -4(n_s - 1)\,. \tag{2.14}$$

ref. [32] noted that for a fixed e-fold, $\Delta N \sim 50 - 60$, the $\mathcal{A} \gg 1$ case has a lower r and larger n_s. However we see from eqs. (2.13) and (2.14) that for the same n_s, the $\mathcal{A} \gg 1$ limit lowers r only by a negligible factor of ≈ 0.97. With recent improvements in the constraints on both parameters, the G-model cannot cure the r-n_s problem of the canonical ϕ^2 model given any choice of M or ΔN. Furthermore no smooth transition or interpolation between these two very close forms can solve this problem either. Monomial potentials with steeper indices than ϕ^2 face a similar issue.

While this might seem like a no-go for simple ϕ^n potentials, we will show in the following sections that a more rapid transition between these two limits provides a solution where

[4]Note that the scalar sound speed is $c_s = \sqrt{2/3}$ for $\mathcal{A} \gg 1$ and $c_s = 1$ for $\mathcal{A} \ll 1$ whereas the tensor sound speed is $c_t = 1$. Even in slow-roll, the freeze-out condition should in principle differ between the two as we discuss below, but given slow variation of the expressions in (2.8) and (2.9), ref. [32] ignored these distinctions.

JCAP04(2018)039

the scalar tilt is substantially but transiently lowered while $\mathcal{A}$ remains sufficiently large to suppress r. Furthermore by allowing a more rapid transition, we automatically cure the gradient instability problem for these models. This problem arises if the transition to $\mathcal{A} < 1$ occurs after the end of inflation such that the scalar sound speed squared c_s^2 oscillates and becomes negative during reheating. In the original G-inflation model, this restriction places a lower limit on M [32] and an upper limit on the enhancements to the scalar power spectrum through $\mathcal{A}$. However, by making the transition more rapid, we can make it complete before the end of inflation for any M.[5]

3 Potential-driven G-inflation with step

As discussed in the previous section, the phenomenological problems of the original version of G-inflation arise because the transition to canonical inflation takes place too slowly. To resolve these problems, we promote f_3 in eq. (2.2) to be a step-like function of ϕ, hereafter called the "Step model",

$$f_3(\phi) = -M^{-3}\left[1 + \tanh\left(\frac{\phi - \phi_r}{d}\right)\right], \tag{3.1}$$

where ϕ_r and d are new parameters of the model related to the position in field space and the width of the step respectively. This allows us to control the epoch and the rapidity of the transition from G-inflation to canonical inflation. By making this transition sufficiently rapid we can evade the observational problems in the r-n_s plane as well as eliminate the gradient instabilities at the end of inflation.

3.1 Background transition

With $f_3(\phi)$ given in eq. (3.1), we can numerically solve the background equations (2.4) following the procedure explained in [32]. As discussed in section 2, the transition from G-inflation to canonical inflation is controlled by $\mathcal{A}$ in eq. (2.7): namely, $\mathcal{A}$ evolves from $\mathcal{A} \gg 1$ to $\mathcal{A} \ll 1$, with the transition occuring at $\mathcal{A} \approx 1$. For the model in eq. (3.1), the rapidity of the transition is controlled by the step width d. Figure 1 shows the evolution of $\mathcal{A}$ for different values of d with m, M and ϕ_r fixed to values which we will motivate below. One can see that the transition takes fewer e-folds N for a sharp step, i.e. for a small d. In these Step model examples N is defined in such a way that at the end of inflation $N_f = 55$. We then take $N = 0$ as the epoch when CMB scales or specifically $k_* = 0.05$ Mpc^{-1} left the scalar sound horizon

$$\int_0^{55} \mathrm{d}N \, \frac{c_s}{aH} = 20\,\mathrm{Mpc}\,. \tag{3.2}$$

Note that the wider the step is, the more the e-fold for which $\mathcal{A} = 1$ lags $N(\phi_r)$ (shown with vertical lines), when the inflaton passes the center of the step.

With a rapid transition, we generically expect that the SR approximation will break down. In figure 2 we show the evolution of ϵ_H for the same cases as figure 1 calculated numerically and through the slow-roll approximation of eq. (2.6). In the slow-roll comparisons here and below we use the numerical computation of $\phi(N)$ to avoid conflating errors in the mapping of eq. (2.12) and local deviations from slow-roll at a given N. Before and after

[5] In [33], the addition of a kinetic X^2 term to the Lagrangian was proposed. This term adds a positive contribution to c_s^2, thus removing gradient instabilities. However, the effect of the Galileon term was weakened.

JCAP04(2018)039

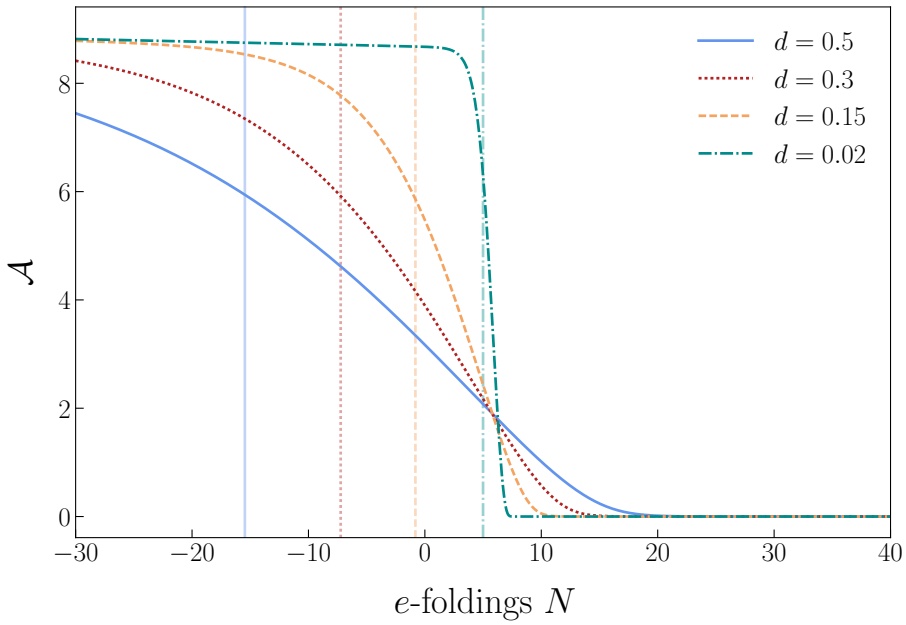

Figure 1. G-inflation transition parameter $\mathcal{A}$ from eq. (2.7) as a function of e-folds N, for the model given in eq. (3.1) and for the values $M = 1.303 \times 10^{-4}$, $m = 2.58 \times 10^{-6}$, $\phi_r = 13.87$ and four different values of the step width d: $d = \{0.5, 0.3, 0.15, 0.02\}$. Vertical lines denote $N(\phi_r)$, the epoch at which the inflaton crosses the center of the step.

the transition (but before the end of inflation), the slow-roll approximation is quite good. Near the transition, however, fractional differences increase as d decreases (figure 2, middle panel). Furthermore, for a rapid evolution of ϵ_H, it is expected that the second SR parameter, $\delta_1 = \frac{1}{2}\frac{\mathrm{d}\ln\epsilon_H}{\mathrm{d}N} - \epsilon_H$, be of order ~ 1, reaffirming the SR breakdown, as shown in the lower panel of figure 2. In both cases, the SR deviations peak near the epoch when $\mathcal{A} = 1$ (vertical lines). The rapid evolution of ϵ_H and corresponding breakdown of the slow-roll approximation requires going beyond the slow-roll approximation for the accurate calculation of scalar and tensor observables as we shall see in the next section.

To finish the discussion on the background solutions, figure 3 shows the evolution of the sound speed squared of scalar perturbations, c_s^2, as a function of N (see eq. (3.4) for details). The value $M = 1.303 \times 10^{-4}$ of the Galileon mass scale used here is below the lower limit obtained in [32] corresponding to the avoidance of gradient instabilities in the G-model case. However, as expected for the Step model, we see that as long as the width is not very large that the transition fails to complete by the end of inflation, the gradient instabilities disappear — c_s^2 is always positive — and this holds independently of the value of the Galileon mass scale M. Since inflation ends at $\phi \sim 1$, this condition corresponds to setting the transition ϕ_r sufficiently large given the width d.

JCAP04(2018)039

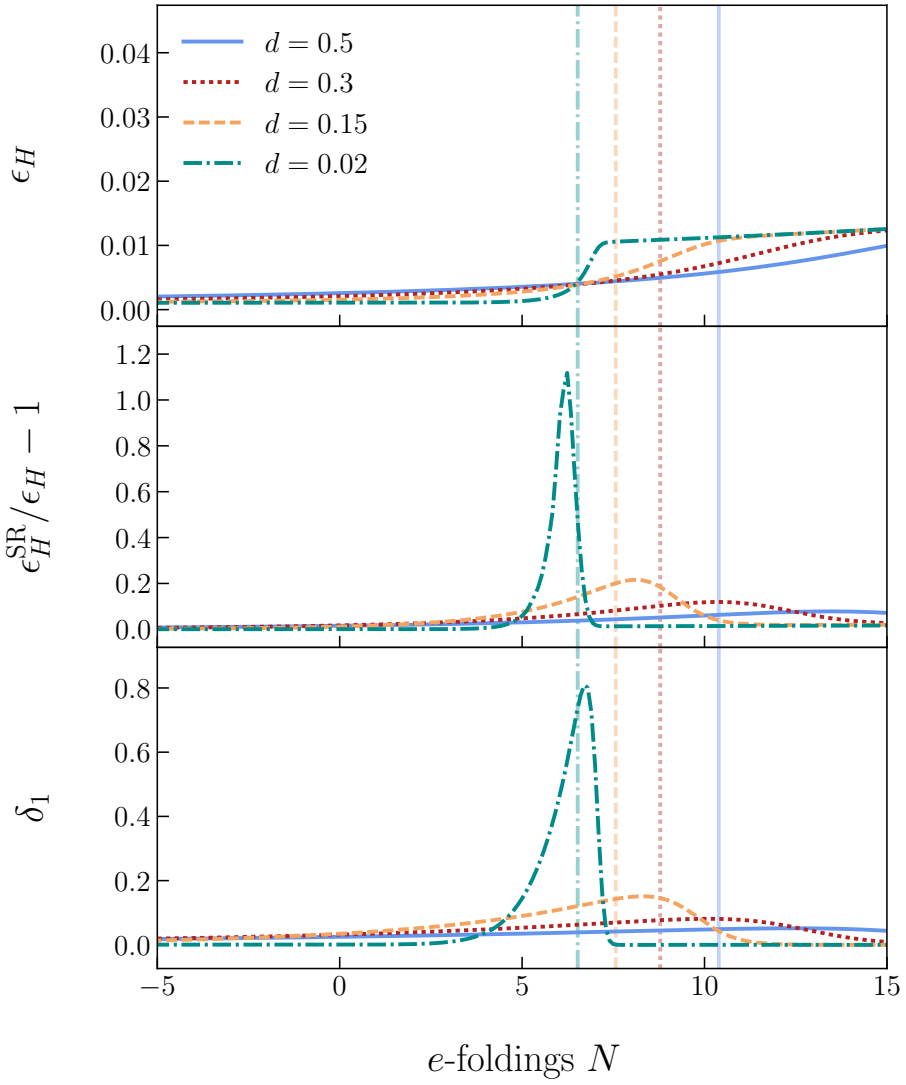

Figure 2. Exact solution for the slow-roll prediction of ϵ_H (r.h.s. of eq. (2.6)) (upper panel), fractional difference between the solution employing the approximation in eq. (2.12) and the exact background value (middle panel), and exact solution for the slow-roll parameter $\delta_1 = \frac{1}{2}\frac{\mathrm{d}\ln\epsilon_H}{\mathrm{d}N} - \epsilon_H$ (lower panel). All as a function of N and for the same models of figure 1. The vertical lines represent $N(\mathcal{A} = 1)$ for each curve where the SR violation is nearly maximal.

3.2 Inflationary observables

In order to compute inflationary observables, we expand to quadratic order in scalar and tensor perturbations the action for $\mathcal{L}_\mathcal{H}$ given in eq. (2.1):

$$S_\zeta^{(2)} = \int \mathrm{d}^4x \frac{a^3 b_s \epsilon_H}{c_s^2}\left(\dot{\zeta}^2 - \frac{c_s^2 k^2}{a^2}\zeta^2\right),$$
$$S_\gamma^{(2)} = \sum_{\lambda=+,\times}\int \mathrm{d}^4x \frac{a^3 b_t}{4c_t^2}\left(\dot{\gamma}_\lambda^2 - \frac{c_t^2 k^2}{a^2}\gamma_\lambda^2\right), \tag{3.3}$$

JCAP04(2018)039

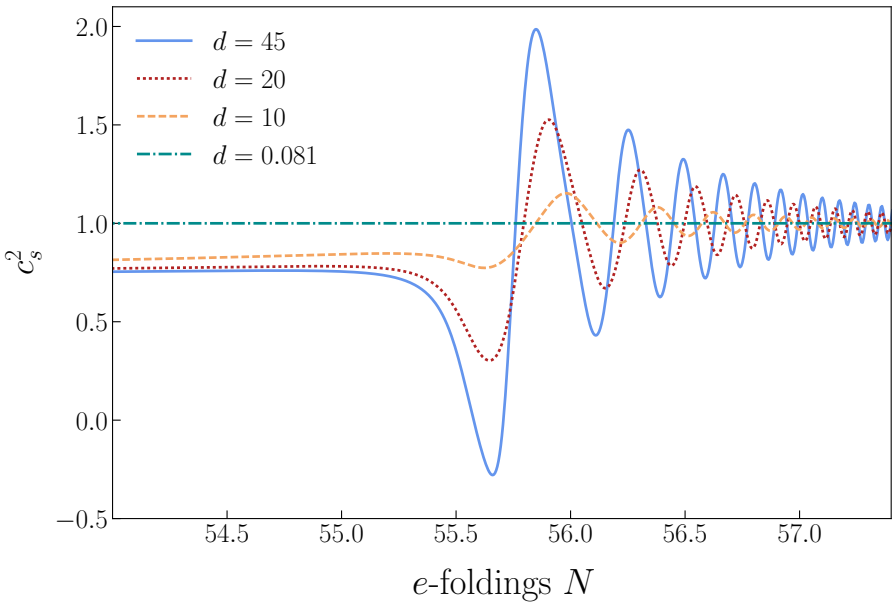

Figure 3. Scalar sound speed squared near the end of inflation $N_f = 55$ for the choice of values $M = 1.303 \times 10^{-4}$, $m = 2.58 \times 10^{-4}$, $\phi_r = 13.87$ and four different values of the step parameter d: $d = \{0.081, 10, 20, 45\}$. Except for the widest case of $d = 45$, the step ensures that the transition completes before the end of inflation, $\mathcal{A}(\phi_f) < 1$, and eliminates the gradient instability, i.e. $c_s^2 > 0$.

parametrized by the sound speeds $c_{s,t}$ and normalization factors $b_{s,t}$ for scalar and tensor perturbations which contain all the information coming from the Horndeski framework [41]. For the choice given in eqs. (2.2) these parameters can be computed as[6]

$$\begin{aligned} b_s &= \frac{2\mu_1 H - 2\mu_1' H - \mu_1^2}{\epsilon_H}\,, \\ c_s^2 &= \frac{3\left(2\mu_1 H - 2\mu_1' H - \mu_1^2\right)}{4\mu_2 + 9\mu_1^2}\,, \\ b_t &= 1\,, \qquad c_t^2 = 1\,, \end{aligned} \tag{3.4}$$

where

$$\begin{aligned} \mu_1 &= 2H - f_3 H^3 \phi'^3\,, \\ \mu_2 &= -9H^2 - 3 f_{3,\phi} H^4 \phi'^4 + \frac{3}{2}\left(1 + 12 H^2 f_3 \phi'\right) H^2 \phi'^2\,. \end{aligned} \tag{3.5}$$

Notice that, for the choice of eqs. (2.2), the tensor action is not modified from that of canonical inflation.

Varying the quadratic actions given in eqs. (3.3) we arrive at the Mukhanov-Sasaki equation

$$\frac{\mathrm{d}^2 u_i}{\mathrm{d}\tau^2} + \left(c_i^2 k^2 - \frac{1}{z_i}\frac{\mathrm{d}^2 z_i}{\mathrm{d}\tau^2}\right) u_i = 0\,. \tag{3.6}$$

Here and below τ is the (positive, decreasing) conformal time until the end of inflation, and $i = s, t$ for the scalar and tensor perturbations respectively. We define the Mukhanov-Sasaki

[6]For the general case in which none of the G_n functions are taken to be equal to zero see [19, 32].

JCAP04(2018)039

variable as $u_s \equiv z_s\zeta$ and $u_t \equiv z_t\gamma$ with

$$z_s = a\frac{\sqrt{2b_s\epsilon_H}}{c_s}\,, \qquad z_t = \frac{a}{c_t}\sqrt{\frac{b_t}{2}}\,, \tag{3.7}$$

for the quadratic actions in eq. (3.3).

As shown in figure 2, for the Step model with a small step width we cannot apply the slow-roll approximation to solve eq. (3.6) due to the fact that the slow-roll conditions are violated near the transition where $\mathcal{A} \sim 1$. We instead solve this equation numerically from Bunch-Davies initial conditions to compute the power spectra as

$$\begin{aligned}\Delta^2_\zeta(k) &= \lim_{k\tau\to 0}\frac{k^3}{2\pi^2}\left|\zeta\right|^2\,,\\ \Delta^2_\gamma(k) &= \lim_{k\tau\to 0}\frac{k^3}{2\pi^2}\left|\gamma_{+,\times}\right|^2\,,\end{aligned} \tag{3.8}$$

which define the inflationary parameters $n_s(k)$ and $r(k)$ through eq. (2.11).

We now construct a working example of transient G-inflation in order to examine its observable phenomenology further. With the convention that the CMB mode exits the scalar sound horizon 55 e-folds before the end of inflation, the Step model has four remaining free parameters: the mass scales M and m, and the step parameters ϕ_r and d. The inflaton mass scale m mainly controls the Hubble rate and hence the amplitude of the power spectra. We choose it to satisfy the *Planck* 2015 TT+lowP measurement of the scalar amplitude $A_s = \Delta^2_\zeta(k_*) = (2.198 \pm 0.08) \times 10^{-9}$ [1]. For a fixed m, the Galileon mass scale M determines $\mathcal{A}$ when the CMB mode leaves the horizon, which sets the tensor amplitude relative to the scalar amplitude. We therefore fix it according to the desired suppression of r, for example $\mathcal{A}(0) \approx 8$. Finally, the step parameters ϕ_r and d are determined by the *Planck* 2015 TT+lowP scalar tilt $n_s = 0.9655 \pm 0.0062$ and bounds on the running of the tilt $\alpha_s = -0.0084 \pm 0.0082$. With four constraints for four parameters, we use slow-roll expressions to find initial parameter guesses which satisfy these conditions and then iterate using numerical results for the background and power spectrum (see section 4) to enforce the Planck constraints beyond slow-roll.

Our resulting fiducial model has the parameter values $M = 1.303 \times 10^{-4}$, $m = 2.58 \times 10^{-6}$, $\phi_r = 13.87$, which are the choices in figures 1–3, and $d = 0.086$, which satisfies the observational constraints on n_s and α_s. Comparing to figures 1 and 2, we see that this model has a relatively fast transition and a moderate violation of slow-roll at the transition. For this set of parameters, we show the resultant scalar power spectrum in figure 4 as computed by solving numerically the Mukhanov-Sasaki equation (3.6) and compare that to the SR formula in eqs. (2.9) using the numerical relationship for $\phi(N)$ with $kc_s/aH = 1$ (upper panel). The discrepancy, which is quantified as the fractional difference between the solutions and shown in the lower panel, is similar to the error in ϵ_H, as shown in figure 2, in that they both peak near the transition where $\mathcal{A} \approx 1$. On the other hand, the slow-roll approximation captures the qualitative behavior of the power spectra and errs mainly in causing a shift in the scale k at which the transition occurs. We shall see in the next section that the optimized evaluation of slow-roll parameters can restore accuracy in the CMB regime by correctly fixing this shift.

We can now see how introducing a more rapid transition from G-inflation can solve the observational problem of having too large r for the observed n_s. Namely, the transition mediates a suppression of the power spectrum or a larger red tilt $1 - n_s$ than predicted by the slow-roll formula in section 2.

JCAP04(2018)039

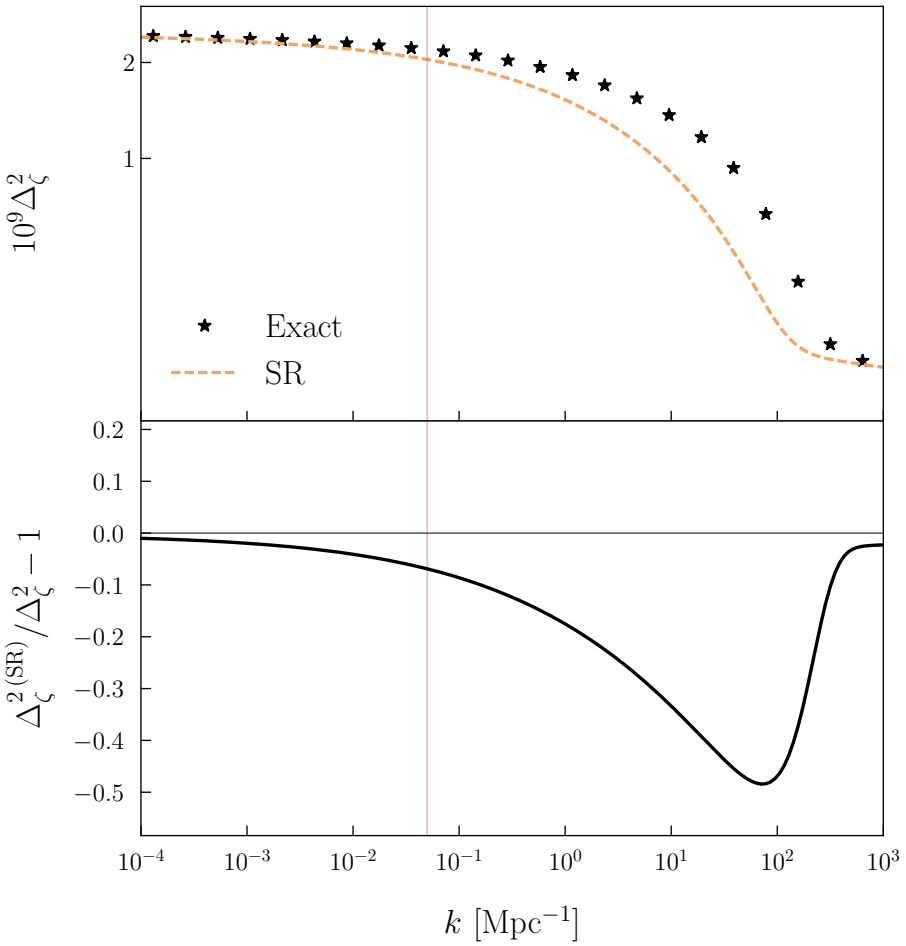

Figure 4. Scalar power spectrum for the Step model computed by solving numerically eq. (3.6) (stars) and by computing eqs. (2.9) with the exact background solutions (dashed orange) (upper panel). Fractional difference between the two solutions (lower panel). The set of parameters used here is $M = 1.303 \times 10^{-4}$, $m = 2.58 \times 10^{-6}$, $\phi_r = 13.87$ and $d = 0.086$. The vertical thin line marks the CMB scale $k_* = 0.05$ Mpc^{-1}.

In figure 5 we show the parametric relationship between r and the n_s for same model. The step model starts at the lower right on the G-model curve but deviates sharply to a lower tilt at the transition before returning to the chaotic inflation curve. In this way, the step solves the observational problem of having a low r and a relatively large red tilt $n_s < 1$. Note that in figure 5 the wavenumber k varies along the curve and so only represents the CMB pivot scale at a single point represented by the star. This model satisfies observational bounds on r and n_s, unlike the G-model and chaotic inflation.

Figure 6 depicts the same (n_s, r) plane but now for the fixed pivot scale k_*. For the G-model and chaotic inflation we show the mapping at $\Delta N = 50$, 60 to provide a reasonable range of possibilities as in ref. [32], whereas for the Step model we keep $\Delta N = 55$. The Galileon mass scale M varies across the curves, where the black star marks the fiducial model $M = 1.303 \times 10^{-4}$, and superimposed are the constraints from the 2015 release of the *Planck* collaboration [1]: we separately consider the full temperature auto-correlation spectrum at all multipoles with the polarization spectra at low multipoles only (*Planck* TT+lowP) plus

JCAP04(2018)039

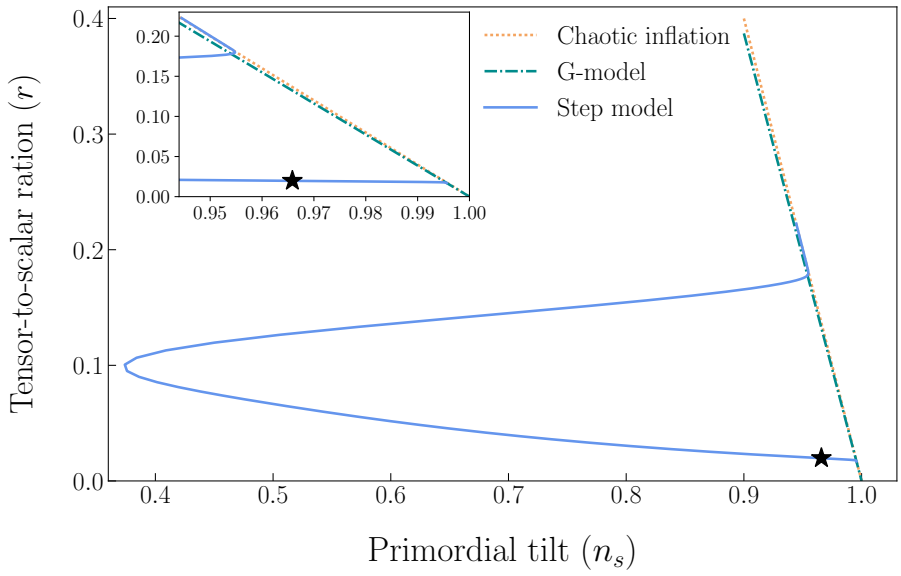

Figure 5. (n_s, r) plane for the three models studied here: chaotic inflation (2.14), G-model (2.13) and the Step model with the values $M = 1.303 \times 10^{-4}$, $m = 2.58 \times 10^{-6}$, $\phi_r = 13.87$ and $d = 0.086$. The wavenumber k varies along the curve in which case the star marks the CMB scale $k_* = 0.05$ Mpc^{-1}.

the joint results of the Bicep2/Keck and *Planck* collaborations (BKP); as well as the *Planck* TT+lowP + BKP combination with Baryon Acoustic Oscillation (BAO) measurements.

As previously discussed, one can see that while the canonical chaotic and G- models are in tension with the latest measurements, the Step model allows for a parameter space of values for M which are in good agreement with the data. Following the methodology explained above, for a given value of M, the inflaton mass m is fixed to obtain the correct scalar amplitude, while the step parameters ϕ_r and d are chosen to keep n_s and α_s fixed. Here we have chosen $\alpha_s \approx -0.01$. Making M smaller allows the Step model to lower the value of r while the transition keeps the CMB scales sufficiently red-tilted.

Furthermore, by varying M away from the fiducial value we encounter two endpoints. As M, and hence r, decreases, the increasing value of $\mathcal{A}(0)$ combined with the requirement that $\mathcal{A} < 1$ at the end of inflation, places a lower limit on $|\alpha_s|$ for a given n_s. This lower limit exceeds $|\alpha_s| = 0.01$ at $r \approx 0.005$ explaining the lower endpoint in figure 6. On the other hand, for large M, CMB scales are no longer in a fully G-inflationary phase so that ϕ_r and d can also no longer be adjusted to match n_s and, more importantly, $\alpha_s \approx -0.01$.

As one might expect, taking a smaller value of $|\alpha_s|$, which still satisfies the Planck constraint, enables a less restrictive upper endpoint that eventually joins with the chaotic or G-model curves. A smaller $|\alpha_s|$ also implies a wider step and increases the lower limit on r from requiring the transition complete before the end of inflation. A larger $|\alpha_s|$ would have the opposite effects but would begin to be in tension with *Planck* constraints. We thus conclude that for the Step model $r \gtrsim 0.005$, and at the lowest r-value $|\alpha_s| > 0.01$, so that tensors and potentially scalar running should be observable with next generation surveys. We comment further on the latter in section 4.2.

For these observationally viable cases, perturbations on CMB scales were frozen in at the very beginning of the transition. As we shall see next, this implies that CMB observables can be accurately predicted by the OSR approximation which takes into account the variation of the slow-roll parameters.

JCAP04(2018)039

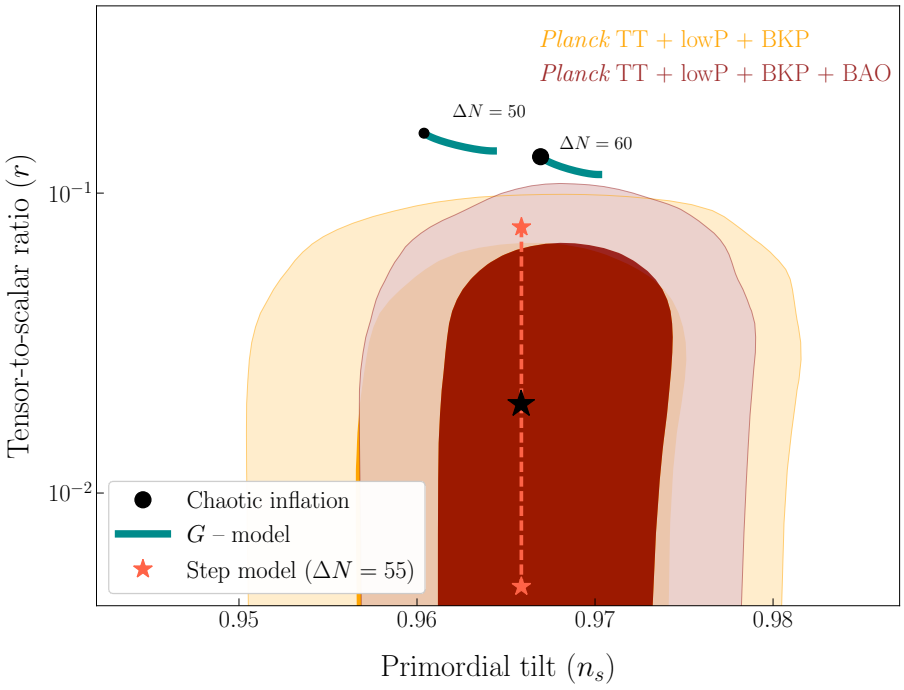

Figure 6. 68% and 95% CL allowed contours from *Planck* TT + lowP+ BKP and from *Planck* TT + lowP + BKP + BAO in the (n_s, r) plane along with the predictions for the canonical chaotic inflation model, the G-model (both for $\Delta N = 50$ and $\Delta N = 60$) and the Step model ($\Delta N = 55$). In both noncanonical cases, M is let to vary from 10^{-4} to 5×10^{-3}, where a smaller M value is associated with a smaller value in r. The black star marks the fiducial-model value $M = 1.303 \times 10^{-4}$, whereas $M = 6.8 \times 10^{-4}$ ($M = 5 \times 10^{-5}$) for the upper (lower) orange stars endpoints determined by requiring the scalar running $\alpha_s \approx -0.01$. Other Step model parameters are fixed by measurements of A_s and n_s as described in the text.

4 Generalized slow-roll

In the previous section we have seen that, by introducing a rapid transition from G-inflation to canonical inflation that completes shortly after the CMB scales leave the horizon, we can avoid the observational problems associated with the original G-model. At the transition, the breakdown of the slow-roll approximation requires numerical solutions for full accuracy, especially for large and sharp steps. On the other hand, CMB scales in observationally viable cases are associated with the very beginning of the transition where there is a much milder breakdown of slow-roll. For CMB observables it is therefore possible to develop a better version of slow-roll that is analytic or semi-analytic. This also helps clarify the phenomenology of the Step model and assists in parameter estimation from the observational data.

Techniques to handle such cases have already been developed for the effective field theory (EFT) of inflation [39, 41], including the Horndeski theory to which our Step model belongs: first the GSR formalism [34–40] allows for formally solving the Mukhanov-Sasaki equation (3.6), in which only the size, but not the evolution, of the slow-roll parameters is required to be small. When the evolution is also slower than the e-folding scale, GSR itself can be systematically expanded in the OSR approximation which fixes the evaluation point of the slow-roll parameters to obtain fully analytic solutions. Since this is the case for the Step model at the beginning of the transition, the OSR approximation is accurate for this model at CMB scales.

JCAP04(2018)039

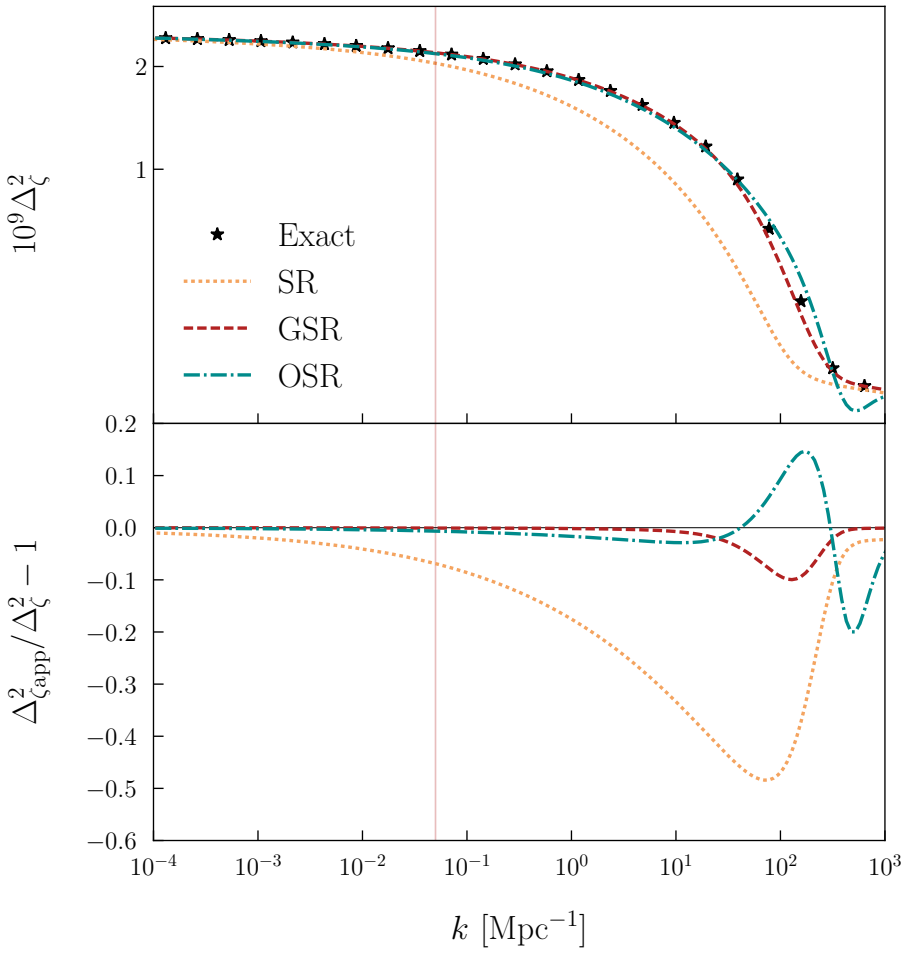

Figure 7. Approximations for the scalar power spectrum of the Step model compared with the exact numerical solution as in figure 4: SR (2.9), GSR (4.6), and OSR (4.9). The thin red vertical line marks the CMB pivot scale $k_* = 0.05$ Mpc^{-1} where GSR and OSR provide a highly accurate description.

4.1 GSR

We can rewrite the Mukhanov-Sasaki equation (3.6), as

$$\frac{\mathrm{d}^2 y}{\mathrm{d}x^2} + \left(1 - \frac{2}{x^2}\right) y = \frac{f_{,\chi\chi} - 3f_{,\chi}}{f} \frac{y}{x^2}\,, \tag{4.1}$$

by defining the new variables $y = \sqrt{2c_i k}u_i$, $x \equiv ks_i$, $\chi \equiv \ln x$, for $i = s, t$ with separate source functions

$$\begin{aligned} f_s &\equiv 2\pi z_s \sqrt{c_s} s_s = \sqrt{8\pi^2 \frac{b_s \epsilon_H c_s}{H^2}} \frac{aH s_s}{c_s}\,, \\ f_t &\equiv 2\pi z_t \sqrt{c_t} s_t = \sqrt{2\pi^2 \frac{b_t c_t}{H^2}} \frac{aH s_t}{c_t}\,, \end{aligned} \tag{4.2}$$

and sound horizons

$$s_{s,t}(N) \equiv \int_N^{N_f} \frac{c_{s,t}}{aH} \mathrm{d}N\,, \tag{4.3}$$

for scalars and tensors, respectively.

JCAP04(2018)039

Notice that the left-hand side of eq. (4.1) corresponds to the evolution of the modefunctions in a de Sitter background and thus the right-hand side encodes deviations from the de Sitter solution into the function f. So far we have not made any assumption for the evolution of ϵ_H or the other slow-roll parameters. In these variables the power spectra, eqs. (3.8), are given by

$$\Delta^2_{\zeta,\gamma} = \lim_{x\to 0} \left| \left(\frac{xy}{f}\right)_{s,t} \right|^2 . \tag{4.4}$$

If deviations from de Sitter remain small in amplitude, eq. (4.1) can be solved iteratively using Green function methods. Starting with the de Sitter solution of the left-hand side of eq. (4.1), i.e. the Bunch-Davies vacuum,

$$y_0(x) = \left(1 + \frac{i}{x}\right) e^{ix} , \tag{4.5}$$

we can take $y \to y_0$ on the right-hand side of eq. (4.1) to obtain the first-order iterative solution (see, e.g., [36] for details),

$$\ln \Delta^{2\,(\mathrm{GSR})} \simeq -\int_0^\infty \frac{\mathrm{d}x}{x} W_{,\chi}(x) G(\chi) , \tag{4.6}$$

where $W(x)$ is a window function given by

$$W(x) = \frac{3\sin(2x)}{2x^3} - \frac{3\cos(2x)}{x^2} - \frac{3\sin(2x)}{2x} , \tag{4.7}$$

and $G(\chi)$ is a source function that now encodes all the deviations from the de Sitter solution and it is written as

$$G \equiv -2\,\ln f + \frac{2}{3}\,(\ln f)_{,\chi} . \tag{4.8}$$

The GSR formula, eq. (4.6), still requires numerical integration, though it remains more computationally efficient than solving eq. (3.6). Moreover, the source function G provides a model-independent means to connect observational constraints with any inflationary model in the EFT class [43, 44]. The scalar tilt n_s and higher order running coefficients can also be efficiently computed numerically by taking derivatives of eq. (4.6) with respect to the scale k.

In figure 7, we compare the GSR approximation to the numerical solution for the same model as in figure 4. GSR provides accurate predictions for the scalar power spectrum along all values of k and only deviates slightly at the transition due to its large amplitude, which can be improved if desired by iterating to higher order. At CMB sales of $k_* = 0.05$ Mpc^{-1}, the approximation is accurate at the $\sim 0.01\%$ level whereas SR deviations are at 7% level.

4.2 OSR

At CMB scales, the source function in eq. (4.8) evolves only over timescales greater than an e-fold ($\Delta N > 1$) as shown for ϵ_H in figure 2. In this case we can Taylor expand the GSR formula, eq. (4.6), around a given evaluation epoch to write down approximate analytical formulas for the power spectra, their tilts and runnings. For the traditional slow-roll expansion, the evaluation epoch is chosen as the horizon exit epoch. However, we can optimize it to minimize an error associated with truncation of the Taylor expansion (see [39, 41] for details). We can then construct the hierarchy of running of power spectrum parameters out of slow-roll

JCAP04(2018)039

parameters associated with the functions H, $b_{s,t}$ and $c_{s,t}$. The OSR formulas which take into account a general background given by eq. (2.1) can then be written to leading order as [39, 41]

$$\begin{aligned}
\ln \Delta_\zeta^{2\,(\mathrm{OSR})} &\simeq \ln\left(\frac{H^2}{8\pi^2 b_s c_s \epsilon_H}\right) - \frac{10}{3}\epsilon_H - \frac{2}{3}\delta_1 - \frac{7}{3}\sigma_{s1} - \frac{1}{3}\xi_{s1}\Big|_{x=x_1}\,, \\
n_s^{(\mathrm{OSR})} - 1 &\simeq -4\epsilon_H - 2\delta_1 - \sigma_{s1} - \xi_{s1} - \frac{2}{3}\delta_2 - \frac{7}{3}\sigma_{s2} - \frac{1}{3}\xi_{s2}\Big|_{x=x_1}\,, \\
\alpha_s^{(\mathrm{OSR})} &\simeq -2\delta_2 - \sigma_{s2} - \xi_{s2} - \frac{2}{3}\delta_3 - \frac{7}{3}\sigma_{s3} - \frac{1}{3}\xi_{s3} - 8\epsilon_H^2 - 10\epsilon_H\delta_1 + 2\delta_1^2\Big|_{x=x_1}\,,
\end{aligned} \tag{4.9}$$

for scalar, and

$$\begin{aligned}
\ln \Delta_\gamma^{2\,(\mathrm{OSR})} &\simeq \ln\left(\frac{H^2}{2\pi^2 b_t c_t}\right) - \frac{8}{3}\epsilon_H - \frac{7}{3}\sigma_{t1} - \frac{1}{3}\xi_{t1}\Big|_{x=x_1}\,, \\
n_t^{(\mathrm{OSR})} &\simeq -2\epsilon_H - \sigma_{t1} - \xi_{t1} - \frac{7}{3}\sigma_{t2} - \frac{1}{3}\xi_{t2}\Big|_{x=x_1}\,, \\
\alpha_t^{(\mathrm{OSR})} &\simeq -\sigma_{t2} - \xi_{t2} - \frac{7}{3}\sigma_{t3} - \frac{1}{3}\xi_{t3} - 4\epsilon_H^2 - 4\epsilon_H\delta_1\Big|_{x=x_1}\,,
\end{aligned} \tag{4.10}$$

for tensor perturbations. Here $\ln x = \ln x_1 \approx 1.06$ is the optimized evaluation point, $\alpha_i = dn_i/d\ln k$ is the running of the tilt, and the slow-roll parameters are defined as:

$$\begin{aligned}
\delta_1 &\equiv \frac{1}{2}\frac{\mathrm{d}\ln\epsilon_H}{\mathrm{d}N} - \epsilon_H\,, & \delta_{p+1} &\equiv \frac{\mathrm{d}\delta_p}{\mathrm{d}N} + \delta_p\left(\delta_1 - p\epsilon_H\right)\,, \\
\sigma_{i,1} &\equiv \frac{\mathrm{d}\ln c_i}{\mathrm{d}N}\,, & \sigma_{i,p+1} &\equiv \frac{\mathrm{d}\sigma_{i,p}}{\mathrm{d}N}\,, \\
\xi_{i,1} &\equiv \frac{\mathrm{d}\ln b_i}{\mathrm{d}N}\,, & \xi_{i,p+1} &\equiv \frac{\mathrm{d}\xi_{i,p}}{\mathrm{d}N}\,,
\end{aligned} \tag{4.11}$$

where $i = s, t$ and $p \geq 1$

Finally, the tensor-to-scalar ratio can be computed in the standard way through eq. (2.11). Note however that the ratio is taken at fixed k which in general gives the $x = x_1$ evaluation point at two different N for scalars and tensors, in which case the sound speeds c_s and c_t differ. Figure 7 shows that although the OSR solution for the scalar power spectrum is slightly less accurate than GSR, it is still a very good approximation with only $\sim 0.6\%$ level deviations at $k_* = 0.05$ Mpc^{-1} (marked by the thin red line).

Furthermore the hierarchy of OSR coefficients $A_s \equiv \Delta_\zeta^{2(\mathrm{OSR})}(k_*)$, $n_s(k_*)$ and $\alpha_s(k_*)$ define a local characterization of the scalar power spectrum in the usual way:

$$\Delta_\zeta^{2(\mathrm{SRH})}(k) = A_s\left(\frac{k}{k_*}\right)^{n_s - 1 + \frac{1}{2}\alpha_s \ln(k/k_*)}\,. \tag{4.12}$$

In figure 8, we show that for the decade below or above the pivot scale k_*, this three-parameter approximation works extremely well with errors less than 1%. This means that observational data in this regime can be analyzed with the usual hierarchy parameterization so long as the implications for inflationary model are extracted from the OSR relations. For example, in the fiducial Step model, $\alpha_s^{(\mathrm{OSR})}(k_*) = -0.011$ can be compared with the *Planck* temperature power spectrum constraint of $\alpha_s = -0.0084 \pm 0.0082$ [1]. Unlike the traditional expansion of the SR approximation to second order in parameters, OSR can accurately relate inflationary models to the SRH observables in such cases when $|\alpha_s|$ is of order $|n_s - 1|$ [39].

JCAP04(2018)039

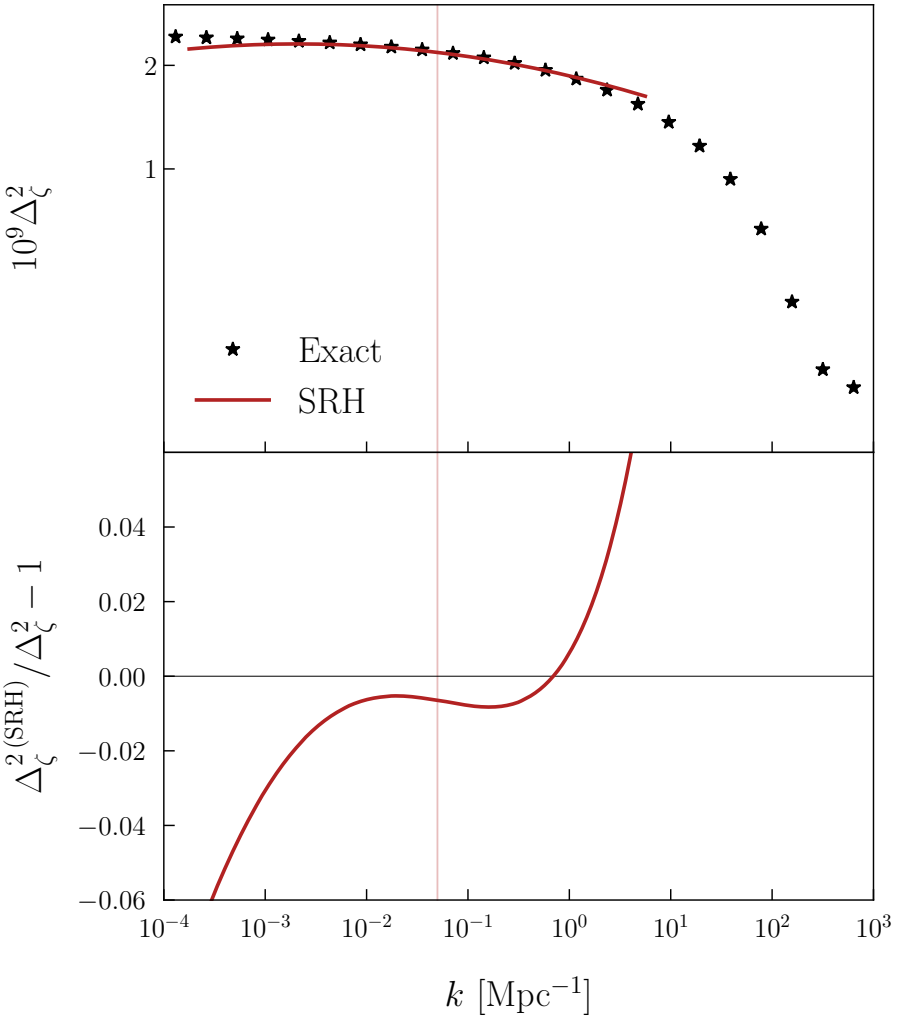

Figure 8. Slow-roll hierarchy (SRH) parameterization, eq.(4.12), of the scalar power spectrum with amplitude A_s, tilt n_s and running of the tilt α_s evaluated at k_* (thin red line) using OSR compared with the exact solution as in figure 4. The three hierarchy parameters provide a good description for more than two decades around k_*.

Finally as discussed in section 3.2, the step model allows for a possible range of values of the running α_s for a given value of r. For $|\alpha_s|$ to be small, the transition must be wide, and enforcing that the transition completes before the end of inflation places a lower bound on $|\alpha_s|$. For instance, for $r = 0.02$, this corresponds to the constraint $|\alpha_s| \gtrsim 0.002$. Furthermore, this lower bound on $|\alpha_s|$ increases as r decreases as the model must transition from an increasingly enhanced scalar power spectrum within the ~ 55 e-folds to the end of inflation; at $r = 0.005$, $|\alpha_s| \gtrsim 0.01$.

5 Conclusions

G-inflation provides the possibility that inflation is driven by simple potentials, like the mass term of chaotic inflation, but with more complex kinetic interactions, while still satisfying observational constraints on the scalar and tensor power spectra. We show that this is not

JCAP04(2018)039

possible with just a cubic Galileon interaction with a constant mass scale since the transition from G-inflation to canonical inflation is too slow, leading to a scalar power spectrum that is either too small relative to the tensors or too close to scale invariant. In addition, failure to complete the transition by the end of inflation leads to gradient instabilities during reheating. By introducing a sufficiently rapid step-like transition, we simultaneously solve both the phenomenological and instability problems of potential driven G-inflation. Although we chose the $m^2\phi^2$ model of chaotic inflation, steeper monomial potentials also suffer from the same problems which can be solved in the same way.

While a fast transition inevitably leads to a breakdown of the traditional slow-roll approximation at the peak of the transition, we show that for phenomenologically viable models, fluctuations on CMB scales freeze out near the beginning of the transition. By comparing exact numerical solutions with the generalized slow-roll approximation and its optimized expansion, we show how to accurately relate the properties of the G-step model, such as the position and width of the step and two mass scales, to the power spectrum observables through the slow-roll parameters. In particular, across the scales that are currently precisely measured by the CMB and large-scale structure, the scalar power spectra can still be described by an amplitude A_s, tilt $n_s - 1$ and running of the tilt α_s.

However the negative running of the tilt can be of order of $n_s - 1$ itself unlike in the traditional slow-roll approximation and necessitates the OSR approximation for its evaluation. In fact for a given tensor-to-scalar ratio r, there is a lower bound on $|\alpha_s|$ since the transition must complete within the ~ 55 e-folds to the end of inflation to avoid gradient instabilities. While the required relatively large running of the tilt can satisfy current constraints if $r \gtrsim 0.005$, it is potentially detectable with future high precision measurements and also suppresses smaller scale structure in observable ways.

Acknowledgments

We thank Eiichiro Komatsu for useful and enlightening discussions. HR and OM would like to thank the Fermilab Theoretical Physics Department and Kavli IPMU for their hospitality. HR and OM were supported in part by MINECO Grant SEV-2014-0398, PROMETEO II/2014/050, Spanish Grants FPA2014-57816-P and FPA2017-85985-P of the MINECO, and European Union's Horizon 2020 research and innovation programme under the Marie Skłodowska-Curie grant agreements No. 690575 and 674896. HM was supported by JSPS KEKENHI Grant No. JP17H06359. WH was supported by U.S. Dept. of Energy contract DE-FG02-13ER41958, NASA ATP NNX15AK22G and the Simons Foundation.

References

[1] Planck collaboration, P.A.R. Ade et al., *Planck 2015 results. XX. Constraints on inflation*, *Astron. Astrophys.* **594** (2016) A20 [arXiv:1502.02114] [INSPIRE].

[2] E. Silverstein and D. Tong, *Scalar speed limits and cosmology: acceleration from D-cceleration*, *Phys. Rev.* **D 70** (2004) 103505 [hep-th/0310221] [INSPIRE].

[3] M. Alishahiha, E. Silverstein and D. Tong, *DBI in the sky*, *Phys. Rev.* **D 70** (2004) 123505 [hep-th/0404084] [INSPIRE].

[4] J.J.M. Carrasco, R. Kallosh and A. Linde, *α-attractors: Planck, LHC and dark energy*, *JHEP* **10** (2015) 147 [arXiv:1506.01708] [INSPIRE].

JCAP04(2018)039

[5] R. Bean, X. Chen, G. Hailu, S.-H. Henry Tye and J. Xu, *Duality cascade in brane inflation*, *JCAP* **03** (2008) 026 [arXiv:0802.0491] [INSPIRE].

[6] E. Silverstein and A. Westphal, *Monodromy in the CMB: gravity waves and string inflation*, *Phys. Rev.* **D 78** (2008) 106003 [arXiv:0803.3085] [INSPIRE].

[7] L. McAllister, E. Silverstein and A. Westphal, *Gravity waves and linear inflation from axion monodromy*, *Phys. Rev.* **D 82** (2010) 046003 [arXiv:0808.0706] [INSPIRE].

[8] R. Flauger, L. McAllister, E. Pajer, A. Westphal and G. Xu, *Oscillations in the CMB from axion monodromy inflation*, *JCAP* **06** (2010) 009 [arXiv:0907.2916] [INSPIRE].

[9] T. Futamase and K.-I. Maeda, *Chaotic inflationary scenario in models having nonminimal coupling with curvature*, *Phys. Rev.* **D 39** (1989) 399 [INSPIRE].

[10] R. Fakir and W.G. Unruh, *Improvement on cosmological chaotic inflation through nonminimal coupling*, *Phys. Rev.* **D 41** (1990) 1783 [INSPIRE].

[11] E. Komatsu and T. Futamase, *Complete constraints on a nonminimally coupled chaotic inflationary scenario from the cosmic microwave background*, *Phys. Rev.* **D 59** (1999) 064029 [astro-ph/9901127] [INSPIRE].

[12] M.P. Hertzberg, *On inflation with non-minimal coupling*, *JHEP* **11** (2010) 023 [arXiv:1002.2995] [INSPIRE].

[13] N. Okada, M.U. Rehman and Q. Shafi, *Tensor to scalar ratio in non-minimal ϕ^4 inflation*, *Phys. Rev.* **D 82** (2010) 043502 [arXiv:1005.5161] [INSPIRE].

[14] A. Linde, M. Noorbala and A. Westphal, *Observational consequences of chaotic inflation with nonminimal coupling to gravity*, *JCAP* **03** (2011) 013 [arXiv:1101.2652] [INSPIRE].

[15] L. Boubekeur, E. Giusarma, O. Mena and H. Ramírez, *Does current data prefer a non-minimally coupled inflaton?*, *Phys. Rev.* **D 91** (2015) 103004 [arXiv:1502.05193] [INSPIRE].

[16] G.W. Horndeski, *Second-order scalar-tensor field equations in a four-dimensional space*, *Int. J. Theor. Phys.* **10** (1974) 363 [INSPIRE].

[17] A. Nicolis, R. Rattazzi and E. Trincherini, *The Galileon as a local modification of gravity*, *Phys. Rev.* **D 79** (2009) 064036 [arXiv:0811.2197] [INSPIRE].

[18] C. Deffayet, X. Gao, D.A. Steer and G. Zahariade, *From k-essence to generalised Galileons*, *Phys. Rev.* **D 84** (2011) 064039 [arXiv:1103.3260] [INSPIRE].

[19] T. Kobayashi, M. Yamaguchi and J. Yokoyama, *Generalized G-inflation: inflation with the most general second-order field equations*, *Prog. Theor. Phys.* **126** (2011) 511 [arXiv:1105.5723] [INSPIRE].

[20] M. Zumalacárregui and J. García-Bellido, *Transforming gravity: from derivative couplings to matter to second-order scalar-tensor theories beyond the Horndeski Lagrangian*, *Phys. Rev.* **D 89** (2014) 064046 [arXiv:1308.4685] [INSPIRE].

[21] J. Gleyzes, D. Langlois, F. Piazza and F. Vernizzi, *Healthy theories beyond Horndeski*, *Phys. Rev. Lett.* **114** (2015) 211101 [arXiv:1404.6495] [INSPIRE].

[22] H. Motohashi and T. Suyama, *Third order equations of motion and the Ostrogradsky instability*, *Phys. Rev.* **D 91** (2015) 085009 [arXiv:1411.3721] [INSPIRE].

[23] D. Langlois and K. Noui, *Degenerate higher derivative theories beyond Horndeski: evading the Ostrogradski instability*, *JCAP* **02** (2016) 034 [arXiv:1510.06930] [INSPIRE].

[24] H. Motohashi, K. Noui, T. Suyama, M. Yamaguchi and D. Langlois, *Healthy degenerate theories with higher derivatives*, *JCAP* **07** (2016) 033 [arXiv:1603.09355] [INSPIRE].

JCAP04(2018)039

[25] R. Klein and D. Roest, *Exorcising the Ostrogradsky ghost in coupled systems*, *JHEP* **07** (2016) 130 [arXiv:1604.01719] [INSPIRE].

[26] J. Ben Achour, M. Crisostomi, K. Koyama, D. Langlois, K. Noui and G. Tasinato, *Degenerate higher order scalar-tensor theories beyond Horndeski up to cubic order*, *JHEP* **12** (2016) 100 [arXiv:1608.08135] [INSPIRE].

[27] M. Crisostomi, R. Klein and D. Roest, *Higher derivative field theories: degeneracy conditions and classes*, *JHEP* **06** (2017) 124 [arXiv:1703.01623] [INSPIRE].

[28] H. Motohashi, T. Suyama and M. Yamaguchi, *Ghost-free theory with third-order time derivatives*, arXiv:1711.08125 [INSPIRE].

[29] T. Kobayashi, M. Yamaguchi and J. Yokoyama, *G-inflation: inflation driven by the Galileon field*, *Phys. Rev. Lett.* **105** (2010) 231302 [arXiv:1008.0603] [INSPIRE].

[30] C. Burrage, C. de Rham, D. Seery and A.J. Tolley, *Galileon inflation*, *JCAP* **01** (2011) 014 [arXiv:1009.2497] [INSPIRE].

[31] K. Kamada, T. Kobayashi, M. Yamaguchi and J. Yokoyama, *Higgs G-inflation*, *Phys. Rev.* **D 83** (2011) 083515 [arXiv:1012.4238] [INSPIRE].

[32] J. Ohashi and S. Tsujikawa, *Potential-driven Galileon inflation*, *JCAP* **10** (2012) 035 [arXiv:1207.4879] [INSPIRE].

[33] K. Kamada, T. Kobayashi, T. Kunimitsu, M. Yamaguchi and J. Yokoyama, *Graceful exit from Higgs G-inflation*, *Phys. Rev.* **D 88** (2013) 123518 [arXiv:1309.7410] [INSPIRE].

[34] E.D. Stewart, *The spectrum of density perturbations produced during inflation to leading order in a general slow roll approximation*, *Phys. Rev.* **D 65** (2002) 103508 [astro-ph/0110322] [INSPIRE].

[35] K. Kadota, S. Dodelson, W. Hu and E.D. Stewart, *Precision of inflaton potential reconstruction from CMB using the general slow-roll approximation*, *Phys. Rev.* **D 72** (2005) 023510 [astro-ph/0505158] [INSPIRE].

[36] C. Dvorkin and W. Hu, *Generalized slow roll for large power spectrum features*, *Phys. Rev.* **D 81** (2010) 023518 [arXiv:0910.2237] [INSPIRE].

[37] W. Hu, *Generalized slow roll for non-canonical kinetic terms*, *Phys. Rev.* **D 84** (2011) 027303 [arXiv:1104.4500] [INSPIRE].

[38] W. Hu, *Generalized slow roll for tensor fluctuations*, *Phys. Rev.* **D 89** (2014) 123503 [arXiv:1405.2020] [INSPIRE].

[39] H. Motohashi and W. Hu, *Running from features: optimized evaluation of inflationary power spectra*, *Phys. Rev.* **D 92** (2015) 043501 [arXiv:1503.04810] [INSPIRE].

[40] V. Miranda, W. Hu, C. He and H. Motohashi, *Nonlinear excitations in inflationary power spectra*, *Phys. Rev.* **D 93** (2016) 023504 [arXiv:1510.07580] [INSPIRE].

[41] H. Motohashi and W. Hu, *Generalized slow roll in the unified effective field theory of inflation*, *Phys. Rev.* **D 96** (2017) 023502 [arXiv:1704.01128] [INSPIRE].

[42] H. Motohashi and W. Hu, *Primordial black holes and slow-roll violation*, *Phys. Rev.* **D 96** (2017) 063503 [arXiv:1706.06784] [INSPIRE].

[43] C. Dvorkin and W. Hu, *Complete WMAP constraints on bandlimited inflationary features*, *Phys. Rev.* **D 84** (2011) 063515 [arXiv:1106.4016] [INSPIRE].

[44] G. Obied, C. Dvorkin, C. Heinrich, W. Hu and V. Miranda, *Inflationary features and shifts in cosmological parameters from Planck* 2015 *data*, *Phys. Rev.* **D 96** (2017) 083526 [arXiv:1706.09412] [INSPIRE].

JCAP04(2018)039

Inflation with mixed helicities and its observational imprint on CMB

Lavinia Heisenberg,[1] Héctor Ramírez,[2,3] and Shinji Tsujikawa[4]

[1]*Institute for Theoretical Physics, ETH Zurich, Wolfgang-Pauli-Strasse 27, 8093 Zurich, Switzerland*
[2]*Departamento de Física Teórica, Universidad de Valencia, Dr. Moliner 50, E-46100 Burjassot, Spain*
[3]*Instituto de Física Corpuscular (IFIC), Universidad de Valencia-CSIC, E-46980, Paterna, Spain*
[4]*Department of Physics, Faculty of Science, Tokyo University of Science, 1-3, Kagurazaka, Shinjuku-ku, Tokyo 162-8601, Japan*

(Received 10 October 2018; published 3 January 2019)

In the framework of effective field theories with prominent helicity-0 and helicity-1 fields coupled to each other via a dimension-3 operator, we study the dynamics of inflation driven by the helicity-0 mode, with a given potential energy, as well as the evolution of cosmological perturbations, influenced by the presence of a mixing term between both helicities. In this scenario, the temporal component of the helicity-1 mode is an auxiliary field and can be integrated out in terms of the time derivative of the helicity-0 mode, so that the background dynamics effectively reduces to that in single-field inflation modulated by a parameter β associated to the coupling between helicity-0 and helicity-1 modes. We discuss the evolution of a longitudinal scalar perturbation ψ and an inflaton fluctuation $\delta\phi$, and we explicitly show that a particular combination of these two, which corresponds to an isocurvature mode, is subject to exponential suppression by the vector mass comparable to the Hubble expansion rate during inflation. Furthermore, we find that the effective single-field description corrected by β also holds for the power spectrum of curvature perturbations generated during inflation. We compute the standard inflationary observables such as the scalar spectral index n_s and the tensor-to-scalar ratio r and confront several inflaton potentials with the recent observational data provided by *Planck* 2018. Our results show that the coupling between helicity-0 and helicity-1 modes can lead to a smaller value of the tensor-to-scalar ratio especially for small-field inflationary models, so our scenario exhibits even better compatibility with the current observational data.

DOI: 10.1103/PhysRevD.99.023505

I. INTRODUCTION

Inflation [1,2] provides a causal mechanism for generating primordial density perturbations responsible for large-scale structures of the Universe [3]. Moreover, the temperature anisotropies observed in the cosmic microwave background (CMB) are overall consistent with the prediction of the inflationary paradigm [4–6]. It is anticipated that the possible detection of B-mode polarizations in the future will offer the opportunity to identify the origin of inflation.

The simplest candidate for inflation is a new scalar field ϕ beyond the Standard Model subject to a particular potential $V(\phi)$. As long as the field evolves slowly along a nearly flat potential, the primordial power spectra of scalar and tensor perturbations generated during inflation are close to scale invariant [7]. The deviation from scale invariance, characterized by the spectral index n_s and the tensor-to-scalar ratio r, depends strongly on the assumption about the inflaton potential. Using the bounds of n_s and r constrained from the CMB data, one can distinguish between different inflationary models [5,6,8–11].

A cosmological accelerated expansion can be driven not only by a scalar field but also by a vector field. Indeed, the accelerated solutions were found in Refs. [12,13] in traditional vector-tensor theories; however, they are generically plagued by instabilities [14–16]. In the so-called generalized Proca theories where an Abelian vector field with broken $U(1)$ gauge symmetry has derivative self-interactions and nonminimal couplings to gravity [17–19] (see also Ref. [20]), the existence of a temporal vector component A_0 can give rise to de Sitter solutions. Indeed, the generalized Proca theories are very successful for describing the late-time cosmic acceleration [21,22].

On the other hand, there are also mechanisms for realizing the cosmic acceleration by using spacelike vector fields [23,24]. Naively this configuration is not compatible with an isotropic cosmological background, but the rotational invariance can be preserved by considering three orthogonal vector fields aligned with three spatial directions. Indeed, three vector fields A^a_μ nonminimally coupled to the Ricci scalar R in the form $RA^a_\mu A^{a\mu}$ can lead to inflation [25], but such accelerated solutions are plagued by either ghosts or Laplacian instabilities [26]. Non-Abelian gauge fields with $SU(2)$ gauge symmetry can also be the source for inflation without instabilities [27,28], but the scalar spectral index n_s and the tensor-to-scalar ratio r are not compatible with the CMB data [29,30]. There exists an

inflationary scenario driven by a nonminimally coupled non-Abelian gauge field [31], but the tensor perturbation is subject to ghost instabilities [32].

Efforts have also been made to construct well-behaved inflationary models in the presence of vector fields but where, as in the standard case, the main source for the accelerated expansion is a scalar field ϕ. It is of particular interest in the case where this field is coupled to an Abelian vector field A_μ. It is known that, for this type of scenario, a stable inflationary solution with an anisotropic hair exists for the coupling of the form $f^2(\phi)F_{\mu\nu}F^{\mu\nu}$, where $F_{\mu\nu} = \nabla_\mu A_\nu - \nabla_\nu A_\mu$ is the field strength tensor with a covariant derivative operator ∇_μ [33]. The same coupling has often been used for the generation of magnetic fields during inflation [34,35], but in such cases the models need to be carefully constructed to avoid the backreaction and strong-coupling problems [36–40].

Moreover, in the presence of a real scalar field ϕ and a vector field A_μ with derivative self-interactions and nonminimal couplings to gravity, the general action of scalar-vector-tensor (SVT) theories was recently constructed by keeping the equations of motion up to second order [41]. In particular, the massive vector field with broken $U(1)$ gauge symmetry is relevant to the cosmological application. In this case, the vector perturbation is subject to exponential suppression by the mass of A_μ.

Among the possible interactions between scalar and massive vector fields, and in particular for inflation, the coupling $A^\mu\nabla_\mu\phi$ is the simplest one modifying the inflaton velocity, $\dot{\phi}$, during the cosmic expansion. This interaction is not only present in SVT theories but arises in many effective field theories as one of the lowest-order operators, once the involved broken gauge symmetries are compensated by the introduction of appropriate Stückelberg fields. In addition, the vector-field contribution to the total energy density during inflation is subdominant relative to the scalar potential $V(\phi)$, yet the modification to the inflaton velocity induced by the vector field can affect the primordial power spectra of scalar and tensor perturbations. See Ref. [42] for a recent review on the systematic construction of modified gravity theories based on additional scalar, vector, and tensor fields (see also [43]).

For the aforementioned type of interaction, $A^\mu\nabla_\mu\phi$, there exists a longitudinal scalar perturbation, ψ, arising from A_μ, besides the inflaton fluctuation $\delta\phi$ [44–46]. This longitudinal perturbation contributes to the total curvature perturbation $\mathcal{R}$ in a nontrivial way. Therefore, the computation of the primordial power spectrum, incorporating both ψ and $\delta\phi$, is not as straightforward as in the standard canonical case. In this paper, we address this problem and derive the standard inflationary observables such as n_s and r under the slow-roll approximation. We show that, as in the canonical case, one can relate these observables with slow-roll parameters but with a rescaling factor β coming from the helicity-0 and helicity-1 mixing. Using these general expressions, we then confront several different inflaton potentials with the recent CMB data provided by the 2018 results from the *Planck* Collaboration [6].

This paper is organized as follows. In Sec. II, we discuss the background inflationary dynamics and show that the system effectively reduces to that of a single-field inflation. In Sec. III, we revisit the primordial tensor power spectrum generated in our scenario and also study the evolution of vector perturbations during inflation. In Sec. IV, we investigate how the perturbations ψ and $\delta\phi$ evolve during inflation and obtain the resulting power spectrum of total curvature perturbations. In Sec. V, we compute inflationary observables and test several inflaton potentials with the latest *Planck* 2018 data. Section VI is devoted to conclusions.

II. INFLATION WITH A SCALAR-VECTOR COUPLING

In many effective field theories, mixings between different helicity modes, even with derivative interactions, arise in a natural way. In massive gravity and massive Proca theories, the decomposition of helicities yields interesting couplings among them [17,19,47]—this, in fact, motivated the construction of SVT theories [41]. The particular mixing of the form $A^\mu\nabla_\mu\phi$ arises quite naturally and is a unique coupling that modifies the involved propagators of scalar and vector fields. As we will see below, one possible origin of this coupling is the standard Proca mass term, which modifies the property of the propagator by the mass parameter.

Let us consider, for instance, the Lagrangian of the standard Proca field:

$$\mathcal{L}_{A_\mu} = -\frac{1}{4}F_{\mu\nu}F^{\mu\nu} - \frac{1}{2}M^2A_\mu A^\mu. \tag{2.1}$$

The existence of the mass term M explicitly breaks the $U(1)$ gauge symmetry and therefore the massive spin-1 field propagates 3 degrees of freedom. Since the gauge invariance is just a redundancy, one can restore it by introducing a Stückelberg field ϕ via the field transformation

$$A_\mu \to A_\mu + \nabla_\mu\phi. \tag{2.2}$$

The initial Lagrangian for the massive spin-1 field (2.1) then modifies to

$$\mathcal{L}_{A_\mu} = -\frac{1}{4}F_{\mu\nu}F^{\mu\nu} - \frac{1}{2}M^2(A_\mu + \nabla_\mu\phi)(A^\mu + \nabla^\mu\phi). \tag{2.3}$$

Notice that the kinetic term $-F_{\mu\nu}F^{\mu\nu}/4$ is not modified under this change of variables since it is gauge invariant. Here, the helicity-0 field ϕ represents the longitudinal mode of the massive vector field. Written in this form, the standard Proca theory is now invariant under the simultaneous

transformations $A_\mu \to A_\mu + \nabla_\mu\theta$ and $\phi \to \phi - \theta$. After canonically normalizing the Stückelberg field $\phi \to \phi/M$, the Lagrangian becomes

$$\mathcal{L}_{A_\mu} = -\frac{1}{4}F_{\mu\nu}F^{\mu\nu} - \frac{1}{2}M^2A_\mu A^\mu - \frac{1}{2}\nabla_\mu\phi\nabla^\mu\phi - MA^\mu\nabla_\mu\phi. \tag{2.4}$$

The last term is exactly the coupling we are interested in. This Lagrangian constitutes our low energy effective field theory.

In the following, we will consider a soft breaking of the shift symmetry of the helicity-0 mode and introduce a scalar potential $V(\phi)$ of the real scalar field ϕ for the purpose of realizing a successful inflationary scenario. Bear in mind that any UV completion will unavoidably introduce the breaking of global symmetry anyway. Our setup consists in an inflationary scenario in which the inflaton field ϕ has a derivative interaction with a massive vector field A^μ of the form $A^\mu\nabla_\mu\phi$, equivalent to that in Eq. (2.4). The inflationary period is mostly driven by the scalar potential $V(\phi)$, but the scalar-vector coupling modifies the dynamics of inflation and the primordial power spectra of cosmological perturbations. We then focus on the action[1]

$$\mathcal{S} = \int d^4x\sqrt{-g}\left[\frac{M_{\rm pl}^2}{2}R + F + X_1 - V(\phi) + \beta_m MX_2 + \beta_A M^2X_3\right], \tag{2.5}$$

where g is the determinant of a metric tensor $g_{\mu\nu}$, $M_{\rm pl}$ is the reduced Planck mass, R is the Ricci scalar, and $F = -(1/4)F_{\mu\nu}F^{\mu\nu}$. The quantity X_1 is the scalar kinetic energy $X_1 = -(1/2)\nabla_\mu\phi\nabla^\mu\phi$, while X_2 and X_3 are defined by

$$X_2 = -\frac{1}{2}A^\mu\nabla_\mu\phi, \qquad X_3 = -\frac{1}{2}A_\mu A^\mu. \tag{2.6}$$

In the last two terms of Eq. (2.5), M is a positive constant (mass of the vector field) relevant to the mass scale of inflation, and β_m and β_A are dimensionless constants associated with the scalar-vector mixing and the vector mass, respectively.

To discuss the background dynamics of inflation, we consider the flat Friedmann-Lemaître-Robertson-Walker (FLRW) spacetime described by the line element $ds^2 = -dt^2 + a^2(t)\delta_{ij}dx^idx^j$, where $a(t)$ is a time-dependent scale factor. The vector-field profile compatible with this metric is of the form $A_\mu = (A_0(t), 0, 0, 0)$, with a time-dependent scalar field $\phi = \phi(t)$. The background equations of motion in full parity-invariant SVT theories were already derived in Refs. [44,45]. For the action (2.5), they are given by

$$3M_{\rm pl}^2H^2 = \frac{1}{2}\dot\phi^2 + V - \frac{1}{2}\beta_A M^2A_0^2, \tag{2.7}$$

$$-2M_{\rm pl}^2\dot H = \dot\phi^2 + \frac{1}{2}\beta_m M\dot\phi A_0, \tag{2.8}$$

$$\ddot\phi + 3H\dot\phi + V_{,\phi} + \frac{1}{2}M\beta_m(\dot A_0 + 3HA_0) = 0, \tag{2.9}$$

$$A_0 = -\frac{\beta_m}{2\beta_A M}\dot\phi, \tag{2.10}$$

where $H \equiv \dot a/a$ is the Hubble expansion rate, a dot represents a derivative with respect to cosmic time t, and $V_{,\phi} \equiv dV/d\phi$. From Eq. (2.10), we notice that the temporal vector component A_0 is simply proportional to $\dot\phi$. Substituting Eq. (2.10) into Eqs. (2.7)–(2.9), we obtain

$$3M_{\rm pl}^2H^2 = \frac{1}{2}\beta\dot\phi^2 + V, \tag{2.11}$$

$$-2M_{\rm pl}^2\dot H = \beta\dot\phi^2, \tag{2.12}$$

$$\ddot\phi + 3H\dot\phi + \frac{V_{,\phi}}{\beta} = 0, \tag{2.13}$$

where we have defined

$$\beta \equiv 1 - \frac{\beta_m^2}{4\beta_A}. \tag{2.14}$$

The coupling β is different from 1 due to the mixing term β_m. This leads to the modified evolution of ϕ compared to the standard case ($\beta = 1$).

In Refs. [44,45], the authors derived conditions for the absence of ghost and Laplacian instabilities of linear cosmological perturbations in the small-scale limit. The propagation speeds of tensor, vector, and scalar perturbations are all equivalent to that of light for the theory given by the action (2.5). The no-ghost conditions of tensor and vector perturbations are trivially satisfied, while the scalar ghost is absent under the condition

[1]It is worth emphasizing that this model propagates 6 degrees of freedom: 2 as in standard GR, 3 from the massive vector field, and 1 from the scalar field. The Proca Lagrangian in (2.1) written as (2.4), on the other hand, propagates only 5 degrees of freedom (including gravity). After introducing the Stückelberg field, the Proca vector field becomes gauge invariant and the longitudinal mode of the initial Proca field is transformed into the Stückelberg field itself. By including a general potential term for the scalar field, we explicitly break the previously restored gauge symmetry (or the related shift symmetry of the scalar field) and the theory propagates one more degree of freedom. This serves just for illustrative purposes, namely, that the operator $A^\mu\nabla_\mu\phi$ is a Hermitian operator.

$$q_s = \frac{M^2}{16}(4\beta_A - \beta_m^2) > 0, \tag{2.15}$$

and hence $4\beta_A > \beta_m^2 \geq 0$. Then, the coupling (2.14) lies in the range

$$0 < \beta \leq 1. \tag{2.16}$$

From Eq. (2.13), the nonvanishing mixing term β_m effectively leads to a faster inflaton velocity.

Employing the slow-roll approximations $\beta\dot{\phi}^2/2 \ll V$ and $|\ddot{\phi}| \ll |3H\dot{\phi}|$ in Eqs. (2.11) and (2.13), it follows that

$$3M_{\rm pl}^2 H^2 \simeq V, \tag{2.17}$$

$$3H\dot{\phi} \simeq -\frac{V_{,\phi}}{\beta}. \tag{2.18}$$

The slow-roll parameter associated with the cosmic expansion rate is given by

$$\epsilon \equiv -\frac{\dot{H}}{H^2} \simeq \frac{\epsilon_V}{\beta}, \tag{2.19}$$

where we used Eq. (2.12), and we define

$$\epsilon_V \equiv \frac{M_{\rm pl}^2}{2}\left(\frac{V_{,\phi}}{V}\right)^2. \tag{2.20}$$

The existence of the nonvanishing mixing term β_m breaks the relation $\epsilon \simeq \epsilon_V$ in standard inflation. The field value $\phi = \phi_f$ at the end of inflation can be derived by the condition $\epsilon(\phi_f) = 1$, i.e.,

$$\epsilon_V(\phi_f) = \beta. \tag{2.21}$$

The number of e-foldings counted to the end of inflation is given by

$$N = \int_{\phi}^{\phi_f} \frac{H}{\dot{\tilde{\phi}}} d\tilde{\phi} \simeq \frac{\beta}{M_{\rm pl}^2}\int_{\phi_f}^{\phi} \frac{V}{V_{,\tilde{\phi}}} d\tilde{\phi}, \tag{2.22}$$

where, in the last approximate equality, we again used the slow-roll approximation. For smaller β, the number of e-foldings gets smaller with a given initial value of ϕ. This is attributed to the fact that the inflaton velocity is effectively increased by the nonvanishing coupling β_m.

If we introduce a rescaled field φ defined by

$$\frac{d\varphi}{d\phi} = \sqrt{\beta}, \tag{2.23}$$

then Eqs. (2.11)–(2.13) reduce, respectively, to

$$3M_{\rm pl}^2 H^2 = \frac{1}{2}\dot{\varphi}^2 + V, \tag{2.24}$$

$$-2M_{\rm pl}^2 \dot{H} = \dot{\varphi}^2, \tag{2.25}$$

$$\ddot{\varphi} + 3H\dot{\varphi} + V_{,\varphi} = 0. \tag{2.26}$$

This means that the background dynamics in the presence of ϕ and $A_0 \propto \dot{\phi}$ is equivalent to the effective single-field dynamics driven by the scalar field φ. From Eq. (2.23), we have $\dot{\phi} = \dot{\varphi}/\sqrt{\beta}$, so the inflaton ϕ evolves faster than the rescaled field φ for $\beta_m \neq 0$.

III. TENSOR AND VECTOR PERTURBATIONS

In this section, we revisit the tensor power spectrum generated during inflation [44,45] and also discuss the evolution of vector perturbations in SVT theories given by the action (2.5).

A. Tensor perturbations

The perturbed line element containing intrinsic tensor modes $h_{ij}(t, x^i)$ on the flat FLRW background is given by

$$ds_t^2 = -dt^2 + a^2(t)(\delta_{ij} + h_{ij})dx^i dx^j, \tag{3.1}$$

where h_{ij} obeys the transverse and traceless conditions $\nabla^j h_{ij} = 0$ and $h_i{}^i = 0$. From Eq. (3.2) of Ref. [44], the second-order action of h_{ij}, for the theory given by Eq. (2.5), is the same as that in GR, i.e.,

$$\mathcal{S}_t^{(2)} = \int dt d^3x \frac{a^3 M_{\rm pl}^2}{8}\delta^{ik}\delta^{jl}\left[\dot{h}_{ij}\dot{h}_{kl} - \frac{1}{a^2}(\partial h_{ij})(\partial h_{kl})\right], \tag{3.2}$$

where the symbol ∂ represents the spatial partial derivative. In Fourier space with the coming wave number k, the equation of motion of h_{ij} is given by

$$\ddot{h}_{ij} + 3H\dot{h}_{ij} + \frac{k^2}{a^2}h_{ij} = 0. \tag{3.3}$$

Deep inside the Hubble radius ($k/a \gg H$), the tensor perturbation is in a Bunch-Davies vacuum state, whereas after the Hubble exit ($k/a < H$) during inflation, h_{ij} soon approaches a constant. Taking into account two polarization states, the primordial tensor power spectrum (per unit logarithmic wave number interval) generated during inflation yields [44]

$$\mathcal{P}_t = \left.\frac{2H^2}{\pi^2 M_{\rm pl}^2}\right|_{k=aH}, \tag{3.4}$$

which should be evaluated at the Hubble exit. By using the slow-roll approximation (2.17), Eq. (3.4) can be expressed in terms of V as

$$\mathcal{P}_t \simeq \left.\frac{2V}{3\pi^2 M_{\rm pl}^4}\right|_{k=aH}. \tag{3.5}$$

B. Vector perturbations

For the vector sector, we choose the perturbed line element in the flat gauge

$$ds_v^2 = -dt^2 + 2V_i dt dx^i + a^2(t)\delta_{ij}dx^i dx^j, \tag{3.6}$$

where the vector perturbation $V_i(t, x^i)$ obeys the transverse condition $\nabla^i V_i = 0$. The spatial component of A_μ contains the intrinsic vector mode Z_i and the longitudinal scalar perturbation ψ, such that

$$A_i = Z_i + \nabla_i \psi, \tag{3.7}$$

where Z_i obeys the condition $\nabla^i Z_i = 0$. In this section, we study the evolution of vector perturbations Z_i during inflation, leaving the analysis of scalar mode ψ for Sec. IV.

Without loss of generality, we can choose the components of V_i and Z_i in the forms $V_i = (V_1(t,z), V_2(t,z), 0)$ and $Z_i = (Z_1(t,z), Z_2(t,z), 0)$. After integrating out the nondynamical field V_i, the second-order action of vector perturbations reduces to [44]

$$\mathcal{S}_v^{(2)} = \int dt d^3x \sum_{i=1}^{2} \frac{a}{2}\left[\dot{Z}_i^2 - \frac{1}{a^2}(\partial Z_i)^2 - \beta_A M^2 Z_i^2\right]. \tag{3.8}$$

Then, in Fourier space, the dynamical perturbation Z_i obeys

$$\ddot{Z}_i + H\dot{Z}_i + \left(\frac{k^2}{a^2} + \beta_A M^2\right) Z_i = 0, \tag{3.9}$$

which can be written as

$$Z_i'' + (k^2 + a^2\beta_A M^2) Z_i = 0, \tag{3.10}$$

where a prime represents the derivative with respect to the conformal time $\tau = \int a^{-1} dt$. For the modes satisfying the condition $k^2 \gg a^2\beta_A M^2$, the perturbation is in a Bunch-Davies vacuum state characterized by $Z_i = e^{-ik\tau}/\sqrt{2k}$. On the other hand, after the mass term $a^2\beta_A M^2$ dominates over k^2 during inflation, we solve Eq. (3.9) for Z_i under the conditions that $H =$ constant and that k^2/a^2 is negligible relative to $\beta_A M^2$. We then obtain the following solution:

$$Z_i = A_+ e^{\lambda_+ t} + A_- e^{\lambda_- t}, \tag{3.11}$$

where $A_\pm$ are integration constants, and

$$\lambda_\pm = \frac{H}{2}\left[-1 \pm \sqrt{1 - \frac{4\beta_A M^2}{H^2}}\right]. \tag{3.12}$$

Since $\beta_A > 0$, the vector mass term leads to the exponential suppression of Z_i after the perturbation enters the region $k^2/a^2 < \beta_A M^2$. The term in the square root of Eq. (3.12) becomes negative for $4\beta_A M^2 > H^2$. Now, we would like to consider the case in which M is of the same order as the Hubble expansion rate H during inflation. Then, for the coupling

$$\beta_A = \mathcal{O}(1), \tag{3.13}$$

the condition $4\beta_A M^2 > H^2$ is satisfied. In this case, the amplitude of Z_i decreases as

$$|Z_i| \propto e^{-Ht/2}, \tag{3.14}$$

with damped oscillations. Then, the vector perturbation decays very fast once it enters the region $k^2/a^2 < \beta_A M^2$. Since $\beta_A M^2$ is of the same order as H^2, this exponential suppression starts to occur around the same moment of the Hubble exit ($k^2/a^2 < H^2$).

In the following, we focus on the coupling β_A of order 1. Then, the amplitude of vector perturbations at the end of inflation is completely negligible relative to those of tensor and scalar perturbations, so we can ignore the contributions of vector perturbations to the total primordial power spectrum.

IV. PRIMORDIAL SCALAR POWER SPECTRUM GENERATED DURING INFLATION

Let us proceed to the derivation of the scalar power spectrum generated in our model given by the action (2.5). In doing so, we begin with the perturbed line element on the FLRW background in the flat gauge:

$$ds_s^2 = -(1+2\alpha)dt^2 + 2\nabla_i \chi dt dx^i + a^2(t)\delta_{ij}dx^i dx^j, \tag{4.1}$$

where α and χ are scalar metric perturbations. We decompose the scalar field ϕ into the background and perturbed parts as

$$\phi = \phi_0(t) + \delta\phi(t, x^i). \tag{4.2}$$

In the following, we omit the subscript "0" from the background value of ϕ. The temporal component of A^μ is expressed in the form

$$A^0 = -A_0(t) + \delta A(t, x^i), \tag{4.3}$$

whereas the spatial vector component A_i contains the longitudinal scalar perturbation ψ as Eq. (3.7).

The second-order action $\mathcal{S}_s^{(2)}$ of scalar perturbations was already computed in full parity-invariant SVT theories [44]. In our theories given by the action (2.5), we show the explicit form of $\mathcal{S}_s^{(2)}$ in Eq. (A1) of the Appendix. Varying the action $\mathcal{S}_s^{(2)}$ with respect to $\alpha, \chi, \delta A$, we obtain the equations of motion for these nondynamical perturbations; see Eqs. (A4)–(A6). After integrating them out from the action, we are finally left with two dynamical real fields, ψ and $\delta\phi$. In general, any real scalar field $\mathcal{X}$ can be expanded in Fourier series, as

$$\mathcal{X} = \int \frac{d^3k}{(2\pi)^3}[\mathcal{X}_k(t)a(\boldsymbol{k})e^{i\boldsymbol{k}\cdot\boldsymbol{x}} + \mathcal{X}_k^*(t)a^\dagger(\boldsymbol{k})e^{-i\boldsymbol{k}\cdot\boldsymbol{x}}], \quad (4.4)$$

where $\boldsymbol{k}$ is a coming wave number and $\mathcal{X}_k(t)$ is the mode function in Fourier space. For a quantized field $\mathcal{X}$, the coefficient $a(\boldsymbol{k})$ and its Hermitian conjugate $a^\dagger(\boldsymbol{k})$ correspond to annihilation and creation operators.

Thus, the second-order action for dynamical perturbations $\mathcal{X}^t = (\psi_k, \delta\phi_k)$ in Fourier space can be written as

$$\mathcal{S}_s^{(2)} = \int dtd^3xa^3\left(\dot{\vec{\mathcal{X}}}^t\boldsymbol{K}\dot{\vec{\mathcal{X}}} - \frac{k^2}{a^2}\vec{\mathcal{X}}^t\boldsymbol{G}\vec{\mathcal{X}} - \vec{\mathcal{X}}^t\boldsymbol{M}\vec{\mathcal{X}}\right), \quad (4.5)$$

where $\boldsymbol{K}, \boldsymbol{G}$, and $\boldsymbol{M}$ are 2×2 matrices. The matrix $\boldsymbol{M}$ does not contain the k^2 term. We note that the term $\vec{\mathcal{X}}^t\boldsymbol{B}\dot{\vec{\mathcal{X}}}$ appearing in Ref. [44] has been absorbed into $\boldsymbol{M}$ after the integration by parts. The nonvanishing matrix components are given by[2]

$$\begin{aligned}
K_{11} &= \frac{k^2\beta_A M^2}{2(k^2+a^2\beta_A M^2)}, \qquad K_{12} = K_{21} = \frac{\beta_m}{2\beta_A M}K_{11},\\
K_{22} &= \frac{1}{2} - \frac{a^2\beta_m^2 M^2}{8(k^2+a^2\beta_A M^2)},\\
G_{11} &= \frac{\beta_A M^2}{2}, \qquad G_{12} = G_{21} = \frac{\beta_m M}{4}, \qquad G_{22} = \frac{1}{2},\\
M_{22} &= \frac{V_{,\phi\phi}}{2} - \frac{(1-\delta_\phi^2)V_{,\phi}^2}{6M_{\rm pl}^2H^2} - \frac{(1+\delta_\phi)^4V_{,\phi}^4}{324\beta H^6M_{\rm pl}^4},
\end{aligned} \quad (4.6)$$

where we used the background Eqs. (2.11)–(2.13) to eliminate $\dot{H}$ and $\ddot{\phi}$. We also introduced the dimensionless quantity

$$\delta_\phi \equiv \frac{\beta\ddot{\phi}}{V_{,\phi}} = -\frac{3\beta H\dot{\phi} + V_{,\phi}}{V_{,\phi}}, \quad (4.7)$$

which is smaller than order 1 during inflation. The off-diagonal components K_{12} and G_{12} do not vanish for $\beta_m \neq 0$.

[2]Unlike Ref. [44], the small-scale limit $k^2 \to \infty$ is not taken here, so that the components of $\boldsymbol{K}$ contain k^2-dependent terms.

To study the evolution of perturbations ψ_k and $\delta\phi_k$ in Fourier space, we introduce the following combination:

$$\delta\chi_k \equiv \psi_k + \frac{\beta_m}{2\beta_A M}\delta\phi_k. \quad (4.8)$$

Varying the action (4.5) with respect to ψ_k and using the properties that both K_{12}/K_{11} and G_{12}/G_{11} are equivalent to $\beta_m/(2\beta_A M)$, we obtain

$$\frac{1}{a^3}\frac{d}{dt}(a^3K_{11}\dot{\delta\chi}_k) + \frac{k^2}{a^2}G_{11}\delta\chi_k = 0. \quad (4.9)$$

For $k^2/a^2 \gg \beta_A M^2$, we have $K_{11} \to \beta_A M^2/2 = G_{11}$ and hence Eq. (4.9) reduces to

$$\ddot{\delta\chi}_k + 3H\dot{\delta\chi}_k + \frac{k^2}{a^2}\delta\chi_k = 0. \quad (4.10)$$

This equation is of the same form as Eq. (3.3) for tensor perturbations, i.e., the equation of motion of a massless field. For the modes deep inside the Hubble radius ($k^2/a^2 \gg H^2$), the canonically normalized field $v_k = \sqrt{2}a\delta\chi_k$ is in a Bunch-Davies vacuum state characterized by $v_k = e^{-ik\int dt/a}/\sqrt{2k}$. Since we are considering the coupling in Eq. (3.13) with $M \simeq H$ during inflation, the transition to another regime $k^2/a^2 < \beta_A M^2$ occurs around the exit of the Hubble radius.

For $k^2/a^2 \ll \beta_A M^2$, we have $K_{11} \to k^2/(2a^2)$, so Eq. (4.9) yields

$$\ddot{\delta\chi}_k + H\dot{\delta\chi}_k + \beta_A M^2\delta\chi_k = 0, \quad (4.11)$$

which is of the same form as Eq. (3.9) after taking the same limit. On the quasi–de Sitter background ($H \simeq$ constant), the solution to Eq. (4.11) is given by

$$\delta\chi_k = A_+e^{\lambda_+ t} + A_-e^{\lambda_- t}, \quad (4.12)$$

where $\lambda_\pm$ are equivalent to those given in Eq. (3.12). Analogous to the intrinsic vector mode Z_i, the perturbation $\delta\chi_k$ starts to be exponentially suppressed after it enters the region $k^2/a^2 < \beta_A M^2$.

For the coupling β_A satisfying $4\beta_A M^2 > H^2$, the amplitude of $\delta\chi_k$ decreases as $|\delta\chi_k| \propto e^{-Ht/2}$. Then, the perturbation $\delta\chi_k$ is vanishing small at the end of inflation, so we can set $\delta\chi_k \simeq 0$ in Eq. (4.8) and hence

$$\psi_k \simeq -\frac{\beta_m}{2\beta_A M}\delta\phi_k. \quad (4.13)$$

One can notice that, from Eq. (2.10), the relation between ψ_k and $\delta\phi_k$ is analogous to that between A_0 and $\dot{\phi}$.

The only possibility for avoiding the above strong suppression is to consider the small coupling $\beta_A \ll 1$.

In this case, there is a period characterized by $H^2 > k^2/a^2 > \beta_A M^2$ during which the perturbation $\delta\chi_k$ is temporally frozen with the value at the Hubble radius crossing. However, after the perturbation enters the region $k^2/a^2 < \beta_A M^2$, $\delta\chi_k$ starts to decay according to Eq. (4.12). It is possible to derive the solution to Eq. (4.11) even for the background where the scale factor evolves as $a \propto t^p$, where p is a positive constant. In this case the resulting solution is given by $|\delta\chi_k| \propto t^{-p/2}$, so the suppression of $\delta\chi_k$ also occurs after inflation whenever H^2 drops below the order of $\beta_A M^2$.

Varying the action (4.5) with respect to $\delta\phi_k$, it follows that

$$\frac{1}{a^3}\frac{d}{dt}[a^3(K_{22}\dot{\delta\phi}_k + K_{12}\dot{\psi}_k)] + \frac{k^2}{a^2}(G_{22}\delta\phi_k + G_{12}\psi_k) + M_{22}\delta\phi_k = 0. \tag{4.14}$$

Now, we employ Eq. (4.8) and its time derivative to eliminate ψ_k and $\dot{\psi}_k$ from Eq. (4.14). In doing so, we also resort to the fact that $\delta\chi_k$ obeys Eq. (4.9). Then, the contributions arising from $\delta\chi_k$ to Eq. (4.14) cancel out, so that

$$\frac{1}{a^3}\frac{d}{dt}(a^3\tilde{K}_{22}\dot{\delta\phi}_k) + \left(\frac{k^2}{a^2}\tilde{G}_{22} + M_{22}\right)\delta\phi_k = 0, \tag{4.15}$$

where

$$\tilde{K}_{22} \equiv K_{22} - \frac{\beta_m}{2\beta_A M}K_{12} = \frac{\beta}{2}, \tag{4.16}$$

$$\tilde{G}_{22} \equiv G_{22} - \frac{\beta_m}{2\beta_A M}G_{12} = \frac{\beta}{2}. \tag{4.17}$$

Taking the limit $\beta \to 1$ in Eq. (4.15) with Eqs. (4.16) and (4.17), we recover the perturbation equation of $\delta\phi_k$ in standard single-field inflation.

We introduce the canonically normalized field $\delta\sigma_k$ as

$$\delta\sigma_k \equiv a\sqrt{\beta}\delta\phi_k. \tag{4.18}$$

Then, we can express Eq. (4.15) in the form

$$\delta\sigma_k'' + \left(k^2 - \frac{a''}{a} + \frac{2a^2 M_{22}}{\beta}\right)\delta\sigma_k = 0. \tag{4.19}$$

On the quasi–de Sitter background characterized by $H \simeq$ constant, the conformal time $\tau = \int a^{-1}dt$ is approximately given by $\tau \simeq -(1+\epsilon)/(aH)$. Applying the slow-roll approximation (2.17) to the mass term M_{22} and picking up next-to-leading order terms in slow roll in Eq. (4.19), we obtain

$$\delta\sigma_k'' + \left[k^2 - 2(aH)^2\left(1 + \frac{5\epsilon_V - 3\eta_V}{2\beta}\right)\right]\delta\sigma_k = 0, \tag{4.20}$$

where we used the relation (2.19) and introduced the second slow-roll parameter

$$\eta_V \equiv \frac{M_{\rm pl}^2 V_{,\phi\phi}}{V}. \tag{4.21}$$

Neglecting the time variations of ϵ_V and η_V, the solution to Eq. (4.20), which recovers the Bunch-Davies vacuum state ($\delta\sigma_k = e^{-ik\tau}/\sqrt{2k}$) in the asymptotic past ($k\tau \to -\infty$), is given by

$$\delta\sigma_k = \frac{\sqrt{\pi|\tau|}}{2}e^{i(1+2\nu)\pi/4}H_\nu^{(1)}(k|\tau|), \tag{4.22}$$

where $H_\nu^{(1)}(k|\tau|)$ is the Hankel function of the first kind, and

$$\nu = \frac{3}{2} + \frac{3\epsilon_V - \eta_V}{\beta}. \tag{4.23}$$

Using the relations $H_\nu^{(1)}(k|\tau|) \to -(i/\pi)\Gamma(\nu)(k|\tau|/2)^{-\nu}$ for $k\tau \to 0$ and $\Gamma(3/2) = \sqrt{\pi}/2$, the solution for $\delta\phi_k$ long after the Hubble exit during inflation is

$$\delta\phi_k = i\frac{H(1-\epsilon)}{k^{3/2}\sqrt{2\beta}}\frac{\Gamma(\nu)}{\Gamma(3/2)}\left(\frac{k|\tau|}{2}\right)^{3/2-\nu}. \tag{4.24}$$

In the de Sitter limit characterized by $\epsilon_V \to 0$ and $\eta_V \to 0$, the solution (4.24) reduces to $\delta\phi_k \to iH/(k^{3/2}\sqrt{2\beta})$.

We introduce the curvature perturbation in a flat gauge incorporating both the field perturbations $\delta\phi_k$ and ψ_k as [46]

$$\mathcal{R} = -\frac{H(\dot{\phi}\delta\phi_k + M^2 A_0\psi_k)}{\dot{\phi}^2 + M^2 A_0^2}. \tag{4.25}$$

By using Eq. (2.10) and eliminating ψ_k on account of Eq. (4.8), we can write Eq. (4.25) in the form

$$\mathcal{R} = \mathcal{R}_\phi + \mathcal{R}_\chi, \tag{4.26}$$

where

$$\mathcal{R}_\phi = -\frac{H\delta\phi_k}{\dot{\phi}}, \qquad \mathcal{R}_\chi = \frac{2\beta_m\beta_A}{4\beta_A^2 + \beta_m^2}\frac{HM\delta\chi_k}{\dot{\phi}}. \tag{4.27}$$

Since $\delta\chi_k$ is exponentially suppressed by the end of inflation, we only need to compute the power spectrum of $\mathcal{R}_\phi$. Taking Eq. (4.15) with the mass term M_{22} given in Eq. (4.6), the perturbation $\mathcal{R}_\phi$ obeys

$$\frac{1}{a^3\epsilon}\frac{d}{dt}(a^3\epsilon\dot{\mathcal{R}}_\phi)+\frac{k^2}{a^2}\mathcal{R}_\phi=0. \tag{4.28}$$

In the large-scale limit ($k^2/a^2\to 0$), we obtain the following solution:

$$\mathcal{R}_\phi=c_1+c_2\int\frac{dt}{a^3\epsilon}, \tag{4.29}$$

where c_1 and c_2 are integration constants. In slow-roll inflation, the second term on the right-hand side of Eq. (4.29) can be identified as a decaying mode. Then, $\mathcal{R}_\phi$ approaches the constant c_1 soon after the Hubble exit. Then, the primordial power spectrum of $\mathcal{P}_{\mathcal{R}_\phi}$ per unit logarithmic wave number interval can be computed at $k=aH$ as

$$\mathcal{P}_{\mathcal{R}_\phi}\equiv\frac{k^3}{2\pi^2}|\mathcal{R}_\phi|^2=\left.\frac{H^4}{4\pi^2\dot{\phi}^2\beta}\right|_{k=aH}, \tag{4.30}$$

where we used the leading-order solution of Eq. (4.24). Applying the slow-roll approximations (2.17)–(2.18) to Eq. (4.30) and neglecting the contribution from $\delta\chi_k$ to the total curvature perturbation $\mathcal{R}$, the resulting primordial scalar power spectrum is given by

$$\mathcal{P}_{\mathcal{R}}\simeq\left.\frac{\beta V^3}{12\pi^2M_{\rm pl}^6V_{,\phi}^2}\right|_{k=aH}. \tag{4.31}$$

In comparison with the canonical picture of single-field inflation, the coupling β induces different behavior for the scalar power spectrum. Using the background field φ defined by Eq. (2.23), the power spectrum (4.31) can be written in the form $\mathcal{P}_{\mathcal{R}}=V^3/(12\pi^2M_{\rm pl}^6V_{,\varphi}^2)|_{k=aH}$. This means that, as long as the perturbation $\delta\chi_k$ is negligibly small compared to $\delta\phi_k$ at the end of inflation, the effective single-field description in terms of φ also works for curvature perturbations.

V. OBSERVATIONAL SIGNATURES IN CMB

In this section, we compute inflationary observables to confront our SVT theories with the CMB data of temperature anisotropies and study how they are modified by the presence of the coupling β.

A. Inflationary observables

In Sec. III, we showed that vector perturbations are exponentially suppressed relative to scalar and tensor perturbations at the end of inflation, so we neglect the contribution of vector modes to the inflationary power spectra. At the pivot wave number $k_0=0.05\ {\rm Mpc}^{-1}$, the amplitude of curvature perturbations constrained from *Planck* 2018 observations is [6]

$$\mathcal{P}_{\mathcal{R}}=\frac{\beta V^3}{12\pi^2M_{\rm pl}^6V_{,\phi}^2}=2.1\times10^{-9}. \tag{5.1}$$

The spectral indices of tensor and scalar perturbations are defined, respectively, by

$$n_t\equiv\left.\frac{d\ln\mathcal{P}_t}{d\ln k}\right|_{k=aH}, \tag{5.2}$$

$$n_s\equiv1+\left.\frac{d\ln\mathcal{P}_{\mathcal{R}}}{d\ln k}\right|_{k=aH}. \tag{5.3}$$

From Eqs. (3.5) and (4.31), we obtain

$$n_t=-\frac{2\epsilon_V}{\beta}, \tag{5.4}$$

$$n_s=1-\frac{1}{\beta}(6\epsilon_V-2\eta_V), \tag{5.5}$$

where we used the slow-roll approximations (2.17)–(2.18). The tensor-to-scalar ratio is given by

$$r\equiv\frac{\mathcal{P}_t}{\mathcal{P}_{\mathcal{R}}}=\frac{16\epsilon_V}{\beta}=16\epsilon. \tag{5.6}$$

From Eqs. (5.4) and (5.6), the following consistency relation holds:

$$r=-8n_t, \tag{5.7}$$

which is of the same form as that in standard single-field inflation. We study how the coupling β modifies the observational prediction of n_s and r. We show that this modification generally depends on the form of inflaton potentials.

B. Different inflaton potentials and *Planck* 2018 constraints

In the following, we consider three different inflaton potentials arising in (i) natural inflation, (ii) α attractors, and (iii) brane inflation. We also discuss whether these models can be consistent with the latest *Planck* 2018 data [6] in the presence of the scalar-vector mixing.

1. Natural inflation

In natural inflation [48], the potential is given by

$$V(\phi)=M^2M_{\rm pl}^2\left[1+\cos\left(\frac{\phi}{f}\right)\right], \tag{5.8}$$

where f is a mass scale associated with the shift symmetry. In this case, the observables (5.1), (5.5), and (5.6) reduce, respectively, to

$$\mathcal{P}_{\mathcal{R}} = \frac{f_\beta^2 M^2 (1+x)^2}{12\pi^2 M_{\rm pl}^2 (1-x)} = 2.1 \times 10^{-9}, \tag{5.9}$$

$$n_s = 1 - \frac{3-x}{f_\beta^2 (1+x)}, \tag{5.10}$$

$$r = \frac{8(1-x)}{f_\beta^2 (1+x)}, \tag{5.11}$$

where $f_\beta \equiv \sqrt{\beta} f/M_{\rm pl}$ and $x \equiv \cos(\phi/f)$. From Eq. (2.22), we obtain $N = f_\beta^2 \ln[(1-x_f)/(1-x)]$, so that

$$x = 1 - (1-x_f) e^{-N/f_\beta^2}, \tag{5.12}$$

where $x_f = (1-2f_\beta^2)/(1+2f_\beta^2)$ is the value of x at the end of inflation determined by the condition (2.21). Substituting Eq. (5.12) into Eqs. (5.10) and (5.11), it follows that n_s and r depend on f_β and N. For a given N, these observables are functions of f_β alone. Hence the theoretical curve in the (n_s, r) plane is the same as that in standard natural inflation. The only difference is that the coupling $f/M_{\rm pl}$ is now modified to $f_\beta = \sqrt{\beta} f/M_{\rm pl}$. From *Planck* 2015 data [5], the coupling is constrained to be $\log_{10}(f_\beta) > 0.84$ at 95% C.L., i.e.,

$$f > \frac{6.9 M_{\rm pl}}{\sqrt{\beta}}. \tag{5.13}$$

As in the standard case, the trans-Planckian problem about the scale f also persists for $\beta < 1$. With given values of f, β, and N, the mass scale M is known from the *Planck* normalization (5.9).

The recent *Planck* 2018 data combined with the data of B-mode polarizations available from the BICEP2/Keck field (BK14) and baryon acoustic oscillations (BAO) indicate that most of the theoretical values of n_s and r in natural inflation are outside of the 95% C.L. observational contour; see Fig. 8 of Ref. [6]. As shown above, this situation is not improved by the mixing term β_m between the inflaton and vector fields.

2. α attractors

The α-attractor model [49] is given by the potential

$$V(\phi) = \frac{3}{4}\alpha_c M^2 M_{\rm pl}^2 \left[1 - \exp\left(-\sqrt{\frac{2}{3\alpha_c}}\frac{\phi}{M_{\rm pl}}\right)\right]^2, \tag{5.14}$$

where α_c is a dimensionless constant.[3] Starobinsky inflation [1] characterized by the Lagrangian $f(R) = R + R^2/(6M^2)$ gives rise to the potential (5.14) with $\alpha_c = 1$ after a conformal transformation to the Einstein frame. In the limit that $\alpha_c \to \infty$, the potential (5.14) reduces to that in chaotic inflation: $V(\phi) = M^2\phi^2/2$.

For α attractors, the inflationary observables are

$$\mathcal{P}_{\mathcal{R}} = \frac{3\alpha_c^2 \beta M^2 (1-y)^4}{128\pi^2 M_{\rm pl}^2 y^2} = 2.1 \times 10^{-9}, \tag{5.15}$$

$$n_s = 1 - \frac{8y(1+y)}{3\alpha_c\beta(1-y)^2}, \tag{5.16}$$

$$r = \frac{64y^2}{3\alpha_c\beta(1-y)^2}, \tag{5.17}$$

where $y \equiv e^{-\sqrt{2/(3\alpha_c)}\phi/M_{\rm pl}}$. The number of e-foldings is given by

$$N = \frac{3}{4}\alpha_c\beta\left(\frac{1}{y} - \frac{1}{y_f} + \ln\frac{y}{y_f}\right), \tag{5.18}$$

where $y_f = (3\alpha_c\beta - 2\sqrt{3\alpha_c\beta})/(3\alpha_c\beta - 4)$ is the value of y at the end of inflation.

For $\alpha_c < \mathcal{O}(10)$, y is smaller than order 1 during inflation. In this case, the dominant contribution to N is the first term in the parentheses of Eq. (5.18), i.e., $y \simeq 3\alpha_c\beta/(4N) \ll 1$. Substituting this expression into Eqs. (5.16) and (5.17), we obtain

$$n_s \simeq 1 - \frac{2}{N}, \qquad r \simeq \frac{12\alpha_c\beta}{N^2}. \tag{5.19}$$

While n_s does not depend on β, the scalar-vector mixing ($\beta_m \neq 0$) leads to a smaller value for the tensor-to-scalar ratio compared to the case $\beta = 1$. The *Planck* normalization (5.15) gives

$$M = 1.3 \times 10^{-5} M_{\rm pl}\sqrt{\beta}\left(\frac{55}{N}\right), \tag{5.20}$$

so that M decreases for smaller β.

For $\alpha_c \gg \mathcal{O}(10)$, y approaches 1 with increasing α_c. Expansion of Eq. (5.18) around $y = 1$ shows that the number of e-foldings long before the end of inflation is approximately given by $N \simeq 3\alpha_c\beta(1-y)^2/8 \gg 1$. In this regime, the observables (5.16) and (5.17) reduce to

$$n_s \simeq 1 - \frac{2}{N}, \qquad r \simeq \frac{8}{N}, \tag{5.21}$$

which are equivalent to those in standard chaotic inflation driven by the potential $V(\phi) = M^2\phi^2/2$ [9]. From Eq. (5.21), the coupling β modifies neither n_s nor r for $\alpha_c \gg \mathcal{O}(10)$.

In Fig. 1, we plot the theoretical curves in the (n_s, r) plane for $\beta = 1$ (red dashed) and $\beta = 0.1$ (black thin solid)

[3] We note that the same potential can be derived from Brans-Dicke theory with the Lagrangian $\mathcal{L} = M_{\rm pl}\phi R/2 - V_0(\phi - M_{\rm pl})^2$ after a conformal transformation to the Einstein frame; see Eq. (109) of Ref. [50]. The observational constraints on this model were already performed in 2011; see Fig. 3 of Ref. [50].

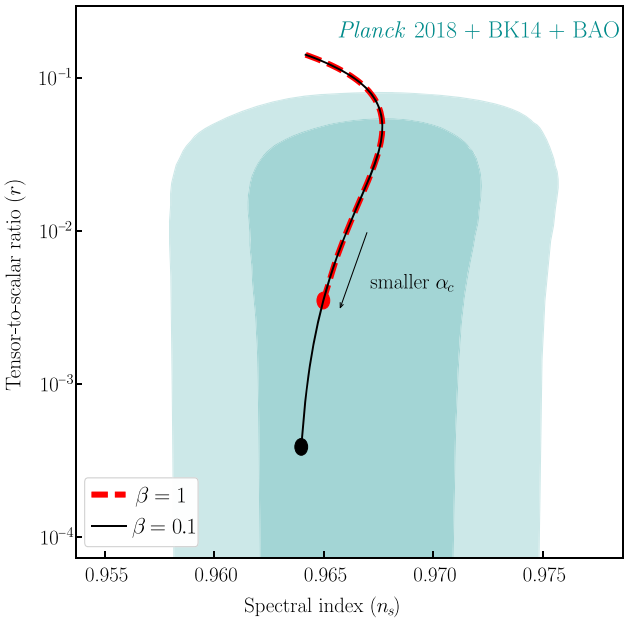

FIG. 1. Observational constraints on α attractors in the (n_s, r) plane. The green contours represent the 68% C.L. (inside) and 95% C.L. (outside) boundaries derived by the joint data analysis of *Planck* 2018 + BK14 + BAO at $k = 0.002$ Mpc^{-1} [6]. The red dashed and black thin solid lines correspond to the cases $\beta = 1$ and $\beta = 0.1$, respectively, with $N = 55$ and $1 \le \alpha_c \le 10^6$. The red and black circles represent Starobinsky inflation ($\alpha_c = 1$) with $\beta = 1$ and $\beta = 0.1$, respectively.

for $N = 55$ and $1 \le \alpha_c \le 10^6$. For $\alpha_c \gg \mathcal{O}(10)$, the observables converge to the values in (5.21) irrespective of the coupling β. With decreasing α_c, the difference of r between the two different values of β tends to be significant. In Starobinsky inflation ($\alpha_c = 1$), e.g., we have $r = 3.9 \times 10^{-4}$ for $\beta = 0.1$. As estimated from Eq. (5.19), this is by 1 order of magnitude smaller than the value $r = 3.5 \times 10^{-3}$ for $\beta = 1$. In both cases, the models are inside a 68% C.L. observational contour constrained from *Planck* 2018 + BK14 + BAO data. Interestingly, even if future observations place the upper limit of r down to 10^{-3}, the model with $\alpha_c = 1$ can be still rescued by the coupling β.

As we observe in Fig. 1, the scalar spectral index n_s for $\beta = 0.1$ and $\alpha_c = 1$ is slightly smaller than that for $\beta = 1$ and $\alpha_c = 1$. This reflects the fact that, in the latter case, the approximation $y \ll 1$ we used for the derivation of n_s in Eq. (5.19) is not completely accurate. As the product $\alpha_c\beta$ decreases toward 0, the observables approach $n_s \to 1 - 2/N$ and $r \to 0$, which are favored in current CMB observations.

Since the coupling β smaller than 1 can reduce the value of r, the bound on α_c is less stringent compared to the case $\beta = 1$. For $\beta = 1$ the observational upper limit is $\alpha_c < 4.4 \times 10$ (68% C.L.), while, for $\beta = 0.1$, the bound is loosened: $\alpha_c < 4.2 \times 10^2$ (68% C.L.). Unless α_c is very much larger than 1 to approach the asymptotic values of n_s and r given by Eq. (5.21), the product $\alpha_c\beta$ is constrained to be

$$\alpha_c\beta \lesssim 40, \tag{5.22}$$

at 68% C.L. The main reason why r is reduced by the mixing term β_m is that the coupling β leads to smaller $y \simeq 3\alpha_c\beta/(4N)$ (i.e., larger ϕ) for $\alpha_c < \mathcal{O}(10)$. This effect overwhelms the coupling β in the denominator of Eq. (5.17), so that r has the dependence $r \propto \alpha_c\beta/N^2$. In other words, for $\beta < 1$, we require that inflation occurs in the region where the potential is flatter relative to the case $\beta = 1$ to acquire the same number of e-foldings. This effectively reduces the value of $r = 16\epsilon$ for a given N.

3. Brane inflation

Finally, we study brane inflation characterized by the effective potential

$$V(\phi) = M^2 M_{\rm pl}^2 \left[1 - \left(\frac{\mu}{\phi}\right)^p + \cdots\right], \tag{5.23}$$

where p and μ are positive constants. The models arising from the setup of a D-brane and anti-D-brane configuration have the power $p = 2$ [51] or $p = 4$ [52,53]. For the positivity of $V(\phi)$, we require that $z \equiv \phi/\mu > 1$. We assume that inflation ends around $\phi \approx \mu$ before the additional terms denoted by the ellipsis in Eq. (5.23) contributes to the potential.

The observables (5.1), (5.5), and (5.6) reduce, respectively, to

$$\mathcal{P}_\mathcal{R} = \frac{\beta M^2\mu^2(z^p - 1)^3}{12\pi^2 M_{\rm pl}^4 p^2 z^{p-2}} = 2.1 \times 10^{-9}, \tag{5.24}$$

$$n_s = 1 - \frac{pM_{\rm pl}^2[2(p+1)z^p + p - 2]}{\mu^2 z^2 (z^p - 1)^2 \beta}, \tag{5.25}$$

$$r = \frac{8p^2 M_{\rm pl}^2}{\mu^2 z^2 (z^p - 1)^2 \beta}. \tag{5.26}$$

The number of e-foldings is given by

$$N \simeq \frac{\beta\mu^2[z^2(2z^p - p - 2) + p]}{2M_{\rm pl}^2 p(p+2)}, \tag{5.27}$$

where we used the fact that the value of z at the end of inflation is $z_f \simeq 1$.

Since inflation occurs in the region $z^p \gg 1$, we pick up the dominant contributions to Eqs. (5.25)–(5.27). Then we have $z^{p+2} \simeq M_{\rm pl}^2 p(p+2)N/\beta\mu^2$, and

$$n_s \simeq 1 - \frac{2(p+1)}{(p+2)N}, \tag{5.28}$$

$$r \simeq 8p^2 \left(\frac{\beta\mu^2}{M_{\rm pl}^2}\right)^{\frac{p}{p+2}} \left[\frac{1}{p(p+2)N}\right]^{\frac{2(p+1)}{p+2}}, \tag{5.29}$$

which show that the β dependence appears in r but not in n_s. From Eq. (5.28), we obtain $n_s = 1\text{–}3/(2N)$, for $p = 2$, and $n_s = 1\text{–}5/(3N)$, for $p = 4$; therefore, one can notice that the value of n_s for these models is larger than the one obtained from Eq. (5.19) for α attractors. From Eq. (5.29), the tensor-to-scalar ratio has the dependence $r \propto \beta^{1/2}/N^{3/2}$ for $p = 2$ and $r \propto \beta^{2/3}/N^{5/3}$ for $p = 4$. In the limit that $p \gg 1$, we have $n_s \simeq 1\text{–}2/N$ and $r \propto \beta/N^2$, so they have the same dependence of N and β as those in the α attractors with $\alpha_c < \mathcal{O}(10)$. The scalar-vector mixing works to reduce the tensor-to-scalar ratio compared to the case $\beta = 1$. Unlike α attractors in which the dependence of r with respect to β depends on α_c, the reduction of r induced by the coupling β occurs irrespective of the values of μ.

In Fig. 2, we plot the theoretical curves in the (n_s, r) plane for the brane inflation scenario with $\beta = 1$ and $\beta = 0.1$ for the mass range $10^{-3/2} \leq \mu/M_{\rm pl} \leq 10$. We consider the models with two different powers: $p = 2$ and $p = 4$.

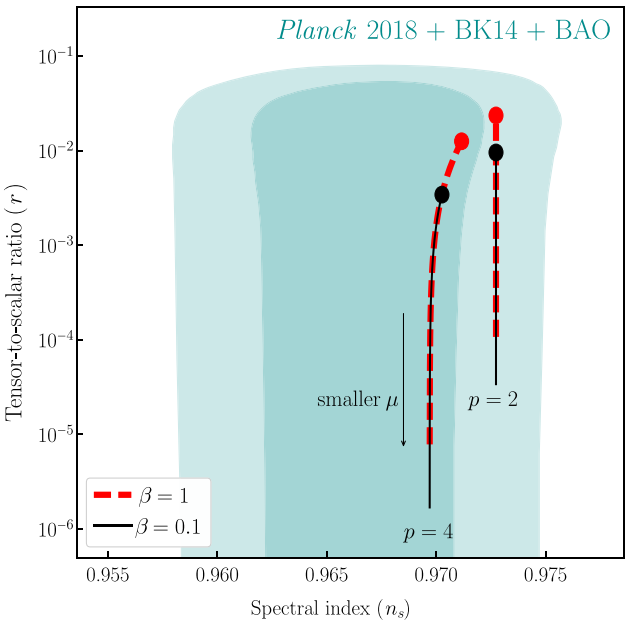

FIG. 2. Observational constraints on brane inflation in the (n_s, r) plane for $p = 2$ and $p = 4$. The green contours are the same as those in Fig. 1. The red dashed and black thin solid lines represent the cases $\beta = 1$ and $\beta = 0.1$, respectively, with $N = 55$ and $-1.5 \leq \log_{10}(\mu/M_{\rm pl}) \leq 1.0$. The red and black circles correspond to $\log_{10}(\mu/M_{\rm pl}) = 1.0$ with $\beta = 1$ and $\beta = 0.1$, respectively.

For smaller μ, z gets larger and hence the approximate results (5.28)–(5.29) tend to be more accurate. As estimated from Eq. (5.28), the scalar spectral index is nearly constant, i.e., $n_s \simeq 0.9727$ for $p = 2$ and $n_s \simeq 0.9697$ for $p = 4$.

The red circle plotted on the line for $p = 2$ of Fig. 2 corresponds to the model parameters $\beta = 1$ and $\mu/M_{\rm pl} = 10$, in which case the model is inside the 95% C.L. observational contour with $r = 2.35 \times 10^{-2}$. From Eq. (5.29), the tensor-to-scalar ratio decreases for smaller values of β and μ. When $p = 2, \beta = 0.1$, and $\mu/M_{\rm pl} = 10$, the numerical value of r is given by 9.53×10^{-3}—see the black circle on the line for $p = 2$ of Fig. 2. The models with $\beta < 1$ and $\mu \lesssim 10 M_{\rm pl}$ are consistent with the current upper bound of r. For $p = 2$, the scalar spectral index is between the 68% C.L. and 95% C.L. observational boundaries.

The model with $p = 4$ gives rise to n_s smaller than that for $p = 2$, so the former model enters the 68% C.L. observational contour for $\mu \lesssim 10 M_{\rm pl}$ and $\beta \leq 1$. The red circle shown on the line for $p = 4$ of Fig. 2 corresponds to $\beta = 1$ and $\mu/M_{\rm pl} = 10$, in which case $r = 1.25 \times 10^{-2}$. For $\beta = 0.1$, this value is reduced to $r = 3.41 \times 10^{-3}$. For smaller β and μ, the tensor-to-scalar ratio approximately decreases as $r \propto (\beta\mu^2)^{2/3}$ for $p = 4$.

We note that the increase of r induced by the coupling $\beta(< 1)$ in the denominator of Eq. (5.26) is switched to the decrease of r by the other term $z^{2+2p} \propto \beta^{-(2+2p)/(2+p)}$. Analogous to α attractors with $\alpha_c < \mathcal{O}(10)$, this behavior occurs in small-field inflation in which the variation of ϕ during inflation does not exceed the order of $M_{\rm pl}$. In α attractors with $\alpha_c \gg \mathcal{O}(10)$, which corresponds to large-field inflation, the decrease of r induced by β is not significant. In chaotic inflation (the limit $\alpha_c \to \infty$ in α attractors), both ϵ_V and η_V are inversely proportional to N, in which case both n_s and r solely depend on N but not on β. In small-field inflation, ϵ_V and η_V have different N dependence with $\epsilon_V \ll |\eta_V|$, in which case the explicit β dependence appears in r.

VI. CONCLUSIONS

This work was devoted to the study of prominent effective field theories with helicity-0 and helicity-1 fields in the presence of a dimension-3 operator that couples the two sectors. We have investigated the implications of this coupling for inflation driven by the helicity-0 mode with a given potential energy, paying particular attention to the evolution of cosmological perturbations. At the background level, the temporal component of the helicity-1 mode, A_0, is just an auxiliary (nondynamical) field, so that it can be directly integrated out in terms of the time derivative of the helicity-0 mode. In this way, the background dynamics resembles that of a single-field inflation modulated by a parameter β associated with the coupling between the helicity-0 and helicity-1 modes.

We studied the evolution of longitudinal scalar perturbation ψ_k in the presence of the inflaton fluctuation $\delta\phi_k$. The perturbation corresponding to the isocurvature mode is given by the combination $\delta\chi_k = \psi_k + \beta_m/(2\beta_A M)\delta\phi_k$. The existence of the vector-field mass M comparable to the Hubble expansion rate during inflation leads to the exponential suppression of $\delta\chi_k$ after the perturbation enters the region $k^2/a^2 < \beta_A M^2$. We then explicitly showed that the power spectrum of the total curvature perturbation, $\mathcal{R}$, generated during inflation, corresponds to that of an effective single-field description also corrected by β. This is possible due to a similar relation between ψ_k and $\delta\phi_k$ to that of A_0 and $\dot{\phi}$ at the background level, obtained in fact by the suppression of $\delta\chi_k$.

After deriving the power spectra of the scalar and tensor perturbations generated during inflation, we computed their spectral indices n_s and n_t as well as the tensor-to-scalar ratio r to confront our inflationary scenario with CMB observations. The mixing between helicity-0 and helicity-1 modes leads to modifications on n_s and r through the parameter β, with the same consistency relation $r = -8n_t$ as in the standard canonical case ($\beta = 1$).

We computed the observables $\mathcal{P}_\mathcal{R}$, n_s, and r for several inflaton potentials to explore the effect of coupling β on CMB. For natural inflation, these observables reduce to those of the canonical case after the rescaling of the mass scale f. In small-field inflation like α attractors and brane inflation, however, the coupling $\beta(< 1)$ can lead to the suppression of $r = 16\epsilon$ compared to the canonical case. This is attributed to the fact that, for smaller β, the total field velocity gets larger and hence inflation needs to start from a region in which the potential $V(\phi)$ is flatter to acquire the sufficient amount of e-foldings. Then, the tensor-to-scalar ratio decreases by the reduction of ϵ on scales relevant to observed CMB anisotropies.

In α attractors given by the potential (5.14), we showed that n_s and r are approximately given by $n_s \simeq 1\text{–}2/N$ and $r \simeq 12\alpha_c\beta/N^2$ for $\alpha_c < \mathcal{O}(10)$. This includes the Starobinsky inflation as a special case ($\alpha_c = 1$). The coupling β smaller than 1 leads to the suppression of r, so that the α-attractor model exhibits even better compatibility with current CMB observations (see Fig. 1). For $\alpha_c < \mathcal{O}(10)$, we obtained the observational bound $\alpha_c\beta \lesssim 40$ (68% C.L.) from the joint analysis based on the *Planck* 2018 + BK14 + BAO data sets. The similar suppression of r and the better compatibility with observations have been also confirmed for brane inflation given by the potential (5.23). For $\beta < 1$, the brane inflation models with $p = 2$ and $p = 4$ are inside the 95% C.L. and 68% C.L. observational contours, respectively, constrained from the *Planck* 2018 + BK14 + BAO data; see Fig. 2.

In this work, we focused on the simple mixing term $A^\mu\nabla_\mu\phi$ as a first step for computing primordial power spectra generated during inflation, but the further generalization of couplings between ϕ and A^μ is possible along the lines of Ref. [41]. It will also be of interest to study potential signatures of such couplings in the CMB bispectrum as well as implications in the physics of reheating. Another direct implication worth studying is the improvement of standard inflationary models with respect to the de Sitter swampland conjecture in the presence of this mixing term [54]. These interesting issues are left for future works.

ACKNOWLEDGMENTS

We would like to thank Jose Beltrán Jiménez, Claudia de Rham, Ryotaro Kase, and Gonzalo Olmo for useful discussions. H. R. would like to thank the Institute of Cosmology and Gravitation in Portsmouth for their kind hospitality. H. R. was supported in part by MINECO Grant No. SEV-2014-0398, PROMETEO II/2014/050, Spanish Grants No. FPA2014-57816-P and No. FPA2017-85985-P of the MINECO, and European Union's Horizon 2020 research and innovation program under the Marie Skłodowska-Curie Grants No. 690575 and No. 674896. S. T. is supported by the Grant-in-Aid for Scientific Research Fund of the JSPS (Grant No. 16K05359) and MEXT KAKENHI Grant-in-Aid for Scientific Research on Innovative Areas "Cosmic Acceleration" (Grant No. 15H05890).

APPENDIX: SECOND-ORDER ACTION FOR SCALAR PERTURBATIONS (4.5)

In this Appendix, we show the details for the derivation of Eq. (4.5). In Eq. (5.4) of Ref. [44], the second-order action $\mathcal{S}_s^{(2)}$ of scalar perturbations was derived in general SVT theories by choosing the flat gauge. For the specific theories given in this work by Eq. (2.5), we have

$$\mathcal{S}_s^{(2)} = \int dtd^3xa^3(\mathcal{L}_s^\phi + \mathcal{L}_s^{\rm GP}), \tag{A1}$$

where

$$\mathcal{L}_s^\phi = \frac{1}{2}\dot{\delta\phi}^2 - \frac{(\partial\delta\phi)^2}{2a^2} - \frac{1}{2}V_{,\phi\phi}\delta\phi^2 - \{\dot{\phi}(2-\beta)\dot{\delta\phi} + V_{,\phi}\delta\phi\}\alpha + \dot{\phi}\beta\delta\phi\frac{\partial^2\chi}{a^2} - \frac{\beta_m M}{2}\left(\dot{\delta\phi}\delta A - \delta\phi\frac{\partial^2\psi}{a^2}\right), \tag{A2}$$

$$\mathcal{L}_s^{\rm GP} = -2HM_{\rm pl}^2\alpha\frac{\partial^2\chi}{a^2} + \frac{\beta_m^2\dot\phi^2}{2\beta_A^2M^2a^2}\left[(\partial\alpha)^2 + \frac{\partial^2\delta A}{A_0}\alpha + \frac{\partial^2\dot\psi}{A_0}\alpha + \frac{(\partial\delta A)^2}{4A_0^2} - \frac{\dot\psi\partial^2\delta A}{2A_0^2} + \frac{(\partial\dot\psi)^2}{4A_0^2}\right]$$
$$+ \left[\dot\phi^2\left(\frac{1}{2}+\frac{3\beta_m^2}{8\beta_A}\right) - 3H^2M_{\rm pl}^2\right]\alpha^2 + \frac{\beta_m^2\dot\phi^2}{8\beta_A}\left(\frac{\delta A^2}{A_0^2} - 4\alpha\frac{\delta A}{A_0}\right) - M^2\beta_A\frac{(\partial\psi)^2}{2a^2}. \tag{A3}$$

Varying the action (A1) with respect to $\alpha, \chi, \delta A$, we obtain the three constraint equations in Fourier space, respectively, as

$$\dot\phi\left(1+\frac{\beta_m^2}{4\beta_A}\right)\dot{\delta\phi} + V_{,\phi}\delta\phi - \left[\dot\phi^2\left(1+\frac{3\beta_m^2}{4\beta_A}\right) - 6H^2M_{\rm pl}^2\right]\alpha + \frac{\beta_m^2\dot\phi^2}{2\beta_A}\frac{\delta A}{A_0}$$
$$+ \frac{k^2}{a^2}\left[\frac{\beta_m^2\dot\phi^2}{2\beta_A^2M^2}\left(\frac{\dot\psi}{A_0}+\frac{\delta A}{A_0}\right) - \frac{\beta_m^2\dot\phi^2}{\beta_A^2M^2}\alpha - 2HM_{\rm pl}^2\chi\right] = 0, \tag{A4}$$

$$\dot\phi\left(1-\frac{\beta_m^2}{4\beta_A}\right)\delta\phi - 2HM_{\rm pl}^2\alpha = 0, \tag{A5}$$

$$\beta_m M\dot{\delta\phi} + \frac{\beta_m^2\dot\phi^2}{2\beta_A}\left(\frac{2\alpha}{A_0} - \frac{\delta A}{A_0^2}\right) - \frac{k^2}{a^2}\frac{1}{A_0}\left[\frac{\beta_m^2\dot\phi^2}{2\beta_A^2M^2}\left(\frac{\dot\psi}{A_0}+\frac{\delta A}{A_0}\right) - \frac{\beta_m^2\dot\phi^2}{\beta_A^2M^2}\alpha\right] = 0. \tag{A6}$$

We solve Eqs. (A4)–(A6) for $\alpha, \chi, \delta A$ and substitute them into Eq. (A1). Then, in Fourier space, we obtain the second-order action (4.5) for dynamical perturbations $\mathcal{X}^t = (\psi_k, \delta\phi_k)$ with the matrix components given by Eq. (4.6).

[1] A. A. Starobinsky, Phys. Lett. **91B**, 99 (1980).
[2] R. Brout, F. Englert, and E. Gunzig, Ann. Phys. (N.Y.) **115**, 78 (1978); D. Kazanas, Astrophys. J. **241**, L59 (1980); K. Sato, Mon. Not. R. Astron. Soc. **195**, 467 (1981); Phys. Lett. **99B**, 66 (1981); A. H. Guth, Phys. Rev. D **23**, 347 (1981).
[3] V. F. Mukhanov and G. V. Chibisov, JETP Lett. **33**, 532 (1981) [Pisma Zh. Eksp. Teor. Fiz. **33**, 532 (1981)]; A. H. Guth and S. Y. Pi, Phys. Rev. Lett. **49**, 1110 (1982); S. W. Hawking, Phys. Lett. **115B**, 295 (1982); A. A. Starobinsky, Phys. Lett. **117B**, 175 (1982); J. M. Bardeen, P. J. Steinhardt, and M. S. Turner, Phys. Rev. D **28**, 679 (1983).
[4] G. Hinshaw *et al.* (WMAP Collaboration), Astrophys. J. Suppl. Ser. **208**, 19 (2013).
[5] P. A. R. Ade *et al.* (Planck Collaboration), Astron. Astrophys. **594**, A20 (2016).
[6] Y. Akrami *et al.* (Planck Collaboration), arXiv:1807.06211.
[7] J. E. Lidsey, A. R. Liddle, E. W. Kolb, and E. J. Copeland, Rev. Mod. Phys. **69**, 373 (1997); D. H. Lyth and A. Riotto, Phys. Rep. **314**, 1 (1999); B. A. Bassett, S. Tsujikawa, and D. Wands, Rev. Mod. Phys. **78**, 537 (2006).
[8] J. Martin, C. Ringeval, and V. Vennin, Phys. Dark Universe **5–6**, 75 (2014).
[9] S. Tsujikawa, J. Ohashi, S. Kuroyanagi, and A. De Felice, Phys. Rev. D **88**, 023529 (2013).
[10] S. Tsujikawa, Prog. Theor. Exp. Phys. **2014**, 6B104 (2014).
[11] M. Escudero, H. Ramírez, L. Boubekeur, E. Giusarma, and O. Mena, J. Cosmol. Astropart. Phys. 02 (2016) 020.
[12] T. Koivisto and D. F. Mota, J. Cosmol. Astropart. Phys. 08 (2008) 021.
[13] J. Beltran Jimenez and A. L. Maroto, Phys. Rev. D **80**, 063512 (2009).
[14] J. Beltran Jimenez and A. L. Maroto, J. Cosmol. Astropart. Phys. 02 (2009) 025.
[15] G. Esposito-Farese, C. Pitrou, and J. P. Uzan, Phys. Rev. D **81**, 063519 (2010).
[16] P. Fleury, J. P. Beltran Almeida, C. Pitrou, and J. P. Uzan, J. Cosmol. Astropart. Phys. 11 (2014) 043.
[17] L. Heisenberg, J. Cosmol. Astropart. Phys. 05 (2014) 015.
[18] E. Allys, P. Peter, and Y. Rodriguez, J. Cosmol. Astropart. Phys. 02 (2016) 004.
[19] J. Beltran Jimenez and L. Heisenberg, Phys. Lett. B **757**, 405 (2016).
[20] G. Tasinato, J. High Energy Phys. 04 (2014) 067; Classical Quantum Gravity **31**, 225004 (2014); L. Heisenberg, R. Kase, and S. Tsujikawa, Phys. Lett. B **760**, 617 (2016); J. Beltran Jimenez and T. S. Koivisto, Phys. Lett. B **756**, 400 (2016); J. Beltran Jimenez, L. Heisenberg, and T. S. Koivisto, J. Cosmol. Astropart. Phys. 04 (2016) 046.
[21] A. De Felice, L. Heisenberg, R. Kase, S. Mukohyama, S. Tsujikawa, and Y. l. Zhang, J. Cosmol. Astropart. Phys. 06 (2016) 048.
[22] A. De Felice, L. Heisenberg, R. Kase, S. Mukohyama, S. Tsujikawa, and Y. l. Zhang, Phys. Rev. D **94**, 044024 (2016).
[23] M. C. Bento, O. Bertolami, P. V. Moniz, J. M. Mourao, and P. M. Sa, Classical Quantum Gravity **10**, 285 (1993).
[24] C. Armendariz-Picon, J. Cosmol. Astropart. Phys. 07 (2004) 007.

[25] A. Golovnev, V. Mukhanov, and V. Vanchurin, J. Cosmol. Astropart. Phys. 06 (2008) 009.
[26] B. Himmetoglu, C. R. Contaldi, and M. Peloso, Phys. Rev. Lett. **102**, 111301 (2009); B. Himmetoglu, C. R. Contaldi, and M. Peloso, Phys. Rev. D **79**, 063517 (2009).
[27] A. Maleknejad and M. M. Sheikh-Jabbari, Phys. Lett. B **723**, 224 (2013); Phys. Rev. D **84**, 043515 (2011).
[28] A. Maleknejad, M. M. Sheikh-Jabbari, and J. Soda, Phys. Rep. **528**, 161 (2013).
[29] R. Namba, E. Dimastrogiovanni, and M. Peloso, J. Cosmol. Astropart. Phys. 11 (2013) 045.
[30] P. Adshead, E. Martinec, and M. Wyman, J. High Energy Phys. 09 (2013) 087.
[31] E. Davydov and D. Gal'tsov, Phys. Lett. B **753**, 622 (2016).
[32] J. Beltran Jimenez, L. Heisenberg, R. Kase, R. Namba, and S. Tsujikawa, Phys. Rev. D **95**, 063533 (2017).
[33] M. a. Watanabe, S. Kanno, and J. Soda, Phys. Rev. Lett. **102**, 191302 (2009); A. E. Gumrukcuoglu, B. Himmetoglu, and M. Peloso, Phys. Rev. D **81**, 063528 (2010); M. a. Watanabe, S. Kanno, and J. Soda, Prog. Theor. Phys. **123**, 1041 (2010); J. Ohashi, J. Soda, and S. Tsujikawa, J. Cosmol. Astropart. Phys. 12 (2013) 009.
[34] M. S. Turner and L. M. Widrow, Phys. Rev. D **37**, 2743 (1988).
[35] B. Ratra, Astrophys. J. **391**, L1 (1992).
[36] K. Bamba and J. Yokoyama, Phys. Rev. D **69**, 043507 (2004).
[37] S. Kanno, J. Soda, and M. a. Watanabe, J. Cosmol. Astropart. Phys. 12 (2009) 009.
[38] V. Demozzi, V. Mukhanov, and H. Rubinstein, J. Cosmol. Astropart. Phys. 08 (2009) 025.
[39] T. Fujita and S. Mukohyama, J. Cosmol. Astropart. Phys. 10 (2012) 034.
[40] S. Mukohyama, Phys. Rev. D **94**, 121302 (2016).
[41] L. Heisenberg, J. Cosmol. Astropart. Phys. 10 (2018) 054.
[42] L. Heisenberg, arXiv:1807.01725.
[43] L. Amendola *et al.* (Euclid Theory Working Group), Living Rev. Relativity **16**, 6 (2013); L. Amendola *et al.*, Living Rev. Relativity **21**, 2 (2018); E. J. Copeland, M. Sami, and S. Tsujikawa, Int. J. Mod. Phys. D **15**, 1753 (2006); A. De Felice and S. Tsujikawa, Living Rev. Relativity **13**, 3 (2010); A. Joyce, B. Jain, J. Khoury, and M. Trodden, Phys. Rep. **568**, 1 (2015).
[44] L. Heisenberg, R. Kase, and S. Tsujikawa, Phys. Rev. D **98**, 024038 (2018).
[45] R. Kase and S. Tsujikawa, J. Cosmol. Astropart. Phys. 11 (2018) 024.
[46] L. Heisenberg, R. Kase, and S. Tsujikawa, Phys. Rev. D **98** 123504 (2018).
[47] C. de Rham, G. Gabadadze, L. Heisenberg, and D. Pirtskhalava, Phys. Rev. D **87**, 085017 (2013).
[48] K. Freese, J. A. Frieman, and A. V. Olinto, Phys. Rev. Lett. **65**, 3233 (1990); F. C. Adams, J. R. Bond, K. Freese, J. A. Frieman, and A. V. Olinto, Phys. Rev. D **47**, 426 (1993).
[49] R. Kallosh, A. Linde, and D. Roest, J. High Energy Phys. 11 (2013) 198; S. Ferrara, R. Kallosh, A. Linde, and M. Porrati, Phys. Rev. D **88**, 085038 (2013).
[50] A. De Felice, S. Tsujikawa, J. Elliston, and R. Tavakol, J. Cosmol. Astropart. Phys. 08 (2011) 021.
[51] J. Garcia-Bellido, R. Rabadan, and F. Zamora, J. High Energy Phys. 01 (2002) 036.
[52] G. R. Dvali, Q. Shafi, and S. Solganik, arXiv:hep-th/0105203.
[53] S. Kachru, R. Kallosh, A. D. Linde, J. M. Maldacena, L. P. McAllister, and S. P. Trivedi, J. Cosmol. Astropart. Phys. 10 (2003) 013.
[54] G. Obied, H. Ooguri, L. Spodyneiko, and C. Vafa, arXiv:1806.08362; P. Agrawal, G. Obied, P. J. Steinhardt, and C. Vafa, Phys. Lett. B **784**, 271 (2018); L. Heisenberg, M. Bartelmann, R. Brandenberger, and A. Refregier, Phys. Rev. D **98**, 123502 (2018); L. Heisenberg, M. Bartelmann, R. Brandenberger, and A. Refregier, arXiv:1809.00154.

Part III

Summary & Conclusions

Inflation elegantly solves the main problems of the standard cosmological model—the observed homogeneity, isotropy, and flatness of the Universe are simple outcomes of an early accelerated epoch. Furthermore, quantum fluctuations during this epoch are stretched by the expansion to classical scales, becoming the seeds for the structures. Yet, the canonical inflationary theory is becoming in worrisome tension with state-of-the-art cosmological observations. Assuming a single-field picture, *i.e.* a scalar field slowly rolling down its sufficiently flat potential, the simplest monomial potential functions and similar constructions are in the edge of being ruled out—indeed, they predict large tensor power, meanwhile upper bounds on the tensor-to-scalar ratio r have been significantly reduced by the latest *Plank* satellite's measurements. In general, models embedded in high-energy particle-physics theories are in better shape, and therefore seeking new inflationary scenarios within the framework of particle physics became a natural approach. However, given the lack of evidence of these theories, different approaches seem more appealing: on the one hand, modeling-independent realizations have the potential of unveiling allowed parameter regions for general classes of inflationary models. On the other hand, a different model-building approach consists on keeping the simplest potentials but at the cost of modifying the underlying theory of gravity. These two alternative approaches constituted the main subject of this thesis.

In canonical single-field scenarios, the equation of state w can be parametrized with only two phenomenological parameters, α and β, in addition to the number of remaining $e$folds of inflation, as discussed in Chapter §3. Also, w is related to the first slow-roll parameter ϵ_H. Consequently, it is possible to relate the tilts $n_{s,t}$ and the tensor-to-scalar ratio r to the parameters α and β. In other words, predictions on $n_{s,t}$ or r can be obtained by constraining the Mukhanov phenomenological parameters without making any reference to a specific potential function $V(\phi)$. Indeed, in §3.1 we showed that a lower bound on r can be predicted only by taking the current constraints on n_s on account of this parametrization, in the case that Nature has chosen canonical single-field inflation. Furthermore, in Ref. [1] we have explicitly shown that this parametrization is in agreement with a more familiar one based on a hierarchy of the slow-roll parameters as they both single out the same parameter space when they are fitted to CMB temperature and polarization data.

The dark energy issue points to the possibility that the laws of gravity, *i.e.* General Relativity, may need to be modified at large scales. This question brought up a large research area from which many theories of mod-

ified gravity have been proposed. Theories based on scalar fields, similar to inflation, led to the proposal of interesting couplings between a scalar field ϕ and the gravity sector. When studied for inflation, nonminimal couplings (expected indeed to be generated at some energy scale) are able to modify the predictions of a canonical potential $V(\phi)$. In particular, we showed in Ref. [2] that a coupling $\xi\phi^2 R$ is favored by present observations for small—$\mathcal{O}(10^{-3})$—and positive values of the coupling parameter ξ at the 2σ level, when a simple quadratic potential function, $m^2\phi^2$ is considered. Furthermore, in the presence of such a coupling, a nonzero value for the tensor-to-scalar ratio is also favored at the same confidence level.

These phenomenological outcomes obtained by simple nonminimal couplings of the inflaton field to the gravity sector lead to the search for phenomenological signatures derived from different types of terms allowed to be present in the theory. Keeping the symmetries and constraints of General Relativity (such as Lorentz invariance, unitarity and locality), along with the condition for second-order equations of motion (in order to avoid Ostrogradsky instabilities), only few combinations between self-derivative terms of ϕ and the gravity sector are allowed. This led to the constructions of general scalar-tensor theories of gravity, discussed in §4.1.1, and from which the Horndeski framework stands out. This framework has become a playground for the construction of well-behaved models of inflation from which G-inflation, discussed in §4.2.2, is the simplest nontrivial one. Its action differentiates from the canonical due to the addition of the self-derivative term $G_3\Box\phi$, which introduces new phenomenology for a given choice of the free function $G_3(\phi, X)$, irrespectively of the potential function $V(\phi)$. Therefore, it allows inflation to be driven by monomial potentials and still satisfy observational constraints. A basic G_3 function with constant mass scale, however, is not able to fit the latest *Planck* 2018 constraints due to their prediction of small scalar power relative to the tensor one as a consequence of a slow transition between the epoch when the mass scale is relevant to the canonical epoch. Furthermore, failure to complete the transition before the end of inflation leads to the appearance of instabilities during the reheating epoch. In Ref. [4] we showed that a sufficiently fast, step-like transition is able to reconcile the monomial potentials (special attention was taken for the simplest $m^2\phi^2$) with observations and, at the same time, to solve the pathological issues presented in this class of models. Interestingly, by assuming a scalar tilt of $n_s \simeq 0.966$, a lower bound on the tensor-to-scalar ratio of $r \gtrsim 5\times10^{-3}$ (*i.e.* potentially observable with next-generation satellites) is obtained for this transient model due to a nontrivial large running α_s originated by the sharp transition.

It is possible that vector fields were also present during the inflationary era. Regardless of their interaction with the inflaton field, they can affect

and modify the dynamics of the expansion. However, couplings between the inflaton and the vector field, on top of the gravitational background, are of special interest and can be tested against CMB observations. In this regard, a general framework of scalar-vector-tensor theories of gravity was recently developed in the same spirit as the scalar-tensor Horndeski theories. Indeed, in §4.1 we showed that any modification of general relativity will introduce new degrees of freedom which can be in the form of new scalar, vector or even tensor fields. The simplest nontrivial combination of a scalar field ϕ and a $U(1)$ vector A_μ, according to the scalar-vector-tensor framework, is given by $\beta_m A^\mu \partial_\mu \phi$. In Ref. [5] we studied the inflationary signatures of several potential functions in the presence of this coupling. At the background level, inflation is still driven by the scalar field, whereas the temporal component of the vector field, A_0, is nondynamical. As a consequence, a single-field description of the background dynamics (modulated by a parameter $\beta = 1 - const. \times \beta_m^2$) arises due to a nontrivial relation between A_0 and the scalar-field velocity $\dot{\phi}$. At the perturbations level, the longitudinal vector mode contributes to an isocurvature perturbation along with the standard inflaton fluctuation. This perturbation, however, is suppressed for a vector-field mass scale comparable to the Hubble parameter H, and, as a result, the power spectrum of the primordial curvature perturbation follows the same single-field description corrected by β. The spectral indices and the tensor-to-scalar ratio are further modified by the presence of β but, interestingly, the canonical consistency relation $r = -8n_t$ is left unmodified. While confronting these results with CMB data, we showed that small-field models of inflation are considerably affected by the presence of the vector coupling. In particular, we found that for α-attractors, $n_s \simeq 1 - 2/N$ and $r \simeq 12\alpha_c\beta/N^2$ for $\alpha_c < \mathcal{O}(10)$ (which includes Starobinsky inflation), *i.e.* there exists a suppression of the tensor-to-scalar ratio for a small β compared to the canonical models ($\beta = 1$). Similar results were obtained for Brane inflation with $p = 2$ and $p = 4$ indices. These results follow from the fact that a nonvanishing β increases $\dot{\phi}$ and, therefore, inflation needs to start from a flatter region of the potential, relevant for CMB scales, where a small value of the slow-roll parameter ϵ_H is maintained compared to the canonical cases.

The computation of the inflationary observables in noncanonical classes of inflation is, in general, far from being trivial. As discussed in §2.4.3, different methods can be used to solve the mode-function equation, from where the slow-roll approximation (SR) usually stands out as the one which leads to analytical results. However, for noncanonical models, the slow-roll conditions are sometimes too restrictive and the use of the slow-roll approximation is not always allowed. This comes from the fact that new noncanonical terms affect the background dynamics of the inflaton field

which usually depart from the standard smooth evolution. Furthermore, the slow-roll approximation is based on an assumed hierarchy of Hubble slow-roll parameters which, in turn, define a restrictive hierarchy of the primordial tilt and its running parameters (α_s, β_s, etc.), as it was discussed at the beginning of §5. To overcome these deficiencies, the generalized (GSR) and optimized (OSR) slow-roll approximations were developed and tested for several inflationary models with features in the potential. Additionally, these techniques were recently promoted to cover inflationary models belonging to the Horndeski and beyond Horndeski classes. Indeed, in Ref. [4] we showed that the predictions of the aforementioned transient G-inflation model can be accurately computed using these techniques. On the one hand, GSR provides accurate results at the $\sim 10\%$ level around the transition (of size $\Delta N \sim 3$) to the canonical epoch; OSR, on the other hand, provides analytical results accurate at the $\sim 20\%$ level. Both being compared with the standard SR approximation which deviates at the $\sim 50\%$ level. However, due to the properties of the model, it is worth mentioning that both GSR and OSR give predictions at the percent level at CMB scales, whereas SR still deviates at the $\sim 10\%$ level. We further showed that these results imply that the scalar power spectrum can still be described in its power-law form, around the relevant scales, as long as n_s and α_s are computed using OSR. This is due to the fact that α_s can be of the same order of n_s and thus the standard slow-roll hierarchy is not valid (in which case, OSR overcomes this wrong order-counting).

Indeed, a correct computation of the inflationary parameters is needed as further parameters, in particular the running of the running of the tilt, β_s, will play an important role to discern between inflationary models of inflation—this in addition to the possibility of a further unobservable amplitude of primordial gravitational waves—, as we showed in Ref. [3]. In this work, a forecast for the CORE mission was carried out and confronted to the most favored models of inflation. We showed that there exists the possibility that the running α_s will not be as important as its own running β_s, as the latter may have the power to exclude all the models studied in the case that the best-fit value of *Planck*, $\beta_s \simeq 0.01$, prevails future observations.

To conclude, in this thesis we have developed a comprehensive novel exploration and a detailed study of the inflationary paradigm using different nonstandard approaches. Firstly, we covered model-independent parametrizations to clarify the allowed parameter space of canonical single-field inflation. Secondly, we demonstrated the potential of nonstandard inflationary parameters, the running of the running of the primordial tilt in particular, which may have the potential of ruling out the vast majority of the currently favored inflationary models. And, finally, we explored the possibility that the inflaton field coupled differently as in the canonical version by in-

troducing self-derivative terms belonging to general scalar-tensor theories; or the possibility that a gauge vector field, coupled to the inflaton, affected the dynamics in an observable way.

Future satellites, interferometers and different ground-based experiments will further guide us towards unveiling the true nature of the early universe. And, whether Nature chose a canonical model embedded in a more fundamental quantum field theory or nontrivial gravitational dynamics, model-building approaches along with a correct understanding of the observational parameters will keep helping in showing us the correct theoretical path.

Part IV

Resumen de la Tesis

1 Inflación cosmológica

1.1 El Modelo Cosmológico Estándar

El Universo a gran escala es un sistema físico que está en constante evolución. Su estudio se basa en el Modelo Cosmológico Estándar (MCS), es decir, en la teoría del *Big Bang* y en las leyes de la Relatividad General. La primera se sustenta en varias observaciones realizadas a lo largo del siglo pasado, y durante el transcurso del presente, sobre la expansión del Universo. En 1929, Edwin Hubble observó que las galaxias se alejaban unas de otras a una velocidad proporcional a la distancia que les separa (Ley de Hubble), lo que implicaba que el Universo se expandía. En 1998, dos grupos astronómicos dedicados a la observación de supernovas del tipo Ia dedujeron que las galaxias más distantes no solo se alejaban unas de otras, sino que lo hacían de forma acelerada, contrario a lo esperado debido a la naturaleza atractiva de la gravedad.

Es intuitivo pensar que en un universo en expansión, toda la materia y energía se encontraban más próximas entre sí en el pasado, a tal punto que en un instante del pasado muy lejano, todo el contenido energético se encontró agrupado en un punto infinitesimal del espacio de densidad infinita denominado *big bang*. La Relatividad General, que describe el movimiento de los planetas, galaxias y el Universo en su totalidad, a través de una reformulación geométrica de la gravedad, deja de ser válida cuando la expansión se extrapola hacia atrás en el tiempo a los instantes del big bang, y una teoría fundamental de la gravedad, que incluya las leyes de la mecánica cuántica, debe remplazarla. Como no conocemos los principios de dicha teoría, el MCS asume ciertas condiciones iniciales, las cuales determinan la subsecuente expansión.

El Universo se comenzó a expander instantes después del big bang, enfriándose y atravesando por varios procesos termodinámicos durante los, aproximadamente, 14 mil millones de años siguientes (equivalentes a la edad del Universo). Durante cada uno de estos procesos, la materia y la energía contenida en el Universo pasó por diferentes fases, cada una de las cuales dejó huellas en las diferentes observaciones cosmológicas que directa o indirectamente se llevan a cabo actualmente, ayudándonos de esta forma a poder explicar de manera detallada la historia del Universo. Particular-

mente relevante para el objeto de estudio de esta tesis, uno de los fenómenos cosmológicos más importantes es la *radiación de fondo de microondas* (CMB, por sus siglas en inglés). Esta es una tenue radiación que llena el universo observable y que, por lo tanto, recibimos de todas direcciones. Su origen se remonta a la época en la que el Universo estaba constituido por núcleos elementales, electrones y fotones, llamada *recombinación*. Cuando la temperatura se redujo aproximadamente por debajo de los 13 eV,[1] correspondientes a la energía de separación del átomo de hidrógeno, los electrones se combinaron con los núcleos atómicos formando átomos neutros, dando lugar a la libre propagación de los fotones a través del Universo, formando el CMB. Por consiguiente, el estudio del CMB nos proporciona las condiciones del Universo en un momento tan lejano en el pasado como lo es la época de la recombinación.

Otra de las observaciones principales del universo actual, y que está sustentada en el CMB, es la isotropía del Universo. A gran escala, la materia se distribuye de tal manera que es indistinguible independientemente del lugar y la dirección en que se mire (como se ejemplifica en la figura 1.4, sección 1.1.6, correspondiente a una simulación por ordenador asumiendo el MCS, donde la escala sobre ella es equivalente a aproximadamente 23 mil trillones de kilómetros). Estas características se encuentran presentes también en la distribución energética del CMB, por lo que se deduce que el *universo primitivo* (como llamaremos a los primeros instantes después del big bang) era también altamente homogéneo e isotrópico. En el MCS no hay ningún mecanismo que conduzca al Universo a este estado, por lo que dichas características se asumen como condiciones iniciales.

Sin embargo, esta isotropía no es perfecta, hay pequeñas variaciones que a escalas ordinarias están dadas por la existencia de sistemas solares y galaxias aleatoriamente distribuidas. La formación de estas *estructuras* se llevó a cabo gracias a la presencia de perturbaciones en la distribución de la materia y energía a través del espacio durante el universo primitivo, y que también dieron lugar a la anisotropía observada en el CMB. Estas perturbaciones se suelen asumir y *poner a mano* en las ecuaciones, ya que el MCS no tiene mecanismo alguno que las cree.

Otra observación sobre la cantidad de materia y energía observable conlleva a estimar la *curvatura* general del Universo. Como ya se mencionó, la Relatividad General es una teoría geométrica de la gravedad donde esta se comporta de una forma u otra dependiendo de la cantidad de materia y/o energía en una cierta región del espacio. Por ello, una vez conocida la cantidad de materia que existe en el Universo, se puede deducir la geometría del mismo. Las observaciones actuales predicen que el Universo es plano. Sin embargo, las mismas leyes dictan que esta geometría es altamente in-

[1] 1 eV=1.602×10^{-19} J.

estable, por lo que el universo primitivo debió haber sido plano a un grado de precisión sumamente inexplicable para tener la planicie actual.

Así, el MCS predice una gran cantidad de observaciones a través de una detallada descripción de varios procesos cosmológicos que dieron lugar al universo actual. Sin embargo, la falta de explicación de las condiciones iniciales que asume (el grado de homogeneidad, isotropía y planicie, así como la naturaleza de las perturbaciones iniciales) hacen del MCS un modelo incompleto. Cualquier teoría que proporcione una explicación natural a estas condiciones iniciales conllevaría a un mejor entendimiento de la historia del Universo. A dicha teoría se le conoce como *inflación cosmológica*.

1.2 El período inflacionario

La inflación cosmológica provee al MCS de un mecanismo en el cual las condiciones iniciales previamente asumidas encuentran una explicación natural, y que al mismo tiempo es capaz de producir las perturbaciones iniciales una vez que las leyes de la mecánica cuántica son tomadas en cuenta.[2] Independientemente del mecanismo, la inflación consiste en una etapa de aceleración del Universo durante el universo primitivo, instantes después del comienzo. Durante esta etapa, el Universo debió haberse expandido en un factor de 10^{24} para lograr reproducir las observaciones actuales, como lo es el grado de isotropía observado en el CMB.

El mecanismo inflacionario fue propuesto por Alan Guth en 1981. Guth demostró que un período de expansión acelerada durante el universo primitivo era capaz de resolver el problema de las condiciones iniciales del MCS, aunque luego se comprobó que el modelo utilizado por él no podría funcionar realmente. Sin embargo, poco después se introdujo un nuevo mecanismo en el cual un campo escalar cuántico, sujeto al movimiento sobre un potencial suficientemente *plano* (es decir, casi invariante), evolucionaba a un ritmo lento comparado con la expansión misma del Universo. Este campo, llamado *inflatón*, transportaría todo el contenido energético del Universo hasta llegar al punto mínimo del potencial donde se desintegraría en las partículas fundamentales conocidas, dando así lugar al big bang. Dicho mecanismo ha prevalecido hasta el día de hoy y se conoce como inflación del tipo *slow-roll* ('rodamiento lento' en español).

Además, en el espacio vacío se producen fluctuaciones cuánticas, creación y subsecuente aniquilación de pares de partícula-antipartícula, como consecuencia del *principio de incertidumbre de Heisenberg*, uno de los principios fundamentales de la mecánica cuántica. En un espacio en expansión acel-

[2]No obstante, la inflacionaria no es una teoría cuántica fundamental de la gravedad, sino una teoría en la que los dos regímenes (el cuántico y el gravitatorio) son igualmente aplicables.

erada, como el inflacionario, la aniquilación de los pares creados en el vacío no se llega a producir ya que el espacio mismo entre el par crece exponencialmente, separando las partículas a una distancia lo suficientemente grande como para ya no poder interaccionar y, por lo mismo, aniquilarse. Estas fluctuaciones suceden a lo largo de todo el Universo y son las que se convierten en las perturbaciones iniciales descritas en el MCS cuando la expansión las extiende a escalas cosmológicas. A su vez, estas perturbaciones se convirtieron en diferencias de densidad de materia y energía a lo largo del espacio que, después de 14 mil millones de años, formaron las estructuras que conforman el universo actual: galaxias, sistemas solares, *nosotros*.

Es así como la teoría inflacionaria no solo resuelve el problema de las condiciones iniciales, sino que también se presenta como la teoría de las fluctuaciones cuánticas primordiales. Sin embargo, el hecho de que hubiera un período de inflación, así como el modelo elegido por la naturaleza, es desconocido. Diferentes tipos de potenciales inflacionarios de slow-roll (cada uno perteneciente a un modelo distinto) dan lugar a ligeras diferencias en las predicciones observacionales, algunas con una mejor concordancia que otras al momento de probarlas con las restricciones experimentales actuales. Una gran variedad de modelos inflacionarios se han propuesto, varios de los cuales se han comprobado falsos dada la cada vez mejor precisión de los datos cosmológicos. Lamentablemente, los modelos más simples (matemáticamente hablando) están muy cerca de ser descartados. Por esta razón, el campo de investigación relacionado con la inflación cosmológica está altamente activo en lo que respecta a la construcción de nuevos modelos de un modo más complejo que el de simplemente modificar el potencial inflacionario.

Efectivamente, una modificación del potencial inflacionario que conlleve a mejores predicciones a costa de complicarlo matemáticamente parece poco natural. En esta tesis se opta por una estrategia alternativa: se asumen los potenciales inflacionarios más simples pero se modifican ligeramente las leyes de la gravedad. Esta estrategia no es nueva, ya que ha sido utilizada para estudiar otros problemas cosmológicos que sugieren que la teoría de la Relatividad General debería ser ciertamente modificada, al menos a escalas cosmológicas (a escalas del sistema solar, en cambio, la Relatividad General describe con alta precisión los fenómenos observables). En el período inflacionario, modificaciones de las leyes de la gravedad dan lugar a distintas predicciones observacionales para el mismo potencial inflacionario, haciéndolas potencialmente mejores cuando se comparan con las mediciones cosmológicas.

Finalmente, la tesis se complementa con un estudio fenomenológico de los parámetros inflacionarios que es independiente del modelo inflacionario que se escoja, así como también con un estudio de parámetros inflacionarios,

distintos de los utilizados típicamente, que podrían ayudar enormemente a identificar el modelo más probable de inflación, dadas las mediciones actuales y futuras.

2 Objetivos

El objetivo general de esta tesis es el estudio del período inflacionario de una manera no estándar. Por un lado, se estudian aproximaciones fenomenológicas a la inflación. Usualmente para estudiar este período se parte de un potencial inflacionario a partir del cual se construyen las ecuaciones de movimiento del inflatón. En esta tesis, en cambio, se parte de parametrizaciones alternativas motivadas por la fenomenología de una ecuación de estado del universo en expansión propuesta en años recientes. Dicha parametrización involucra parámetros libres que son acotados usando los datos observacionales actuales.

Asimismo, se realiza un estudio de los parámetros inflacionarios alternativos a los estándares que pudieran ser importantes para discernir entre los modelos inflacionarios más populares. Actualmente, las pruebas más importantes del período inflacionario involucran el estudio de dos parámetros: la razón entre las amplitudes de los espectros de potencias de las perturbaciones escalares y tensoriales, r, y la razón del cambio en el espectro de potencias escalar con respecto a la escala, n_s. Sin embargo, observaciones actuales y futuras no pueden discernir entre modelos usando solo estos dos parámetros. Por ello, se estudia la importancia de varios parámetros que no suelen tomarse en cuenta, y se discute su relevancia actual y en futuros experimentos como lo es el futuro satélite CORE.

Por otro lado, se estudian modelos de inflación no estándares. Usualmente se asume que el inflatón interacciona con la gravedad de forma *mínima* (o, equivalentemente, que el inflatón se encuentra *mínimamente acoplado*). En realidad, esta 'simplicidad' no es necesaria y, además, se ha demostrado que para ciertos potenciales inflacionarios con interacciones más complejas conllevan a mejores resultados. En esta tesis se estudia un modelo en el que el inflatón está *no mínimamente acoplado* a la gravedad a través de un parámetro adicional. En el estudio se ha acotado este parámetro usando los datos cosmológicos actuales y, también, se realiza una comparación estadística entre los modelos *mínimamente* y *no mínimamente acoplados*, encontrando el segundo caso como el más favorecido.

Finalmente, también se estudian modelos no estándares que requieren de una modificación aún más trascendental de la Relatividad General, pertenecientes al marco de teorías generales escalar-tensor llamada *Horndeski*.[3] Di-

[3]En honor a Gregory Horndeski, quien en 1974 fue el primero en estudiar estas teorías.

chos modelos resuelven varios problemas que presentaban los modelos no estándares propuestos anteriormente y también conllevan a predicciones de los parámetros inflacionarios que se encuentran en mejor concordancia con los datos observacionales actuales. Se estudian además modelos pertenecientes a un nuevo marco del tipo escalar-vector-tensor en donde existe un campo vectorial acoplado al inflatón capaz de afectar la expansión del Universo, analizando las consecuencias de esta interacción sobre las predicciones cosmológicas.

3 Metodología

El trabajo de investigación relativo al estudio del universo primitivo requiere tanto de técnicas analíticas de estadística y cálculo matemático como también de técnicas numéricas. Para ello se han empleado las herramientas y técnicas de cálculo y de computación aprendidas durante los estudios de grado y máster.

En particular, desde la perspectiva teórica de esta tesis, que requiere un entendimiento adecuado del Modelo Cosmológico Estándar (y por lo tanto de la Relatividad General), se han empleado métodos de resolución de ecuaciones diferenciales lineales y de grados superiores, técnicas numéricas de integración, funciones de Green, expansiones en series numéricas, entre otras. Estas técnicas son necesarias para calcular y resolver las ecuaciones de movimiento clásicas y de perturbaciones en un modelo inflacionario específico, así como también para calcular los parámetros inflacionarios. La mayor parte de estos cálculos se realizan o comprueban con ayuda de software para cálculo matemático.

Por otro lado, la perspectiva fenomenológica de la tesis requiere de estudio y procesado de datos experimentales, provenientes de mediciones cosmológicas, que se utilizan para contrastar los modelos teóricos con las observaciones. Para ello son necesarias herramientas de probabilidad y estadística para la realización de diferentes análisis, como lo son la prueba de hipótesis χ^2, el teorema de Bayes, la *información de Fisher* o técnicas de Monte Carlo, por mencionar algunas.

4 Estructura de la tesis

La tesis está dividida en tres partes. La primera, conteniendo cinco capítulos, consiste en una introducción al trabajo de investigación llevado a cabo durante el doctorado: el Capítulo 1 ofrece una corta introducción al Modelo Cosmológico Estándar, prestando especial atención a las épocas relevantes para el estudio del período inflacionario (tal como lo es la época que

da origen a la radiación de fondo de microondas), así como también a los problemas principales que dan lugar a la propuesta de la inflación cosmológica. En el Capítulo 2 se ofrece un resumen exhaustivo de la dinámica de la inflación cosmológica del tipo slow-roll estándar donde se muestra que una expansión acelerada del Universo resuelve los problemas del MCS y cómo un campo cuántico escalar satisface los requerimientos de dicha expansión. También se explica la teoría de las fluctuaciones cuánticas primordiales, las ecuaciones de movimiento de estas, su evolución y las señales que dejan en las observaciones actuales. En el Capítulo 3 se discute la parametrización de Mukhanov, una aproximación independiente de modelos para estudiar el espacio de parámetros permitido de la teoría inflacionaria estándar. Por otro lado, la aproximación de modificaciones de gravedad se estudia en el Capítulo 4. Primero, discutimos la construcción de las teorías más generales de gravedad de los tipos scalar-tensor y scalar-vector-tensor que dan lugar a ecuaciones de movimiento de segundo orden; luego, se discuten los principales modelos inflacionarios construidos a partir de estas teorías. Finalmente, en el Capítulo 5, demostramos las capacidades de técnicas *más allá de slow-roll* para calcular los parámetros inflacionarios en modelos inflacionarios estándares y no estándares. Completamos esta primera parte con un apéndice detallado sobre la Teoría de Perturbaciones Cosmológicas, seguido de un segundo apéndice que contiene ecuaciones útiles para los capítulos principales.

En la Parte II se muestran los artículos de investigación publicados en revistas *peer-reviewed*. Allí, el lector encontrará los resultados principales obtenidos a lo largo del doctorado. En la Parte III se resumen estos resultados y se concluye.

5 Resultados y Conclusiones

La inflación cosmológica resuelve de una manera elegante los problemas principales del MCS: la homogeneidad, isotropía y planicie del Universo son simples resultados de una época de aceleración temprana. Más aún, fluctuaciones cuánticas durante esta época son expandidas a escalas clásicas por la expansión, transformándose en las perturbaciones iniciales que dan lugar a las estructuras cosmológicas. Sin embargo, la teoría inflacionaria estándar está en peligro de ser descartada por los datos experimentales. Es por esto que nuevos métodos para estudiar la teoría deben ser considerados: por un lado, aproximaciones independientes de modelos específicos tienen el potencial de descifrar el espacio de parámetros permitido según las mediciones cosmológicas. Por otro lado, la construcción de modelos inflacionarios puede realizarse manteniendo los potenciales inflacionarios más simples pero a costa de modificar las leyes de la gravedad. Estas dos aprox-

imaciones alternativas constituyeron el objeto de estudio principal de esta tesis.

En modelos de inflación estándares, la ecuación de estado puede ser parametrizada con solo dos parámetros fenomenológicos, con los que equivalentemente se pueden escribir relaciones analíticas para los parámetros inflacionarios. De esta forma, se puede obtener un espacio de parámetros inflacionarios permitido acotando los parámetros fenomenológicos con las mediciones experimentales. En [1] mostramos explícitamente que esta parametrización está en concordancia con parametrizaciones más familiares, y que cubren el mismo espacio de parámetros permitido, cuando son confrontadas con datos del CMB.

Existe la posibilidad de que las leyes de la gravedad, descritas por la Relatividad General, necesiten ser modificadas. Esta posibilidad trae consigo un amplio campo de investigación a partir del cual muchas teorías de *gravedad modificada* has sido propuestas. Teorías basadas en campos escalares como el inflatón conllevan al estudio de interesantes tipos de acoplamientos entre el campo escalar y el sector gravitatorio. Cuando estos acoplamientos se aplican para la inflación cosmológica, acoplamientos *no mínimos* pueden modificar las predicciones de potenciales inflacionarios estándares. En este aspecto, en [2] se demostró que un acoplamiento *no mínimo* específico entre el inflatón y la gravedad es favorecido por las mediciones observacionales cuando se mantiene un potencial inflacionario simple que, de otra forma, estaría descartado.

Estos resultados fenomenológicos obtenidos a partir de simples acoplamientos entre el inflatón y el sector gravitatorio conllevaron a la búsqueda de nuevos resultados provenientes de términos diferentes y más complejos permitidos en la teoría. Manteniendo las simetrías y restricciones de la Relatividad General (como lo es la invariancia Lorentz, la unitariedad y localidad), así como la restricción de obtener una teoría que conlleve a ecuaciones de movimiento de segundo orden (para evitar inestabilidades), solo unas pocas combinaciones entre el inflatón y el sector gravitatorio son permitidas. Esto en su momento conllevó a la construcción de teorías gravitatorias generales del tipo escalar-tensor. El marco teórico de Horndeski, representa un punto de partida para la construcción de atractivos modelos inflacionarios, de los cuales *G-inflation* es el más sencillo. En este modelo, un término *autoderivativo* del inflaton es introducido que, al igual que en el caso de acoplamientos *no mínimos*, permite modificar las predicciones observacionales para un potencial inflacionario específico. Sin embargo, el modelo de *G-inflation* original estaba también en tensión con respecto a los datos actuales por lo que, en [4], se propuso una modificación de este modelo con la que se mejoran las predicciones inflacionarias y se resuelven los problemas de inestabilidades que el modelo original presentaba.

Es posible también que campos cuánticos vectoriales hayan estado presentes durante el período inflacionario. Independientemente de su interacción con el inflatón, estos campos pueden afectar y modificar la expansión del Universo. De cualquier manera, acoplamientos entre el inflatón y el campo vectorial, sobre el campo gravitatorio, son de especial interés y pueden ser acotados de igual forma con mediciones del CMB. En este respecto, un marco de teorías generales de gravedad del tipo escalar-vector-tensor fue construido recientemente. En [5] se estudiaron las predicciones observacionales del acoplamiento más sencillo proveniente de este marco de teorías. Se demostró que, aunque la inflación cosmológica es llevada a cabo por el campo escalar como en el caso estándar, la presencia del campo vectorial produce una disminución en el factor de expansión del Universo. Con base en estos resultados, se demostró que en ciertos modelos se pueden obtener mejores predicciones con respecto a los datos experimentales dependiendo de la intensidad del acoplamiento entre el inflatón y el campo vectorial.

Por otro lado, el cálculo de los parámetros inflacionarios en modelos no estándares como los descritos anteriormente es lejos de ser sencillo, en general. Existen diferentes métodos para resolver la ecuación de movimiento de las perturbaciones primordiales, como la aproximación *slow-roll* que provee soluciones analíticas para los parámetros inflacionarios. Sin embargo, en modelos inflacionarios no estándares, esta aproximación no es siempre válida. Para tratar estos modelos, nuevas técnicas han sido desarrolladas, entre las cuales las técnicas *slow-roll generalizado* (GSR, por sus siglas en inglés) y *slow-roll optimizado* (OSR) han sido probadas satisfactoriamente. Recientemente, estas técnicas fueron extendidas para modelos provenientes de marcos teóricos del tipo Horndeski y, en [4], se demostró que las predicciones obtenidas para el modelo del tipo *G-inflation* propuesto podían ser calculadas con estas técnicas y con una alta precisión. Por ejemplo, en casos en los que la aproximación *slow-roll* tiene una precisión del 90% (no lo suficientemente alta para las precisiones requeridas en Cosmología), GSR provee de resultados con una precisión de más del 99% con un bajo coste computacional.

Finalmente, en [3] se demostró la importancia de parámetros inflacionarios diferentes de los típicos para discernir entre modelos inflacionarios con futuras mediciones experimentales como lo serían aquellas dadas por futuros satélites como CORE.

Para concluir, en esta tesis se desarrolló una exhaustiva exploración y un estudio detallado de la teoría de la inflación cosmológica usando diferentes aproximaciones no estándares. Primero, cubrimos parametrizaciones independientes de modelos específicos. Luego, se demostró el potencial de parámetros diferentes de los típicos para discernir entre modelos inflacionar-

ios. Finalmente, se exploró la posibilidad de que el inflatón se haya acoplado de una manera no estándar al sector gravitatorio o a campos vectoriales presentes durante el período inflacionario y que pueden afectar la expansión del Universo.

Part V

Bibliography

[1] L. Boubekeur, E. Giusarma, O. Mena and H. Ramírez, *Phenomenological approaches of inflation and their equivalence*, *Phys. Rev.* **D91** (2015) 083006, [1411.7237]. Cited on page v, 50, 167, and 182.

[2] L. Boubekeur, E. Giusarma, O. Mena and H. Ramírez, *Do current data prefer a nonminimally coupled inflaton?*, *Phys. Rev.* **D91** (2015) 103004, [1502.05193]. Cited on page v, 35, 65, 168, and 182.

[3] M. Escudero, H. Ramírez, L. Boubekeur, E. Giusarma and O. Mena, *The present and future of the most favoured inflationary models after Planck 2015*, *JCAP* **1602** (2016) 020, [1509.05419]. Cited on page v, 45, 170, and 183.

[4] H. Ramírez, S. Passaglia, H. Motohashi, W. Hu and O. Mena, *Reconciling tensor and scalar observables in G-inflation*, *JCAP* **1804** (2018) 039, [1802.04290]. Cited on page v, 36, 68, 69, 79, 168, 170, 182, and 183.

[5] L. Heisenberg, H. Ramírez and S. Tsujikawa, *Inflation with mixed helicities and its observational imprint on CMB*, *Phys. Rev.* **D99** (2019) 023505, [1812.03340]. Cited on page v, 63, 69, 72, 169, and 183.

[6] S. Gariazzo, O. Mena, H. Ramírez and L. Boubekeur, *Primordial power spectrum features in phenomenological descriptions of inflation*, *Phys. Dark Univ.* **17** (2017) 38–45, [1606.00842]. Cited on page vi, and 51.

[7] S. Gariazzo, O. Mena, V. Miralles, H. Ramírez and L. Boubekeur, *Running of featureful primordial power spectra*, *Phys. Rev.* **D95** (2017) 123534, [1701.08977]. Cited on page vi.

[8] E. Hubble, *A relation between distance and radial velocity among extra-galactic nebulae*, *Proceedings of the National Academy of Sciences* **15** (1929) 168–173. Cited on page 3, and 4.

[9] P. Ferreira, *The Perfect Theory: A Century of Geniuses and the Battle over General Relativity*. Little, Brown, 2014. Cited on page 3.

[10] Supernova Search Team collaboration, A. G. Riess et al., *Observational evidence from supernovae for an accelerating universe and a cosmological constant*, *Astron. J.* **116** (1998) 1009–1038, [astro-ph/9805201]. Cited on page 4.

[11] Supernova Cosmology Project collaboration, S. Perlmutter et al., *Measurements of Omega and Lambda from 42 high redshift supernovae*, *Astrophys. J.* **517** (1999) 565–586, [astro-ph/9812133]. Cited on page 4.

[12] S. Dodelson, *Modern Cosmology*. Academic Press, Amsterdam, 2003. Cited on page 4, 5, 10, and 12.

[13] L. Amendola and S. Tsujikawa, *Dark Energy*. Cambridge University Press, 2015. Cited on page 4, 54, and 57.

[14] E. W. Kolb and M. S. Turner, *The Early Universe*, *Front. Phys.* **69** (1990) 1–547. Cited on page 5, 7, 31, and 32.

[15] V. Mukhanov, *Physical Foundations of Cosmology*. Cambridge University Press, Oxford, 2005. Cited on page 5, 12, 31, 38, 40, 81, and 84.

[16] S. Weinberg, *Cosmology*. Oxford, UK: Oxford Univ. Pr. (2008) 593 p, 2008. Cited on page 5, 12, 32, and 84.

[17] V. A. Rubakov and D. S. Gorbunov, *Introduction to the Theory of the Early Universe*. World Scientific, Singapore, 2017, 10.1142/10447. Cited on page 5, 6, 7, 10, 12, 31, and 35.

[18] S. Weinberg, *The Quantum theory of fields. Vol. 1: Foundations*. Cambridge University Press, 2005. Cited on page 6.

[19] S. Weinberg, *The quantum theory of fields. Vol. 2: Modern applications*. Cambridge University Press, 2013. Cited on page 6.

[20] Particle Data Group collaboration, C. Patrignani et al., *Review of Particle Physics*, *Chin. Phys.* **C40** (2016) 100001. Cited on page 6, and 8.

[21] D. A. Kirzhnits and A. D. Linde, *Macroscopic Consequences of the Weinberg Model*, *Phys. Lett.* **42B** (1972) 471–474. Cited on page 6.

[22] L. Dolan and R. Jackiw, *Symmetry Behavior at Finite Temperature*, *Phys. Rev.* **D9** (1974) 3320–3341. Cited on page 6.

[23] S. Weinberg, *Gauge and Global Symmetries at High Temperature*, *Phys. Rev.* **D9** (1974) 3357–3378. Cited on page 6.

[24] H. Georgi, *Unity of all elementary-particle forces*, *Physical Review Letters* **32** (1974) 438–441. Cited on page 6.

[25] F. Englert and R. Brout, *Broken Symmetry and the Mass of Gauge Vector Mesons*, *Phys. Rev. Lett.* **13** (1964) 321–323. Cited on page 7.

[26] P. W. Higgs, *Broken Symmetries and the Masses of Gauge Bosons*, *Phys. Rev. Lett.* **13** (1964) 508–509. Cited on page 7.

[27] H. Fritzsch, M. Gell-Mann and H. Leutwyler, *Advantages of the Color Octet Gluon Picture*, *Phys. Lett.* **47B** (1973) 365–368. Cited on page 7.

[28] C. Quigg, *Gauge Theories Of The Strong, Weak And Electromagnetic Interactions*, *Front. Phys.* **56** (1983) 1–334. Cited on page 7.

[29] A. Pich, *Aspects of quantum chromodynamics*, in *Proceedings, Summer School in Particle Physics: Trieste, Italy, June 21-July 9, 1999*, pp. 53–102, 1999. hep-ph/0001118. Cited on page 7.

[30] D. J. Gross and F. Wilczek, *Ultraviolet Behavior of Nonabelian Gauge Theories*, *Phys. Rev. Lett.* **30** (1973) 1343–1346. Cited on page 7.

[31] H. D. Politzer, *Reliable Perturbative Results for Strong Interactions?*, *Phys. Rev. Lett.* **30** (1973) 1346–1349. Cited on page 7.

[32] J. Lesgourgues and S. Pastor, *Massive neutrinos and cosmology*, *Phys. Rept.* **429** (2006) 307–379, [astro-ph/0603494]. Cited on page 7.

[33] S. Betts, W. R. Blanchard, R. H. Carnevale, C. Chang, C. Chen, S. Chidzik et al., *Development of a relic neutrino detection experiment at ptolemy: Princeton tritium observatory for light, early-universe, massive-neutrino yield*, 1307.4738. Cited on page 7.

[34] S. Bashinsky and U. Seljak, *Signatures of relativistic neutrinos in cmb anisotropy and matter clustering*, *Phys.Rev.D* **69** (2004) 083002, [astro-ph/0310198]. Cited on page 7.

[35] B. Follin, L. Knox, M. Millea and Z. Pan, *A first detection of the acoustic oscillation phase shift expected from the cosmic neutrino background*, *Phys. Rev. Lett.* **115** (2015) 091301, [1503.07863]. Cited on page 7.

[36] D. Baumann, F. Beutler, R. Flauger, D. Green, A. Slosar, M. Vargas-Magaña et al., *First constraint on the neutrino-induced phase shift in the spectrum of baryon acoustic oscillations*, *Nature Physics* (Feb, 2019) . Cited on page 7.

[37] R. A. Alpher, H. Bethe and G. Gamow, *The origin of chemical elements*, *Phys. Rev.* **73** (1948) 803–804. Cited on page 8.

[38] R. V. Wagoner, W. A. Fowler and F. Hoyle, *On the Synthesis of elements at very high temperatures*, *Astrophys. J.* **148** (1967) 3–49. Cited on page 8.

[39] B. D. Fields, *The primordial lithium problem*, *Ann. Rev. Nucl. Part. Sci.* **61** (2011) 47–68, [1203.3551]. Cited on page 8.

[40] R. H. Cyburt, B. D. Fields, K. A. Olive and T.-H. Yeh, *Big Bang Nucleosynthesis: 2015*, *Rev. Mod. Phys.* **88** (2016) 015004, [1505.01076]. Cited on page 8.

[41] P. J. E. Peebles, *Recombination of the Primeval Plasma*, *Astrophys. J.* **153** (1968) 1. Cited on page 8.

[42] Ya. B. Zeldovich, V. G. Kurt and R. A. Sunyaev, *Recombination of hydrogen in the hot model of the universe*, *Sov. Phys. JETP* **28** (1969) 146. Cited on page 8.

[43] D. J. Fixsen, E. S. Cheng, J. M. Gales, J. C. Mather, R. A. Shafer and E. L. Wright, *The Cosmic Microwave Background spectrum from the full COBE FIRAS data set*, *Astrophys. J.* **473** (1996) 576, [astro-ph/9605054]. Cited on page 8.

[44] D. J. Fixsen, *The Temperature of the Cosmic Microwave Background*, *Astrophys. J.* **707** (2009) 916–920, [0911.1955]. Cited on page 8.

[45] A. A. Penzias and R. W. Wilson, *A Measurement of excess antenna temperature at 4080-Mc/s*, *Astrophys. J.* **142** (1965) 419–421. Cited on page 8.

[46] R. H. Dicke, P. J. E. Peebles, P. G. Roll and D. T. Wilkinson, *Cosmic Black-Body Radiation*, *Astrophys. J.* **142** (1965) 414–419. Cited on page 9.

[47] Planck collaboration, N. Aghanim et al., *Planck 2018 results. VI. Cosmological parameters*, 1807.06209. Cited on page 9, 13, and 14.

[48] M. J. Rees, *Polarization and spectrum of the primeval radiation in an anisotropic universe*, *The Astrophysical Journal* **153** (Jul, 1968) L1. Cited on page 10.

[49] J. Negroponte, *Polarization of the primeval radiation in an anisotropic universe*, *Physical Review Letters* **44** (1980) 1433–1437. Cited on page 10.

[50] J. R. Bond and G. Efstathiou, *Cosmic background radiation anisotropies in universes dominated by nonbaryonic dark matter*, *The Astrophysical Journal* **285** (Oct, 1984) L45. Cited on page 10.

[51] S. Weinberg, *Gravitation and Cosmology*. John Wiley and Sons, New York, 1972. Cited on page 10.

[52] M. Kamionkowski, A. Kosowsky and A. Stebbins, *A Probe of primordial gravity waves and vorticity*, *Phys. Rev. Lett.* **78** (1997) 2058–2061, [astro-ph/9609132]. Cited on page 11.

[53] U. Seljak and M. Zaldarriaga, *Signature of gravity waves in polarization of the microwave background*, *Phys. Rev. Lett.* **78** (1997) 2054–2057, [astro-ph/9609169]. Cited on page 11.

[54] POLARBEAR collaboration, P. A. R. Ade et al., *A Measurement of the Cosmic Microwave Background B-Mode Polarization Power Spectrum at Sub-Degree Scales from 2 years of POLARBEAR Data*, *Astrophys. J.* **848** (2017) 121, [1705.02907]. Cited on page 11.

[55] D. S. Gorbunov and V. A. Rubakov, *Introduction to the theory of the early universe: Cosmological perturbations and inflationary theory*. 2011, 10.1142/7874. Cited on page 11, 32, 33, and 87.

[56] G. Bertone, D. Hooper and J. Silk, *Particle dark matter: Evidence, candidates and constraints*, *Phys.Rept.* **405** (2005) 279–390, [hep-ph/0404175]. Cited on page 11.

[57] L. Bergström, *Dark matter evidence, particle physics candidates and detection methods*, 1205.4882. Cited on page 11.

[58] A. Kusenko and L. J. Rosenberg, *Snowmass-2013 cosmic frontier 3 (cf3) working group summary: Non-wimp dark matter*, 1310.8642. Cited on page 11.

[59] V. Springel et al., *Simulating the joint evolution of quasars, galaxies and their large-scale distribution*, *Nature* **435** (2005) 629–636, [astro-ph/0504097]. Cited on page 12.

[60] D. Baumann, *Inflation*, in *Physics of the large and the small, TASI 09, proceedings of the Theoretical Advanced Study Institute in Elementary Particle Physics, Boulder, Colorado, USA, 1-26 June 2009*, pp. 523–686, 2011. 0907.5424. DOI. Cited on page 12, 19, 38, 81, and 87.

[61] D. Baumann, *Primordial Cosmology*, *PoS* **TASI2017** (2018) 009, [1807.03098]. Cited on page 12.

[62] P. J. E. Peebles, *Principles of physical cosmology*. Princeton, USA: Univ. Pr. (1993) 718 p, 1994. Cited on page 14.

[63] Ã. Aubourg et al., *Cosmological implications of baryon acoustic oscillation measurements*, *Phys. Rev.* **D92** (2015) 123516, [1411.1074]. Cited on page 14.

[64] Planck collaboration, P. A. R. Ade et al., *Planck 2015 results. XIII. Cosmological parameters*, *Astron. Astrophys.* **594** (2016) A13, [1502.01589]. Cited on page 14.

[65] A. H. Guth, *The Inflationary Universe: A Possible Solution to the Horizon and Flatness Problems*, *Phys. Rev.* **D23** (1981) 347–356. Cited on page 21.

[66] A. H. Guth and E. J. Weinberg, *Cosmological Consequences of a First Order Phase Transition in the SU(5) Grand Unified Model*, *Phys. Rev.* **D23** (1981) 876. Cited on page 22.

[67] G. P. Cook and K. T. Mahanthappa, *Supercooling in the SU(5) Phase Transitions and Magnetic Monopole Suppression*, *Phys. Rev.* **D23** (1981) 1321. Cited on page 22.

[68] J. D. Barrow and M. S. Turner, *Inflation in the Universe*, *Nature* **292** (1981) 35–38. Cited on page 22.

[69] A. Linde, *A new inflationary universe scenario: A possible solution of the horizon, flatness, homogeneity, isotropy and primordial monopole problems*, *Physics Letters B* **108** (1982) 389 – 393. Cited on page 22, and 33.

[70] A. Albrecht, *Cosmology for grand unified theories with radiatively induced symmetry breaking*, *Physical Review Letters* **48** (1982) 1220–1223. Cited on page 22, and 33.

[71] V. F. Mukhanov and G. V. Chibisov, *Quantum Fluctuations and a Nonsingular Universe*, *JETP Lett.* **33** (1981) 532–535. Cited on page 22.

[72] S. Hawking, *The development of irregularities in a single bubble inflationary universe*, *Physics Letters B* **115** (1982) 295 – 297. Cited on page 22.

[73] A. Starobinsky, *Dynamics of phase transition in the new inflationary universe scenario and generation of perturbations*, *Physics Letters B* **117** (1982) 175 – 178. Cited on page 22.

[74] A. H. Guth, *Fluctuations in the new inflationary universe*, *Physical Review Letters* **49** (1982) 1110–1113. Cited on page 22.

[75] J. M. Bardeen, *Spontaneous creation of almost scale-free density perturbations in an inflationary universe*, *Physical Review D* **28** (1983) 679–693. Cited on page 22.

[76] A. H. Guth, *The inflationary universe: The quest for a new theory of cosmic origins*. 1997. Cited on page 22.

[77] L. Kofman, A. D. Linde and A. A. Starobinsky, *Towards the theory of reheating after inflation*, *Phys. Rev.* **D56** (1997) 3258–3295, [hep-ph/9704452]. Cited on page 31.

[78] B. A. Bassett, S. Tsujikawa and D. Wands, *Inflation dynamics and reheating*, *Rev.Mod.Phys.* **78** (2006) 537–589, [astro-ph/0507632]. Cited on page 31.

[79] D. H. Lyth and A. R. Liddle, *The primordial density perturbation: Cosmology, inflation and the origin of structure*. 2009. Cited on page 31, 32, 33, and 35.

[80] J. Martin, C. Ringeval and V. Vennin, *Encyclopdia Inflationaris*, *Phys. Dark Univ.* **5-6** (2014) 75–235, [1303.3787]. Cited on page 32.

[81] A. Linde, *Chaotic inflation*, *Physics Letters B* **129** (1983) 177 – 181. Cited on page 33, and 34.

[82] P. Collaboration, Y. Akrami, F. Arroja, M. Ashdown, J. Aumont, C. Baccigalupi et al., *Planck 2018 results. x. constraints on inflation*, 1807.06211. Cited on page 33, 34, 45, 46, 49, and 64.

[83] L. Boubekeur and D. H. Lyth, *Hilltop inflation*, *JCAP* **0507** (2005) 010, [hep-ph/0502047]. Cited on page 33.

[84] F. L. Bezrukov and M. Shaposhnikov, *The Standard Model Higgs boson as the inflaton*, *Phys. Lett.* **B659** (2008) 703–706, [0710.3755]. Cited on page 34, and 35.

[85] G. Dvali, Q. Shafi and R. Schaefer, *Large scale structure and supersymmetric inflation without fine tuning*, *Phys.Rev.Lett.* **73** (1994) 1886–1889, [hep-ph/9406319]. Cited on page 34.

[86] K. Freese, *Natural Inflation*, in *Evolution of the universe and its observational quest. Proceedings, 37th Yamada Conference, Tokyo, Japan, June 8-12, 1993*, pp. 49–58, 1993. astro-ph/9310012. Cited on page 34.

[87] J. E. Kim, H. P. Nilles and M. Peloso, *Completing natural inflation*, *JCAP* **0501** (2005) 005, [hep-ph/0409138]. Cited on page 34.

[88] N. Arkani-Hamed, H.-C. Cheng, P. Creminelli and L. Randall, *Pseudonatural inflation*, *JCAP* **0307** (2003) 003, [hep-th/0302034]. Cited on page 34.

[89] N. Arkani-Hamed, H.-C. Cheng, P. Creminelli and L. Randall, *Extra natural inflation*, *Phys. Rev. Lett.* **90** (2003) 221302, [hep-th/0301218]. Cited on page 34.

[90] J. Garcia-Bellido, R. Rabadan and F. Zamora, *Inflationary scenarios from branes at angles*, *JHEP* **01** (2002) 036, [hep-th/0112147]. Cited on page 34.

[91] G. R. Dvali, Q. Shafi and S. Solganik, *D-brane inflation*, in *4th European Meeting From the Planck Scale to the Electroweak Scale (Planck 2001) La Londe les Maures, Toulon, France, May 11-16, 2001*, 2001. hep-th/0105203. Cited on page 34.

[92] S. Kachru, R. Kallosh, A. D. Linde, J. M. Maldacena, L. P. McAllister and S. P. Trivedi, *Towards inflation in string theory*, *JCAP* **0310** (2003) 013, [hep-th/0308055]. Cited on page 34.

[93] R. Kallosh, A. Linde and D. Roest, *Superconformal Inflationary α-Attractors*, *JHEP* **11** (2013) 198, [1311.0472]. Cited on page 34.

[94] S. Ferrara, R. Kallosh, A. Linde and M. Porrati, *Minimal Supergravity Models of Inflation*, *Phys. Rev.* **D88** (2013) 085038, [1307.7696]. Cited on page 34.

[95] D. Wands, *Multiple field inflation*, *Lect. Notes Phys.* **738** (2008) 275–304, [astro-ph/0702187]. Cited on page 35.

[96] C. Armendariz-Picon, T. Damour and V. F. Mukhanov, *k - inflation*, *Phys. Lett.* **B458** (1999) 209–218, [hep-th/9904075]. Cited on page 35.

[97] J. Garriga and V. F. Mukhanov, *Perturbations in k-inflation*, *Phys. Lett.* **B458** (1999) 219–225, [hep-th/9904176]. Cited on page 35.

[98] D. S. Salopek, J. R. Bond and J. M. Bardeen, *Designing Density Fluctuation Spectra in Inflation*, *Phys. Rev.* **D40** (1989) 1753. Cited on page 35, and 64.

[99] T. Futamase and K.-i. Maeda, *Chaotic Inflationary Scenario in Models Having Nonminimal Coupling With Curvature*, *Phys. Rev.* **D39** (1989) 399–404. Cited on page 35, and 64.

[100] R. Fakir and W. G. Unruh, *Improvement on cosmological chaotic inflation through nonminimal coupling*, *Phys. Rev.* **D41** (1990) 1783–1791. Cited on page 35, and 64.

[101] D. I. Kaiser, *Primordial spectral indices from generalized Einstein theories*, *Phys. Rev.* **D52** (1995) 4295–4306, [astro-ph/9408044]. Cited on page 35, and 64.

[102] E. Komatsu and T. Futamase, *Complete constraints on a nonminimally coupled chaotic inflationary scenario from the cosmic microwave background*, *Phys. Rev.* **D59** (1999) 064029, [astro-ph/9901127]. Cited on page 35, and 64.

[103] A. O. Barvinsky, A. Yu. Kamenshchik and A. A. Starobinsky, *Inflation scenario via the Standard Model Higgs boson and LHC*, *JCAP* **0811** (2008) 021, [0809.2104]. Cited on page 35.

[104] A. O. Barvinsky, A. Yu. Kamenshchik and A. A. Starobinsky, *Inflation in the Standard Model with a strong non-minimal curvature coupling and the Higgs boson mass*, in *Proceedings, 15th International Seminar on High Energy Physics (Quarks 2008): Sergiev Posad, Russia. May 23-29, 2008*, 2008. Cited on page 35.

[105] F. Bezrukov and M. Shaposhnikov, *Standard Model Higgs boson mass from inflation: Two loop analysis*, *JHEP* **07** (2009) 089, [0904.1537]. Cited on page 35.

[106] M. P. Hertzberg, *On Inflation with Non-minimal Coupling*, *JHEP* **11** (2010) 023, [1002.2995]. Cited on page 35, and 64.

[107] N. Okada, M. U. Rehman and Q. Shafi, *Tensor to Scalar Ratio in Non-Minimal ϕ^4 Inflation*, *Phys. Rev.* **D82** (2010) 043502, [1005.5161]. Cited on page 35, and 65.

[108] A. Linde, M. Noorbala and A. Westphal, *Observational consequences of chaotic inflation with nonminimal coupling to gravity*, *JCAP* **1103** (2011) 013, [1101.2652]. Cited on page 35, and 65.

[109] G. W. Horndeski, *Second-order scalar-tensor field equations in a four-dimensional space*, *Int. J. Theor. Phys.* **10** (1974) 363–384. Cited on page 35, and 58.

[110] A. Nicolis, R. Rattazzi and E. Trincherini, *The Galileon as a local modification of gravity*, *Phys. Rev.* **D79** (2009) 064036, [0811.2197]. Cited on page 35, and 57.

[111] C. Deffayet, S. Deser and G. Esposito-Farese, *Generalized Galileons: All scalar models whose curved background extensions maintain second-order field equations and stress-tensors*, *Phys. Rev.* **D80** (2009) 064015, [0906.1967]. Cited on page 35.

[112] C. Deffayet, G. Esposito-Farese and A. Vikman, *Covariant Galileon*, *Phys. Rev.* **D79** (2009) 084003, [0901.1314]. Cited on page 35, and 58.

[113] J. Gleyzes, D. Langlois, F. Piazza and F. Vernizzi, *Healthy theories beyond Horndeski*, *Phys. Rev. Lett.* **114** (2015) 211101, [1404.6495]. Cited on page 35.

[114] D. Langlois and K. Noui, *Degenerate higher derivative theories beyond Horndeski: evading the Ostrogradski instability*, *JCAP* **1602** (2016) 034, [1510.06930]. Cited on page 35, and 59.

[115] J. M. Ezquiaga, J. García-Bellido and M. Zumalacárregui, *Towards the most general scalar-tensor theories of gravity: a unified approach in the language of differential forms*, *Phys. Rev.* **D94** (2016) 024005, [1603.01269]. Cited on page 35.

[116] H. Motohashi, K. Noui, T. Suyama, M. Yamaguchi and D. Langlois, *Healthy degenerate theories with higher derivatives*, *JCAP* **1607** (2016) 033, [1603.09355]. Cited on page 35.

[117] M. Crisostomi, K. Koyama and G. Tasinato, *Extended Scalar-Tensor Theories of Gravity*, *JCAP* **1604** (2016) 044, [1602.03119]. Cited on page 35.

[118] J. Ben Achour, M. Crisostomi, K. Koyama, D. Langlois, K. Noui and G. Tasinato, *Degenerate higher order scalar-tensor theories beyond Horndeski up to cubic order*, *JHEP* **12** (2016) 100, [1608.08135]. Cited on page 35, and 59.

[119] J. Ben Achour, D. Langlois and K. Noui, *Degenerate higher order scalar-tensor theories beyond Horndeski and disformal transformations*, *Phys. Rev.* **D93** (2016) 124005, [1602.08398]. Cited on page 35, and 59.

[120] H. Motohashi, T. Suyama and M. Yamaguchi, *Ghost-free theory with third-order time derivatives*, 1711.08125. Cited on page 35.

[121] A. Starobinsky, *A new type of isotropic cosmological models without singularity*, *Physics Letters B* **91** (1980) 99 – 102. Cited on page 36.

[122] L. E. Parker and D. Toms, *Quantum Field Theory in Curved Spacetime*. Cambridge Monographs on Mathematical Physics. Cambridge University Press, 2009, 10.1017/CBO9780511813924. Cited on page 36.

[123] B. Whitt, *Fourth Order Gravity as General Relativity Plus Matter*, *Phys. Lett.* **145B** (1984) 176–178. Cited on page 36.

[124] D. H. Coule and M. B. Mijic, *Quantum Fluctuations and Eternal Inflation in the r^2 Model*, *Int. J. Mod. Phys.* **A3** (1988) 617–629. Cited on page 36.

[125] J. D. Barrow and S. Cotsakis, *Inflation and the Conformal Structure of Higher Order Gravity Theories*, *Phys. Lett.* **B214** (1988) 515–518. Cited on page 36.

[126] K.-i. Maeda, *Towards the Einstein-Hilbert Action via Conformal Transformation*, *Phys. Rev.* **D39** (1989) 3159. Cited on page 36.

[127] C. Burrage, C. de Rham, D. Seery and A. J. Tolley, *Galileon inflation*, *JCAP* **1101** (2011) 014, [1009.2497]. Cited on page 36.

[128] K. Kamada, T. Kobayashi, M. Yamaguchi and J. Yokoyama, *Higgs G-inflation*, *Phys. Rev.* **D83** (2011) 083515, [1012.4238]. Cited on page 36, and 66.

[129] J. Ohashi and S. Tsujikawa, *Potential-driven Galileon inflation*, *JCAP* **1210** (2012) 035, [1207.4879]. Cited on page 36, 66, 67, and 68.

[130] K. Kamada, T. Kobayashi, T. Kunimitsu, M. Yamaguchi and J. Yokoyama, *Graceful exit from Higgs G inflation*, *Phys. Rev.* **D88** (2013) 123518, [1309.7410]. Cited on page 36, and 66.

[131] R. L. Arnowitt, S. Deser and C. W. Misner, *The Dynamics of general relativity*, *Gen. Rel. Grav.* **40** (2008) 1997–2027, [gr-qc/0405109]. Cited on page 37.

[132] K. A. Malik and D. Wands, *Cosmological perturbations*, *Phys.Rept.* **475** (2009) 1–51, [0809.4944]. Cited on page 38, 81, 82, and 88.

[133] J. M. Maldacena, *Non-Gaussian features of primordial fluctuations in single field inflationary models*, *JHEP* **05** (2003) 013, [astro-ph/0210603]. Cited on page 39.

[134] C. Dvorkin and W. Hu, *Generalized Slow Roll for Large Power Spectrum Features*, *Phys. Rev.* **D81** (2010) 023518, [0910.2237]. Cited on page 44, and 76.

[135] P. Adshead, W. Hu, C. Dvorkin and H. V. Peiris, *Fast Computation of Bispectrum Features with Generalized Slow Roll*, *Phys. Rev.* **D84** (2011) 043519, [1102.3435]. Cited on page 44.

[136] P. Adshead, C. Dvorkin, W. Hu and E. A. Lim, *Non-Gaussianity from Step Features in the Inflationary Potential*, *Phys. Rev.* **D85** (2012) 023531, [1110.3050]. Cited on page 44, and 79.

[137] W. Hu, *Generalized Slow Roll for Non-Canonical Kinetic Terms*, *Phys. Rev.* **D84** (2011) 027303, [1104.4500]. Cited on page 44.

[138] V. Miranda, W. Hu and P. Adshead, *Warp Features in DBI Inflation*, *Phys. Rev.* **D86** (2012) 063529, [1207.2186]. Cited on page 44, and 79.

[139] V.-c. Miranda and W. Hu, *Inflationary Steps in the Planck Data*, *Phys. Rev.* **D89** (2014) 083529, [1312.0946]. Cited on page 44, and 79.

[140] P. Adshead, W. Hu and V. Miranda, *Bispectrum in single-field inflation beyond slow-roll*, 1303.7004. Cited on page 44.

[141] W. Hu, *Generalized slow roll for tensor fluctuations*, *Phys. Rev.* **D89** (2014) 123503, [1405.2020]. Cited on page 44.

[142] V.-c. Miranda, W. Hu and P. Adshead, *Steps to Reconcile Inflationary Tensor and Scalar Spectra*, *Phys. Rev.* **D89** (2014) 101302, [1403.5231]. Cited on page 44, and 79.

[143] G. Obied, C. Dvorkin, C. Heinrich, W. Hu and V. Miranda, *Inflationary versus reionization features from Planck 2015 data*, *Phys. Rev.* **D98** (2018) 043518, [1803.01858]. Cited on page 44.

[144] H. Motohashi and W. Hu, *Running from Features: Optimized Evaluation of Inflationary Power Spectra*, *Phys. Rev.* **D92** (2015) 043501, [1503.04810]. Cited on page 44, 76, 77, 78, and 79.

[145] H. Motohashi and W. Hu, *Generalized Slow Roll in the Unified Effective Field Theory of Inflation*, *Phys. Rev.* **D96** (2017) 023502, [1704.01128]. Cited on page 44, 75, 77, 78, and 79.

[146] G. Cabass, E. D. Valentino, A. Melchiorri, E. Pajer and J. Silk, *Running the running*, *Phys. Rev. D* **94** (2016) 023523, [1605.00209]. Cited on page 45.

[147] C. van de Bruck and C. Longden, *Running of the running and entropy perturbations during inflation*, *Phys. Rev. D* **94** (2016) 021301, [1606.02176]. Cited on page 45.

[148] BICEP2, Keck Array collaboration, P. A. R. Ade et al., *Improved Constraints on Cosmology and Foregrounds from BICEP2 and Keck Array Cosmic Microwave Background Data with Inclusion of 95 GHz Band*, *Phys. Rev. Lett.* **116** (2016) 031302, [1510.09217]. Cited on page 46.

[149] CORE collaboration, F. Finelli et al., *Exploring cosmic origins with CORE: Inflation*, *JCAP* **1804** (2018) 016, [1612.08270]. Cited on page 47.

[150] CORE collaboration, M. Remazeilles et al., *Exploring cosmic origins with CORE: B-mode component separation*, *JCAP* **1804** (2018) 023, [1704.04501]. Cited on page 47.

[151] CORE collaboration, J. Delabrouille et al., *Exploring cosmic origins with CORE: Survey requirements and mission design*, *JCAP* **1804** (2018) 014, [1706.04516]. Cited on page 47.

[152] J. Aasi, B. P. Abbott, R. Abbott, T. Abbott, M. R. Abernathy, K. Ackley et al., *Advanced ligo*, *Classical and Quantum Gravity* **32** (Mar, 2015) 074001. Cited on page 47.

[153] *Gw150914: The advanced ligo detectors in the era of first discoveries*, *Physical Review Letters* **116** (2016) . Cited on page 47.

[154] P. Amaro-Seoane, H. Audley, S. Babak, J. Baker, E. Barausse, P. Bender et al., *Laser interferometer space antenna*, 1702.00786. Cited on page 47.

[155] G. Hobbs, A. Archibald, Z. Arzoumanian, D. Backer, M. Bailes, N. D. R. Bhat et al., *The international pulsar timing array project: using pulsars as a gravitational wave detector*, *Classical and Quantum Gravity* **27** (Apr, 2010) 084013. Cited on page 47.

[156] M. Kramer, D. Backer, J. Cordes, T. Lazio, B. Stappers and S. Johnston, *Strong-field tests of gravity using pulsars and black holes*, *New Astronomy Reviews* **48** (2004) 993 – 1002. Cited on page 47.

[157] LIGO Scientific, Virgo collaboration, B. P. Abbott et al., *Observation of Gravitational Waves from a Binary Black Hole Merger*, *Phys. Rev. Lett.* **116** (2016) 061102, [1602.03837]. Cited on page 48, and 53.

[158] LIGO Scientific, Virgo collaboration, B. P. Abbott et al., *GW151226: Observation of Gravitational Waves from a*

22-Solar-Mass Binary Black Hole Coalescence, *Phys. Rev. Lett.* **116** (2016) 241103, [1606.04855]. Cited on page 48, and 53.

[159] LIGO Scientific, Virgo collaboration, B. P. Abbott et al., *Binary Black Hole Mergers in the first Advanced LIGO Observing Run*, *Phys. Rev.* **X6** (2016) 041015, [1606.04856]. Cited on page 48, and 53.

[160] LIGO Scientific, Virgo, Fermi GBM, INTEGRAL, IceCube, AstroSat Cadmium Zinc Telluride Imager Team, IPN, Insight-Hxmt, ANTARES, Swift, AGILE Team, 1M2H Team, Dark Energy Camera GW-EM, DES, DLT40, GRAWITA, Fermi-LAT, ATCA, ASKAP, Las Cumbres Observatory Group, OzGrav, DWF (Deeper Wider Faster Program), AST3, CAASTRO, VINROUGE, MASTER, J-GEM, GROWTH, JAGWAR, CaltechNRAO, TTU-NRAO, NuSTAR, Pan-STARRS, MAXI Team, TZAC Consortium, KU, Nordic Optical Telescope, ePESSTO, GROND, Texas Tech University, SALT Group, TOROS, BOOTES, MWA, CALET, IKI-GW Follow-up, H.E.S.S., LOFAR, LWA, HAWC, Pierre Auger, ALMA, Euro VLBI Team, Pi of Sky, Chandra Team at McGill University, DFN, ATLAS Telescopes, High Time Resolution Universe Survey, RIMAS, RATIR, SKA South Africa/MeerKAT collaboration, B. P. Abbott et al., *Multi-messenger Observations of a Binary Neutron Star Merger*, *Astrophys. J.* **848** (2017) L12, [1710.05833]. Cited on page 48, and 53.

[161] LIGO Scientific, Virgo collaboration, B. P. Abbott et al., *GW170817: Observation of Gravitational Waves from a Binary Neutron Star Inspiral*, *Phys. Rev. Lett.* **119** (2017) 161101, [1710.05832]. Cited on page 48, and 53.

[162] LIGO Scientific, Virgo collaboration, B. P. Abbott et al., *GW170814: A Three-Detector Observation of Gravitational Waves from a Binary Black Hole Coalescence*, *Phys. Rev. Lett.* **119** (2017) 141101, [1709.09660]. Cited on page 48, and 53.

[163] LIGO Scientific, Virgo collaboration, B. P. Abbott et al., *GW170608: Observation of a 19-solar-mass Binary Black Hole Coalescence*, *Astrophys. J.* **851** (2017) L35, [1711.05578]. Cited on page 48, and 53.

[164] LIGO Scientific, VIRGO collaboration, B. P. Abbott et al., *GW170104: Observation of a 50-Solar-Mass Binary Black Hole*

Coalescence at Redshift 0.2, *Phys. Rev. Lett.* **118** (2017) 221101, [1706.01812]. Cited on page 48, and 53.

[165] LIGO Scientific, Virgo, Fermi-GBM, INTEGRAL collaboration, B. P. Abbott et al., *Gravitational Waves and Gamma-rays from a Binary Neutron Star Merger: GW170817 and GRB 170817A*, *Astrophys. J.* **848** (2017) L13, [1710.05834]. Cited on page 48, and 53.

[166] LIGO Scientific, Virgo collaboration, B. P. Abbott et al., *GWTC-1: A Gravitational-Wave Transient Catalog of Compact Binary Mergers Observed by LIGO and Virgo during the First and Second Observing Runs*, 1811.12907. Cited on page 48, and 53.

[167] C. J. Moore, R. H. Cole and C. P. L. Berry, *Gravitational-wave sensitivity curves*, *Classical and Quantum Gravity* **32** (Dec, 2014) 015014. Cited on page 48.

[168] C. Caprini and D. G. Figueroa, *Cosmological Backgrounds of Gravitational Waves*, *Class. Quant. Grav.* **35** (2018) 163001, [1801.04268]. Cited on page 48.

[169] J. L. Cook and L. Sorbo, *Particle production during inflation and gravitational waves detectable by ground-based interferometers*, *Phys. Rev.* **D85** (2012) 023534, [1109.0022]. Cited on page 48.

[170] L. Senatore, E. Silverstein and M. Zaldarriaga, *New Sources of Gravitational Waves during Inflation*, *JCAP* **1408** (2014) 016, [1109.0542]. Cited on page 48.

[171] M. Mylova, O. zsoy, S. Parameswaran, G. Tasinato and I. Zavala, *A new mechanism to enhance primordial tensor fluctuations in single field inflation*, 1808.10475. Cited on page 48.

[172] V. Mukhanov, *Quantum Cosmological Perturbations: Predictions and Observations*, *Eur. Phys. J.* **C73** (2013) 2486, [1303.3925]. Cited on page 49, 50, and 51.

[173] L. Barranco, L. Boubekeur and O. Mena, *A model-independent fit to Planck and BICEP2 data*, *Phys. Rev.* **D90** (2014) 063007, [1405.7188]. Cited on page 50.

[174] C. Collaboration, C. Armitage-Caplan, M. Avillez, D. Barbosa, A. Banday, N. Bartolo et al., *Core (cosmic origins explorer) a white paper*, 1102.2181. Cited on page 51.

[175] P. Draper, P. Meade, M. Reece and D. Shih, *Implications of a 125 GeV Higgs for the MSSM and Low-Scale SUSY Breaking*, *Phys. Rev.* **D85** (2012) 095007, [1112.3068]. Cited on page 53.

[176] L. Heisenberg, *A systematic approach to generalisations of general relativity and their cosmological implications*, 1807.01725. Cited on page 54, 56, 58, 59, and 61.

[177] C. de Rham, *Massive Gravity*, *Living Rev. Rel.* **17** (2014) 7, [1401.4173]. Cited on page 56.

[178] C. de Rham, G. Gabadadze, L. Heisenberg and D. Pirtskhalava, *Cosmic Acceleration and the Helicity-0 Graviton*, *Phys. Rev.* **D83** (2011) 103516, [1010.1780]. Cited on page 56.

[179] H. Motohashi, *Third order equations of motion and the ostrogradsky instability*, *Physical Review D* **91** (2015) . Cited on page 56.

[180] G. R. Dvali, G. Gabadadze and M. Porrati, *4-D gravity on a brane in 5-D Minkowski space*, *Phys. Lett.* **B485** (2000) 208–214, [hep-th/0005016]. Cited on page 57.

[181] D. Langlois and K. Noui, *Hamiltonian analysis of higher derivative scalar-tensor theories*, *JCAP* **1607** (2016) 016, [1512.06820]. Cited on page 59.

[182] C. Deffayet, S. Deser and G. Esposito-Farese, *Arbitrary p-form Galileons*, *Phys. Rev.* **D82** (2010) 061501, [1007.5278]. Cited on page 60.

[183] C. Deffayet, A. E. Gmrkolu, S. Mukohyama and Y. Wang, *A no-go theorem for generalized vector Galileons on flat spacetime*, *JHEP* **04** (2014) 082, [1312.6690]. Cited on page 60.

[184] C. Deffayet, S. Mukohyama and V. Sivanesan, *On p-form theories with gauge invariant second order field equations*, *Phys. Rev.* **D93** (2016) 085027, [1601.01287]. Cited on page 60.

[185] C. Deffayet, S. Garcia-Saenz, S. Mukohyama and V. Sivanesan, *Classifying Galileon p-form theories*, *Phys. Rev.* **D96** (2017) 045014, [1704.02980]. Cited on page 60.

[186] G. W. Horndeski, *Conservation of charge and the einstein–maxwell field equations*, *Journal of Mathematical Physics* **17** (1976) 1980–1987, [https://doi.org/10.1063/1.522837]. Cited on page 60.

[187] J. D. Barrow, M. Thorsrud and K. Yamamoto, *Cosmologies in Horndeski's second-order vector-tensor theory*, *JHEP* **02** (2013) 146, [1211.5403]. Cited on page 60.

[188] J. Beltran Jimenez, R. Durrer, L. Heisenberg and M. Thorsrud, *Stability of Horndeski vector-tensor interactions*, *JCAP* **1310** (2013) 064, [1308.1867]. Cited on page 60.

[189] L. Heisenberg, *Generalization of the Proca Action*, *JCAP* **1405** (2014) 015, [1402.7026]. Cited on page 61.

[190] E. Allys, P. Peter and Y. Rodriguez, *Generalized Proca action for an Abelian vector field*, *JCAP* **1602** (2016) 004, [1511.03101]. Cited on page 61.

[191] J. Beltran Jimenez and L. Heisenberg, *Derivative self-interactions for a massive vector field*, *Phys. Lett.* **B757** (2016) 405–411, [1602.03410]. Cited on page 61.

[192] G. Tasinato, *Cosmic Acceleration from Abelian Symmetry Breaking*, *JHEP* **04** (2014) 067, [1402.6450]. Cited on page 61.

[193] G. Tasinato, *A small cosmological constant from Abelian symmetry breaking*, *Class. Quant. Grav.* **31** (2014) 225004, [1404.4883]. Cited on page 61.

[194] A. De Felice, L. Heisenberg, R. Kase, S. Mukohyama, S. Tsujikawa and Y.-l. Zhang, *Effective gravitational couplings for cosmological perturbations in generalized Proca theories*, *Phys. Rev.* **D94** (2016) 044024, [1605.05066]. Cited on page 61.

[195] A. De Felice, L. Heisenberg, R. Kase, S. Mukohyama, S. Tsujikawa and Y.-l. Zhang, *Cosmology in generalized Proca theories*, *JCAP* **1606** (2016) 048, [1603.05806]. Cited on page 61.

[196] A. de Felice, L. Heisenberg and S. Tsujikawa, *Observational constraints on generalized Proca theories*, *Phys. Rev.* **D95** (2017) 123540, [1703.09573]. Cited on page 61.

[197] A. Cisterna, M. Hassaine, J. Oliva and M. Rinaldi, *Static and rotating solutions for Vector-Galileon theories*, *Phys. Rev.* **D94** (2016) 104039, [1609.03430]. Cited on page 61.

[198] M. Minamitsuji, *Solutions in the generalized Proca theory with the nonminimal coupling to the Einstein tensor*, *Phys. Rev.* **D94** (2016) 084039, [1607.06278]. Cited on page 61.

[199] A. De Felice, L. Heisenberg, R. Kase, S. Tsujikawa, Y.-l. Zhang and G.-B. Zhao, *Screening fifth forces in generalized Proca theories*, *Phys. Rev.* **D93** (2016) 104016, [1602.00371]. Cited on page 61.

[200] Z.-Y. Fan, *Black holes with vector hair*, *JHEP* **09** (2016) 039, [1606.00684]. Cited on page 61.

[201] J. Chagoya, G. Niz and G. Tasinato, *Black Holes and Abelian Symmetry Breaking*, *Class. Quant. Grav.* **33** (2016) 175007, [1602.08697]. Cited on page 61.

[202] L. Heisenberg, R. Kase, M. Minamitsuji and S. Tsujikawa, *Hairy black-hole solutions in generalized Proca theories*, *Phys. Rev.* **D96** (2017) 084049, [1705.09662]. Cited on page 61.

[203] L. Heisenberg, R. Kase, M. Minamitsuji and S. Tsujikawa, *Black holes in vector-tensor theories*, *JCAP* **1708** (2017) 024, [1706.05115]. Cited on page 61.

[204] J. Chagoya, G. Niz and G. Tasinato, *Black Holes and Neutron Stars in Vector Galileons*, *Class. Quant. Grav.* **34** (2017) 165002, [1703.09555]. Cited on page 61.

[205] L. Heisenberg, R. Kase and S. Tsujikawa, *Beyond generalized Proca theories*, *Phys. Lett.* **B760** (2016) 617–626, [1605.05565]. Cited on page 61.

[206] L. Heisenberg, *Scalar-Vector-Tensor Gravity Theories*, *JCAP* **1810** (2018) 054, [1801.01523]. Cited on page 62.

[207] R. Kase and S. Tsujikawa, *Dark energy in scalar-vector-tensor theories*, *JCAP* **1811** (2018) 024, [1805.11919]. Cited on page 63.

[208] L. Heisenberg and S. Tsujikawa, *Hairy black hole solutions in $U(1)$ gauge-invariant scalar-vector-tensor theories*, *Phys. Lett.* **B780** (2018) 638–646, [1802.07035]. Cited on page 63.

[209] T. Kobayashi, M. Yamaguchi and J. Yokoyama, *Generalized G-inflation: Inflation with the most general second-order field equations*, *Prog. Theor. Phys.* **126** (2011) 511–529, [1105.5723]. Cited on page 64, 66, 67, 89, and 90.

[210] M. B. Einhorn and D. R. T. Jones, *Inflation with Non-minimal Gravitational Couplings in Supergravity*, *JHEP* **03** (2010) 026, [0912.2718]. Cited on page 64.

[211] R. Kallosh and A. Linde, *New models of chaotic inflation in supergravity*, *JCAP* **1011** (2010) 011, [1008.3375]. Cited on page 64.

[212] S. Ferrara, R. Kallosh, A. Linde, A. Marrani and A. Van Proeyen, *Jordan Frame Supergravity and Inflation in NMSSM*, *Phys. Rev.* **D82** (2010) 045003, [1004.0712]. Cited on page 64.

[213] H. M. Lee, *Chaotic inflation in Jordan frame supergravity*, *JCAP* **1008** (2010) 003, [1005.2735]. Cited on page 64.

[214] S. Ferrara, R. Kallosh, A. Linde, A. Marrani and A. Van Proeyen, *Superconformal Symmetry, NMSSM, and Inflation*, *Phys. Rev.* **D83** (2011) 025008, [1008.2942]. Cited on page 64.

[215] R. Kallosh, A. Linde and T. Rube, *General inflaton potentials in supergravity*, *Phys. Rev.* **D83** (2011) 043507, [1011.5945]. Cited on page 64.

[216] D. I. Kaiser and E. I. Sfakianakis, *Multifield Inflation after Planck: The Case for Nonminimal Couplings*, *Phys. Rev. Lett.* **112** (2014) 011302, [1304.0363]. Cited on page 65.

[217] T. Chiba and K. Kohri, *Consistency Relations for Large Field Inflation: Non-minimal Coupling*, *PTEP* **2015** (2015) 023E01, [1411.7104]. Cited on page 65.

[218] C. Pallis and Q. Shafi, *Gravity Waves From Non-Minimal Quadratic Inflation*, *JCAP* **1503** (2015) 023, [1412.3757]. Cited on page 65.

[219] T. Tenkanen, *Resurrecting Quadratic Inflation with a non-minimal coupling to gravity*, *JCAP* **1712** (2017) 001, [1710.02758]. Cited on page 65.

[220] T. Kobayashi, M. Yamaguchi and J. Yokoyama, *G-inflation: Inflation driven by the Galileon field*, *Phys. Rev. Lett.* **105** (2010) 231302, [1008.0603]. Cited on page 66.

[221] A. De Felice and S. Tsujikawa, *Primordial non-Gaussianities in general modified gravitational models of inflation*, *JCAP* **1104** (2011) 029, [1103.1172]. Cited on page 66.

[222] H. Bazrafshan Moghaddam, R. Brandenberger and J. Yokoyama, *Note on Reheating in G-inflation*, *Phys. Rev.* **D95** (2017) 063529, [1612.00998]. Cited on page 66.

[223] L. Heisenberg, R. Kase and S. Tsujikawa, *Cosmology in scalar-vector-tensor theories*, *Phys. Rev.* **D98** (2018) 024038, [1805.01066]. Cited on page 69, 71, 72, 89, 91, and 92.

[224] J. A. Adams, B. Cresswell and R. Easther, *Inflationary perturbations from a potential with a step*, *Phys. Rev.* **D64** (2001) 123514, [astro-ph/0102236]. Cited on page 74.

[225] L. Covi, J. Hamann, A. Melchiorri, A. Slosar and I. Sorbera, *Inflation and WMAP three year data: Features have a Future!*, *Phys. Rev.* **D74** (2006) 083509, [astro-ph/0606452]. Cited on page 74.

[226] J. Hamann, L. Covi, A. Melchiorri and A. Slosar, *New Constraints on Oscillations in the Primordial Spectrum of Inflationary Perturbations*, *Phys. Rev.* **D76** (2007) 023503, [astro-ph/0701380]. Cited on page 74.

[227] C. Pahud, M. Kamionkowski and A. R. Liddle, *Oscillations in the inflaton potential?*, *Phys. Rev.* **D79** (2009) 083503, [0807.0322]. Cited on page 74.

[228] M. Joy, A. Shafieloo, V. Sahni and A. A. Starobinsky, *Is a step in the primordial spectral index favored by CMB data ?*, *JCAP* **0906** (2009) 028, [0807.3334]. Cited on page 74.

[229] M. J. Mortonson, C. Dvorkin, H. V. Peiris and W. Hu, *CMB polarization features from inflation versus reionization*, *Phys. Rev.* **D79** (2009) 103519, [0903.4920]. Cited on page 74.

[230] E. D. Stewart, *The Spectrum of density perturbations produced during inflation to leading order in a general slow roll approximation*, *Phys.Rev.* **D65** (2002) 103508, [astro-ph/0110322]. Cited on page 74.

[231] R. Kase and S. Tsujikawa, *Effective field theory approach to modified gravity including Horndeski theory and Hořava–Lifshitz gravity*, *Int. J. Mod. Phys.* **D23** (2014) 1443008, [1409.1984]. Cited on page 75.

[232] C. Dvorkin and W. Hu, *Complete WMAP Constraints on Bandlimited Inflationary Features*, *Phys. Rev.* **D84** (2011) 063515, [1106.4016]. Cited on page 76.

[233] G. Obied, C. Dvorkin, C. Heinrich, W. Hu and V. Miranda, *Inflationary Features and Shifts in Cosmological Parameters from Planck 2015 Data*, *Phys. Rev.* **D96** (2017) 083526, [1706.09412]. Cited on page 76.

[234] V. Miranda, W. Hu, C. He and H. Motohashi, *Nonlinear Excitations in Inflationary Power Spectra*, *Phys. Rev.* **D93** (2016) 023504, [1510.07580]. Cited on page 77.

[235] H. Motohashi and W. Hu, *Primordial Black Holes and Slow-Roll Violation*, *Phys. Rev.* **D96** (2017) 063503, [1706.06784]. Cited on page 79.

[236] P. Adshead and W. Hu, *Fast computation of first-order feature-bispectrum corrections*, *Phys. Rev. D* **85** (2012) 103531, [1203.0012]. Cited on page 79.

[237] P. Adshead, W. Hu and V. Miranda, *Bispectrum in single-field inflation beyond slow-roll*, *Phys. Rev. D88 023507 (2013)* (03, 2013) , [1303.7004]. Cited on page 79.

[238] S. Passaglia and W. Hu, *Scalar bispectrum beyond slow-roll in the unified eft of inflation*, *Phys. Rev. D* **98** (2018) 023526, [1804.07741]. Cited on page 79.

[239] J. M. Bardeen, *Gauge Invariant Cosmological Perturbations*, *Phys. Rev.* **D22** (1980) 1882–1905. Cited on page 86.

⋆ ⋆ ⋆